An experimental procedure for Reaction Injection Moulding – RIM – materials formulation design

Ph.D. Dissertation
in
Chemical and Biological Engineering
by

Marina Verenčević Lima Torres

Supervisors

Ricardo Jorge Nogueira dos Santos

Mário Rui Pinto Ferreira Nunes da Costa

Laboratory of Separation and Reaction Engineering
Departamento de Engenharia Química
Faculdade de Engenharia
Universidade do Porto

May 2014

Acknowledgments

Here I wish to thank some people for their support during these four years of work on the dissertation:

- To my supervisor Dr. Ricardo Santos, for his support and motivation during this four years of professional and personal growth.
- To my co-supervisor Prof. Dr. Mário Rui Costa, for his motivation and friendship.
- I wish to acknowledge Prof. Dr. José Carlos Lopes for his guidance in the world of scientific research in the beginning of this work, as well as his friendship and motivation.
- To Prof[a] Dr[a] Madalena Dias, for her help and support always when needed.
- To Prof. Dr. Alírio Rodrigues, director of LSRE – Laboratory of Separation and Reaction Engineering, where this work was developed.
- To Fundação de Ciência e Tecnologia, for the financial support through Ph.D. scholarship with the reference SFRH/BD/64344/2009.
- To my friends and colleagues from "Mixing" group and LSRE. To my friend Cláudio Fonte, with whom I learned a lot, for his friendship and motivation. To my friends Marina Manić and Gabriela Ruphuy. To Carlos Fonte, Marcelo Costa, Nuno Gomes, António Gouveia, Paulo Gomes, Ashar Sultan, Kateryna Krupa, Ângela Novais, Romulo Oliveira, Enis Leblebici, Pelin Leblebici, Anna Harcinska and Franziska Fehst, for the great moments that we shared during years. To Anna Karpinska Portela for her help and friendship in the very beginning of this work.
- To all my family and friends, especially my husband Pedro, my mother and my parents in law.
- To all my friends from Serbia, especially Ljubica Mitrović, Marija Jović, Viktorija Kočeski and Biljana Jovanović.

To my family

"A happy man is too satisfied with the present to think too much about the future."

Albert Einstein

Abstract

A method for efficient mixing at rheometer called the Holding Cell (HC) of two components of a reactive polymerisation was developed and it was proven that it can be applied for the measurement of rheological properties of a mixture of reactive monomers (poyol and isocyanate), in situ. This method enables the simultaneous measurement of the gel point and to obtain a solid product that can be tested mechanically to assess characteristics such as the compression strength and the deflection temperature. These mechanical characterisations are limited by the dimensions of the sample, depending on the rheometer measuring system and can be as high as: diameter 75 mm and height approx. 10 mm. Viscosity rise due to the polymerisation was modelled. Particular attention was paid to the study of the mixing of the monomers in a rotational rheometer, and this was proven to be a step that has a critical effect on the results of the rheochemical characterisation.

A method for the functionalisation of crystalline nanometric hydroxyapatite (HAp) water paste was developed, and involves: mixing the HAp paste with ethylene glycol and distillation to extract water and obtain stable dispersion of HAp in ethylene glycol. This dispersion was mixed with polyol and afterwards the Holding Cell method was applied and rheological properties of this reactive formulation were measured. It is concluded that HAp acts as a catalyst when high shear rates are applied.

A method for the synthesis of the zinc oxide nanoparticles and transfer to the polyol was developed and the rheochemical characteristics of the processing of this nanocomposite were measured by the HC method. This study showed that zinc oxide acts as a catalyst for the polymerisation and increases the viscosity rise.

The optimal initiator/catalyst ratio of the polyamide-6 reactive formulation for Reaction Injection Moulding (RIM) was found by measuring the complex viscosity rise using the HC rheometry method.

Resumo

Um método para a mistura eficiente de dois componentes duma polimerização reativa, designado de Método da Célula de Suporte, foi desenvolvido e a sua aplicação demonstrada na caracterização reológica de um mistura reativa de dois monómeros (poliol e isocianato), *insitu*. Este método permite simultaneamentea medição do tempo de gelificação a obtenção dum produto sólido que pode ser submetido a ensaios mecânicos, tais como o teste de compressão e de temperatura de deflexão. Estes testes são limitados em função das dimensões da amostra, que dependem da geometria do sistema usado no reómetro e que pode ser de até 75mm de diâmetro e 10mm de altura. O aumento da viscosidade por efeito da polimerização foi modelizado. Particular atenção foi dada ao estudo da mistura dos monómeros no reómetro rotacional, e foi demonstrado que esta etapa tem um efeito crucial nos resultado da caracterização reoquímica da polimerização.

Um método para a funcionalização de pasta aquosa de hidroxiapatita (HAp) cristalina nanométrica foi desenvolvido. O método consiste na mistura da pasta de HAp em etileno glicol, seguida de uma destilação para extrair a água e obter uma dispersão estável de HAp. A dispersão de HAp foi incorporada no poliol, e de seguida foi usado o Método da Célula de Suporte para medição das propriedades reológicas da formulação reativa. Conclui-se que HAp age como catalisador às taxas de deformação altas.

Um método para a síntese de nanopartículas de óxido de zinco e transferência para o poliol foi desenvolvido e as características reoquímicas do processamento deste nanocompósito foram medida, com o Método da Célula de Suporte. Este estudo mostrou que o óxido de zinco age com o catalisador da polimerização e promove o aumento de viscosidade.

A razão ótima de iniciador/catalisador para formulações de poliamida-6 para Moldagem de Injecção Reactiva (RIM) foi determinada usando a curva de subida da viscosidade complexa com o Método da Célula de Suporte.

Резиме

У овој дисертацији развијен је поступак за ефикасно мешање два реактанта реакционих полимеризација путем реометра назван “The holding cell” и доказано је да се може применити за мерење реолошких својстава смеше реактивних мономера (полиола и изоцијаната), *insitu*. Овај поступак омогућава симултано мерење тачке формирања гела и добијање производа у крајњој форми, који накнадно подлеже мерењу механичких својстава - компресивне јачине и температуре дефлекције. Карактерисање механичких својстава је ограничено димензијама узорка, а које зависе од мерног система реометра и могу бити максималне величине: пречника $75\,\mathrm{mm}$ и висине (приближно) $10\,\mathrm{mm}$. Моделован је пораст вискозности услед полимеризације. Посебна пажња посвећена је проучавању мешања мономера путем ротационог реометра, и доказано је да је овај корак има критично дејство на резултате рео-хемијског карактерисања.

Развијен је поступак за функционализацију кристалног нанометарског хидроксиапатита (ХАп) у облику водене пасте, и укључује: мешање водене ХАп пасте са етилен гликолом и дестилацију ради екстракције воде и добијања стабилне дисперзије ХАп у етилен гликолу. Последња дисперзија је помешана са полиолом и након тога примењен је “The holding cell” поступак и мерене су реолошке карактеристике реактивне формулације.

Још је развијен метод за синтезу наночестица цинк оксида и њихов трансфер у полиол као и мерење рео-хемијских карактеристика током реактивне прераде овог нанокомпозита путем методе “The holding cell”.

Одређен је оптималан иницијатор/катализатор однос за реактивну формулацију полиамида-6 за примену у Реакционом Инјекционом Бризгању путем мерења пораста комплексне вискозности користећи “The holding cell” методу путем реометра.

Table of Contents

Table of Figures

Table of Tables

Notation

A	Area $[m^2]$
A_{HAp}	Area of a hydroxyapatite nanoparticle $[m^2]$
A_{EG}	Area of a ethylene glycol molecule $[m^2]$
A	Absorbance
b	Sample width for DMA tests $[m]$
D	Tube diameter $[m]$
E'	Storage modulus $[Pa]$
E"	Loss modulus $[Pa]$
E *	Complex modulus $[Pa]$
F	Force $[N]$
G'	Storage modulus $[Pa]$
G"	Loss modulus $[Pa]$
h	Sample height for DMA tests $[m]$
L	Sample length $[m]$
L_0	Initial sample length $[m]$
M	Torque $[Nm]$
M_W	Molecular weight $[g / mole]$
M_W^{EG}	Molecular weight of ethylene glycol $[g / mole]$
m_{pack}^{C10}	C10 package weight
m_{pack}^{C20}	C20 package weight
$m_{CL,add}^{A}$	Pure CL mass to be added into tank A
$m_{CL,add}^{B}$	Pure CL mass to be added into tank A
m_{C10}^{A}	Mass of C10 to be added into tank A
m_{C20}^{B}	Mass of C20 to be added into tank B
m_{CL}^{C10}	Mass of CL from C10
m_{CL}^{C20}	Mass of CL from C20
$m_{CL,tot}^{A}$	Total mass of CL in tank A (the sum of pure CL to be added into tank A, $m_{CL,add}(A)$ and CL from C10, $m_{CL}(C10)$)
$m_{CL,tot}^{B}$	Total mass of CL in tank B (the sum of pure CL to be added into tank B, $m_{CL,add}(B)$ and CL from C20, $m_{CL}(C20)$)
$m_{Na-\ CL}^{C10}$	Mass of sodium-CL from C10 (equals to the mass of CL in tank A)
$m_{B-\ iso}^{C20}$	Mass of B-iso from C20 (equals to the mass of CL in tank B)
m_{tot}^{A}	Total mass of tank A

m^{B}_{tot}	Total mass of tank B
$m^{A}_{Na\text{- }CL}$	Mass of sodium-CL in tank A
$m^{B}_{B\text{- }iso}$	Mass of B-iso in tank B
m^{samp}	Mass of the solidified sample of polyamide-6
n_X	Number of moles [mole]
n'	Number of moles [mole]
N	Number of the cone turns
N_A	Avogadro constant [molecules / mole]
N^{tot}_{HAp}	Total number of hydroxyapatite molecules
N^{tot}	Total number of molecules
R	Cone radius [m]
T	Temperature [°C]
T_b	Boiling point [°C]
T_{iso}	Isocyanate temperature [°C]
T_m	Melting point [°C]
T_{pol}	Polyol temperature [°C]
T_{rheo}	Rheometer temperature [°C]
T_{room}	Room temperature [°C]
t	Time [s]
$t_{M,max}$	Time when the torque is maximum [s]
t_{tot}	Total time of experiment [s]
t_s	Sample thickness for DMA [mm]
t_{out}	Time when sample gets out of the gap [s]
s	Scale of the lamina
v	Velocity [m / s]
V	Volume of tank A or B in PA-6 synthesis
V^A	Volume of tank A in PA-6 synthesis
V^B	Volume of tank B in PA-6 synthesis
V'	Specific volume [m^3]
V_{prop}	Volume of isopropanol [m^3]
V^{tot}	Total volume [m^3]
V^{tot}_{EG}	Total volume of ethylene glycol [m^3]
V^{tot}_{HAp}	Total volume of hydroxyapatite [m^3]
ω^{C10}_{Na-CL}	Weight fraction of sodium-CL in C10
y	Initial thickness of the lamina
ω^{C20}_{B-iso}	Weight fraction of B-iso in C20
ω^{A}_{Na-CL}	Weight fraction of sodium-CL in tank A

ω^{B}_{B-iso}	Weight fraction of B-iso in tank B
ω^{samp}_{Na-CL}	Weight fraction of sodium-CL in solidified sample of polyamide-6
ω^{samp}_{B-iso}	Weight fraction of B-iso in solidified sample of polyamide-6

Greek letters

α	Angle of the cone [°]
γ	Shear strain
γ_0	Shear strain amplitude
$\dot{\gamma}$	Shear rate [s^{-1}]
ε	Elongation [m]
μ	Dynamic viscosity [Pa.s]
μ_{init}	Initial dynamic viscosity [Pa.s]
η	Dynamic viscosity [Pa.s]
π	Mathematical constant
ρ	Density [kg / m^3]
ρ_{CL}	Density of pure CL monomer in synthesis of PA-6
ρ^{A}	Density of the mixture in tank A in synthesis of PA-6
ρ^{B}	Density of the mixture in tank B in synthesis of PA-6
ρ_{HAp}	Hydroxyapatite density [kg / m^3]
ρ_{EG}	Ethylene glycol density [kg / m^3]
σ	Shear stress [Pa]

Abbreviations

AP	Anionic polymerisation
BSED	Back Scattered Electron Detector
CFD	Computational Fluid Dynamics
CL	Caprolactam
DBTDL	Dibutyltin dilaurate
DCP	Dicyclopentadiene
DIN	Deutsche Institut fur Normung (German Institute for Standardization)
DRIFT	Diffuse Reflectance Infrared Fourier Transform
DSC	Differential Scanning Calorimetry
DTUL	Deflection Temperature Under Load
EDS	Energy Dispersive Spectrometer
EG	Ethylene Glycol
FTIR	Fourier Transform Infrared
HAp	Hydroxyapatite
HC	Holding cell
KBr	Potassium Bromide

LFD	Large Field Detector
LSRE	Laboratory of Separation and Reaction Engineering
MDI	Methylene Difenyl Diisocyanate
OPO	One top other
PA	Polyamide
PEG	Polyehtylene Glycol
PDCP	Polydicyclopentadiene
PU	Polyurethane
Ren	Rencast
RIM	Reaction Injection Moulding
RRIM	Reinforced Reaction Injection Moulding
SEM	Scanning Electron Microscopy
SRIM	Structural Reaction Injection Moulding
TC	Temperature controller
TDI	Toluene Diisocyanate
TEK	Thermostatting and measuring device for cone/plate geometry
TEZ	Thermostatting and measuring device for cylinder geometry
TG	Thermogravimetry
TPU	Thermoplastic Polyurethane

1 Introduction

1.1 Reactive formulations for RIM

The work presented in this thesis is focused at Reaction Injection Moulding (RIM) formulations, typically polyurethanes (PU) and polyamide-6. Although both of the mentioned materials are possible to produce throughout different addition reactions onto isocyanate group, only reactions with fast kinetics at relatively low temperatures are considered for RIM. Polyurethanes and polyureas are widely used in many applications in everyday life such as: automotive parts, aeronautical parts, cushions and mattresses, faux leather for garments and furniture etc. Such a wide range of products is possible to obtain due to the very rich chemistry of polyurethanes (isocyanates) – multiple possibilities of addition onto isocyanate functional group – and many combinations of catalysts/additives (Szycher 1999). Polyurethanes and polyureas formation reactions are characterised by very fast kinetics even at low temperatures. Viscosity rise and the gel time of the reaction mixture are two of the most important material parameters that affect the optimal processing parameters for their production. Polyurethane formulations are characterised by the gel time, which

is the time when the viscosity of the forming polymer is still low enough for the reactive mixture to be modified and moulded before getting its final shape.

Nowadays, one of the most common processes used in industrial production of polyurethanes and polyureas is RIM process. Two (oligomerized) monomers are used: an extremely reactive isocyanate and a polyol (amine). Their viscosities range from $10\,\mathrm{mPa.s}$ to $5000\,\mathrm{mPa.s}$ at room temperature. Those monomers impinge and mix inside the mixing chamber of the RIM machine during the time of $10\,\mathrm{ms}$ to $100\,\mathrm{ms}$, and afterwards the reactive mixture is pushed into the mould where the polymerisation takes place. Mechanical and physical properties of the final product depend highly on the mixing of the two monomers inside the mixing chamber of the RIM machine. Efficient mixing of the two monomers is essential for achieving a good quality product. Problems with the clogged mixing head caused by the polymerisation of the reactive mixture inside it have been one of the major problems in RIM industry requiring often maintenance of the RIM machines and tuning of the processing parameters for each specific formulation. For a successful mould filling, gel time of the formulation must be larger than the mould filling time.

Polyurethanes are mainly produced in one of the major international chemical companies such as BASF (BASF 2012), Bayer AG (Bayer 2012), and Huntsman (Huntsman 2012) In Table 1.1 are represented annual revenues in Euros of the mentioned industries with the indicated polyurethanes and plastics share in it. It is observed that the polyurethanes represent a large fraction of the total sales for each one of these companies. The values reported by Huntsman were converted from Dollars to Euros at an average exchange rate over the last 5 years of $0.74\,€/\$$.

Table 1.1. Annual sales in billions of Euros of some of the major chemical companies.

Company	Total		Plastics		Polyurethanes	
	2011	2012	2011	2012	2011	2012
BASF	73.5	78.8	11	11.4	5.85	6.3
Bayer AG	36.5	39.8	-	-	5.36	6
Huntsman	8.31	8.31	-	-	3.26	3.63

1.2 Previous work

The work presented in this thesis is a complementary study to the Ph.D. thesis on mixing mechanisms in RIM (Fonte 2012) and recently patented RIM technology and moulds (Gomes 2014). Nevertheless, before presenting the objectives and layout of this dissertation, it is relevant to summarize their works here.

Fonte (2012) studied mixing mechanisms in impinging jets with the dominant application in RIM. CFD simulations on the mixing mechanisms were performed and the successful pattern of the mixing determined, consisting of stretching, folding and break up of the fluid stream. Critical Reynolds number for the effective mixing was calculated and it was 110. CFD simulations were confirmed by the experimental studies with Particle Image Velocimetry and Planar Laser Induced Fluorescence.

A detailed study on moulds for RIM machines including CFD simulation on the flow dynamics inside the mould was done by Gomes (2014). Recently developed RIM technology that enables the control of the mixing of the two monomers by a differential pressure sensor (Patent number WO 2005/097477) was studied on the production of the polyurethane RenCast reactive formulation in a prototype machine. Optimal process parameters for this specific formulation were determined. Compressive strength and deflection temperature of the products were measured and morphology was studied from the Scanning Electron Microscopy (SEM) micrographs.

1.3 Thesis Objectives and Layout

The main objectives of this study are the determination of the viscosity rise and the gel point of the reactive formulations in order to provide data that can feed the design of RIM processes, mainly using the new mixing head design novelties

introduced by Fonte (2012). Mixing efficiency of the rheometry method was assessed by comparing two methods: One Top Other – two reactants are placed one on the top of the other and The Holding Cell method – two reactants are placed next to each other with a separator between them assuring the delay of the mixing and polymerisation compared to the One Top Other method. Shear rate and angular frequency effect on the viscosity rise and the gel point, respectively are studied. This study shows the Newtonian nature of the reactive mixture of monomers used to form the solid polyurethane. Many authors (Castro and Macosko 1980, Richter and Macosko 1980, Sun, Toth et al. 1997, Dimier, Sbirrazzuoli et al. 2004, Haddadi, Nazockdast et al. 2008) had already stated that the reacting mixture of monomers is Newtonian and the shear rate effect on the chemorheological properties can be neglected. A method for the production of solid polymerised samples using the holding cell was developed, and mechanical properties of the samples are related with the experimental parameters, mainly the premixing shear rate. Viscosity rise was modelled and compared to experimental results.

A method for the functionalisation of an inorganic nanoparticle, hydroxyapatite was developed. The functionalised nanoparticles were blended with polyol and this mixture reacted with isocyanate in the rheometer using the Holding Cell (HC) method. The solid samples of produced nanocomposite were examined by SEM. Zinc oxide nanoparticles were also incorporated into the RenCast reactive formulation and the polyurethane matrix was produced by The Holding Cell method. The viscosity rise and the gel point of the nanocomposites processing were measured and the effect of nanoparticles on processing conditions was assessed.

Polyamide-6 formulation for RIM was characterised using the HC method and an optimal initiator/catalyst ratio was found by the determination of the complex viscosity rise of the reactive formulations.

The thesis is divided as follows:

- In Chapter 2, state of the art on reactive formulations for RIM and nanocomposites and bibliography revision are presented. This chapter is divided into sub-chapters including: RIM process - industrial significance and recent developments, mixing in RIM machines; reinforced RIM process; rheological behaviour of fluids, mechanical properties of polymeric materials; polyurethanes chemistry and applications to RIM; polyamide-6 chemistry and applications to RIM; polymer nanocomposites with special interest in hydroxyapatite and zinc oxide polymer nanocomposites;
- Chapter 3 describes theoretical basis of the experimental techniques that are used throughout all the experimental work in this thesis: rheometry, FTIR-ATR, SEM, spray-drying, and DSC-TG.
- In Chapter 4 development of the thermosetting polyurethane products is presented. This included development of the mixing technology using two methods One Top Other and the Holding Cell and production of the final product by the Holding Cell method using cone and plate rheometer. A model for the viscosity rise of the reactive mixture is developed and presented. Mechanical analysis of the polyurethane samples produced at rheometer was carried out.
- The optimal initiator/catalyst ratio of the polyamide-6 reactive formulation for RIM was determined by The Holding Cell method and presented in Chapter 5.
- Chapter 6 describes the method for the development and functionalisation of hydroxyapatite nanoparticles in organic solvent and their incorporation into the thermosetting polyurethane matrix. Nanocomposite reactive formulation of RenCast polyurethane and functionalized hydroxyapatite nanoparticles was developed and its viscosity rise and the gel point were determined by The Holding Cell method. Final product was characterised by the SEM in order to determine the morphology. Another polymer nanocomposite containing zinc oxide nanoparticles is synthesised and characterised at rheometer.

1.4 References

BASF (2012). Annual Report 2012. Germany, BASF Group.

Bayer (2012). Annual Report 2012. Germany, Bayer AG.

Castro, J. M. and C. W. Macosko (1980). "Kinetics and rheology of typical polyurethane reaction injection molding systems." Society of Plastics Engineers (Technical Papers): 434-438.

Dimier, F., N. Sbirrazzuoli, B. Vergnes and M. Vincent (2004). "Curing kinetics and chemorheological analysis of polyurethane formation." Polymer Engineering & Science **44**(3): 518-527.

Fonte, C. P. (2012). Mixing Studies with Impinging Jets (PIV/PLIF Experiments and CFD Simulation). Ph.D., Universidade do Porto, Porto, Portugal.

Gomes, N. (2014). Protótipo Industrial RIMCop: Projecto, Construção e Operação. Ph.D., Universidade do Porto, Porto, Portugal.

Haddadi, H., E. Nazockdast and B. Ghalei (2008). "Chemorheological characterisation of thermosetting polyurethane formulations containing different chain extender contents." Polymer Engineering and Science **48**(12): 2446-2453.

Huntsman (2012). Annual Report 2012, Huntsman International.

Richter, E. B. and C. W. Macosko (1980). "Viscosity changes during isothermal and adiabatic urethane network polymerisation." Polymer Engineering & Science **20**(14): 921-924.

Sun, X., J. Toth and L. James Lee (1997). "Chemorheology of poly(urethane/isocyanurate) formation." Polymer Engineering & Science **37**(1): 143-152.

Szycher, M. (1999). Szycher's Handbook of Polyurethanes, CRC Press.

2 State of the art

2.1 Reaction Injection Moulding of fast reactive formulations

Reaction Injection Moulding (RIM) is an industrial process for production of large plastic parts, generally made of polyurethanes, polyureas or polyamide-6. In a RIM process the reactants that are the base monomers for the final plastic, are introduced as high-speed jets into a mixing chamber, where they impinge and mix within 10 to 100 ms. The mixing chamber diameter is typically in the range of 3 to 15 mm, and the diameter of the injectors ranges from 1 to 3 mm. Typical jets velocities are in the range of 10 to 150 m / s, although Reynolds numbers are low between 100 and 500 due to the values of viscosity of the fluids that range from 20 to 2000 mPa.s.

The reactive mixture of monomers, catalysts and chain extenders is injected into a mould where the polymerisation takes place. The critical step of the process is mixing because the quality of the final product depends on the degree of mixing of the two reactants (Tucker and Suh 1980, Kolodziej, Macosko et al. 1982, Kolodziej, Yang et al. 1986). The choice of formulations of polymers suitable for reactive processing in RIM is limited by the impact of the polymer cure time in the production cycle length

of a RIM plastic part, therefore only polymerisations with fast kinetics are generally considered in industrial processes for medium size series (around 10000 moulded parts).

Figure 2.1 shows the major components of a RIM machine: storage tanks for the reactants (7) with low pressure recirculation pumps (4), high pressure lance pistons (6) and mixing chamber (1). Thermal stabilisation of the reactants is achieved through the recirculation of the reactants with the recirculation pumps. The lance pistons (6) are filled with the reactants before delivering the reactants to the mixing chamber (1). The process starts by injection of the reactants into the mixing chamber where the monomers are mixed and discharged into a mould until the mould is filled up. Afterwards, the polymer stays in the mould curing and the mixing chamber is cleaned by means of a cleanout piston (3). Curing in the mould is the limiting step of the process, and some RIM machines can have more than one mould to enhance the production times. After the piston descends over the mixing chamber and cleans it and blocks the monomer jets, the RIM machine is kept in recirculation mode until the next injection. In order to protect the reactants from air humidity contamination, dry air or nitrogen can be dispersed in one or both reactant tanks. The gas bubbles that get stuck in the monomer collapse in the high pressure metering cylinders, but can reappear in the mixing head during decompression.

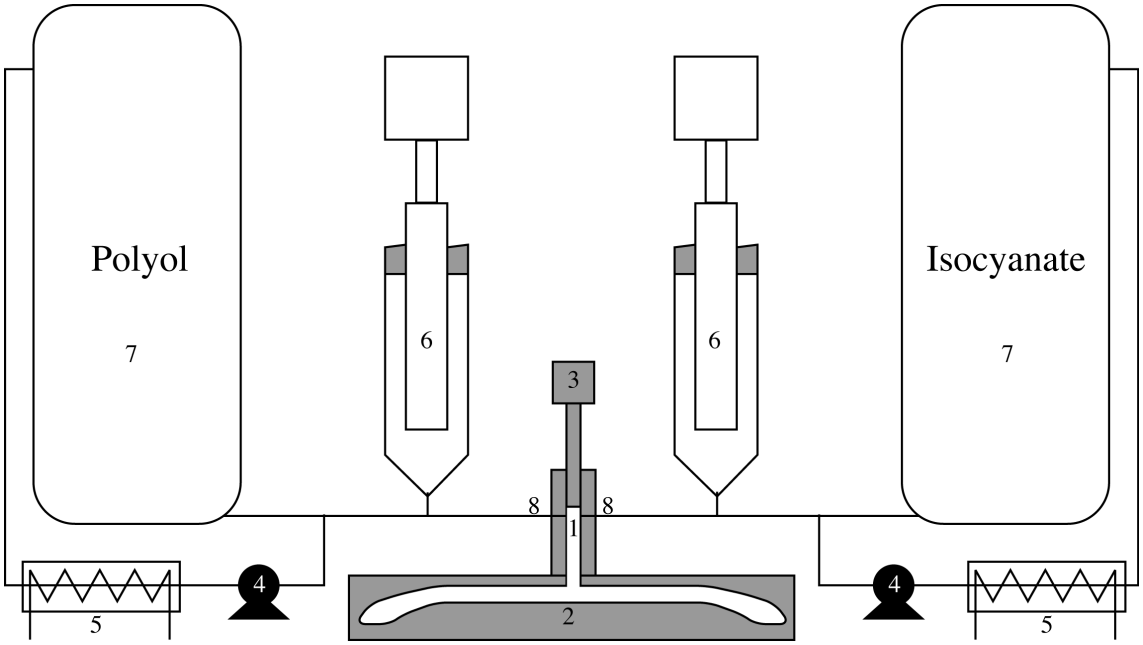

1 – Mixing chamber 2 – Mould

3 – Cleanout piston 4 – Recirculation pumps

5 – Heat exchangers 6 – Lance pistons

7 – Storage tanks 8 – Injectors

Figure 2.1. Scheme of a RIM machine.

The reactions in RIM are typically step growth polymerisations without by-product that yield in formation of polyurethanes and polyureas, ring-opening anionic polymerisation of caprolactam monomer to form polyamide-6, and ring-opening metathesis polymerisation of dicyclopentadiene (DCP) to form polydicyclopentadiene (PDCP). In step growth polymerisation without by-product both reactants contain at least two functional groups, which can bond covalently and generate new linkages in form of linear, branched and highly crosslinked macromolecules. Step growth polymerisation without by-products shows some advantages compared to other types of polymerisations, namely: all monomers disappear early in the reaction, initiator is not necessary, no secondary products are formed, and no solvent is needed. Listed advantages lead to a decrease of the costs, because further operations such as separation of the secondary products and/or extractions of the solvent or non-reacted monomers are not necessary. Furthermore, total time of the production of polymerised product is shortened.

In production of polyurethane products, the monomers are mixed, reacted, and cured into the final shape in a single process, whereas to obtain products of radical polymerisations such as poly (methyl methacrylate), polystyrene etc., synthesis and processing are separated into two different technologies.

Main advantages and disadvantages of the RIM process are listed below (Torcato 2013). The main advantages are:

- Production of large plastic parts with low weight;
- Low costs of moulds;
- Energy consumption is reduced because of the low viscosity reactants;
- Possibility of in-mould painting;
- Variation of the thickness of the product walls from 5 to 25 mm.

The main problems associated with the polymer processing in RIM technology are:

- High variable costs;
- Air entrapment inside the product;
- Necessity for mould release agent;
- Lack of know-how in the RIM machine design;
- Visible parts may require painting;
- In-mold painting is not reliable.

2.1.1 Reinforced RIM and Structural RIM

In order to improve mechanical properties, thermal and dimensional stability and resistance to flame, fillers or particles may be added into reactive formulations. Fillers that are typically used to mix with polyurethanes are milled, chopped glass or glass flakes (Macosko 1989). In Reinforced RIM (RRIM) the process filler is premixed with one of the reactants before transporting the reactant into the storage tank of the RIM machine. The moulding process itself remains exactly the same as in traditional RIM. The problem that may appear is lack of the orientation of the filler in the final product, since there is no control of it. This is only possible if the filler is micro or a

nanosize particle. Maximum content of the reinforcing materials in RRIM is up to 25 wt.%.

If the filler is larger such as fibres, more appropriate method is placing the filler inside the mould cavity and inject the reactive mixture from the RIM mixing chamber into the mould with the fillers. This method is used in processes called structural RIM (SRIM). In SRIM process reinforcing materials are preplaced in an empty mould cavity and reactive mixture has to fill the mould and wet all the fibbers quickly before the polymerisation takes place. Maximum glass fibre loadings are up to 60 wt.%, because there is no problem with the filler orientation. Mechanical properties, such as flexural modulus and tensile strength of the SRIM products are higher than in RRIM, due to higher content of the reinforcing materials.

In the last two decades the development on analytical methods and physical-chemical characterisation methods for the detection and on the production of nanosized materials increased the availability of these materials, and also their use in reinforcement of the polymers has also started to become exploited.

Kim and Macosko (2000) studied the efficiency of the SRIM process that was assessed by measuring adiabatic temperature rise, viscosity rise, pressure rise during the mould filling, temperature profile inside a mould (experiment and simulation), and dimensional stability of the final products. The material tested was a thermosetting polyurethane formulation consisting of MDI, poly(propyleneoxide) tryol and DBTDL with continuous glass fibre mats having a diameter of 15 μm and a fiber bundle diameter ranging from 80 to 200 μm. Viscosity of the reactive system was measured by Rheometrics System IV and RMS-800 with parallel plates geometry having 25 mm diameter. The authors reported that viscosity of the reactive mixture is independent on the shear rate and that the linear shrinkage of the reinforced moulded part was considerably lower than of the moulded part containing no fibre mats.

2.1.2 Mixing effect on the product quality

Product properties are highly affected by the mixing of two monomer jets in the RIM process. It was found that mixing phenomenon depends on the hydrodynamic regime of the reactor which is associated to the Reynolds number of the jets (Kolodziej, Macosko et al. 1982, Santos R. J., Teixeira A.M. et al. 2002). The Reynolds number of the injectors of the RIM mixing chamber was originally defined by Malguarnera and Suh (1977)

$$\mathrm{Re} = \frac{\rho v_{inj} d}{\mu} \tag{2.1}$$

where v_{inj} is the superficial velocity of the jets at the injectors, d is the injectors' diameter, ρ is the fluid density, and μ is the fluid viscosity. The Reynolds number is the ratio of the inertial to viscous forces of the fluid.

One of the first research works on the impingement mixing in RIM was done by Malguarnera and Suh (1977) who used glycerol as a model fluid and acetic acid solution as a tracer in one of the streams. The concentration of acetic acid in the outlet mixture was used as a measure of mixing quality. This work contained the first dimensional analysis of impingement mixing. This study paid a special attention to the Reynolds number and concluded that in order to obtain effective mixing, the Reynolds number must be greater than 50, and in the range from 500 to 4000 there is no change of the mixing quality. Another critical parameter for mixing in RIM process was the momentum ratio between the jets, which must be equal to unity. When momentum ratio was not equal to one, only the fluid from the higher momentum jet was sampled at the outlet indicating complete absence of mixing. Influence of some geometrical parameters on mixing was also studied and it was concluded that the distance between nozzles was not important for the mixing quality; however the smaller diameter of the chamber means that less air will be entrapped in the mixture, yielding a momentum ratio closer to unity.

Tucker and Suh (1980) used a clear and coloured stream for impingement mixing experiments and measured the mixing quality by a light transmittance technique. This study also showed that the transition from laminar to turbulent motion occurs at the Reynolds number of 140 for a mixing chamber with directly opposed jets. The authors found that the size of the "smallest eddies" of the turbulent flow is responsible for the scale of segregation of the final mixture.

Lee, Ottino et al. (1980) measured the adiabatic temperature rise for various Reynolds numbers and mixing head geometries. The experiments led to conclusion that the maximum adiabatic temperature rise increases with the Reynolds number, until the critical value of the Reynolds number of 200 beyond which there is no improvement in the adiabatic temperature rise. The most significant changes occurred in the Reynolds number range from 100 to 160. Higher mixing efficiency was obtained using the chamber with the jets not directly opposed.

Sebastian and Boukobbal (1986) studied the effect of momentum ratio between the two streams of monomers. The momentum ratio was changed by using different nozzle diameters. The maximum adiabatic temperature rise was observed for the momentum ratio equal to one. The existence of critical ratio between nozzle and chamber diameter was proven, and below this critical value of ratio there was no mixing observed.

Kolodziej, Macosko et al. (1982) studied the effects of the impingement mixing on adiabatic temperature rise, molecular weight of final polymer and the striation thickness distribution. Carbon black was used as a tracer in one of the streams. Thinner strias are clear indication of more intensive mixing, so the mixing efficiency can be evaluated by the observation of the final polymer. The segmented thermoplastic polyurethane system that was studied comprised polyol, MDI isocyanate and a low molecular weight chain extender. The authors concluded that with the Reynolds number up to 200, strias were getting thinner, and beyond 200 there was no improvement on striation thickness, and therefore on mixing.

Kolodziej, Yang et al. (1986) continued the previous work of (Kolodziej, Macosko et al. 1982), but focus was on the microstructure of polyurethanes. It was found that a higher mixing level yields higher molecular weight of polymer.

Mixing in RIM was studied at Laboratory of Separation and Reaction Engineering (LSRE) using Computational Fluid Dynamics (CFD) simulations (Santos R.J., Teixeira A.M. et al. 2002, Santos, Teixeira et al. 2005, Erkoc, Santos et al. 2007, Santos, Erkoç et al. 2009, Santos, Teixeira et al. 2010, Fonte, Santos et al. 2011), experimental laser techniques (Teixeira, Santos et al. 2005, Santos, Erkoç et al. 2008, Santos, Erkoç et al. 2009) and test reactions – micromixing in chemical reactors (Nunes 2007). These studies showed that in RIM mixing chambers two flow regimes occur, and only the flow regime that is associated with the formation of vortices that engulf both liquid monomer jets promotes an intense mixing of both monomers. This flow regime was described as a self-sustainable chaotic flow and it has been shown that this flow regime only occurs under very well defined and controlled operational conditions. Transition from steady to self-sustainable chaotic flow regime occurs at critical Reynolds number of 120 (Fonte, Santos et al. 2011). The findings of the LSRE's group on RIM were incorporated into a novel RIM process, the RIMcop®.

2.1.3 RIMcop® technology

RIMcop® innovative technology involves changes in the RIM machine and therefore the RIM process itself. The main novelty of RIMcop® is the control of mixing, which is ensured by two means: dynamic measurements of static pressure upstream of the injectors using pressure transducers, and/or imposing a chaotic flow regime through the pulsation of the opposed jets (Lopes, Santos et al. 2005).

The pilot RIMcop® has been compared to the traditional RIM process using non-reactive and reactive fluids and it was proven to enable increase of the quality and the degree of mixing of the monomers (Erkoc, Santos et al. 2007). A pilot RIMcop® machine was built in the LSRE and the implementation of some of the patented concepts in (Lopes, Santos et al. 2005) is described and shown in Figure 2.2:

- The mixing chamber is a cylinder where one of its ends is closed by a piston, used for cleaning the chamber and stopping the process; when the piston is lowered the machine is in recirculation and when the piston is up the machine is in mixing mode. The other end of the mixing chamber is opened and discharges into a mould;
- The injectors are located at a distance from the closed end of the chamber approximately equal to half the diameter of the chamber. Injectors are circular directly opposite and are positioned at right angle to the mixing chamber axis. The injectors have a conical section, which ensures acceleration of the fluids when entering the chamber. The design of the RIMcop® machine enables replacement of these injectors;
- A third needlelike injector was proposed and implemented in the prototype RIMcop® machine. The third injector is located within the impact region of the two opposed jets. So far this novelty was not validated experimentally.

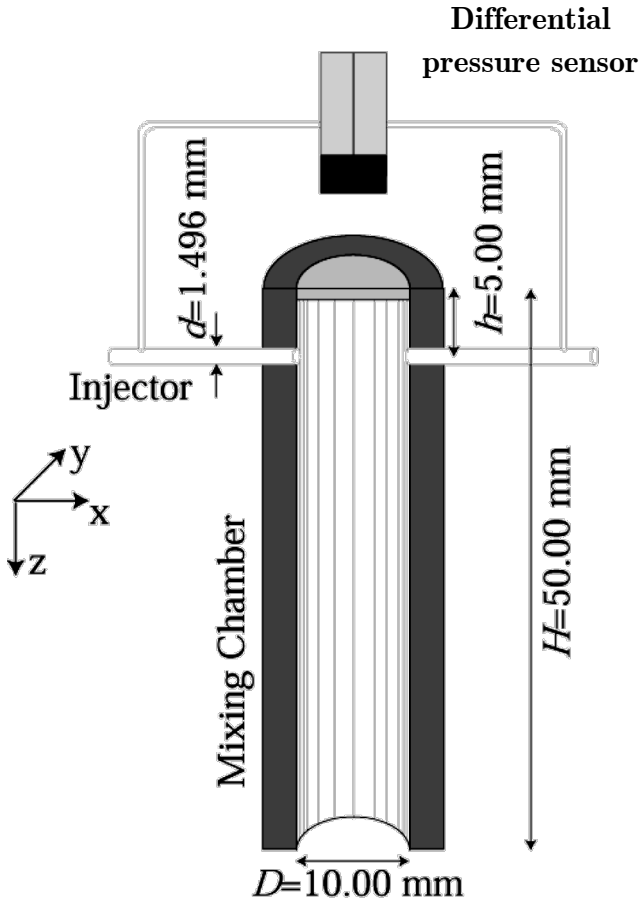

Figure 2.2. Scheme of the differential pressure sensor mounted on the mixing head.

The third injector is foreseen to be used for reactions where flow rate ratio is as low as 1:1000, which is the case of anionic polymerisations, where monomer is mixed with initiator. Reactant with higher feed flow rate would be injected in equal amounts through each of the two opposed injectors, and reactant with lower feed flow rate would be injected through the third injector.

In Figure 2.3 is represented the cylindrical mixing chamber with diameter 10 mm and 50 mm height, with two opposed injectors having each a diameter of 1.496 mm and positioned at 5 mm from the closed chamber top. The differential pressure sensor is connected to the injectors feed lines and it dynamically measures the static pressure inside the injectors. This pressure transducer is connected to the computer and it automatically controls the pressure in one or both of the injectors if needed.

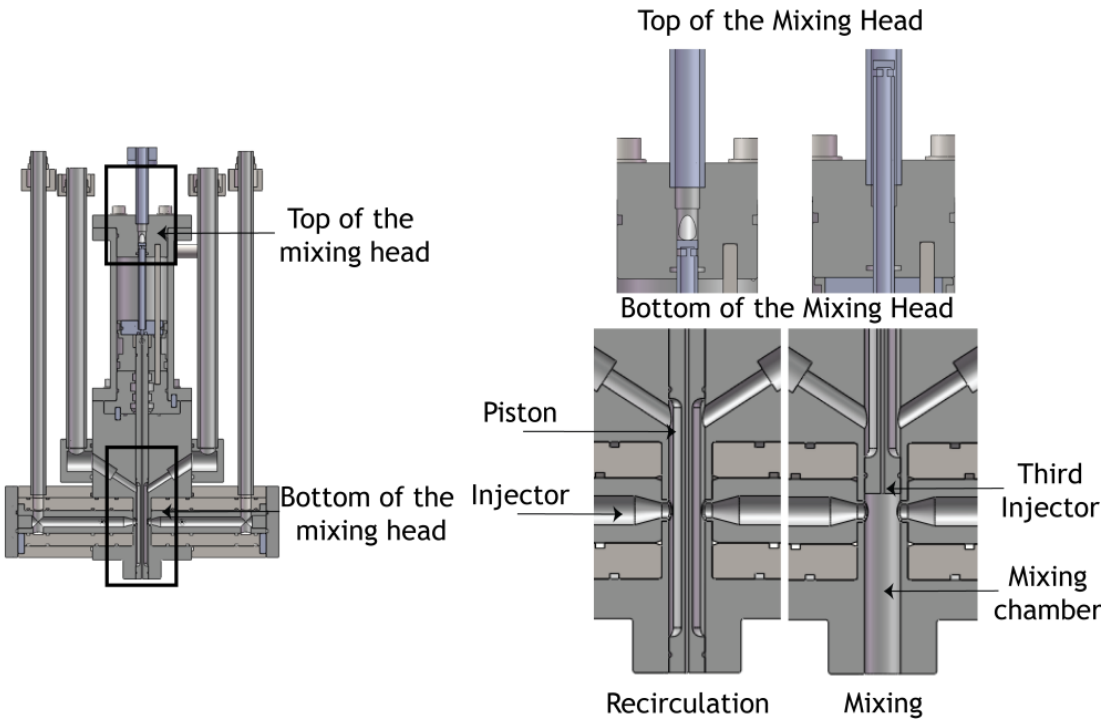

Figure 2.3. Scheme of the RIMcop® mixing head prototype.

2.2 Rheological behaviour of fluids

When a fluid is being deformed by shearing as it occurs in a cone and plate rheometer, simple shear flow is generated where hypothetical adjacent layers of the

fluid slide over each other with different speeds. Existing gradient of the velocity in the normal direction to the flow is called shear rate

$$\dot{\gamma} = \frac{dv_X}{dy} \tag{2.2}$$

Where v is the velocity, x is the direction of the flow and y is the normal direction to the flow. Flow of the fluid generates a tangential stress to the flow direction, called shear stress

$$\sigma_{YX} = \frac{F}{A} \tag{2.3}$$

That is determined by the force F per unit area A .

Many liquid materials (water, air) show Newtonian behavior, which means that shear stress is proportional to the shear rate at any point of the fluid, described by the

$$\sigma_{YX} = \mu \frac{dv_X}{dy} \tag{2.4}$$

Where μ is called viscosity, and it represents the property of the fluid to resist the deformation (Barnes, Hutton et al. 1989). Polyurethane reactive mixtures are known to have Newtonian behaviour (Castro and Macosko 1980, Dimier, Sbirrazzuoli et al. 2004). On the other hand, non-Newtonian fluids (polymer melts, polymer solutions, non-drip paints, blood) are characterised by the shear stress that is not directly proportion to the shear rate. Viscosity of the non-Newtonian fluids depends on the shear rate as shown

$$\sigma_{YX} = \eta(\dot{\gamma}) \frac{dv_X}{dy} \tag{2.5}$$

Where $\eta(\dot{\gamma})$ is the dynamic viscosity.

Viscosity of all fluids decreases exponentially with temperature by the Andrade-Eyring equation (Macosko 1994).

$$\eta = K \exp\left[\frac{E_\eta}{RT}\right] \tag{2.6}$$

Where K is a kinetic constant E_h is activation energy of the viscous flow, R is universal gas constant and T is the absolute temperature. For reacting mixtures of polymerisations the increase in temperature has two opposite effects: it decreases the viscosity of the mixture but also increases the rate of the reaction which promotesa viscosity rise (Haddadi, Nazockdast et al. 2008).

In addition to viscosity, some fluids namely polymeric fluids have elastic behaviour. Elasticity is measured through oscillatory tests, i.e. rather than making the fluid flow with a continuous shear, the fluid is subjected to small deformations. When a viscoelastic sample is being submitted to the oscillatory test, first it is needed to assure that the test parameters are in linear viscoelastic region. This is relevant, because in linear viscoelasticity the material response (strain) is directly proportional at any time to the initiating signal (stress) (Barnes, Hutton et al. 1989). In order to perform rheometry experiments in linear viscoelastic region, it is needed to assure a small-amplitude of the oscillatory shear. This is made by chosing low values of shear stress amplitude and angular frequency.

In oscillatory rheometry the shear strain is represented by (Barnes, Hutton et al. 1989):

$$\gamma = \gamma_0 \cos \omega t \tag{2.7}$$

Where γ is strain, γ_0 is a strain amplitude small enough to assure linearity, ω is the angular frequency and t is the time. Oscillatory rheometry tests are generally performed in strain control mode where the setting parameters are strain amplitude

and angular frequency. The strain rate is obtained by deriving the previous equation by time and substituting $\frac{d\gamma}{dt} = \dot{\gamma}$

$$\dot{\gamma} = -\gamma_0 \omega \sin \omega t \tag{2.8}$$

The fluid behaviour in the oscillatory shear may be represented by the Maxwell model of the viscoelastic fluid which is represented by the differential equation of the first order (Barnes, Hutton et al. 1989):

$$\sigma + \frac{\eta}{G}\dot{\sigma} = \eta\dot{\gamma} \tag{2.9}$$

Where σ is the shear stress, η is the viscosity, G is the elastic modulus, $\dot{\sigma}$ is the shear stress rate. When combining Eq. 2.8 and Eq. 2.9 the solution of the differential equation is obtained:

$$\sigma = \frac{\eta\omega\gamma_0}{\left(1+\omega^2\tau^2\right)}\left(\omega\tau\cos\omega t - \sin\omega t\right) \tag{2.10}$$

Where τ is relaxation time. In order to obtain the part of the stress that is in phase with the strain $\sigma_0^{'}$, $\sin\omega t$ should equal to zero, and

$$\sigma_0^{'} = G'\gamma \tag{2.11}$$

Where G' is called the storage modulus and it is equalto

$$G' = \frac{\eta\tau\omega^2}{1+\omega^2\tau^2} \tag{2.12}$$

In order to obtain the part of the stress that is out phase with the strain $\sigma_0^{''}$, $\cos\omega t$ should be equal to zero, and

$$\sigma_0^{''} = \frac{G''}{\omega}\dot{\gamma} \tag{2.13}$$

Where $G"$ is called the loss modulus, and it is equal to

$$G" = \frac{\eta\omega}{1+\omega^2\tau^2} \tag{2.14}$$

Complex viscosity η^* is defined as a ratio of the shear stress to the shear rate.

$$\eta^* = \frac{\sigma(t)}{\dot{\gamma}(t)} \tag{2.15}$$

An additional but useful parameter that is derivative from the storage and loss modulus is the loss factor (damping factor) $\tan\delta$ is calculated from

$$\tan\delta = \frac{G"}{G'} \tag{2.16}$$

In rheological experiments most useful material parameters that are calculated are storage and loss moduli, complex viscosity and loss factor. In order to obtain the gel point of the polymerizing polyurethane, evolution of the storage and loss moduli is monitored and the point where they crossover is the gel point. Consequently, a gel point is when loss factor equals one.

2.3 Mechanical properties of polymers and nanocomposites

In the compression test the specimen is being compressed at constant speed, until it fractures. Parameters measured in this test are the force sustained by the sample, F (N), and the decrease in the specimen length between the gauge marks, ΔL_0 (mm). Specimen should be cut by machining and have dimensions as stated in International Standard ISO 604, where L_0 is length, b is width and h is height. The initial cross-sectional area A (mm) of sample is calculated from

$$A = bh \tag{2.17}$$

The compressive load or stress, σ (MPa), is calculated from

$$\sigma = \frac{F}{A} \tag{2.18}$$

The strain is calculated from

$$\varepsilon = \frac{\Delta L_0}{L_0} \times 100 \tag{2.19}$$

Stress, σ and strain, ε are used to plot typical engineering stress-strain graph (see Figure 2.4).

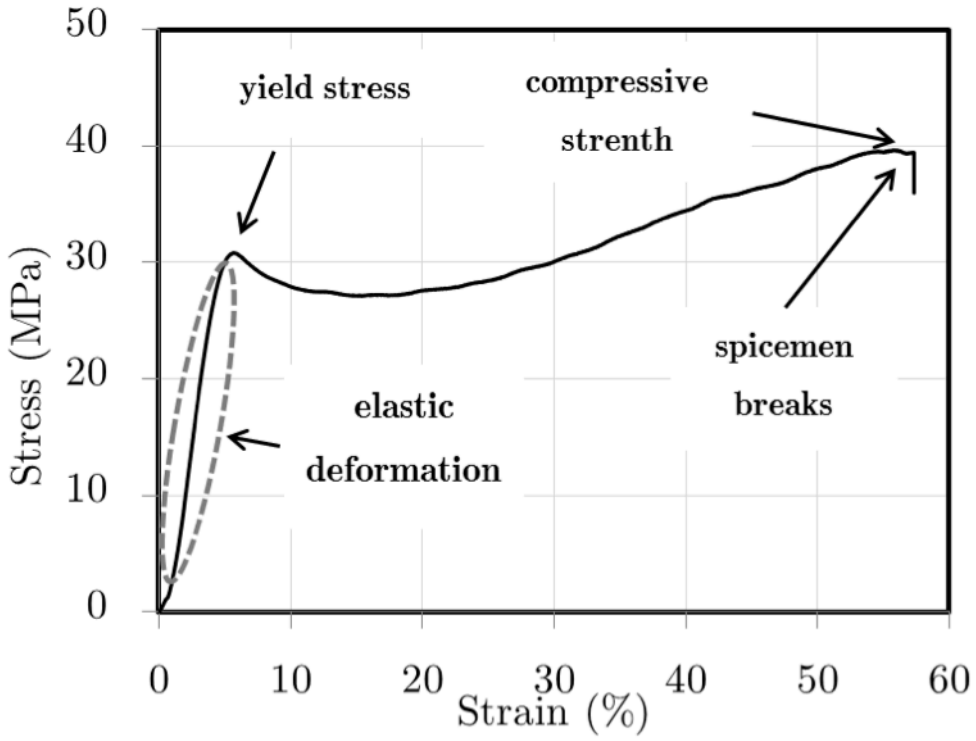

Figure 2.4. Typical stress vs. strain curve.

From the Figure 2.4 is observed the region with linear slope at low strains, which corresponds to the elastic deformation of the specimen and it is described by the Hooke's law. The compressive stress at yield is defined as the first stress at which an increase in strain occurs without an increase in stress. The compressive strength is defined as the maximum compressive stress sustained by the sample during a

compressive test. The last point in the graph before the stress curve starts do decrease corresponds to the break of the specimen.

The deflection temperature under load (DTUL) is defined as a temperature at which sample deflects when it is submitted to heating under constant load at flexure test (Menard 2008). In this test a sinusoidal stress, σ is applied, and the resultant sinusoidal strain, ε is measured, and δ is the phase lag between the strain and stress. From these values complex modulus, E^* is calculated from

$$E^* = \frac{\sigma}{\varepsilon} \tag{2.20}$$

Storage modulus E' , and loss modulus E'' are calculated from

$$E' = E^* \cos\delta \tag{2.21}$$

and

$$E'' = E^* \sin\delta \tag{2.22}$$

And loss factor, $\tan\delta$ is calculated from

$$\tan\delta = \frac{E''}{E'} \tag{2.23}$$

In this thesis test conditions for measurement of DTUL and complex modulus by DMA are: single cantilever bending, with constant oscillatory frequency of $1\,\mathrm{Hz}$, single strain of 0.05% and temperature sweep with ramp $20-200\,^{\circ}\mathrm{C}$.

2.4 Polyurethanes and polyureas

2.4.1 Chemistry

Polyurethanes are synthetic polymers containing urethane linkages. They are synthesised from the very reactive isocyanate compound and a hydroxyl group compound. Some amount of amine groups, whether they come from catalyst or

formulated polyol (with additives) are usually present in polyurethane formulations. If there is amine present in the formulation, isocyanate reacts with it to form urea bonds. Therefore, formation of polyurethanes and polyureas is very closely related, and their functional groups are represented in Figure 2.5.

Urethane linkage Urea linkage

Figure 2.5. Urethane and urea linkage

An isocyanate is an organic compound containing (-NCO) functional group. The number of functional groups can be two, three or more and the compound is called diisocyanate, triisocyanate or polyisocyanates, respectively. The isocyanate group has three resonance structures as shown in Equation (2.24):

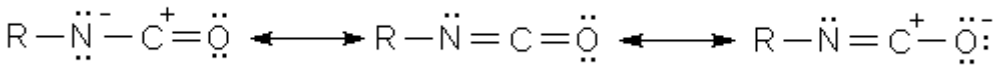

(2.24)

Where R is the organic substituent. The reactivity of the isocyanate depends on the structure of the substituent, which can be aliphatic, alicyclic or aromatic. If the isocyanate has an aromatic ring in its structure, then the electrons from the ring withdraw negative charge from the isocyanate group leaving carbon with increased partial positive charge. This makes the transfer of the electron from the donor to the carbon easier, and causes faster reaction (Szycher 1999). Therefore, aromatic isocyanates generally have higher reactivity than aliphatic.

Figure 2.6 shows two of the most commonly used isocyanates in the production of polyurethanes, 4,4'-diphenylmethane diisocyanate (MDI) and 2,4-toluene diisocyanate (TDI). They are commonly used due to their high reactivity and low price.

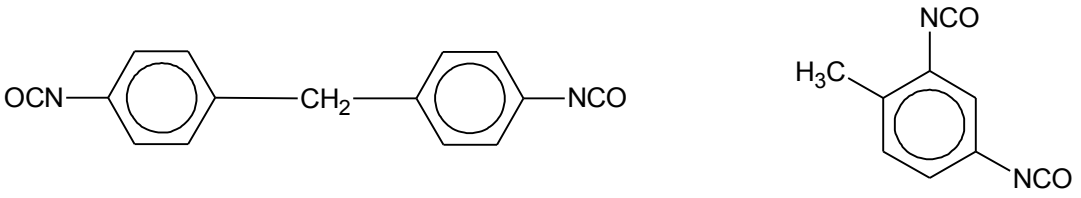

4,4'-diphenylmethane diisocyanate (MDI) 2,4-toluene diisocyanate (TDI)

Figure 2.6. Chemical structurediisocyanates MDI and TDI.

Due to the high reactivity of isocyanates, they are able to undergo reaction of self-condensation at room or higher temperatures forming different products. One of these reactions is trimerization reaction, it is favoured by selective catalysts at $120\,^{\circ}\mathrm{C}$ to $140\,^{\circ}\mathrm{C}$ and the product obtained is called isocyanurate. Isocyanurate can also be formed at room temperature in the presence of the epoxy moiety and a tertiary amine catalyst. The advantage of the isocyanurate presence in the polyurethane formulation is that this moiety is stable at high temperatures and it can improve the thermal stability of the final product.

In order to form polyurethane, isocyanates react with compounds that contain at least one exchangeable hydrogen atom. Such compounds are generally alcohols or amines, or a compound containing both hydroxyl and amino groups. In the presence of the amine groups, urea is always formed and reaction of formation of urea is faster than of the formation of polyurethane (Macosko 1989). Hydrogen atom from the hydroxyl group in alcohol can react with isocyanate group. In order to form polyurethane, alcohol must contain at least two hydroxyl groups. Polyols used in polyurethane synthesis are compounds with molecular weight in the range of $0.4\times10^{3}\ \mathrm{g/mole}$ to $10\times10^{3}\ \mathrm{g/mole}$. There is a wide variety of polyols, but the two major groups are polyols with hydroxyl functional groups (typically polyether, polyester-based polyols and polycarbonates) and compounds where one of the hydroxyl frunctional groups was replaced with an amine (typically amine-terminated polyethers). Each type of polyol will give very distinct properties to the final polyurethane. Polyether polyols are synthesised in reaction between an initiator (ethylene glycol, propylene glycol, glycerol etc.) and cyclic ether (ethylene oxide,

propylene oxide, tetrahydrofuran etc.). Adipic, glutaric and azeolic polyester polyols and caprolactone polyesters are widely used. In Figure 2.7 are represented a polyether-based and a polyester-based polyol.

The catalysts for polyurethanes production are generally amines, which are organic compounds with amino group and mixtures of tertiary amine and tin catalysts. One of the most commonly used tin catalysts is dibutyltindilaurate (DBTDL). As already mentioned above, isocyanates react with compounds that contain active hydrogen. Hydrogen atom of the active hydrogen compound reacts with nitrogen atom of the isocyanate compound by breaking the double bond between the nitrogen and carbon in the isocyanate compound.

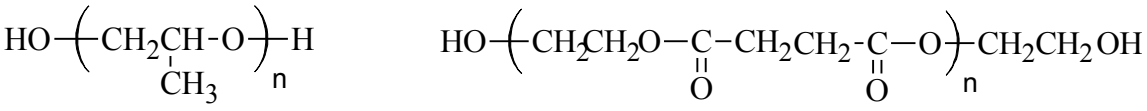

Poly(oxytetramethylene glycol) Poly(ethylene adipate)

Figure 2.7.Examples of the most common polyols: poly(oxytetramethylene glycol) – polyethertype and poly(ethylene adipate) - polyester type.

Typically commercial RIM polyurethane formulations consist of two preformulated reactants, polyol and isocyanate. Polyols are typically ether or ester based with viscosity at $25\,^{\circ}C$ up to $3\,Pa.s$ - $4\,Pa.s$. Other additives, such as catalysts are usually added into the preformulated polyol. Isocyanates viscosity compared to polyols is typically relatively low, having values around $0.3\,Pa.s$ - $0.4\,Pa.s$. Isocyanates used in RIM are typically aromatic, MDI and TDI. Polyol and isocyanate mix in the mixing head of the RIM machine and form the reactive mixture that gets discharged into a mould where the polymerisation reaction takes place.

Reaction between isocyanate group and hydroxyl group from alcohol where urethane is formed in the simplified form is shown in Equation (2.25).

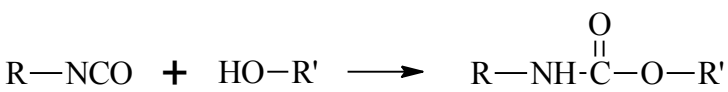

(2.25)

Isocyanate and amine react to form urea, which is shown in Equation (2.26).

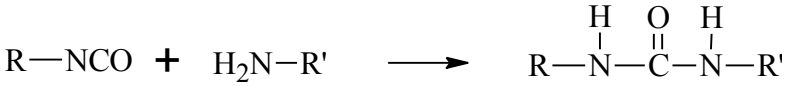

(2.26)

The mechanism of the addition of hydroxyl group onto isocyanate group in the presence of catalyst (A) is shown in Equation (2.27). In the first step of the mechanism, anion of the catalyst (A:) bonds with carbon from the isocyanate group to form an intermediary compound with polarized carbon-nitrogen bond. In the next step, alcohol attacks this carbon-nitrogen bond to form second intermediary compound, which will then split into catalyst (A:) and the product polyurethane, a mechanism that is represented as:

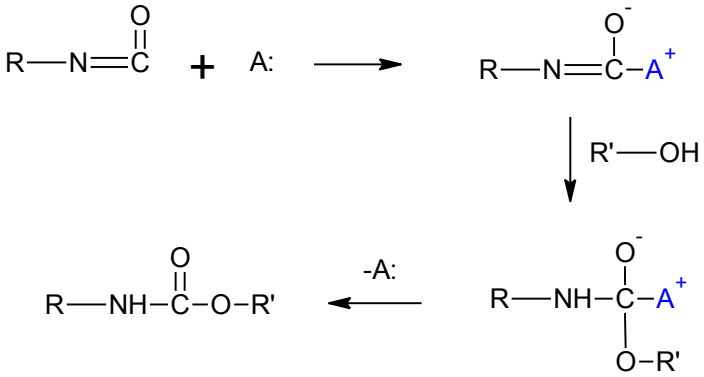

(2.27)

In addition to the urethane reaction, other reactions may occur during the curing stage of the RIM process. Typical reactions that occur are the reaction of isocyanates with urethanes to form allophanates, and isocyanates with urea to form biurets. These reactions are favoured by the higher temperatures up to 150 °C, and they result in branching and cross-linking (Macosko 1989). The formation of the allophanate bonds in the reaction with the excess of isocyanate groups occurs as follows:

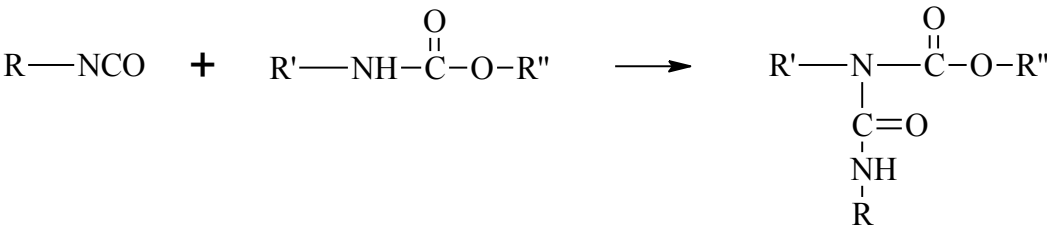

(2.28)

Isocyanates react with urea to form biurets according to the following mechanism;

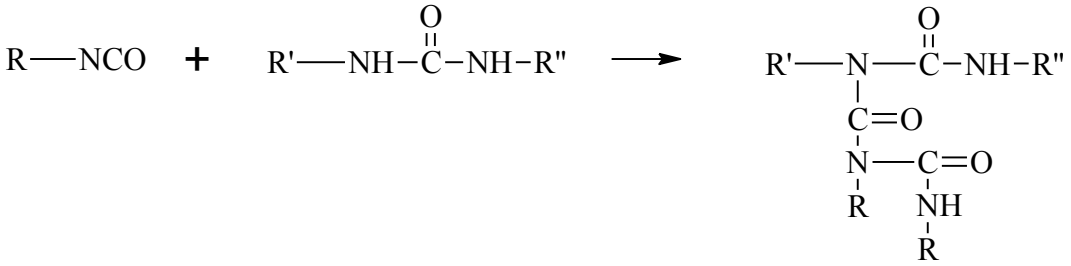

(2.29)

This reaction may take place in the mould of the RIM machine, with excess of isocyanates and at temperatures as high as 150 °C.

Isocyanates react with water to form carbamic acid which breaks down into an amine and carbon dioxide as follows:

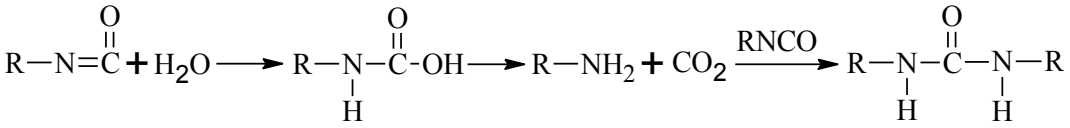

(2.30)

Urea is formed as a by-product of this reaction between the generated amine and other isocyanate molecules present in the mixture. If the desired polyurethane product is not foam, water should be eliminated from the formulation by drying of the reactants. Typically RIM products have less than 0.07% of water (Macosko 1989).

Polymerisation reaction mainly takes place in the mould of the RIM machines, because residence time in the mixing chamber is too short when compared with reaction time scale. Besides formation of the polyurethane, other structures may be formed as previously represented such as polyureas, allophanates and biurets. Reactive mixture that is formed in the mixing chamber polymerises and solidifies in the mould in a process that can be assessed by the rapid increase in viscosity up to few thousands of Pa.s.

2.4.2 Thermal stability, degradation, decomposition and flammability of polyurethanes

In general, polyurethanes have low thermal stability at high temperatures, and thermal degradation can begin at 180 °C (Chattopadhyay and Webster 2009). Thermal stability of polyurethanes may be increased by incorporation of nanosized fillers such as silicate nanolayers, carbon nanotubes or even some other cyclic compounds such as fullerene.

When submitted to heating, the covalent bonds in PU chains are submitted to complex vibration and rotation within their local space. If the heating continues, these bonds can break to form different small molecules and chain fragments that can undergo mutual recombination. Ultimately, they can vaporize, diffuse or carbonise.

Thermal decomposition of PU involves release of the volatile compounds and scission and depolymerisation resulting in loss of weight and mechanical degradation. The decomposition process ends with the loss of all volatile compounds and formation of char, which is a polynuclear aromatic carbon that can contain compounds with heteroatoms such as oxygen, nitrogen, phosphor and sulphur and can consist of amorphous and crystalline regions.

There are different ways of improvement of the thermal stabilization of the polyurethanes such as: formation of poly(urethane-isocyanurate), poly(urethane-oxazolidone) and poly(urethane-imide), increase in aromatic ring content, use of hyperbranched polyols as crosslinkers, hybrid formation using fillers nano-silica, titanium oxide, silica grafting, incorporation of carbon nanotubes.

Chattopadhyay and Webster (2009) reported that the thermal stability derives from the hard segments formed during polyurethane formation according to the following order: isocyanurate>urea>urethane>biuret>allophanate. Thermal stability of the crosslinked polymers depends highly on the crosslinking concentration.

2.4.3 Polyurethane product types

Thermoset polyurethanes are formed when polyols and isocyanates have functionalities higher than 2, NCO:OH ratios are higher than 1, and if the crosslinkers are introduced into the formulation. Their structure is highly crosslinked with covalent bonds, giving them superior mechanical properties and high resistance to many chemicals. Their glass transition temperature is higher than their decomposition temperature. When heating is applied thermosets cannot be molten and modified in that state.

Thermoplastic polyurethane (TPU) is a group of polyurethanes that contains two types of sequences: hard (HS) and soft segments (SS), where soft domains are responsible for high elasticity of the product and hard domains are interconnected into the network by the hydrogen bonds that is responsible for good mechanical properties. HS consists of diisocyanate and short chain extender and SS of linear long-chain diols and polyols. At room temperature HSs have high melting temperature and SSs low glass temperature. In segmented PU, urea groups typically exist in the interior of the HSs, and urethane groups on the boundaries of the HSs and SSs. Hydrogen bonds in polyurethanes may be formed between proton donator groups which are urethane ($\mathrm{N-H}$) or urea ($\mathrm{N-H}$) and proton acceptor which can be oxygen from hydroxyl group ($\mathrm{O\text{-}\ H}$), ether ($\mathrm{C\text{-}\ O\text{-}\ C}$), urethane ($\mathrm{C=O}$) or urea ($\mathrm{C=O}$).

Higher content of HS improves the elastic modulus and tensile stress at break, and SS increase strain at failure. One of the ways of improving the mechanical properties of TPUs is incorporation of nanoparticles such as nanometric clay into HS in the way that the structure of SS and therefore the elastic properties remain intact.

Rigid polyurethane foams are highly used as insulating materials due to its porous structure. In order to form a porous structure a blowing agent is required, and in some cases if water is present in the reacting formulation, there is no need for the blowing agent, since carbon dioxide is released from the reaction of isocyanate and

water. Insulating properties of foam materials may reduce over time because blowing agents may diffuse out of the closed cells and get replaced by the air diffusing in. This can be avoided by developing foam with smaller cell size or by reducing gas diffusion by adding filler that act as a diffusion barrier.

2.4.4 Viscosity rise of the reactive mixture

In synthesis of polymers monomers of water-like viscosity mix and form a reactive mixture with a viscosity that is approximately the viscosity of the monomers, which is followed by a dramatic increase in viscosity of the mixture until the solid product is formed after curing. From the liquid stage to the solid stage, reactive mixture passes through the gelation point, which is defined as the point where the entire reactive sample corresponds to one infinite macromolecule. In polymer processing this point is taken as the limit that marks the end of the mixture possibility to change the shape of the reactive mixture (below the gelation point) or not (after the gelation point). Gel point is a rheological characteristic of a material and its component in time, called gel time, is a specific value at defined temperature for each polymer. In rheometry, gel time is measured in oscillation experiments at a specific temperature and depending on the reaction rate it can be detected with high precision.

Literature revision on processing parameters and properties of polyurethane reactive mixtures during curing is listed below.

- Valles and Macosko (1979) assumed that the viscosity of the branched system is higher than of the linear system for the same molecular weight. In their study a defined ideal non-linear system of long difunctional and short trifunctional and tetrafunctional monomers of poly(dimethylsiloxanes) with known functionalities is chosen. Monomers were mixed for 30 s by a motorized stirrer, degassed and kinetics and viscosity were simultaneously measured over time. Extent of the reaction was measured by infrared spectrometry and viscosity and normal forces by a Rheometrics mechanical spectrometer. Molecular weight was measured by the low-angle light scattering

photometer. The authors developed the theoretical equation for the calculation of the molecular weight of the nonlinear stepwise polymers. This calculated value was used for the comparison to the measured value of the molecular weight. In order to calculate the molecular weight, extent of the reaction measured by infrared was used. For this specific polymeric formulation, normal forces were possible to detect only very close to the gel point, after which a sudden increase in the normal force occurred. Rotation speed was initially of $1\,\mathrm{rad}/\mathrm{s}$ and when the viscosity increased, rotation speed decreased for 1000 fold in order not to destroy the sample. Furthermore, the authors were able to determine the critical molecular weight for the onset of entanglement process and to correlate it with the corresponding viscosity, which for the trifunctional system is $98000\,\mathrm{g}/\mathrm{mole}$ and $2.35\,\mathrm{Pa.s}$.

- One of the firsts studies on rheokinetics of a monomers' reactive mixture while it cures in RIM machine was done by Castro and Macosko (1980). These authors modelled the mould filling of the RIM machine with a commercial three components polyurethane system. In this study it was assumed that viscosity rise depended only on the extent of the reaction and temperature but not on the shear rate. Polyurethane reactive mixture was obtained in a small laboratory RIM machine. Extent of the reaction of the mixture was found from the kinetics of the reaction that was measured experimentally by the adiabatic temperature rise. Viscosity rise over time was measured by the Rheometrics mechanical spectrometer. By measuring the extent of the reaction vs. time and viscosity vs. time at different temperatures, a graph of viscosity vs. extent of the reaction was obtained. The authors obtained an equation where the reduced viscosity was related to the extent of the reaction. The change in transparency of the separate reactants and the reactive mixture soon after it starts to react was explained by the formation of phase-separated polyurethane, which was turbid. Empirical viscosity model where viscosity is independent on the shear rate developed in this work is called Castro-Macosko model and is used and cited in some of the following studies.

- The objective of the Richter and Macosko (1980) study was to determine the relation between the viscosity and the extent of reaction for a MDI, polyester triol and DBTDL system. Reactants were mixed in the laboratory impingement mixer and transferred to the viscometer shortly after that. Viscosity and normal forces were measured by Rheometric Mechanical Spectrometer and viscosity was found to be independent on the shear rate and the normal force only appeared at approximately 60% of conversion. The authors reported that normal force did not decrease immediately when the rotation of the cone stopped as a consequence of change in volume or phase separation occurrence. Using the branching theory, a model relating viscosity to the molecular weight was developed. Adiabatic viscosity rise model was found to be a reasonably good fit with the experimental viscosity rise, and that the occurring errors could be reduced with the better isolation of the rheometer.
- Chambon, Petrovic et al. (1986) researched rheology of three concentrations crosslinking polyurethane systems at the gel point. Reactive formulation is a very slow one, having total curing time of at least 15 hours. In the first experimental part an oscillatory time sweep measurement was carried out in the rheometer and the gel time at specified frequency was determined as a crossover of the storage and loss moduli. In the following experimental part, three oscillatory measurements were carried out: time sweep, frequency sweep in the vicinity of the already determined gel time, and time sweep until the end of curing. From the frequency sweep near the gel point it was determined that at lower frequencies than the gel point frequency both moduli decrease to zero. At frequencies shortly after the gel point frequency, permanent elasticity was observed, and at frequencies much higher than the gel point frequency both moduli crossover and pass each other in a continuous fashion. The authors reported that elastic and loss moduli are congruent and proportional to the square root of the angular frequency at the gel point.

- Elwell (1995) studied the formation of the flexible polyurethane foam with urea segments, and urea hydrogen-bonded sequences by forced-adiabatic rheometry and identified four regions of the rheological: (i) bubble nucleation where viscosity of the mixture is equal to actual viscosity of the reactants; (ii) second region is the liquid foam formation and microphase separation characterised with higher elastic modulus than the loss one; (iii) third region of the physical gelation with increase in the elastic modulus of two decades; during the physical gelation increase in the elastic modulus is the consequence of the vitrification of the urea segments that masks the effect of the microphase separation; and (iv) the last region is characterised with further but not as dramatic increase in the elastic modulus, which is the consequence of formation of the cross-linked network.
- Macosko (1996) made a review of the rheology models that can be applied for the characterisation of the polymers. The author illustrated the rheology phenomena of the thermoplastic polymers with the suspension of the particles in a Newtonian fluid. In order to calculate the intrinsic viscosity models for the particles in Newtonian liquids (such as spheres, ellipsoids and flocculated network) were represented and compared to the models to calculate the molecular weight of the polymers such as rigid and flexible polymer coils, entangled and crosslinked network and branched, entangled chains.
- On another study on chemorheology of a MDI, polyether triol and DBTDL were mixed by the laboratory impingement mixer (Kim and Macosko 1996). Kinetic parameters were obtained via adiabatic temperature rise measurements. Viscosity was measured by Rheometrics Mechanical Spectrometer and found to be independent on the shear rate and to fit well with the Castro-Macosko viscosity model.
- Sun, Toth et al. (1997) also studied chemorheology of poly(urethane/isocyanurate) by adiabatic temperature rise, viscosity rise and DSC. Viscosity was measured and experimental results were fitted by the Castro-Macosko model. Since this formulation induces trimerization reactions,

and molecular weight depends on the network formation, viscosity was related to the molecular weight, which was determined by the recursive method.

- Dimier, Sbirrazzuoli et al. (2004) measured complex viscosity rise of the commercial polyurethane reactive formulation at different temperatures. The authors also modelled viscosity rise of the system based on Castro-Macosko model. Gelation time was measured by oscillation test and determined from the loss tangent intersection at different frequencies.
- Haddadi, Famili et al. (2006) tested commercial RIM polyurethane formulation to investigate its rheological properties such as viscosity rise and gel point as a function of temperature. Activation energy of the polymerisation was calculated. Gel point was measured by oscillatory tests and found as a point where the loss factor becomes independent on the angular frequency.

2.5 Polyamide-6

Polyamide-6, commercially called Nylon 6 (Du Pont) is a polymer produced by anionic polymerisation (in spite of the most polyamides that are produced by polycondensation), and it is a crystallinic thermoplastic. Due to the polar $C=O$ groups, polyamide-6 is highly hygroscopic and moisture has a plasticizing effect, which causes a decrease in the gel point. The glass temperature of polyamide-6 is around $75\,^{\circ}C$, and melting temperature is $232\,^{\circ}C$ (Sibal, Camargo et al. 1983). Polyamide-6 is generally synthesised from caprolactam monomer (CL), and different combinations and concentrations of initiators and activators. Figure 2.8. represents chemical formulas of caprolactam monomer, typical catalysts are N-acetyl caprolactam and hexamethylene-1,6-dicarbamoyl caprolactam and typical initiators are sodium caprolactamate, magnesium bromide caprolactam and isophthaloyl-bis-caprolactam.

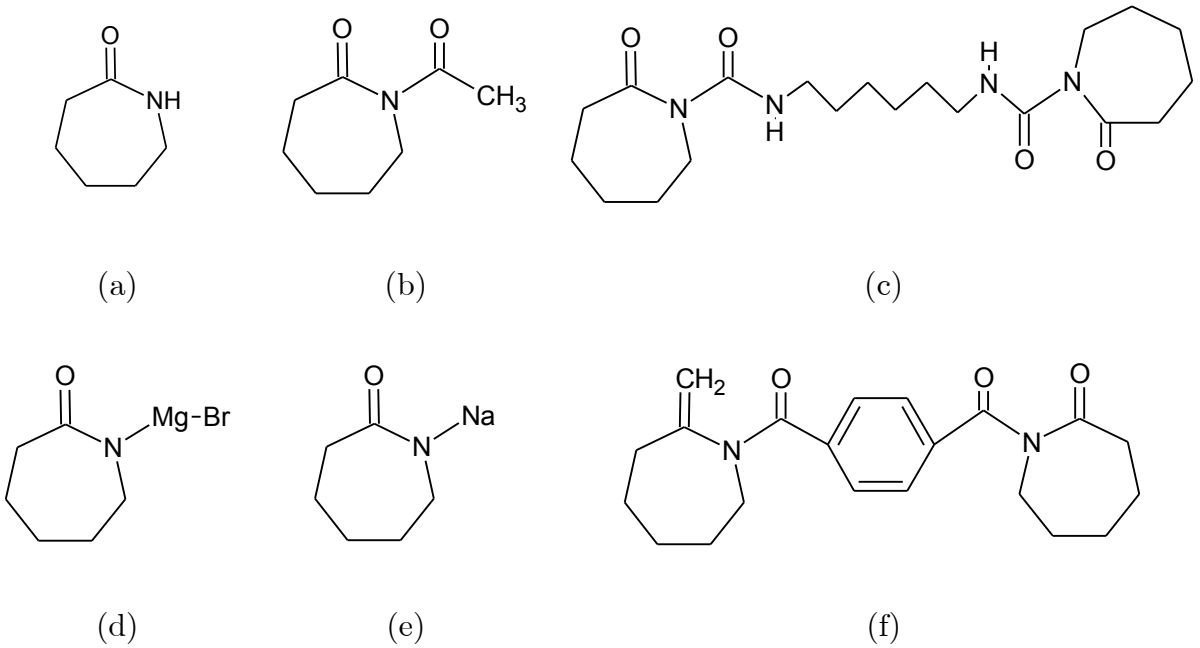

Figure 2.8. Chemical formulas of reactants for anionic polymerisation of polyamide-6: (a) ε- caprolactam; (b) N-acetyl caprolactam; (c) hexamethylene-1,6-dicarbamoyl caprolactam; (d) magnesium bromide caprolactam; (e) sodium caprolactamate; (f) isophthaloyl-bis-caprolactam.

Caprolactam is used as a monomer in the formation of polyamide-6, and the reaction takes place by the opening of the cyclic ring of the caprolactam. Initiators for this polymerisation are typically magnesium bromide caprolactam and sodium caprolactamate. They initiate the polymerisation by reacting with the caprolactam and forming an anion. This anion reacts with one of the catalysts N-acetyl caprolactam or hexamethylene-1,6-dicarbamoyl caprolactam and forms an imide group, which is necessary for the faster reaction. Polymerisation takes place through adding of anions to the growing macromolecular chain.

Caprolactam is a cyclic amide of aminocaproic acid, which is represented in Figure 2.9. Caprolactam is soluble in water, and as a product of the reaction between the caprolactam and water, aminocaproic acid is formed. Caprolactam is a white crystal substance at room temperature with melting point of $68\,^{\circ}\mathrm{C}$.

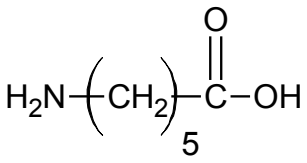

Figure 2.9. Aminocaproic acid structural formula.

Some combinations of initiators and catalysts used in the reaction of formation of polyamide-6 studied in literature are as follows:

- Sodium hydroxide (NaOH) as a initiator and toluene 2,4-diisocyanate (TDI) as an catalyst (Gong, Liu et al. 2010);
- Magnesium bromide incaprolactam (CL) as a initiator, and two catalysts isophthalolyl-bis-caprolactam and N-acetylcaprolactam (Udipi, Davé et al. 1997);
- Van Rijswijk, Bersee et al. (2006) used as initiators monofunctional N-acetylcaprolactam and difunctional hexamethylene-1,6-dicarbamoyl-caprolactam. As catalysts were used sodium caprolactamate and caprolactam magnesium bromide. The objective was vacuum infusion of large plastic parts.

Increase in catalyst concentration causes increase in the number of chains and decrease in molecular weight and consequently toughness of the product. Increase in initiator concentration causes reduction of the final conversion degree, which is caused by the fact that some residual monomer remains non-reacted and this residual monomer may act as a plasticizer and diffuse to the product surface and make the product unpaintable and tacky (Van Rijswijk, Bersee et al. 2006).

Temperatures higher than 160 °C may cause de-blocking of caprolactam-blocked isocyanate activator as represented in Figure 2.10. A compound containing free isocyanate groups with much higher reactivity than the initial activator is formed, and it is able to react with the amide-groups of PA-6 to form branches as shown in Figure 2.11.

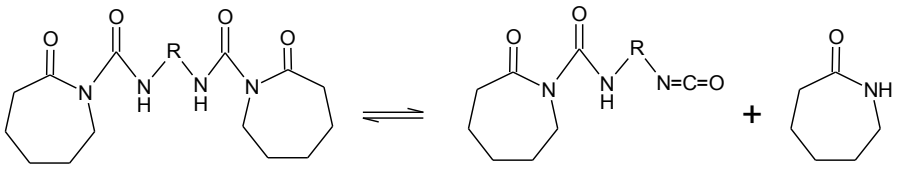

Figure 2.10. De-blocking reaction of difunctional blocked isocyanate catalyst.

In order to check the formation of branching, a solubility test in an aqueous solution of sulfuric acid (40%) may be carried out. However, when using more stable activators at high temperatures such as acyllactam, de-blocking reaction is avoided.

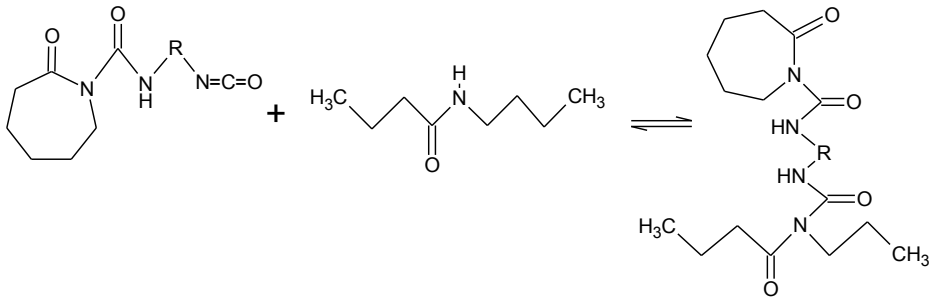

Figure 2.11. Branching reaction of difunctional blocked isocyanate catalyst.

Polyamide-6 is synthesised in anionic ring-opening polymerisation of monomer caprolactam which can be divided into three steps as shown in Figure 2.12:

1) Anion formation, which is actually dissociation of the initiator;
2) Complex formation between the initiator and the activator;
3) Polymerisation through the anions, during which an anion is regenerated after every monomer addition.

Giving the facts that nylon-6 is synthesised in anionic ring-opening of $\varepsilon-$caprolactam polymerisation, and that the polymer crystallizes, the reaction temperature has two opposite effects on the polymerisation and product. Raising the temperature, polymerisation rate is higher, but crystallisation rate is slower. Mechanical properties of PA-6 depend on the build-up of its crystallinic structure. Increase in temperature affects the anionic polymerisation of nylon-6 in two ways, increasing the reaction rate and decreasing the crystallization rate. An increase of some mechanical properties, such as better chemical resistance, lower water

absorption, higher modulus and lower toughness are favoured by the higher crystalline fraction.

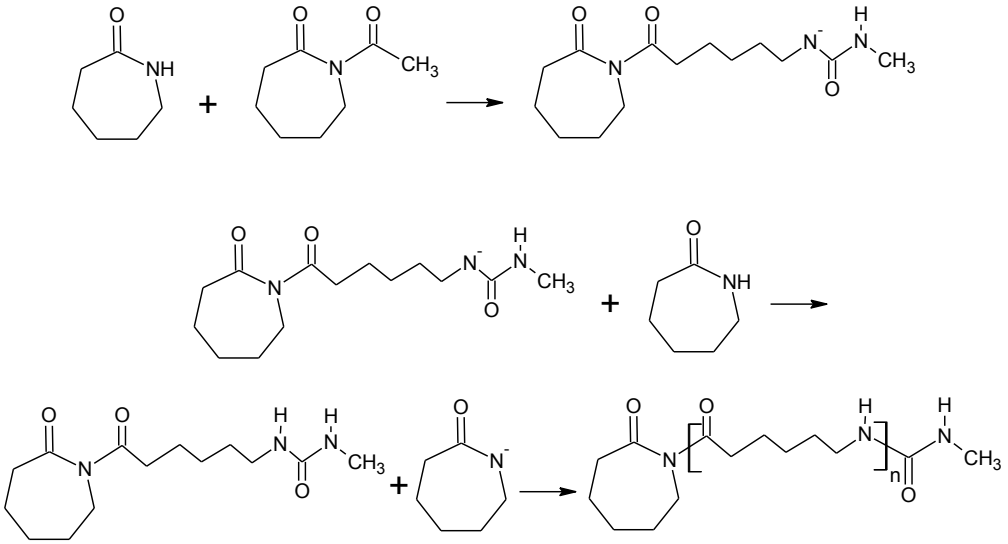

Figure 2.12. Three steps of the reaction of polymerisation of polyamide-6.

The highest value that can be obtained for the crystalline fraction is 50% and is obtained in the temperature range 145°C to 150°C (van Rijswijk, Bersee et al. 2006). If the temperature is lower than 130°C the crystallisation rate is too high causing low conversions and poor mechanical properties. At temperatures higher than 180°C the exothermic effect of the reaction is added to the total reaction temperature, and it may increase up to the melting temperature of the product which is 220°C resulting in modified morphology followed by modified mechanical properties (Van Rijswijk, Bersee et al. 2006). In order to measure the degree of crystallinity, PA-6 may be dissolved in 40% aqueous sulfuric acid, and residual monomer, which is the amount of the initially added monomer caprolactam that did not react, but remains entrapped inside the polymer that it is extracted by refluxing in demineralized water. The degree of crystallinity and melting point may be measured by DSC. Equation for the degree of the crystallinity, X_c, that is used is the following (van Rijswijk, Bersee et al. 2006):

$$X_c = \frac{\Delta H_m}{\Delta H_{100}} 100\% \tag{2.31}$$

Where ΔH_m is the melting enthalpy measured by the DSC, and ΔH_{100} is the melting enthalpy of fully crystalline polyamide-6.

Viscosity rise of the reactive mixture of the polyamide-6 depends primarily on the molecular weight, but there are other factors that may influence an increase in viscosity such as: temperature, solid crystallites that may appear and act as fillers and therefore increase the viscosity, large degree of crystallisation influencing physical gelation that may occur before complete polymerisation and branching reactions leading to increase in molecular weight (Sibal, Camargo et al. 1983).

- One of the first studies on processing guidelines and basic parameters for production of polyamide-6 in RIM process was carried out by (Sibal, Camargo et al. 1983). Sodium caprolactam (NaCL) was the initiator, and a phenyl isocyanate (PhI) and hexamethylene diisocyanate (HMDI) caprolactam the catalysts. Viscosity rise was measured during the polymerisation by Rheometrics Mechanical Spectrometer that has parallel plates geometry and can operate in the temperature range from $100\,^{\circ}\mathrm{C}$ to $170\,^{\circ}\mathrm{C}$. Minimum measurable viscosity was $0.01\,\mathrm{Pa.s}$, and maximum of $10^{30}\,\mathrm{Pa.s}$ at temperature values ranging from $140\,^{\circ}\mathrm{C}$ to $170\,^{\circ}\mathrm{C}$ and the time interval for the measurements was in the range $5\,\mathrm{s}$ to $50\,\mathrm{s}$. At temperatures $100, 120$ and $130\,^{\circ}\mathrm{C}$ experiment duration was $60\,\mathrm{s}$, and measured viscosity at this point was $0.05, 0.15$ and $10\,\mathrm{Pa.s}$, respectively. Adiabatic temperature rise was measured during the polymerisation in an isolated beaker using copper-constantan thermocouple. The authors stated that shear rate effect on the viscosity of the reactive mixture of polyamide-6 in most of the cases is negligible. Rheokinetics data for NaCL/HMDI system showed existence of three temperature regimes: below $130\,^{\circ}\mathrm{C}$ where the viscosity versus conversion data is temperature dependent, $130\,^{\circ}\mathrm{C}$ to $160\,^{\circ}\mathrm{C}$ curves for each temperature are nearly identical, above $160\,^{\circ}\mathrm{C}$ viscosity rise is much sharper because at

these temperatures crystallization rate is slower and branching formation rate is higher.

- Davé, Kruse et al. (1997) measured complex viscosity rise in-situ during reaction injection pultrusion process in the temperature range 120°C to 160°C. The authors used system of isophtaloyl-bis-caprolactam and caprolactam-magnesium-bromide as initiator and catalyst. Mixing of the two-reactant streams was accomplished using a spiral static mixer which is laboratory made unit for mixing and injecting into Rheometrics Mechanical Spectrometer measuring system. Two monomer streams were injected from syringes into the mixer and immediately introduced into the gap between two parallel plates, and after the oscillatory rheometry measurements were made. Measurement parameters used for oscillation test were strain of 10% and angular frequency of 100 rad / s. The rheometer geometry was parallel plates of 50 mm diameter and 0.5 mm gap. The maximum measureable complex viscosity by spectrometer used in this study was 10^3 Pa.s This value was obtained at different times depending on the temperature: at 120 °C maximum complex viscosity was obtained at 89 s and at the highest temperature of 160 °C maximum complex viscosity was obtained at 40 s.
- Van Rijswijk, Bersee et al. (2006) studied the optimal combination of activator/initiator for vacuum infusion process, which is characterized with relatively high moulding times that require formulation of polyamide-6 with relatively slow kinetics. Mixing of the two streams monomer/catalyst and monomer/initiator was carried out in lab-scale mixing unit with the static mixer. Different combinations of initiator-catalyst were assessed regarding their ability to form complexes between catalyst and initiator or monomer and consequently anions. Formation of complex early in reaction leaded to high reaction rate, comparing to the complex formation later in reaction or no complex formation at all. The authors observed that the complex was formed early in the reaction when using caprolactam magnesium bromide initiator and

monofunctional N-acetylcaprolactam, and sodium caprolactamate and difunctional hexamethylene-1,6-dicarbamoylcaprolactam. In case of sodium caprolactamate and N-acetylcaprolactam no complex was formed, and caprolactam magnesium bromide and hexamethylene-1,6-dicarbamoylcaprolactam complex was formed later in the reaction. Furthermore Rijswijk et al. stated three characteristic stages of polymerisation: first stage where the fluid surface remains fixed even under agitation of the container, second stage is the "cloudy" liquid, where the polymer chains are longer and are no longer soluble in monomer, the third stage is the shrinkage of the polymer as a consequence of the crystallisation.

- As an extension of the previous publication, van Rijswijk, Bersee et al. (2006) studied reaction temperature effect on final product properties using carbamoyl caprolactam initiator with a caprolactam magnesium bromide catalyst, a combination that was specifically formulated for vacuum infusion process with long time mould-filling. The procedure to mix the reactants was the same as in the previous publication. The physical aspect of the final product was studied to obtain data on the crystalline structure. At 140 °C white and opaque stains appear, having few millimeters these stains are characteristic of crystalline structures, whereas the product obtained at 150 °C to 170 °C was amorphous being homogeneous and translucent. Conversion during time was calculated at 140 °C, 150 °C and 160 °C and it was found that the conversion and therefore the reaction rate increase with temperature. The viscosity average molecular weight was measured and was found that it increased rapidly with an increase in temperature. Final conversion was measured and found to increase in the range 140 °C to 150 °C and decrease in the range 150 °C to 170 °C , which was related with the degree of crystallinity. Higher crystallinity degree corresponds to the higher conversion. At 140 °C it is believed the crystallization rate is so high that monomer is being trapped inside crystals, reducing the measured conversion and causing white colour of the product. Furthermore, at higher temperatures

branching may occur and decrease the degree of crystallinity, which reduces the conversion. The authors pointed out that for their specific system the optimal polymerisation temperature is between 140 °C to 150 °C. Increasing the temperature to 150°C to 170°C decreases the measured tensile properties and density due to the lower crystallinity degree. However at 140 °C the sudden drop in density and tensile properties were explained by the formation of shrinkage induced internal voids, while outer dimensions of the product remain intact.

- Work on optimal catalyst/initiator combination for reactive rotational moulding, and the optimization of the processing parameters using reactive rheometry and DSC was carried out by (Barhoumi, Maazouz et al. 2013). Combinations of catalyst/initiator were: complex forming sodium caprolactamate in caprolactam (C10) / hexamethylene-1,6-dicarbamoyl-caprolactam in caprolactam (C20), and initially no complex caprolactam magnesium bromide in caprolactam (C1) / hexamethylene-1,6-dicarbamoyl-caprolactam in caprolactam (C20). Monomer/initiator and monomer/catalyst mixtures were melted separately at 80°C under nitrogen, afterwards both mixtures were blended together and immediately characterised at Rheometric Scientist ARES rheometer, with cone and plate geometry using a gap with 0.06 mm. Oscillatory test was set to constant shear stress of 0.5 Pa and 1 rad / s angular frequency. The maximum values of complex viscosities at 160 °C were of 10^{40} Pa.s at 550 s for C10/C20 and at 1100 s for C1/C20. Viscosity value of 2×10^{40} Pa.s was reached at 410 s and 900 s for C10/C20 and C1/C20 respectively. The heat flow evolution of the reactive mixture was measured in DSC equipment during three consecutive intervals: heating from room temperature to 240 °C, cooling from 240 °C to 25 °C, and heating from 25 °C to 240 °C. Authors determined that an increase in catalyst/initiator ratio had higher impact on the viscosity rise than increasing the temperature.

Melting temperature of the solid sample obtained at the polymerisation at the rheometer at different reaction temperatures was measured and found that with an increase in polymerisation temperature, melting temperature of the solid sample decreased approximately 6 °C. Less crystalline polymer was obtained when content of the residual caprolactam was high and branching occurred at high temperatures. Monomer conversion was calculated by the determination of the residual monomer (reflux in demineralized water), molecular weight was calculated by determination of intrinsic viscosity (Ubbelohde viscometer) at 25 °C. The authors also reported typical mechanical test values for rotation moulded polyamide-6: Young's modulus 750 MPa to 1560 MPa, yield stress 62 MPa to 80 MPa, elongation at break 32% to 64%.

In Table 2.1 a comparison between polyurethanes and polyamide-6 reactive formulations for RIM is presented. Special importance is given to the main differences in the characteristics of each group of polymers (PU and PA-6).

Table 2.1. Reactive formulations for RIM: polyurethanes and polyamide-6 comparison.

RIM formulations	
Polyurethanes	**Polyamide-6**
Polycondensation	Anionic polymerisation
2 reactants	3 reactants
Molar ratio of the reactants highly important for the product quality	Material properties are less sensitive to molar ratio than polyurethanes
Gel temperature higher than degradation temperature	Gel temperature=75°C
Covalent bonds network	Hydrogen bonds network
Thermoset	Thermoplastic
Low reaction temperatures and fast demoulding times	Higher reaction temperatures and longer demoulding times
Low viscosity reactants	Low viscosity reactants
Not hygroscopic	Hygroscopic (dimensional changes and mechanical property variation with humidity changes)
Not recyclable	Recyclable

2.6 Polymer nanocomposites

2.6.1 Hybrid materials and nanocomposites

These materials consist of relatively strongly interacting components that are blended on molecular scale and can be divided into two classes depending on the strength of the interaction between two moieties (Kickelbick 2006, Chattopadhyay and Webster 2009):

- Class I consists of materials with weak interactions between the two phases, such as van der Waals, hydrogen bonding and electrostatic forces. These materials are blends (inorganic and organic building blocks without strong interactions) and interpenetrating networks (inorganic and organic network interpenetrate each other without strong interactions);

- Class II materials have strong interactions such as covalent bonds and these are discrete inorganic blocks/clusters or inorganic polymers that are linked to the organic polymers.

A nanocomposite is is a hybrid material if one of its structural units (organic or inorganic) size ranges from 1 to 10 nm . Nanomaterials usually exist in one of the following morphologies: nanoparticle, nanorod, nanotube (carbon nanotubes) and galleries/layers (clay materials). Nanomaterials are characterised by a large surface area, which has a large number of atoms in their surface available to make bonds with other materials. Nanosized objects such as inorganic particles show very high surface energy and because of that they tend to agglomerate in organic medium, and as a consequence of that a surfactant should be used in order to make a stable dispersion of nanoparticles. The degree of dispersion of nanoparticles depends on the factors such as: particle size, particle wettability by the dispersing medium and the nature of the attractive forces between the particles and medium.

Inorganic particles can improve many properties of the hybrid materials such as: long-term stability, electronic, mechanical and thermal properties, mechanical strength and biocompatibility.

In order to synthesize mechanically resistant nanocomposite, an organic polymer matrix must wet sufficiently enough inorganic nanoparticle. In general inorganic fillers are hydrophilic and form hydrogen bonds with other hydrophilic substances; on the other hand polymers are hydrophobic and are connected to other substances through van der Waals forces. A composite material consists of at least two phases and one or more interfaces between them. In order to form mechanically strong nanocomposite during high temperature processing, better adhesion between polymer and inorganic nanoparticle is achieved when nanoparticle has irregular shape rather than spherical, because the surface area is greater when the shape is irregular. Particles can be embedded into polymer matrix, chemically bonded to the polymer chains, form chemical network and inorganic-organic hybrid polymer. The amount of

filler can also affect the mechanical properties of the nanocomposite, for example if the filler content is too high the composite material can be more heterogeneous and therefore more brittle. Inorganic nanoparticles have tendency to aggregate forming agglomerates by the adhesion forces such as: van der Waals force, electrostatic forces, interlocking and liquid and solid bridges. In order to break the agglomerates, processing equipment or laboratory ultrasonication is required. This equipment produces shear forces larger than particle adhesion forces. Efficiency of inorganic particle dispersion is generally assessed using SEM and TEM. Most of the ceramic particles have bi-modal size distribution which is preferred because smaller particles can penetrate into spaces between larger particles (upová 2009).

The two most common methods of nanocomposite synthesis are: 1 - a method based on thermo-mechanical forces to join polymer matrix and inorganic fillers; and 2 – a method based on physical-chemical methods that involves precipitation and dispersion of particles into polymer matrix/solution. One of the methods of production of nanocomposites is polymer shell formation, where monomers polymerise on the top of particles, forming coated particles that are more resistant to the agglomeration. The nucleation of the hydroxyapatite crystals is affected by the functional groups as follows: PO_4H_2> COOH >>$CONH_2$~OH>NH_2>>CH_3 =0 (upová 2009). For production of biocompatible scaffold electro-spinning is often used. For the problem of agglomeration of hydroxyapatite, surfactant (with one hydrophilic and other hydrophobic end) is often used.

2.6.2 Polyurethanes with inorganic particles

Formation of nanocomposite polyurethane materials increases thermal and oxidative stability because of interfacial interaction between the filler and polymer chains, which is improved when the surface area of the filler is larger. Efficiency against thermal degradation increases by decreasing the size of filler and increasing the aspect ratio of it (Chattopadhyay and Webster 2009). Conventional polyurethane composites are made by premixing the inorganic compound with the polyol and then reacting this mixture with isocyanate.

2.6.2.1 Titanium (IV) oxide

Titanium (IV) oxide (TiO_2) is highly used as filler in polymer industry due to its extraordinary properties such as: photocatalytic activity, strong redox ability, UV resistance and excellent transparency in the range of visible light (tengl, Hou ková et al. 2008). Besides those, low costs of production and low toxicity also have played an important role in the expansion of TiO_2 particles usage.

A new nanocomposite polyurethane material reinforced with titanium dioxide nanoparticles was developed from toluene diisocyanate and castor oil without a catalyst in bulk polymerisation (Ristić, Budinski-Simendić et al. 2012). Nanofiller suspension in acetone was added to the molten castor-oil and stirred vigorously, after what isocyanate was added to form reactive mixture and it was casted into the preheated mould. The size of the titanium dioxide nanoparticles in suspension in acetone was measured with zetasizer and it was found that the number based average size of nanofiller was approx. 100 nm. An increase in the filler content increased the tensile strength, hardness and elongation at break due to the increase in intermolecular entanglement and interactions and higher cross-linking density. Glass temperature measured by DSC and DMS decreased with an increase in the filler content. This is explained by the macromolecular chains moving due to the presence of the filler, and this consequently increased the elastic properties such as elongation at break. Filler component might have induced higher degree of noncovalent bonding and entanglements of the polymeric chains which might have increased the compatibility between the filler and the macromolecular chains, by forming a strong interface interaction and more non-covalent linkages and entanglements.

Golaz, Tetouani et al. (2012) studied the formation of TPU reinforced with SiO_2 nanoparticles and titanium dioxide microparticles by extrusion and compression moulding. The rheological, thermal and mechanical properties were measured. Viscosity was measured by AR2000, TA Instruments in an oscillation test with a strain sweep and a flow test with a shear rate sweep at 200 °C and shear-thinning

behaviour was confirmed. No significant influence on the gel temperature of the SiO_2 and titanium dioxide on TPU was observed by DSC. Elastic modulus, strain at break and ultimate strength were slightly increased with an addition of filler.

2.6.2.2 Silicate nanolayers

Silica layers or clay are natural minerals containing silicon, oxygen, water and some other element typically, sodium, potassium, calcium, magnesium or aluminum. They exist in different sizes depending on the chemical structure such as: Laponite of 25 nm diameter and 1 nm thickness, Montmorillonite and Hectorite of 100-300 nm diameter (Liff, Kumar et al. 2007). All of these clays have hydrophilic character and due to the fact they retain water, they require modification for addition in a reactive PU process.

Completely delaminated hybrid silicate layers were homogeneously dispersed in a polymer matrix (Dai, Xu et al. 2004). When processing the hybrid material, if the silicate layers content is too high, an effective entry of the monomers into the organically modified silicate layers may be very difficult.

In order to modify inorganic silicate layers to be able to disperse and mix with an organic polymer, an exfoliation (separation of the stacked clay particles and dispersion of the separated particles) is carried out by the means of melt extrusion or organic modification. High degree dispersion of the organically modified clay nanoparticles is typically obtained from one of the following methods: in-situ polymerisation of previously intercalated monomers between silicate layers, thermoplastic polymers melt intercalation and further exfoliation and combining with polymer solution. Chemical modification or functionalisation of the silica nanoparticles and attachment of the modified silica to polyurethanes is called silica grafting (Chattopadhyay and Webster 2009).

Thermal stability of polyurethane nanocomposite with silica clay is ensured by the fact that clay acts as a thermal insulator and mass transport barrier to the volatile compounds that are formed during decomposition.

Mechanical properties of solution cast TPU-montmorillonite nanocomposites were studied by Dai, Xu et al. (2004). Sodium montmorillonite was chemically treated to exchange hydrophilic inorganic cations with more organophylic alkylammonium ions and dissolved in dimethylformamide. Polyol and MDI were added to the mixture and stirred. Dai, Xu et al. (2004) reported that with an increase in the clay content molecular chains have less space to move, therefore even with the application of the strain the SSs are oriented in the direction of the strain but their crystallisation is suppressed. As a consequence of the decreasing rate of the crystallisation, elongation at break is improved. The authors also reported that higher clay content increases the degree of hydrogen bonding, gel temperature of the soft domain and Young's modulus of the nanocomposite.

Mechanical properties of nanocomposite containing TPU and silica obtained by extrusion and solvent casting were studied by (Finnigan, Martin et al. 2004). Commercial nanosized layered silica organically modified to have hydroxyl functional groups was blended with commercial TPU. It was reported that efficient dispersion of the filler in TPU matrix was obtained, showing organosilicate filler bonded with the hard segments of TPU by hydrogen bonds. Large improvement in the Young's modulus was obtained when the filler was used from both processing methods, but on the other hand, tensile strength and elongation of the nanocomposite decreased with an addition of the filler.

(Finnigan, Martin et al. 2004) continued the study on the effect of nanosilica on mechanical properties of TPU nanocomposite, researching the effect of tensile strain on tensile stress of the films prepared by the solvent casting (Finnigan, Jack et al. 2005). In this study it was reported that a significant increase in tensile properties of the prepared films occurred when the diameter of the disks decreased. When strain is applied, microphase structure of phase-separated polyurethane depends on the size of

the fillers: small fillers did not affect the microphase structure because they align with the strain and form hydrogen bonds with TPU sequences. These hydrogen bonds increased the stiffness of the material; larger fillers affected the formation of voids between the polymer and filler, because filler particles were unable to align with the strain. Additional tensile stress caused voids formation, reduction of the tensile properties at low strains and whitening of the material. Only at high strains stiffness of the material increased, because the microphase structure is disassembled and fillers can align in the strain direction and form hydrogen bonds.

Properties of rigid polyurethane foam reinforced with montmorillonite in which natural sodium was exchanged with a quaternary ammonium salt with hydroxyl functionality was studied by Widya and Macosko (2005). Nanoclay was previously dispersed in toluene and afterwards stirred with MDI until the MDI diffused into the intergallery spacing of the clay and reacted with the hydroxyl groups. Mixture of nanoclay and MDI was sonicated, afterwards the toluene was extracted by evaporation. These operations were followed by the mixing with polyol mixture (which contained catalysts and other additives) in a laboratory mixing head and discharging the mixture into a mould. Authors reported that intergallery spacing in the clay increased with toluene present in the formulation. Viscosity of the mixture was found to significantly increase with the addition of the nanoclay, and also at higher concentration clay platelets can form a network which may result in the appearance of yield stress, the fluid does not flow until the critical yield stress is reached. This phenomenon influences mixing between the polymeric matrix and the nanoclay, in the way that mixing will only be possible close to the stirrer (where stresses are higher than the yield stress). Because of this, authors chose nanoclay with the smallest diameter for this study.

A method for exfoliation of the clay particles is described in the patent WO 2007/011394 that uses two solvents exchange method. This method consists of: dispersion of the particles into the first solvent resulting in the first particle/solvent dispersion, adding the second solvent to it which results in the second

particle/solvent dispersion, and extracting the first solvent from it to form the third particle/solvent dispersion. First solvent must disperse the particles, and have lower boiling point than the second one. The second solvent must dissolve polymeric matrix, and both solvents must be miscible. This method may include one or more drying steps of the third particle/solvent dispersion. The solvent extraction may include distillation. The first solvent may be water, methanol, chloroform, dichloromethane, glycerol; the second solvent may be tetrahydrofuran, dimethylformamide, dimethylsulfoxide...The particle size may be from 1nm to 5microns or higher. Particles may be smectite clays, silica nanoparticles, carbon black, carbon nanoparticles and nanotubes and also semiconductor particles and quantum dots.

Two solvent exchange method for exfoliation of Laponite previously described in WO 2007/011394 was applied for the synthesis of Laponite - TPU nanocomposite (Liff, Kumar et al. 2007). Authors reported that the addition of Laponite significantly increases the elastic modulus of TPU and this increases with the Laponite content, which is consequence of the interfacial adhesion of the Laponite with the HS of TPU. Laponite increases the strength, toughness and extensibility of the TPU nanocomposite but not as much as it affects the elastic modulus. Changes in mechanical properties of nanoreinforced TPU were due to changes in polymer morphology cause by addition of Laponite.

Ari and Aydin (2011) studied rheological and thermal properties of micro and nanocomposites of thermoplastic, commercial formulation of PVC and SiO_2. PVC and SiO_2 were blended in a Haake rheometer and mixture showed shear-thinning behaviour. Furthermore, an effect of the rotor speed on viscosity was measured, and it was found that at low rotor speeds viscosity of composites increased with increase in the silica particle size. Higher rotor speeds did not have a significant effect on viscosity except for the filler of the smallest size ($25\ \mathrm{nm}$). Particles of size lower than $100\ \mathrm{nm}$ showed higher apparent viscosity when compared to the larger particles, which was a consequence of the increased interfacial interaction between the smaller

particles and polymer. It was also reported that for smaller silica particles the temperature of the initial stage of thermal degradation of the composite decreased.

2.6.2.3 Carbon nanotubes

Carbon nanotubes (CNT) are very interesting reinforcing fillers for nanocomposites because they have nanometric diameters, aspect ratios ranging 100-1000 and low density. If the CNTs are uniformly dispersed in polyurethane, they offer thermal and oxidative stability, higher thermal conductivity which effects increased heat transfer and therefore the polyurethane decomposition is delayed (Chattopadhyay and Webster 2009).

2.6.2.4 Hydroxyapatite nanoparticles

Hydroxyapatite (HAp) is a natural, crystalline, inorganic mineral and one of many calcium phosphates that exhibit different properties with Ca^{2+} to PO_4^{3-} stoichiometric ratio. This ratio in HAp is 1.67 and it corresponds to the chemical formula $Ca_{10}(PO_4)_6(OH)_2$.

Natural hydroxyapatite occurs as a constituent of bones and teeth (upová 2009), having nanometric dimensions of approx. 4x50x50 nm. Besides natural, synthetic HAp has been produced in the last two decades, most commonly by wet chemical precipitation between a source of calcium ions, Ca^{2+}, which is generally calcium nitrate $Ca(NO_3)_2$ solution, and of phosphorous ions, PO_4^{3-} which is monoammonium phosphate $(NH_4)H_2PO_4$ as represented in Equation (2.32). In order to obtain the product with 1.67 stoichiometric ratio between calcium and phosphate ions, pH should be maintained in the range from 9 to 12 (Silva, Quadros et al. 2008, Gomes, Silva et al. 2009). For that reason, reaction should occur in an alkaline medium, for example ammonium hydroxide NH_4OH or potassium hydroxide KOH.

$$10Ca^{2+}(aq.) + 6PO_4^{3-}(aq.) \xrightarrow{OH^-} Ca_{10}(PO_4)_6(OH)_2(s) \qquad \textbf{(2.32)}$$

Synthesis of crystalline nanosized HAp is possible in the novel reactor NETmix® that was designed for fast reactions (patent EP1720643). This mixer consists of a continuous network of interconnected chambers where complete mixing occurs and channels where complete segregation occurs, and it controls the micromixing which is where the reaction occurs (at molecular level). In order to increase crystallinity of the HAp formed by a NETmix® reaction and also to approach Ca/P ratio to stoichiometric value additional maturation by stirring of the HAp slurry may be conducted (Silva, Quadros et al. 2008).

In order to replace hydrophilic hydroxyl groups of HAp with some more hydrophobic groups to enable HAp to mix more efficiently with polymeric materials, surface modification is required.

Wang, Li et al. (2002) tested the effect of surface modified HAp on the mechanical properties and crystallinity of the nanocomposite material containing crystalline polyamide-6,6 and HAp. Hap nanosized crystals surface was modified with polyethylene glycol (PEG) at 145°C, using the ratio of PEG and HAp of 20:100 wt. %. Surface modified HAp was tested by TEM and found that particles had size 10-30 nm in diameter and 50-93 nm in length comparing to the pure HAp (diameter 5-26 nm and length 30-84 nm). This mixture of HAp with PEG was then added to the commercial formulation of crystalline polyamide 6,6 that was previously dissolved in dimethyl acetamide (DMAC). The authors reported that the degree of crystallinity of the PA-6,6 nanocomposite decreased with the addition of HAp because of the lower number of hydrogen bonds inside polyamide chains, that is the consequence of the formed interface between HAp and PA. Tensile, bending and impact strength of synthesised nanocomposite material were measured and found to increase with HAp present in nanocomposites.

In the work of Dai, Xu et al. (2012) HAp was synthesised by wet chemical precipitation and then it was treated with 3-aminopropyltriethoxysilane to exchange hydroxyl groups with amine groups. Obtained amine-terminated HAp was then reacted with L-phenylalanine N-carboxyanhydride to form poly (L-phenylalanine)

hydroxyapatite, the surface modified HAp. The authors reported that modified HAp had almost the same crystalline structure as pure HAp as well as successful prevention of HAp particles aggregation up to 24h by dispersion test in dichloromethane (DCM), due to the hydrophobic surface that was formed by poly(L-phenylalanine). TEM analysis showed that surface modification method did not affect the bulk structure of HAp, and also that only few nanoparticles were aggregated into aggregates of approximately 200x800 nm and polymer chains were grafted onto the surface of those initial HAp aggregates that prevented further aggregation. Weight loss of the HAp modified with poly(L-phenylalanine) was measured by Thermal Gravimetric Analysis (TGA). With an increase in the concentration of poly(L-phenylalanine), measured weight loss of the modified HAp increased..

Adamska, Szubert et al. (2013) developed a method for surface modification of hydroxyapatite powder with two compounds PEG and polyhexaethylmetacrylate (pHEMA). Method consisted of HAp dispersing N,N-dimethyelformamide (DMF), and reacting it with hexamethylenediisocyanate (HMDI) and dibutyltindilaurate (DBTDL). In the next step previously obtained mixture was stirred with PEG and/or pHEMA and filtrated. Suggested reaction mechanism included: beginning of the reaction between the hydrogen from hydroxyl group of HAp and isocyanate group from HMDI to form an intermediate product having one NCO end group that can react later with hydroxyl group from PEG and/or pHEMA. Authors reported that modification with pHEMA showed higher modification than with PEG.

2.6.2.5 Zinc oxide-nanoparticles

Inorganic zinc oxide (ZnO) is an advantageous material for incorporation in polymeric matrices due to its superior UV-blocking, photocatalytic, electrical, electronic, optical, antibacterial and dermatological properties. ZnO together with TiO2 are non-toxic and stable at high temperatures and UV radiation (Becheri, Dürr et al. 2008).

ZnO nanoparticles are synthesised in two steps reaction: first step involves reaction between zinc chloride ($ZnCl_2$) and sodium hydroxide ($NaOH$) to form zinc hydroxide ($Zn(OH)_2$) as

$$ZnCl_2 + 2NaOH \rightarrow Zn(OH)_2 + 2NaCl \quad \textbf{(2.33)}$$

Both reactants $ZnCl_2$ and $NaOH$ are solid and therefore require dissolving in an appropriate solvent. Second step is aging (calcination) at high temperature to obtain solid ZnO. Solvent influence on the particle size of ZnO was studied by (Moroni, Borrini et al. 2005, Becheri, Dürr et al. 2008). They used water at 90°C and ethylene glycol at 150°C and reported that smaller particle size was obtained with ethylene glycol. Zinc hydroxide and sodium chloride generated in the reaction between $ZnCl_2$ and $NaOH$, are washed with water and silver nitrate ($AgNO_3$) in order to eliminate sodium chloride ($NaCl$) and sonicated with 2-propanol in order to destroy microaggregates and finally centrifuged. Second step of the synthesis is the thermal treatment called calcination at 550-750°C to obtain solid ZnO (Moroni, Borrini et al. 2005).

In the study of Becheri, Dürr et al. (2008) the ability of synthesised ZnO to absorb UV radiation, and the influence of the nanoparticles on the mechanical properties of the reinforced fabrics are reported. ZnO nanoparticles were applied onto the fabrics and then washed in repeated cycles and it was reported that large aggregates were removed from fabric surface, while nanoparticles remained at the textile surface. Textiles with nanosized zinc oxide particles incorporated showed higher absorption of UV radiation than textiles not treated with zinc oxide. Mechanical strength increased and elongation decreased with materials with ZnO.

2.7 Conclusions

Given the above overview of the reactive formulations of polyurethanes, polyamide-6 and their nanocomposites for application in RIM process, one may conclude that

there is still a need for the assessment of the methodologies used on the mixing of monomers in laboratory test to obtain final solid products, as well as the determination of the correlation between the product properties and mixing and productions conditions. Each of the mentioned groups of materials are studied in the following chapters of this thesis, all of them having the same objectives: definition of the reactants characteristics, eventual modification of the reactants in order to become more easily mixed with other reactants, assessment of the mixing procedure, assessment of the synthesis parameters, obtainment the final product and measure its characteristics and correlate this with the production parameters.

2.8 References

Adamska, K., M. Szubert, A. Voelkel and Z. Okulus (2013). "Characterisation of hydroxyapatite surface modified by poly(ethylene glycol) and poly(hydroxyethyl methacrylate) grafting." Chemical Papers**67**(4): 429-436.

Ari, G. A. and I. Aydin (2011). "A study on fusion and rheological behaviors of PVC/SiO 2 microcomposites and nanocomposites: The effects of SiO 2 particle size." Polymer Engineering and Science**51**(8): 1574-1579.

Barhoumi, N., A. Maazouz, M. Jaziri and R. Abdelhedi (2013). "Polyamide from lactams by reactive rotational molding via anionic ring-opening polymerisation: Optimization of processing parameters." Express Polymer Letters**7**(1): 76-87.

Barnes, H. A., J. F. Hutton and K. Walters (1989). An Introduction to Rheology Elsevier.

Becheri, A., M. Dürr, P. Lo Nostro and P. Baglioni (2008). "Synthesis and characterisation of zinc oxide nanoparticles: application to textiles as UV-absorbers." Journal of Nanoparticle Research**10**(4): 679-689.

Castro, J. M. and C. W. Macosko (1980). "Kinetics and rheology of typical polyurethane reaction injection molding systems." Society of Plastics Engineers (Technical Papers): 434-438.

Chambon, F., Z. S. Petrovic, W. J. MacKnight and H. H. Winter (1986). "Rheology of model polyurethanes at the gel point." Macromolecules**19**(8): 2146-2149.

Chattopadhyay, D. K. and D. C. Webster (2009). "Thermal stability and flame retardancy of polyurethanes." Progress in Polymer Science**34**(10): 1068-1133.

Dai, X., J. Xu, X. Guo, Y. Lu, D. Shen, N. Zhao, X. Luo and X. Zhang (2004). "Study on Structure and Orientation Action of Polyurethane Nanocomposites." Macromolecules**37**(15): 5615-5623.

Dai, Y., M. Xu, J. Wei, H. Zhang and Y. Chen (2012). "Surface modification of hydroxyapatite nanoparticles by poly(l-phenylalanine) via ROP of l-phenylalanine N-carboxyanhydride (Pha-NCA)." Applied Surface Science**258**(7): 2850-2855.

Davé, R. S., R. L. Kruse, K. Udipi and D. E. Williams (1997). "Polyamides from lactams via anionic ring-opening polymerisation: 3. Rheology." Polymer**38**(4): 949-954.

Dimier, F., N. Sbirrazzuoli, B. Vergnes and M. Vincent (2004). "Curing kinetics and chemorheological analysis of polyurethane formation." Polymer Engineering & Science**44**(3): 518-527.

Elwell, M. J. (1995). "Forced-adiabatic sampling environments: useful tools for the study of structure development during polymerisation." Thermochimica Acta**269–270**(0): 145-157.

Erkoc, E., R. J. Santos, M. I. Nunes, M. M. Dias and J. C. B. Lopes (2007). "Mixing dynamics control in RIM machines." Chemical Engineering Science**62**(18-20): 5276-5281.

Finnigan, B., K. Jack, K. Campbell, P. Halley, R. Truss, P. Casey, D. Cookson, S. King and D. Martin (2005). "Segmented Polyurethane Nanocomposites: Impact of Controlled Particle Size Nanofillers on the Morphological Response to Uniaxial Deformation." Macromolecules**38**(17): 7386-7396.

Finnigan, B., D. Martin, P. Halley, R. Truss and K. Campbell (2004). "Morphology and properties of thermoplastic polyurethane nanocomposites incorporating hydrophilic layered silicates." Polymer**45**(7): 2249-2260.

Fonte, C. P., R. J. Santos, M. M. Dias and J. C. B. Lopes (2011). "Quantification of Mixing in RIM Using a Non-Diffusive Two-Phase Flow Numerical Model." International Journal of Chemical Reactor Engineering**9**(A114).

Golaz, B., S. Tetouani, N. Diomidis, V. Michaud and S. Mischler (2012). "Processing and tribology of thermoplastic polyurethane particulate composite materials." Journal of Applied Polymer Science**125**(5): 3745-3754.

Gomes, P. J., V. M. Silva, P. A. Quadros, M. M. Dias and J. C. B. Lopes (2009). "A Highly Reproducible Continuous Process for Hydroxyapatite Nanoparticles Synthesis." Journal of Nanoscience and Nanotechnology**9**(6): 3387-3395.

Gong, Y., A. Liu and G. Yang (2010). "Polyamide single polymer composites prepared via in situ anionic polymerisation of -caprolactam." Composites Part A: Applied Science and Manufacturing**41**(8): 1006-1011.

Haddadi, H., M. H. N. Famili, E. Nazokdast and S. Moradi (2006). "Chemorheological analyses of a reaction injection moulding polyurethane formulation." Iranian Polymer Journal (English Edition)**15**(12): 967-977.

Haddadi, H., E. Nazockdast and B. Ghalei (2008). "Chemorheological characterisation of thermosetting polyurethane formulations containing different chain extender contents." Polymer Engineering and Science**48**(12): 2446-2453.

Kickelbick, G. (2006). Hybrid Materials.

Kim, D. S. and C. W. Macosko (1996). "Reaction kinetics and chemorheology of a highly reactive PU system." Korea Polymer Journal**4**(1): 54-60.

Kim, D. S. and C. W. Macosko (2000). "Reaction injection molding process of glass fiber reinforced polyurethane composites." Polymer Engineering and Science**40**(10): 2205-2216.

Kolodziej, P., C. Macosko and W. Ranz (1982). "The influence of impingement mixing on striation thickness distribution and properties in fast polyurethane polymerisation." Polymer Engineering & Science**22**(6): 388-392.

Kolodziej, P., W. P. Yang, C. W. Macosko and S. T. Wellinghoff (1986). "Impingement Mixing And its Effect on the Microstructure of RIM Polyurethanes." Journal of Polymer Science, Part B: Polymer Physics**24**(10): 2359-2377.

Lee, L. J., J. M. Ottino, W. E. Ranz and C. W. Macosko (1980). "Impingement mixing in reaction injection molding." Polymer Engineering & Science**20**(13): 868-874.

Liff, S. M., N. Kumar and G. H. McKinley (2007). "High-performance elastomeric nanocomposites via solvent-exchange processing." Nature Materials**6**(1): 76-83.

Lopes, J. C. B., R. J. Santos, Teixeira A.M. and C. M.R.P.F.N. (2005). Production Process of Plastic Parts by Reaction Injection Moulding, and Related Head Device. Portugal.

Macosko, C. W. (1989). Fundamentals of Reaction Injection Molding. Minneapolis.

Macosko, C. W. (1989). RIM, Fundamentals of Reaction Injection Molding, Hanser

Macosko, C. W. (1994). Rheology: Principles, Measurements, and Applications, Wiley-VCH.

Macosko, C. W. (1996). "Application of rheology to polymer characterisation."

Malguarnera, S. C. and N. P. Suh (1977). "Liquid injection molding I. An investigation of impingement mixing." Polymer Engineering & Science**17**(2): 111-115.

Menard, K. P. (2008). Dynamic Mechanical Analysis: A Practical Introduction, CRC Press.

Moroni, M., D. Borrini, L. Calamai and L. Dei (2005). "Ceramic nanomaterials from aqueous and 1,2-ethanediol supersaturated solutions at high temperature." Journal of Colloid and Interface Science**286**(2): 543-550.

Richter, E. B. and C. W. Macosko (1980). "Viscosity changes during isothermal and adiabatic urethane network polymerisation." Polymer Engineering & Science**20**(14): 921-924.

Ristić, I. S., J. Budinski-Simendić, I. Krakovsky, H. Valentova, R. Radičević, S. Cakić and N. Nikolić (2012). "The properties of polyurethane hybrid materials based on castor oil." Materials Chemistry and Physics**132**(1): 74-81.

Santos R. J., Teixeira A.M., Costa M.R.P.F.N. and L. J. C. B. (2002). "Operational and Design Study of RIM machines." International Polymer Processing.

Santos R.J., Teixeira A.M., Costa M.R.P.F.N. and L. J. C. B. (2002). "Operational and Design Study of RIM machines." International Polymer Processing.

Santos, R. J., E. Erkoç, M. M. Dias and J. C. B. Lopes (2009). "Dynamic behavior of the flow field in a RIM machine mixing chamber." AIChE Journal**55**(6): 1338-1351.

Santos, R. J., E. Erkoç, M. M. Dias, A. M. Teixeira and J. C. B. Lopes (2008). "Hydrodynamics of the mixing chamber in RIM: PIV flow-field characterisation." AIChE Journal**54**(5): 1153-1163.

Santos, R. J., A. M. Teixeira, E. Erkoç, M. A. Sultan, A. Karpinska, M. M. Dias and J. C. B. Lopes (2010). "Validation of a 2D CFD Model for Hydrodynamics' Studies in CIJ Mixers." International Journal of Chemical Reactor Engineering**8**: A32.

Santos, R. J., A. M. Teixeira and J. C. B. Lopes (2005). "Study of mixing and chemical reaction in RIM." Chemical Engineering Science**60**(8-9): 2381-2398.

Sebastian, D. H. and S. Boukobbal (1986). "Mixhead Parameters Governing Impingement Mixing Effectiveness for Polyurethane Reactive Injection Molding Processes." Polymer Process Engineering**4**(1): 53-70.

Sibal, P. W., R. E. Camargo and C. W. Macosko (1983). "Designing Nylon-6 Polymerisation Systems for RIM " Polymer Process Engineering**1**(2): 147-169.

Silva, V. M. T. M., P. A. Quadros, P. E. M. S. C. Laranjeira, M. M. Dias and J. C. B. Lopes (2008). "A Novel Continuous Industrial Process for Producing Hydroxyapatite Nanoparticles." Journal of Dispersion Science and Technology**29**(4): 542-547.

tengl, V., V. Hou ková, S. Bakardjieva, N. Murafa and V. Havlín (2008). "Optically transparent titanium dioxide particles incorporated in poly(hydroxyethyl methacrylate) thin layers." Journal of Physical Chemistry C**112**(50): 19979-19985.

Sun, X., J. Toth and L. James Lee (1997). "Chemorheology of poly(urethane/isocyanurate) formation." Polymer Engineering & Science**37**(1): 143-152.

upová, M. (2009). "Problem of hydroxyapatite dispersion in polymer matrices: A review." Journal of Materials Science: Materials in Medicine**20**(6): 1201-1213.

Szycher, M. (1999). Szycher's Handbook of Polyurethanes, CRC press.

Teixeira, A. M., R. J. Santos, M. R. P. F. N. Costa and J. C. B. Lopes (2005). "Hydrodynamics of the mixing head in RIM: LDA flow-field characterisation." AIChE Journal**51**(6): 1608-1619.

Torcato, R. O. (2013). Modeling the Product Development Process: The RIM case study. Doctor of Philosophy in Leaders for Tecnological Industries of the MIT - Portugal Program, Faculdade de Engenharia da Universidade do Porto.

Tucker, C. L. and N. P. Suh (1980). "Mixing for reaction injection molding. I. Impingement mixing of liquids." Polymer Engineering & Science**20**(13): 875-886.

Udipi, K., R. S. Davé, R. L. Kruse and L. R. Stebbins (1997). "Polyamides from lactams via anionic ring-opening polymerisation: 1. Chemistry and some recent findings." Polymer**38**(4): 927-938.

Valles, E. M. and C. W. Macosko (1979). "Structure and viscosity of poly(dimethylsiloxanes) with random branches." Macromolecules**12**(3): 521-525.

van Rijswijk, K., H. E. N. Bersee, A. Beukers, S. J. Picken and A. A. van Geenen (2006). "Optimisation of anionic polyamide-6 for vacuum infusion of thermoplastic composites: Influence of polymerisation temperature on matrix properties." Polymer Testing**25**(3): 392-404.

Van Rijswijk, K., H. E. N. Bersee, W. F. Jager and S. J. Picken (2006). "Optimisation of anionic polyamide-6 for vacuum infusion of thermoplastic composites: Choice of activator and initiator." Composites Part A: Applied Science and Manufacturing**37**(6 SPEC. ISS.): 949-956.

Wang, X., Y. Li, J. Wei and K. De Groot (2002). "Development of biomimetic nano-hydroxyapatite/poly(hexamethylene adipamide) composites." Biomaterials**23**(24): 4787-4791.

Widya, T. and C. W. Macosko (2005). "Nanoclay-modified rigid polyurethane foam." Journal of Macromolecular Science - Physics**44 B**(6): 897-908.

3 Experimental techniques

In this chapter, the experimental techniques that were used in this thesis are described, namely: Rheometry, Fourier Transform Infrared with Attenuated Total Reflectance (FTIR-ATR), Diffuse Reflectance Infrared Fourier Transform Spectroscopy (DRIFTs), Differential Scanning Calorimetry (DSC) and Thermogravimetry (TG), Spray drying, Scanning Electron Microscopy (SEM) and Dynamical Mechanical Analysis (DMA) and Compression.

3.1 Rheometry

Rheometry is an experimental technique used for measurement of the rheological properties of fluids, such as viscosity, yield stress, storage and loss moduli. The model of the rheometer used for experiments in this work is Anton Paar Physica UDS200 (Universal Dynamic Spectrometer) and it is shown in Figure 3.1. This rheometer consists of the rheometer measuring drive (1), rheometer electronics (2), thermostatic bath (3) and computer with the control program(4).

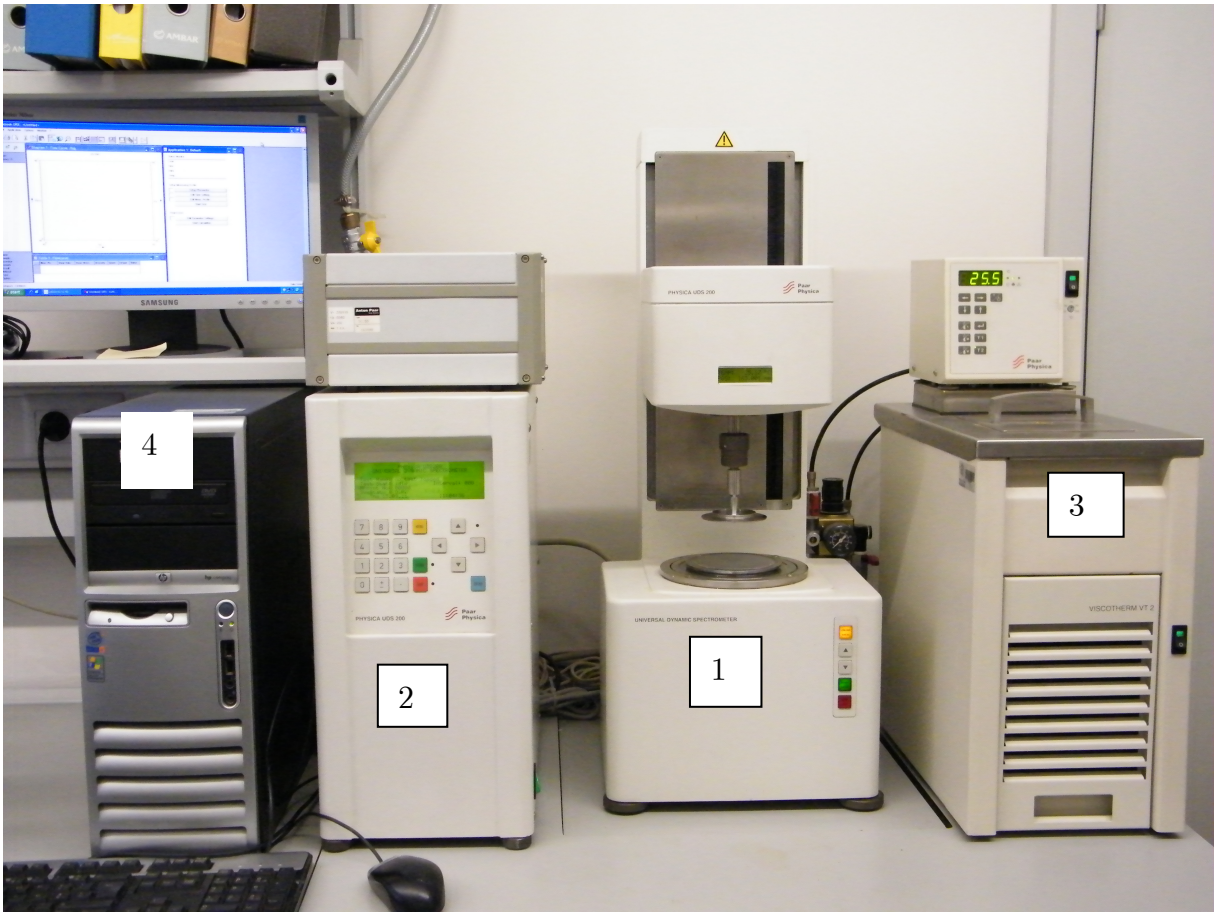

Figure 3.1. Rheometer containing computer, electronic unit, measuring unit and thermostatic bath.

Measuring system geometries that are compatible with UDS 200 are cone and plate, plate and plate, concentric cylinders. For high viscosity fluids cone/plate and plate/plate with smaller plate diameter are recommended; for very low viscosity fluids (waterlike viscosities) concentric cylinders is recommended; for suspensions plate/plate would be the best option.

Measuring system used in all experiments in this thesis was cone and plate, see Figure 3.2, with different cone diameter depending on the specific test. In this geometry the cone is the moving part and the plate is the fixed part of the measuring system of the rheometer. When performing experiments, the sample is always added onto the fixed plate, afterwards the cone is lowered to the measuring position, which can have a gap to the plate from 0.5 mm to 10 mm or more depending on the type of sample that is used. Cone and plate rheometer can be used for measurements of both Newtonian and non-Newtonian fluids, due to its constant shear rate throughout the

entire sample and direct measurement of the normal force for non-Newtonian materials. Figure 3.2 shows schematically a cone and plate geometry, where R(mm) is cone radius, $\beta(^{o})$ is cone angle, M(Nm) is torque, and Ω(rad/s) is angular velocity. The variable measured by the rheometer is torque, and rheological characteristics of the samples (such as shear stress, viscosity, storage and loss moduli etc.) are derived from the torque and geometrical parameters of the cone and plate system.

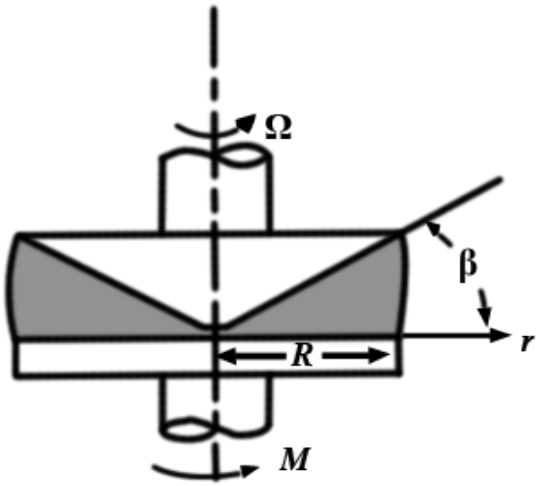

Figure 3.2. Drawing of the cone and plate geometry.

In this work two measuring cone-plate systems were used, MK22 and MK24 and the respective dimensions are presented in Table 3.1.

Table 3.1 Dimensions of the measuring cones.

	MK22	MK24
R(mm)	25	37.5
$\beta(^{o})$	1	1
V(ml)	0.7	2.2

In order to control the temperature of the sample, thermostating units may be connected to the measuring system depending on the temperature that is needed for the specific experiment. In this thesis two thermostating units were used, TEK 180 for lower temperature measurements (maximum operating temperature is 180 °C) and TEK 350 for higher temperature (up to 350 °C). TEK 180 is a heating bath that operates with a fluid that is circulated through a chamber in the plate and controls

the temperature of the plate. In this thesis water is used as fluid, enabling maximum temperature values with the TEK 180 of $95\,^{\circ}\mathrm{C}$. This unit is able to control the temperature of the plate for very thin layers of the samples, therefore it is recommended a maximum value for the cone/plate gap of $0.5\,\mathrm{mm}$.

The temperature control unit TEK 350 has two parts, plate TCS-TEK 350 and thermostat hood EHH-TEK 350. In order to control the temperature of the plate, a temperature control unit TC20 is connected to both parts of TEK 350. Inside the plate temperature is measured through a Pt100 resistance sensor and is transmitted to the temperature control unit, which is a Proportional Intergral Derivative (PID) controller. Sample temperature is the same as the hood temperature that may differ from the plate temperature. Therefore, a calibration of the temperature control unit is required.

Technical specifications of the UDS200 rheometer are: torque range $0.5\,\mu\mathrm{Nm} - 150\,\mathrm{mNm}$, torque resolution $0.1\,\mu\mathrm{Nm}$, angular resolution $< 1\,\mu\mathrm{rad}$, frequency range $10^{-4} - 100\,\mathrm{Hz}$, shear stress range $10^{-8} - 10^{50}\,\mathrm{Pa}$, shear rate range $10^{-6} - 10^{50}\,\mathrm{s}^{-1}$, viscosity range depending on the measuring system $0.5\times10^{-8} - 8.5\times10^{80}\,\mathrm{Pa.s}$.

UDS200 Paar Physica rheometer can carry out rotation (shear rate and shear stress control) and oscillation tests (strain amplitude and stress amplitude control). This means that, if the shear rate controlled mode is chosen, the set variable is the shear rate and measured property is the torque. From these two values, and using the geometry constants of the measuring system that are given by the supplier, other rheological characteristics are calculated. In the case of shear stress controlled mode, shear stress is the parameter that is set during the test. For oscillation tests, strain or stress amplitude control modes are possible, and setting parameters are strain or stress amplitude and in both modes, angular frequency is also required as a setting parameter.

Rotation tests include flow curve tests, temperature ramp, time test measurement, creep and relaxation test. Flow curve test is used in order to obtain flow properties, it is conducted in shear rate control mode defining a linear or logarithmic scale shear rate ramp. Temperature rotation test is conducted by maintaining constant shear rate in shear rate control mode and applying temperature ramp. Objective of this test is to assess the temperature dependence of the viscosity of the tested material. Time test rotation is carried out at constant shear rate and constant temperature in order to research ageing and reaction dependent changes in the sample. Creep test is conducted in shear stress control, by application of constant stress and consequent release of the stress. Creep test is used to measure elastic properties in rotation test. For structure analysis it is recommended to conduct relaxation test by applying constant deformation over a time range in shear rate control mode.

Oscillation tests include amplitude and frequency sweep, temperature ramp oscillation and time test. When the objective is to determine the linear viscoelastic range of a material it is recommended to conduct amplitude sweep test by applying constant angular frequency and setting a ramp for the deformation amplitude. This test is usually carried out in preparation for further tests, such as investigation of the structure of material. Non-destructive structure test is a frequency sweep using constant amplitude and varying angular frequency. Temperature ramp oscillation is carried out with constant oscillation parameters and temperature ramp, with the objective of determining the sample behaviour with temperature evolution, regarding the phase and structure transformations of the material. Time test oscillation is the oscillatory equivalent of the time test rotation, that is made by applying constant frequency and amplitude strain and temperature.

In this thesis, two types of formulations are used: one is a low temperature formulation, thermosetting polyurethane that is also used for nanocomposites with different nanoparticles; and the other polymer is a high temperature formulation, the, polyamide-6. The low temperature formulations were characterized using TEK 180

equipped with water bath. High temperature polyamide-6 formulation is analysed using TEK 350 due to the polymerisation temperatures that were as high as 170°C.

3.2 Infrared spectroscopy

3.2.1 Fourier Transform Infrared with Attenuated Total Reflectance

Fourier Transform Infrared (FTIR) spectroscopy is used for qualitative and quantitative measurements and it operates by measuring the absorbance of energy of the characteristic functional groups in materials. Attenuated Total Reflectance (ATR) is one of the possible accessories for infrared spectrometry, and it is used mainly for liquid samples. ATR cell consists of two pairs of mirrors that direct the infrared beam and crystal, which is used to place the sample on top of it and to reflect the beam. The crystal is placed on a metal plate and has trapezoidal shape. An ATR measures the change in energy that occurs in a totally internally reflected infrared beam, when the beam comes in contact with the sample.

Infrared radiation passes through a set of mirrors, enters into optically dense crystal at one end of the crystal, and reflects various times until it goes out of the crystal through the opposite end. This internal reflectance generates an evanescent wave, which is able to penetrate through crystal surface into the sample, which is in direct contact with the crystal surface. Sample absorbs part of the evanescent radiation, and the detector of the infrared spectrometer produces the spectra. In spectrum region where the sample absorbs energy, the evanescent wave is attenuated or altered. Resulting intensity of absorption is proportional to number of reflections (from infrared beam in crystal), for typical ATR crystals is 1-15, and it is adapted to optical scale ranging $1\mu m - 25\mu m$. In order to successfully obtain the spectrum, the following conditions are required: contact between sample and crystal must be excellent because the evanescent wave penetrates into the sample up to 0.5-5 mm; index of refraction of the crystal must be much greater than that of the sample or else internal reflectance will not happen. Detector might be one of the following: room temperature detector deuterated triglycinesulfate (DTGS) which is pyroelectric

detector that measures changes in temperature, it can provide fast response; and low temperature detector using liquid nitrogen, mercury cadmium telluride (MCT) which is a photon detector and it depends on the quantum nature of radiation.

Equipment used in this thesis is FTIR Bomem MB series machine (Quebec, Canada) represented in Figure 3.3. It consists of:

- Michelson interferometer (Model MB104) with infrared operating range from $650\text{cm}^{-1} - 4000\text{cm}^{-1}$;
- Horizontal ATR Graseby Specac cell, (Smyrna, GA, USA) with an input for inert gas purge. Silica or zinc selenide crystal may be installed;
- Graseby Specac temperature controller controlling the temperature of the crystal and sample with temperature range from room temperature up to 200°C.

Figure 3.3. Bomem (Arid-Zone) Fourier Transformation Infrared spectrometer with ATR cell.

The characteristics of some of the most common crystals for ATR cell are represented in the text below. Zinc selenide crystal is a hard, brittle and inertcrystal, it is appropriate for analysing liquids, pastes and gels. This crystal requires careful handling, and it is not recommended to work in pH range from 5-9. Transmittance range of this crystal is from $10^4\,\text{cm}^{-1}$ to $1540\,\text{cm}^{-1}$. Silica crystal is also hard, brittle

and inert crystal, also it is chemically inert. A major disadvantage of this crystal is the limited spectral range for strong absorbing bands. Silica transmittance range is from $2\times10^{4}\,\mathrm{cm}^{-1}$ to $454\,\mathrm{cm}^{-1}$.

The depth of penetration of the evanescent wave on the sample depends on the crystal, and it influences the intensity of the final spectrum and is calculated from

$$d_p = \frac{\lambda}{\left[4\pi n_1\left[\sin^2\theta - \left(\frac{n_2}{n_1}\right)^2\right]\right]^{0.5}} \qquad \textbf{(3.1)}$$

Where λ is the wavelength, θ is the incidence angle of the evanescent wave, n_1 and n_2 the refractive indices of the crystal and the sample, respectively. For the calculation of the depth of penetration, it was considered for all crystals that were used that the wavelength is $0.001\mathrm{cm}$ and the incidence angle of 90^{o}. Refractive indices of ZnSe and Si crystals are 2.4 and 3.4, respectively. Refractive index of the polyurethane sample is 1.4 (Barreiro 2000).

The calculated depth of penetration of the ZnSe crystal is $2.24\,\mu\mathrm{m}$ and of Si is $1.68\,\mu\mathrm{m}$. ATR cell with zinc selenide crystal is shown in Figure 3.4.

Figure 3.4. ATR cell with zinc selenide crystal.

In this thesis FTIR is used to perform qualitative analysis of pure and modified reactants, such as thermosetting polyurethane formulation reactants (polyol and isocyanate). No direct analyses of the kinetics of the polyurethanes reaction were performed in this work. Some of the most important absorbance bands for this work are listed as it follows. Stretching bands of hydrocarbons occur in wavenumbers region of $3300\,\mathrm{cm}^{-1} - 2800\,\mathrm{cm}^{-1}$:

- $3300\,\mathrm{cm}^{-1}$ is the characteristic band of acetylenic carbon-hydrogen bond;
- $3100\,\mathrm{cm}^{-1} - 3000\,\mathrm{cm}^{-1}$ is the region for alkene and aromatic carbon-hydrogen structures;
- $3000\,\mathrm{cm}^{-1} - 2850\,\mathrm{cm}^{-1}$ is the region where aliphatic carbon-hydrogen stretching bands occur;
- $2900\,\mathrm{cm}^{-1}$ and $2700\,\mathrm{cm}^{-1}$ are two sharp adsorption bands characteristic for aldehydes.

Triple bonds and other limited types of functional groups have bands in the range of $2700\mathrm{cm}^{-1}$ - $1850\mathrm{cm}^{-1}$:

- $2260\,\mathrm{cm}^{-1} - 2100\,\mathrm{cm}^{-1}$ is the region for triple carbon-carbon covalent bond;
- $2260\,\mathrm{cm}^{-1} - 2220\,\mathrm{cm}^{-1}$ is the characteristic region for double carbon-nitrogen bond;
- $2260\,\mathrm{cm}^{-1}$ is the characteristic band for triple nitrogen-nitrogen bond;
- $2000\,\mathrm{cm}^{-1} - 1900\,\mathrm{cm}^{-1}$ is the region for triple carbon atoms bonded with two double covalent bonds structure.

Variety of double-bonded functional groups has adsorption bands in region $1950\,\mathrm{cm}^{-1} - 1450\,\mathrm{cm}^{-1}$:

- $1870\,\mathrm{cm}^{-1} - 1550\,\mathrm{cm}^{-1}$ the characteristic region for carbonyl group carbon-oxygen double bond vibration;

- $1850\,\mathrm{cm}^{-1} - 1750\,\mathrm{cm}^{-1}$ is the region for acid chlorides and acid anhydrides;
- $1750\,\mathrm{cm}^{-1} - 1650\,\mathrm{cm}^{-1}$ is the region for aldehydes, ketones, carboxylic acids, amides and esters;
- $1610\,\mathrm{cm}^{-1} - 1550\,\mathrm{cm}^{-1}$ and $1420\,\mathrm{cm}^{-1} - 1300\,\mathrm{cm}^{-1}$ for carboxylate ions.

The region $600\,\mathrm{cm}^{-1} - 1600\,\mathrm{cm}^{-1}$ is the typical peaks pattern for each compound and it is called the fingerprint region.

Shifts in absorption frequencies may appear if some of the following effects exist: non-conjugated aliphatic bonds double carbon-carbon bonds and double carbon-nitrogen show vibrations in $1690\,\mathrm{cm}^{-1} - 1620\,\mathrm{cm}^{-1}$ region; aromatic compounds show strong vibrations in $1650\,\mathrm{cm}^{-1} - 1400\,\mathrm{cm}^{-1}$ and weak in $2000\,\mathrm{cm}^{-1} - 1650\,\mathrm{cm}^{-1}$ region; molecules containing nitro group show vibrations in the wavenumber ranges $1660\,\mathrm{cm}^{-1} - 1500\,\mathrm{cm}^{-1}$ and $1390\,\mathrm{cm}^{-1} - 1260\,\mathrm{cm}^{-1}$. Hydrogen bonding shows adsorption bands for stretching vibrations in the region of $4000\,\mathrm{cm}^{-1} - 2500\,\mathrm{cm}^{-1}$; carboxyl and amide hydrogen bonding adsorption bands appear in $3700\,\mathrm{cm}^{-1} - 2500\,\mathrm{cm}^{-1}$ region. Additionally, hydrogen bonds tend to broaden the peaks.

3.2.2 Diffuse Reflectance Infrared Fourier Transform Spectroscopy

Diffuse Reflectance Infrared Fourier Transform Spectroscopy (DRIFTs) is typically used for powder samples. In general sample preparation is not needed, although if the sample shows high absorptivity it should be diluted with some non-absorbent materials such as potassium bromide (KBr) or potassium chloride (KCl). Equipment used in this thesis was FTIR Nicolet 510-P equipped with a DRIFT accessory from Spectratech.

Data obtained from DRIFTs analysis is usually plotted as Kubelka-Munk function versus wavelength of infrared light. Kubelka-Munk, $F(R)$ is directly proportional to the absorbance of the sample and is calculated from

$$F(R) = \frac{(1 - R)^2}{2R} = \frac{k}{s}\frac{Ac}{s} \quad \textbf{(3.2)}$$

where R is the reflectance, k is the absorption coefficient, A is sample absorbance, c is sample concentration and s is scattering coefficient.

3.3 Differential Scanning Calorimetry and Thermogravimetric Analysis

Differential Scanning Calorimetry (DSC) is a thermal technique based on the principle of measuring the difference in the amount of heat absorbed by the sample and reference sample as a function of temperature. Reference sample should have well defined thermal capacity. DSC is used to measure different physical and chemical properties of materials such as specific heat, transition enthalpies, melting and crystallisation temperatures, glass transition temperature and specific capacity, degree of crystallinity, decomposition effect, thermokinetics and phase transformations and diagrams.

Thermogravimetry (TG) is the method used for measurement of the weight loss of the sample during heating. Materials properties such as thermal stability, decomposition, dehydration, oxidation, volatile compounds determination etc. are obtained with TG.

Combining DSC and TG technique into one technique and one equipment it is possible simultaneously to measure the heat absorption and weight loss of the sample. Equipment used in this thesis was STA 490 PC Luxx Netzsch thermal analyser at the Laboratory of Catalysis and Materials (LCM) at the University of Porto. In this thesis DSC-TG is used in order to measure samples mass loss, and therefore calculate the evaporated quantity of the water and EG. The samples were heated in a nitrogen flow from 50 °C to 400 °C at the heating range of 5 °C/min.

3.4 Spray drying

Spray drying is used to dry aqueous or organic solutions, dispersions, emulsions etc. In order to obtain dried powder, liquid solution/dispersion feed is sprayed into a hot drying medium, which is generally air. After the drying, resultant powder has a reduced weight and volume. Spray drying of HAp dispersions was performed on a BÜCCHI Mini Spray Dryer B-290 equipment, which is shown in Figure 3.5. The inlet feed enters the equipment through the tube (1) and flows into the drying chamber (2) where the suspension feed meets the hot air. The dried powder is collected in a recipient (3), and the solution is collected in another recipient (4).

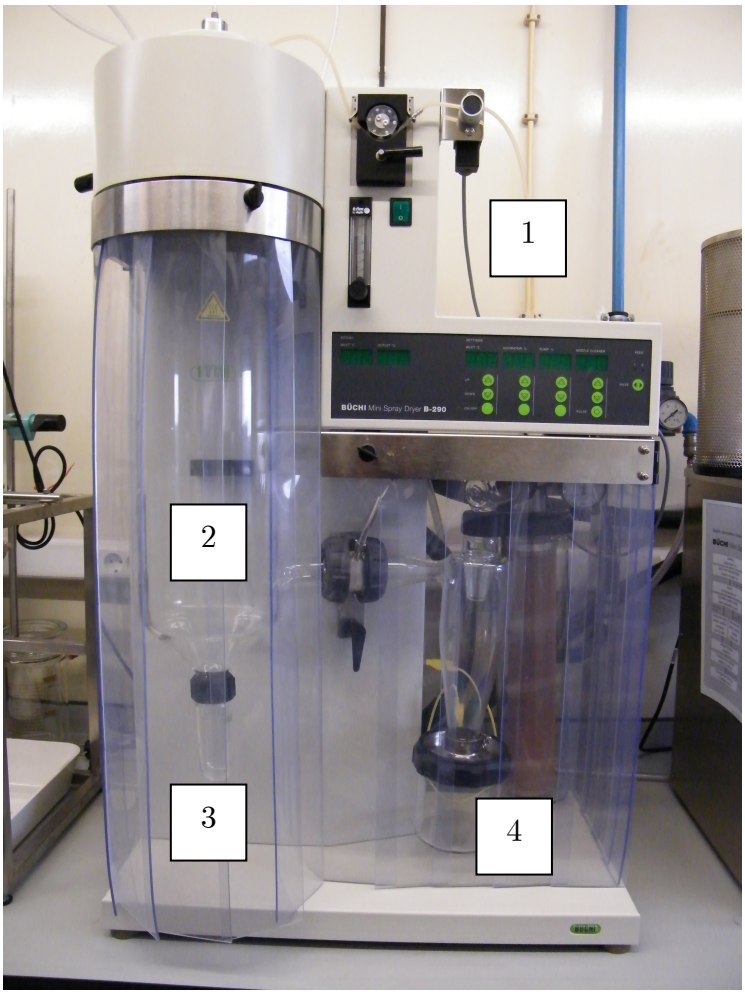

Figure 3.5. BÜCCHI Mini Spray Dryer B-290.

3.5 Scanning Electron Microscopy

In order to obtain high-resolution images of polymeric nanocomposites samples Scanning Electron Microscopy (SEM) was used. In this technique electrons generated by electron gun of the equipment interact with atoms in the sample and produce different signals that can be detected by detectors. SEM gives information about topography, which is sample surface and composition.

In this thesis two models of SEM were used: Quanta and Phenom G2 Pro. Quanta model have two types of electron detectors, Large Field Detector (LFD) and Backscattered Electron Detector (BSED), and X-ray detector Energy Dispersive spectrometer (EDS) that is used for elemental analysis of the samples. LFD is used in low vacuum for detection of the secondary, high-energy electrons. BSED is used for detection of the backscattered, low energy electrons (10-50 eV) and it enables topographic images. EDS is used in order to obtain total collected X-ray spectrum, with fingerprint peak signals of each element in the sample. This SEM model operates at three electron accelerating voltages $5.00\,\mathrm{kV}$, $10.00\,\mathrm{kV}$ and $15.00\,\mathrm{kV}$. To obtain images of the samples in this thesis was used a Jeol JSM 6301F microscope with Oxford Inca Energy 350 energy dispersive X-ray system at CEMUP – Centro de Materiais da Universidade do Porto. All the samples were treated with gold for 200 seconds in order to avoid the accumulation of electrical charges and after that were fixed with a carbon tape to a metallic holder.

The Phenom G2 Pro SEM is equipped with two imaging modes, light optical with magnification in the range of $20-120\,\mathrm{times}$, and electron optical with magnification ranging 80 – 450 000 times. Electron optical illumination is long lifetime thermionic source, with acceleration voltage $5.00\,\mathrm{kV}$ and resolution $25\,\mathrm{nm}$. Detector used is high-sensitivity backscattered electron detector, which enables the composition determination and topographical modes. Maximum diameter of the sample is $25\,\mathrm{mm}$ and maximum height $30\,\mathrm{mm}$, and sample loading time is less than $30\,\mathrm{seconds}$. The Phenom equipment used in this work is shown in Figure 3.6. It is compact equipment

containing the electronic microscope unit (1), a computer (2) and a vacuum pump (not shown in this figure).

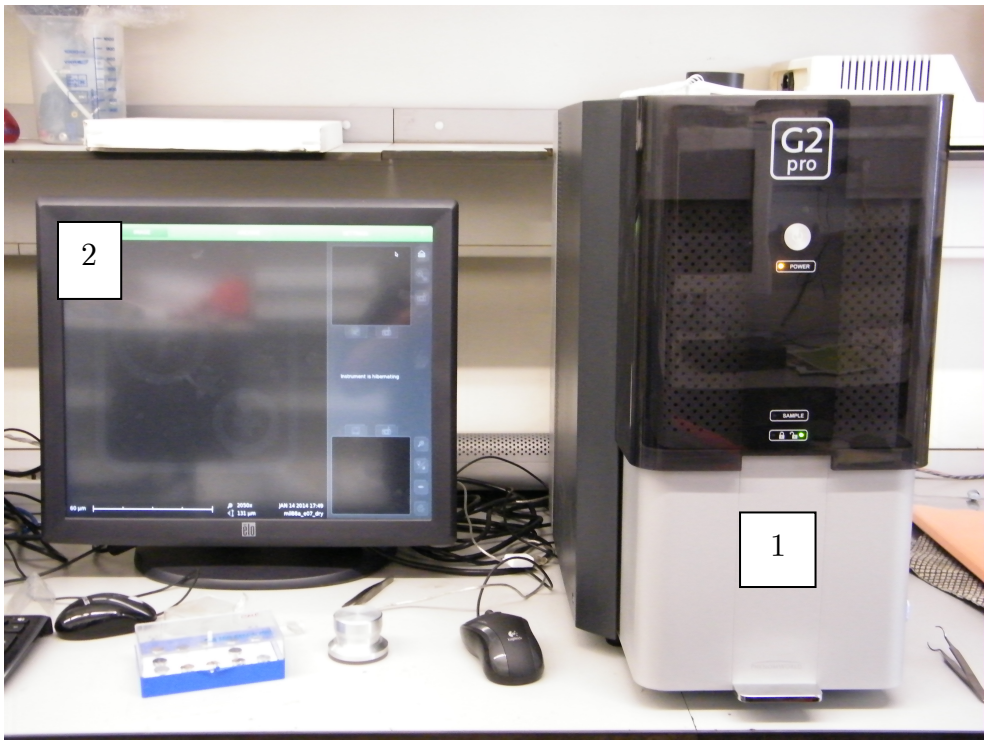

Figure 3.6. Phenom G2 pro Scanning Electron Microscope.

3.6 Mechanical Analysis

Mechanical properties of polymeric products were determined by Dynamical Mechanical Analysis (DMA) and compression tests. DMA tests were performed to measure the deflection temperature using Dynamic Mechanical Analyzer, model Tritec 2000, Triton at the Polytechnic Institute of Leiria. Deformation mode was single cantilever bending; experiment test was time/temperature scan; using single frequency mode and frequency was set to 1Hz. Total experiment duration was 90 min, temperature ramp rate 2°C / min, starting temperature 20°C, ending temperature 200°C. Compression tests were performed on a Zwick model Z100 DMA equipment (see Figure 3.7) with the aid of the compressive strength unit (see Figure 3.8) at the Polytechnic Institute of Leiria. All the samples had dimensions of $10 \times 4 \times 4$ mm.

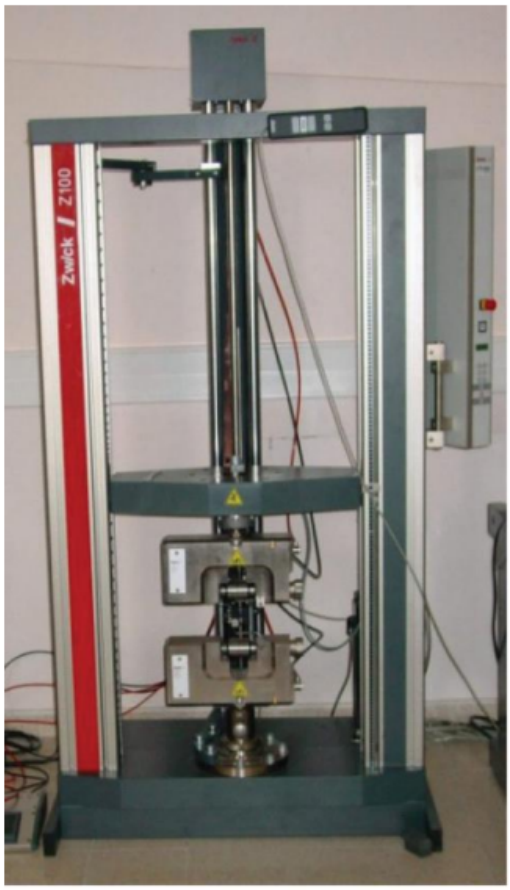

Figure 3.7. Zwick model Z100 DMA.

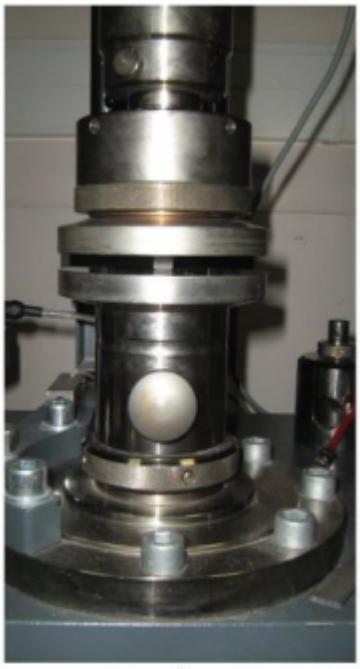

Figure 3.8. Compressive strenght test.

4 Polyurethanes product development by rheometry

4.1 Introduction

The formation of polyurethanes is characterised by a huge change of the viscosity of a reactive mixture of monomers. This reactive mixture generally consists of two components, formulated and prepolymerised polyol and thermally modified or oligomerized isocyanate, but this can vary depending on the formulation. Reactants of most industrial formulations have viscosities of order of magnitude of $0.3\,\mathrm{Pa.s} - 0.4\,\mathrm{Pa.s}$ for isocyanate and $1\,\mathrm{Pa.s} - 2\,\mathrm{Pa.s}$ for polyol. From the relatively low initial values, the viscosity changes approximately 10^5 times in few minutes to viscosity values around $10^5\,\mathrm{Pa.s}$ while polymerisation takes place. Monitoring the viscosity rise of the reactive mixture at a rheometer is therefore a useful tool for the prediction of the demoulding time in RIM processes, as well as for the measurement of the gel time of the formulation. In the rheometer it is also possible to produce a solid sample under very controlled mixing conditions that can be afterwards used in mechanical tests.

This chapter introduces an experimental method based on the use of a rotational rheometer with cone and plate geometry, that enables the measurement of the

viscosity rise, gel time and determination of the rheological behaviour during the polymerisation of a polyurethane. Several mechanical properties are measured in the samples produced with the rheometer, such as compressive strength and deflection temperature. Rheological experiments are performed using different sets or parameters for rotational and oscillatory tests. Two different methods for premixing the monomers are also presented and from this it is assessed the effect of mixing.

4.2 Methods and experimental set up

4.2.1 Formulation and reactants preparation

Commercial Huntsman formulation of polyurethanes RenCast© FC 52 Isocyanate / FC 52 Polyol was used in this work. From now on these reactants are referred to as isocyanate and polyol. This formulation is specified as a casting resin and quick setting polyurethane system. Recommended mixing ratio is 100:100 w/w (Huntsman 2007). In Table 4.1 are represented some of the most important properties of the reactants for this study: viscosity and density at $25\,^{\circ}\mathrm{C}$ (Huntsman 2007). These values were measured in the rheometer using the following experimental conditions: constant shear rate of $100\,\mathrm{s}^{-1}$ and test duration $100\,\mathrm{s}$.

Table 4.1. Pysical properties at 25°C of RenCast© reactants.

Reactant	Viscosity $\left[\mathrm{mPa.s}\right]$	Density $\left[\mathrm{g/cm^3}\right]$
Polyol	65	0.98
Isocyanate	20	1.12

Datasheet of the polyol indicates that this is a formulated polyol containing $5-15\%$ petroleum distillates, $5-15\%$ ethylene diamine propoxylated, $1-10\%$ terphenyl hydrogenated and $0.1-1\%$ terphenyl (Huntsman 2007). Other information on chemical composition of formulated polyol is not specified in the datasheet. Isocyanate prepolymer consists of: $30-60\%$ diphenylmethane diisocyanate (isomers and homologues), $13-30\%$ o-(p-isocyanatobenzyl)phenylisocyanate, $13-30\%$ 4,4' – methylenediphenyl diisocyanate, $7-13\%$ terphenyl and $0.1-1\%$ hydrogenated terphenyl (Huntsman 2011).

In order to determine the chemical composition of both reactants, FTIR measurements were made with an ATR cell having a ZnSe crystal. The analysis of the polyol and isocyanate were made at room temperature. The background scanning with nitrogen purge was carried out in the first phase and afterwards the sample was added onto the ATR crystal and the scanning started. Wavelength resolution used was $4\,\mathrm{cm}^{-1}$, and the scanning was repeated three times for each reactant. Figure 4.1 shows the polyol spectrum of the transmittance versus wavenumber.

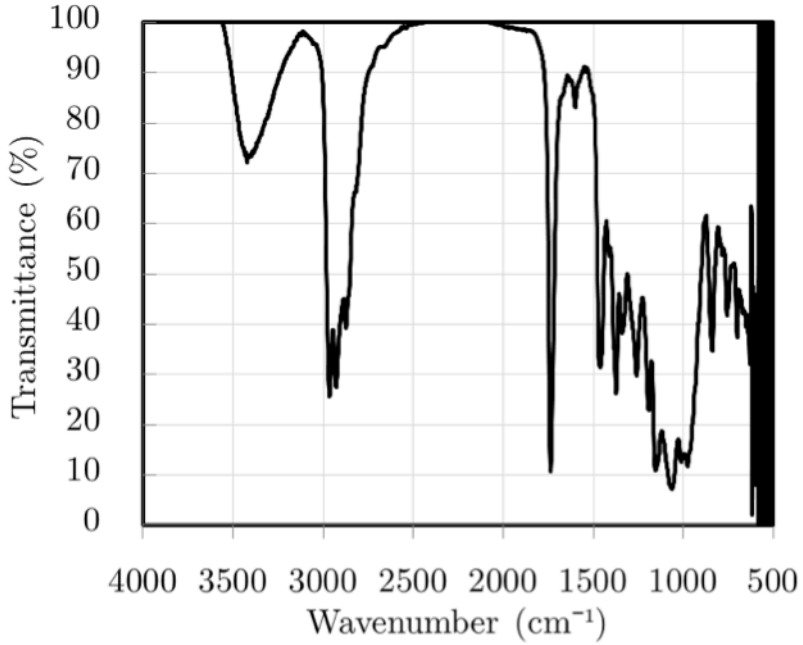

Figure 4.1. FTIR spectrum of a polyol sample.

Looking at the spectrum in Figure 4.1, four characteristic peaks may be identified:

- Broad peak in the region $3100-3500\,\mathrm{cm}^{-1}$ that are related with hydroxyl and also amine groups;
- Double sharp peaks at $2800-3000\,\mathrm{cm}^{-1}$ identify saturated hydrocarbon chain;
- Sharp peak at approx. $1750\,\mathrm{cm}^{-1}$ is typically assigned to C=O groups (aldehydes, ketones, esters, carboxylic acids or amides); since this is a polyol and in polyurethane formulations it is known that polyol may typically be ether or ester based, this peak indicates the existence of an ester;

- Broad peaks made of some sharper peaks, in the region of $500-1500\,\mathrm{cm}^{-1}$, are the fingerprint of the specific compound.

Isocyanate spectrum is represented in Figure 4.2 where transmittance versus wavenumber is plotted.

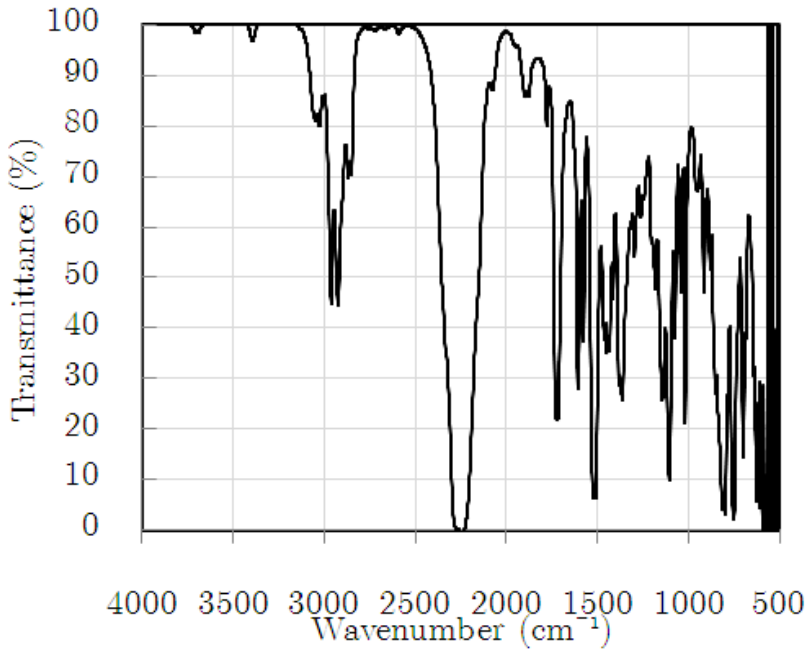

Figure 4.2. FTIR spectrum of an isocyanate sample.

Analysing the peaks in Figure 4.2 it can be observed:

- Two sharp peaks at $2900-3000\,\mathrm{cm}^{-1}$ that are assigned to aliphatic C-H stretching bands;
- Long and relatively broad peak at around $2250\,\mathrm{cm}^{-1}$ that is typical for the isocynate group N=C=O;
- Many sharp peaks in the region $600-700\,\mathrm{cm}^{-1}$, which are assigned to fingerprint region of this isocyanate.

After the analysis of the power spectra it is concluded that:

- This polyol is ester type, which is confirmed by the presence of the sharp peak at $1750\,\mathrm{cm}^{-1}$ characteristic for carboxyl group;

- Polyol has saturated hydrocarbon chain(s);
- Isocyanate contains aliphatic hydrocarbon chain(s).

Before conducting experiments the reactants were pre-treated with nitrogen and heated. In Figure 4.3 is represented the polyol after agitation, and after settling. When agitated the polyol is white and has a milky aspect, and after settling two distinguishable phases are observed, a white precipitate in the bottom of the bottle and a clear bright yellow phase on the top of the bottle. In the experimental work, in order to avoid the settling of the solid content, the polyol was always agitated with a magnetic stirrer before every experiment. Furthermore, the polyol was treated with a nitrogen stream that was introduced through the bottom of the bottle during 15 min in the beginning of each experimental set. The nitrogen stream flushes any moist from the air and avoids possible reactions with the isocyanate.

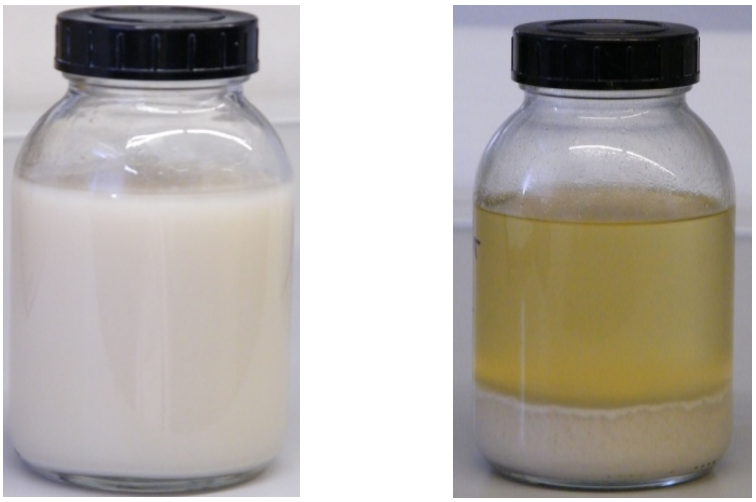

(a) (b)

Figure 4.3. Physical aspect of the polyol: (a) homogenised, (b) settled.

Figure 4.4 (a) shows a sample of isocyanate just taken off the bottle that is characterised by a clear, bright yellow colour, and (b) shows an isocyanate which underwent some self-condensation reaction and its colour turned into opaque yellow. This opaque yellow coloured sample was heated and then the clear appearance was regained. This opaque colour is characteristic of formation of dimer that dissociates at higher temperatures. When doing experiments special attention was paid to the

preparation of isocyanate. Experiments at 25 °C involved using small quantities of freshly open reactant with clear, bright yellow colour. Experiments at 40 °C involved heating the isocyanate on a hot plate so it had a clear physical aspect before every experiment.

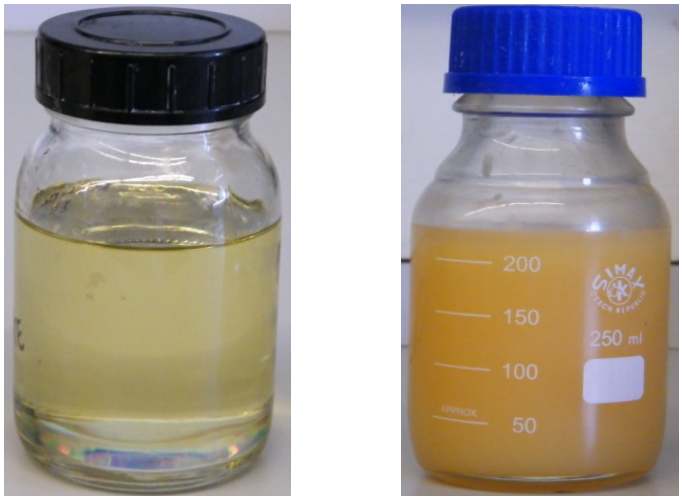

(a) (b)

Figure 4.4. Isocyanate physical aspect: (a) new or heated, (b) with dimer formation.

The effect of the reactant pre-treatment on the viscosity rise during the reactive mixing of polyol and isocyanate at 25 °C is represented in Figure 4.5. This experiment was conducted in a rotational rheometer (premixing interval 100 s at shear rate of $500\,s^{-1}$ and reaction rotation interval at $100\,s^{-1}$) at 25 °C. Three samples of reactive mixture were tested:

- *Dimer* reactive mixture sample, where the isocyanate was in previous contact with air and polyol was not agitated nor treated with a nitrogen stream;
- *New reactants* sample, which means that the isocyanate was from a newly opened package and polyol was not agitated nor treated with nitrogen;
- *Nitrogen* reactive mixture sample, where the isocyanate is from a newly opened package and the polyol was agitated and treated with nitrogen for 30 min before the experiment.

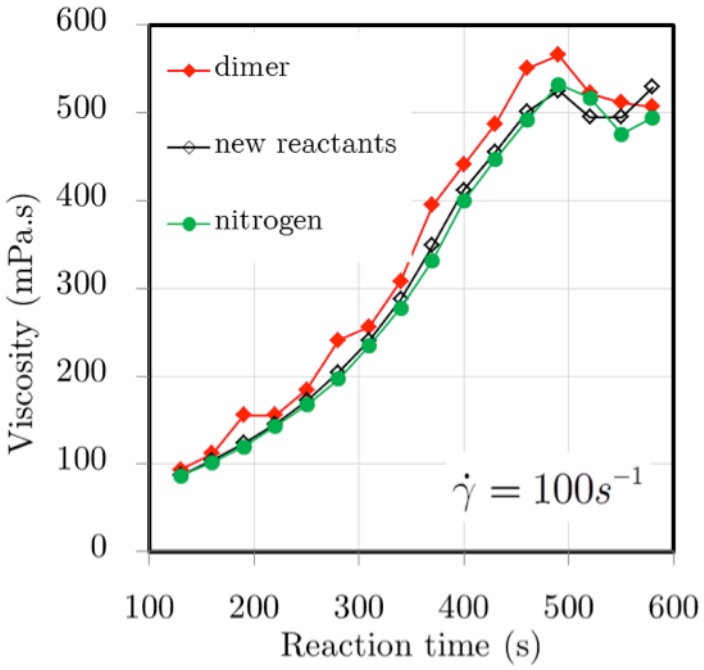

Figure 4.5. Viscosity rise of the reactive mixture of polyol and isocyanate.

In Figure 4.5 is seen that the viscosity rise is slightly faster for the *Dimer* sample and the slower for the *Nitrogen* sample. In the *Nitrogen* sample, reaction between the moisture from air present in polyol and isocyanate that could result in formation of urea and/or bubble appearance from formation of carbon dioxide is reduced because of the treatment with nitrogen. Occurrence of this reaction could give a rise in viscosity due to the rise in molecular weight. That is why the viscosity rise is slower for *nitrogen* sample than for *new reactants* sample. *Dimer* sample has the fastest viscosity rise because the molecular weight of polyurethane grows faster in the presence of the dimer that enables branching reactions, which also increase the final molecular weight.

4.2.2 Experimental set-up

Experimental set-up is shown in Figure 3.1 and consisted of the rheometer measuring drive (1), rheometer electronics module (2), thermostatic bath (3) and computer (4). Measuring drive is equipped with different measuring systems, and in the following experiments the system that was used was the cone and plate, where the cone has a

diameter of 50 mm and an angle of 1° and the plate was connected to the thermostating unit TEK 180, which used water as the working fluid.

Measuring gap, which is the distance between the centre of the cone and the plate in the rheometer during measurements was different depending on the objective of the test:

- Measurements of the rheological characteristics of the material, the measuring gap was set to 50 μm ;
- Experiments with objective to produce the solid sample to be tested mechanically afterwards, the measuring gap was set to 8 mm.

Two different combinations of the cone and plate system were used in order to enable two different premixing methods of the reactants:

- Simple cone and plate – where reactants were placed one on the top of the other; the method based on this configuration is called hereafter One Top Other (OTO) method.
- Cone and plate with the holding cell – where the reactants were placed in separate compartments; the method based on this configuration is called hereafter the Holding Cell (HC) method.

Figure 4.6 represents the simple cone (1) and plate (2) measuring system that is used for the OTO method. The sample of the two reactants on top of each other is placed in the center of the plate, after the measuring cone is lowered over the plate until it reaches a distance from the plate corresponding to the value of the measuring gap that is set in the rheometer control program. After the test starts with the rotation of the cone the shearing of the cone will mix the two fluids in the sample.

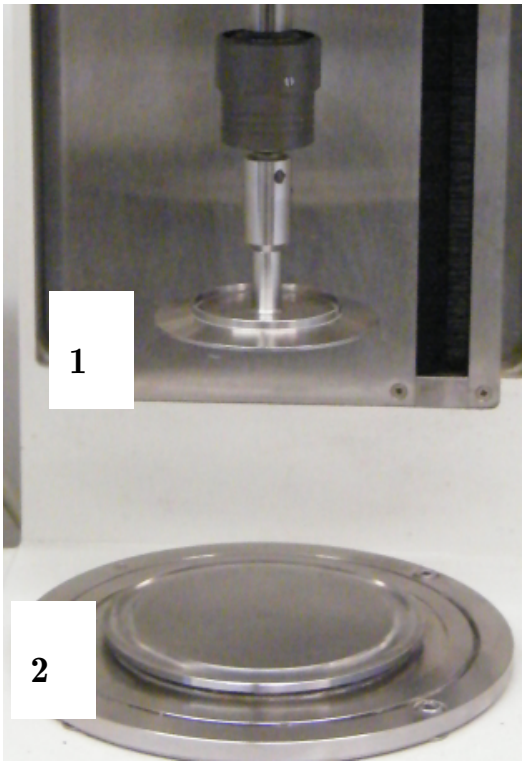

Figure 4.6. Photo of the cone and plate geometry. 1 – Cone; 2 – Plate.

The HC method requires some modifications of the measuring system described for the OTO method. Cone and plate measuring system with the holding cell is shown in Figure 4.7 where the holding cell (1) is placed on the top of the plate (2) by the aid of three guiding screws (3) the cell is placed concentrically with the plate and the cone (4). The holding cell has a separator so the fluids are placed segregatedly. Both the cell and the separator are made of stainless steel. Before the cone is placed in the measuring position and in order to successfully place the reactants onto the plate, the separator is adjusted into the holding cell as represented in Figure 4.8, where it can be observed: the holding cell (1) and the separator (2).

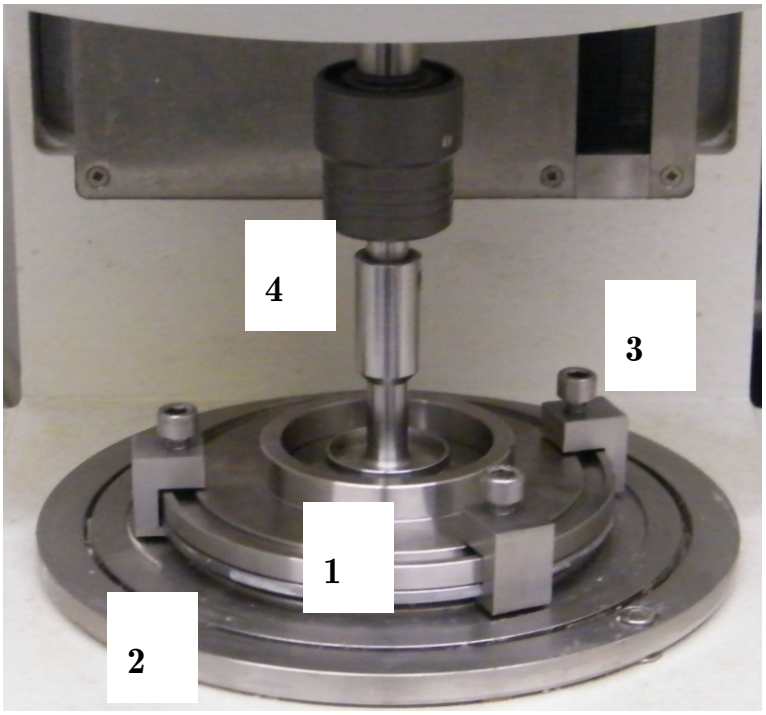

Figure 4.7. The holding cell with cone at the measuring position. 1 – The holding cell; 2 – Plate; 3 – Screws; 4 – Cone.

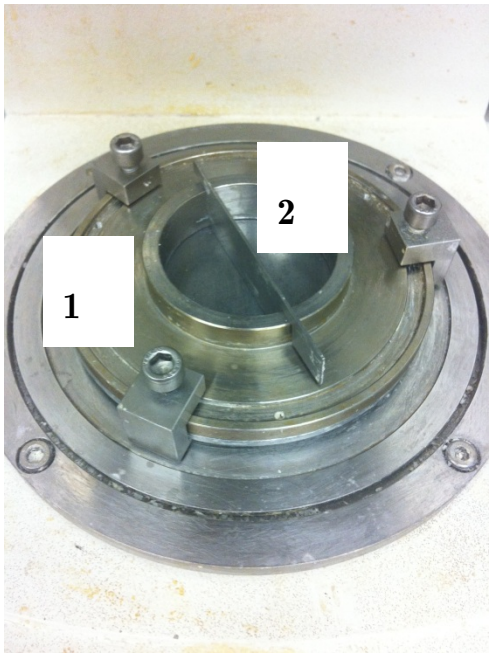

Figure 4.8. The holding cell with the separator. 1 – The holding cell; 2 – Separator.

4.2.3 Experimental method

Two methods of contacting the reactants in the plate for premixing, were developed:

- The OTO (one top other) method, using simple cone and plate set-up;

- The HC (holding cell) method, using the holding cell set-up.

In rheological experiments with the RenCast reactive mixture, the two reactants were only mixed in the rheometer plate few seconds before the actual rheological test starts. By this way rheological experiment had two functions: to mix the reactants and to measure the evolution of rheological properties with reaction, which was consequently divided into two test intervals, premixing and reaction interval. This way of premixing of the reactants was chosen in order to be able to control the mixing. Alternative method of premixing would be stirring both reactants in a cup. This method proved to cause much higher variation of the experimental results on the sequent rheological tests than premixing at the rheometer.

First premixing method OTO was developed throughout this work and it involved the following steps shown in Figure 4.9:

- Lay the polyol over the rheometer plate using a piston pipette and slowly place the isocyanate exactly in the centre of the polyol sample(a);
- Placing the cone in the measuring position, on the top of the reactive mixture (b). Looking at the reactive mixture, it is clear that after putting the isocyanate on the polyol, there is the appearance of white concentric circles of the isocyanate that propagate from the centre to the outside border although they do not completely reach the outside border;
- Start of the test.

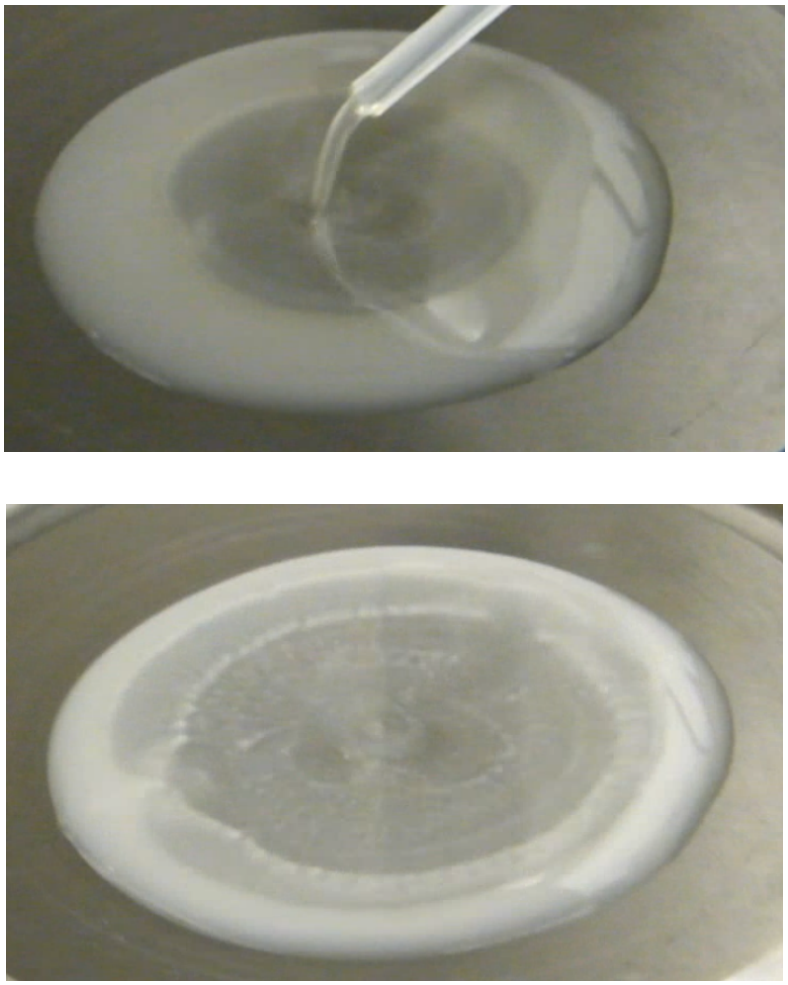

(a)

(b)

Figure 4.9. OTO sample: (a) addition of the isocyanate onto the top of the polyol and (b) reactive mixture.

The HC method involved a physical limit outside the sample, and the physical separation between the two reactants at the time of their placement onto the plate. This method consists on the next steps:

- Place the holding cell to the correct position using the guiding screws and with the separator adjusted;
- Place the stoichiometric amount of the reactants to each of the compartments of the holding cell;
- Simultaneously place the cone in the measuring position and takeaway the separator;
- Start the test.

Figure 4.10 represents the opening inside the holding cell with the separator in the middle of it, and two reactants placed each one in a separate compartment, isocyanate (1) and polyol (2).

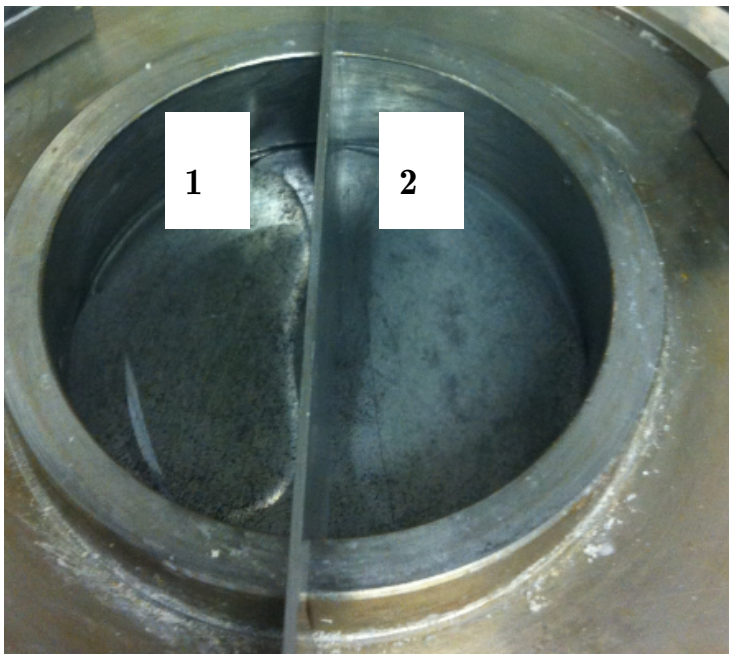

Figure 4.10. The HC: polyol and isocyanate separated by the separator. 1 – Isocyanate; 2 – Polyol.

4.3 Experiments

The objective of this study was to assess the effect of mixing conditions by measuring the evolution of rheological properties of the reactive mixture, in particular viscosity rise and the gel time and correlating them to the initial mixing conditions. This study also aims at assessing the usage of rheology to define the set of parameters in a RIM machine for the processing of a reactive polymer, generally thermosets.

For this end, the reactive formulation chosen was a thermosetting polyurethane from Huntsman with commercial name RenCast FC52 having pot life of 6 – 8 minutes at 25 °C and consisting of two preformulated reactants each having viscosity less than 100 mPa.s at 25 °C. These properties enabled to successfully conduct the rheometry experiments at temperatures as low as 25 °C and 40 °C to obtain the viscosity rise, gel time and polymerised solid product.

The major concern in this study was to control the mixing of the two reactants because the reaction kinetics is fast and final product properties highly depend on the mixing. Once the control of mixing was successful the same mixing conditions can be applied on the viscosity rise and gel time measurements in order for them to be comparable. Therefore it was decided to design the experimental interval with the objective to mix and control the mixing of the two reactants. This interval is called the premixing interval. The second interval is specifically designed to measure the rheological properties of the reacting mixture, and it is called the reaction interval. In this thesis premixing interval was always carried out in rotation mode, while the reaction interval was carried out in rotation, to assess the viscosity rise, or in oscillation mode, to assess the gel time.

For the premixing interval rotation test was chosen because the interfacial area between the two reactants increases with every rotation of the cone. When the interfacial area is large, the laminas of the two reactants are thin enough for the reactants molecules to diffuse into one another and by this way ensuring the conditions for the polymerisation to be only controlled by the reaction kinetics without being limited by mass transfer rate. With the polymerisation onset, polymeric chains start to form and grow, subsequently leading to the formation of the network, which is followed by an increase in molecular weight and therefore viscosity. The parameters for the premixing interval (shear rate and duration) and their effect on viscosity rise are assessed and described next. First, the gel time of the formulation at the specific temperature is estimated from the oscillation test. In the following, different effects on the gel time at the same chosen temperature are estimated from the experiments, such as: the effect of the premixing shear rate, angular frequency of the oscillation test interval and the temperature effect.

The experiments are divided into the following groups:

1) Viscosity rise measurement:
    1.a) Reaction shear rate effect;
    1.b) Premixing duration effect;

2) Gel time estimation:
   2.a) Premixing shear rate effect;
   2.b) Premixing duration effect;
3) Rheological behaviour:
   3.a) Premixing shear rate effect;
   3.b) Premixing time effect.

Table 4.2 has a summary of the experimental conditions. Detailed experimental conditions for each experiment are presented in the following sub-chapters.

Table 4.2. Summary of experimental conditions for the rheometry tests.

	Viscosity rise	Gel time	Rheological behaviour
Shear rate effect	$1, 50, 100, 500, 1000$ and $3000\ s^{-1}$ *	100, 500, and $1000\ s^{-1}$ **	1^o range: $1-100\ s^{-1}$ *** 2^o range: $100-3000\ s^{-1}$ ***
Premixing duration effect	10, 50 and 100 s	10, 50 and 100 s	10, 50 and 100 s

* constant shear rate in reaction interval;
** constant shear rate in premixing interval;
*** shear rate range with logarithmic increase, without the premixing interval.

4.3.1 The end of experiment

The end of rheometry experiments was established experimentally, when one of the three phenomena occurred:

- Maximum torque ($150\,mN.m$) is reached;
- Sharp decrease in the torque occurs;
- An experimental value of viscosity for rotation or complex viscosity and elastic modulus for oscillation is reached. In rotation tests, the set viscosity value is reached and in oscillation tests the complex viscosity and/or optimal elastic modulus are reached. These values of viscosity/complex viscosity/elastic

modulus are determined experimentally, and set the time for the end of the test, due to:

- Rotation test: for shear rate of $1 s^{-1}$, as a general rule edge fracture does not occur, therefore viscosity could rise infinitely. However, in order to make it possible or easier to clean the polymerised sample from the rheometer plate it is useful to stop the experiment before a very adhesive solid is formed. This point is experimentally determined, and is assumed to occur at a viscosity of 250 Pa.s. This rule does not apply to higher shear rates, due to the appearance of the edge fracture, which terminates the experiment.
- Oscillation test: the objective of the oscillation tests is to determine the gel point and to assess the evolution of the storage and loss moduli over time. Furthermore, some oscillation tests are used to produce solid samples for mechanical tests; in this case the test should be stopped before the solid sample gets to sticky to the plate and cone, in order to avoid damaging the rheometer plate and cone by the demoulding/cleaning operations.

Measuring rheological characteristics during the reactive polymerisation depends on the maximum value of the torque of the instrument. Polymerisation of the reactive mixture is followed by the increase in molecular weight and increase in the resistance of the monomers mixture to the deformation imposed by the cone. As the reaction continues, higher torque is needed to deform the reacting sample. Other rheological properties of the sample (such as viscosity, complex viscosity, elastic modulus etc.) are calculated from the measured torque and geometrical constants of the measuring system. Rheometry experiments are conducted by setting constant shear rate/shear stress/angular frequency/strain depending on the type of the experiment. However, when the maximum torque is reached, the parameter set to a constant value starts to decrease as a consequence of the permanent increase in the resistance of the sample to deformation of the mixture.

In rotation experiments a common phenomenon that occurs is the edge fracture. This is explained as the breakdown of the sample at its edges and consequent expelling of the lost sample mass outside the cone and it is shown in Figure 4.11 from the white circle of reacting material that is seen around the cone. The concentric circle of material has 3 - 4 mm and is visible both on the top and at the edge of the cone showing that some part of the sample was expelled to outside the measuring gap.

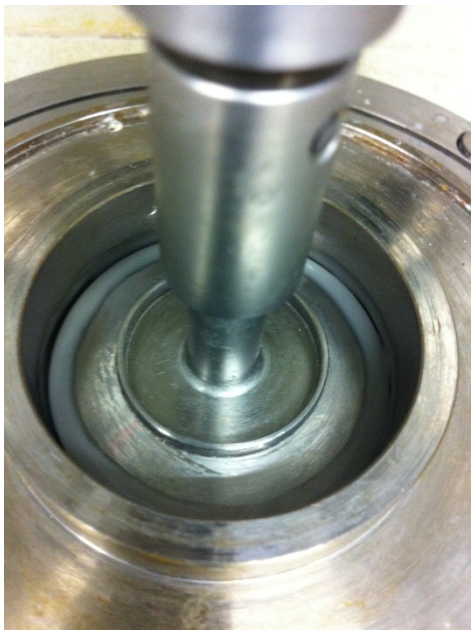

Figure 4.11. The edge fracture of the sample in the holding cell.

The edge fracture is often associated to a sharp decrease of the measured torque and of the sample viscosity. In rotation tests, even if the maximum torque has not been achieved, the point when the viscosity starts to decrease is taken as the end of the experiment. It is reported in literature that edge fracture usually occurs at low shear rates (Macosko 1994), but it also may occur at higher and critical shear rates as will be presented later in this chapter.

When the objective of the experiment is to obtain solid polyurethane sample with sufficient mechanical resistance to demould it without fracturing the sample, maximum torque value may be ignored and the end of experiment is the point where elastic modulus and complex viscosity are in a specified range. This range is experimentally determined for the elastic modulus to be $2000-3000\,\mathrm{kPa}$ and for the

complex viscosity it is $50-70\,\mathrm{kPa.s}$. Below this range, the sample may not be mechanically resistant and it may fracture easily by demoulding. Above this range, the sample may stick to the cone or the plate and demoulding can be rather difficult. Besides the laborious demoulding, leaving the sample at the rheometer for a longer period is not necessary, because the sample viscosity rapidly increases to out of the rheometer measuring range, and furthermore curing in reactive polymerisations occurs in moulds where shearing stops after the mould filling.

4.4 Viscosity rise

4.4.1 No premixing on OTO method

Since control of mixing of the reactants was very important for this study, and in order to be able to correlate rotation and oscillation results, unique premixing interval is designed and applied to both rotation and oscillation experiments as previously described. However, it was also relevant to study material behaviour without the premixing interval and compare with the cases where the sample undergone a premixing period. For that purpose, viscosity rise was measured in the rheometer under shear mixing caused by the cone rotation, but without previous premixing. Reactants were joined and stirred by magnetic stirrer for 30 s in a disposable plastic cup and the reactive mixture was then immediately transferred to the rheometer by a disposable pipette and after the test started.

In these experiments cone and plate geometry was used, cone diameter is 75 mm and the angle is 1°, recommended sample volume for this cone diameter is 2.1 ml. Polyol and isocyanate were pretreated by heat and nitrogen as previously described. In order to sample 2.1 ml of the reactive mixture at rheometer, it was decided to join 2.10 ml of each reactant into a disposable plastic cup and stir the mixture. Immediately after stirring, 2.1 ml of this mixture were pipetted onto the plate of the rheometer and then the test started. The test consisted of only one interval, called reaction interval in rotation mode, using different shear rates $1\,\mathrm{s}^{-1}$ and $50\,\mathrm{s}^{-1}$ at $40\,^{\circ}\mathrm{C}$. The end of the

test was set to 1500 s , except for the measurements where torque started to decrease or exceeded the maximum value of 150 mNm .

In each experiment at least three measurements using identical experimental conditions were taken in order to assure repeatability of the results. The mean value was calculated from

$$\overline{x} = \frac{1}{n}\sum_{i=1}^{n} x_i \tag{4.1}$$

Where n is the number of the measurements, x is the measured property (viscosity) and the standard deviation was calculated from

$$s_d = \sqrt{\frac{1}{n-1}\sum_{i=1}^{n}(x_i - \overline{x})^2} \tag{4.2}$$

The lower and upper limits of the confidence interval of $95\,\%$ were calculated from

$$\overline{x} \pm \frac{t_{0.975}}{\sqrt{n}} s_d \tag{4.3}$$

Where $t_{0.975}$ is the correspondent quantile of the cumulative t distribution, and it has value of 4.303.

Figure 4.12 shows the viscosity versus reaction time at $40\,^{\circ}\mathrm{C}$, without the premixing period. Figure 4.12 shows two plots, one with maximum values that were obtained in the experiment and the other is a detailed view in order to get a better insight of the viscosity rise for different shear rates at the initial reaction time. Viscosity values on the graph represent average values of three measurements. The objective of this study was to show that viscosity rise is faster for the lower shear rate.

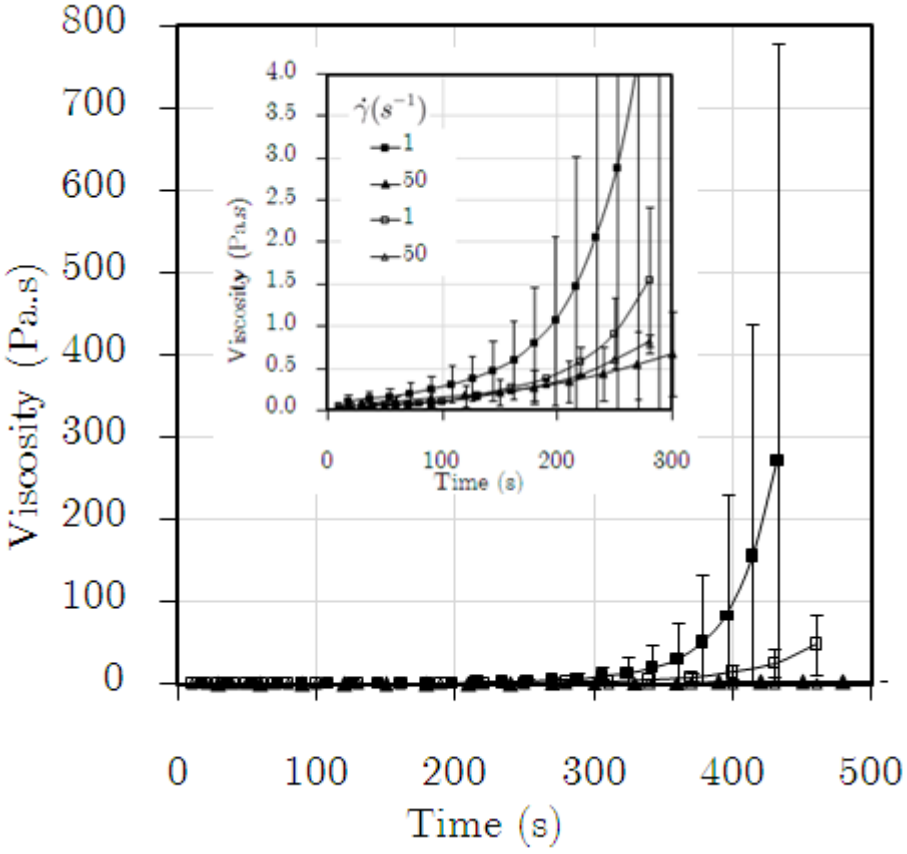

Figure 4.12. Viscosity vs. reaction time without premixing interval at 40 °C for four different constant values of the shear rate. Full symbols - mixed outside the rheometer, open symbols - mixed at the rheometer.

Maximum viscosity rise is achieved for shear rate of $1\,s^{-1}$ as observed in Figure 4.12 and it is 280 Pa.s at 440 s. Difference of the viscosity rise with the shear rates is also observed, and at 250 s, at $1\,s^{-1}$ mixed at rheometer viscosity achieved the value of 0.9 Pa.s and mixed outside of the rheometer viscosity achieved 2.9 Pa.s.

4.4.2 Effect of reactants contacting procedure

The polymerisation reaction to produce polyurethanes is very sensitive to the stoichiometric ratio of the reactants (Macosko 1989). In the RIM process, the quality of the final product highly depends on the mixing degree of the two reactants. Mixing step at industrial RIM machine is well below 1s, and the curing step (depending on the formulation) of the process typically takes less than a minute (Macosko 1989). Mixing of the reactants is efficient if there is a flow regime in the mixing chamber of

RIM machines where the formation of vortices engulfing both reactants (Fonte, Santos et al. 2011). Although polymerisation onsets in the mixing head the significant viscosity rise of the reacting mixture takes place during curing in the mould. Incomplete mould filling could happen because of the unexpected viscosity rise inside some mould section that could also lead to formation of the solid product blocking other sections of the mould. Therefore, measuring the viscosity rise of the reactive formulation, and its correlation with the degree of mixing is a useful tool for designing RIM machines to a specific formulation.

The reactive mixture for testing at the rheometer was sampled according to a procedure previously described. The reactants were mixed in a cup with a magnetic stirrer, after the reacting mixture was transferred to the rheometer. The viscosity rise curve obtained with this procedure was affected by the poor control of mixing in the magnetic stirrer which lacked repeatability from test to test, particularly as far as the initial contacting of the monomers is regarded. In order to enable better control of the mixing of the reactants, a new method was developed, here called OTO, which consists in adding the separate reactants directly on the rheometer plate, and mixing them by the shearing caused by the rotation of the cone. By setting the shear rate of the cone and the time duration it is enabled to always mix the reactants in the same way, as long as the setting parameters are the same. Shear rates employed in this experiment were $1\,s^{-1}$ and $50\,s^{-1}$. Figure 4.13 shows the viscosity rise at $40\,^{o}C$ measured with the OTO for premixing by the open symbols, and viscosity rise of the reactants mixed in the disposable cup by magnetic stirrer by the full symbols. It is observed, that all curves that correspond to the mixing by the magnetic stirrer have 2-3 times higher value of viscosity than curves obtained at OTO method without the premixing interval in the first 100 seconds of reaction. This result is expected because the viscosity starts to rise as soon as the two reactants enter into contact, and lower values for OTO without the premixing interval are the consequence of the later onset of the mixing and polymerisation.

The standard deviation values from the sample that were mixed in the sample were larger than 60% of the average viscosity value in the first 100 seconds, while for the OTO method the standard deviation values in the same interval were less than 10% of the average. The contacting of reactants in polyurethane polymerisation is thus a critical step, and so the control of this step has a huge impact on the course of the reaction. This result confirms the findings of (Tucker and Suh 1980, Kolodziej, Yang et al. 1986) that mixing has a huge impact on the polymers made with RIM.

Faster viscosity rise at lower shear rates suggests that polymerisation is faster and the product with higher molecular weight is formed earlier in time when lower shear rates are employed. This observation is confirmed in other experiments and is going to be explained in more detail later on in this chapter. Viscosity rise curves at higher reaction times for the samples shown in Figure 4.13, are in Figure 4.14.

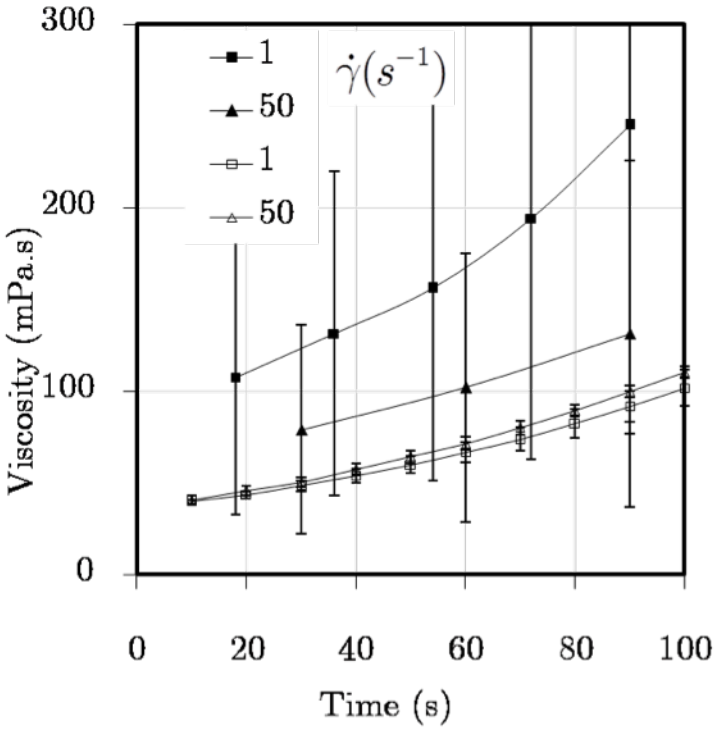

Figure 4.13. Viscosity vs. time at early reaction times at 40°C: full symbols - mixed outside rheometer, open symbols - mixed at rheometer.

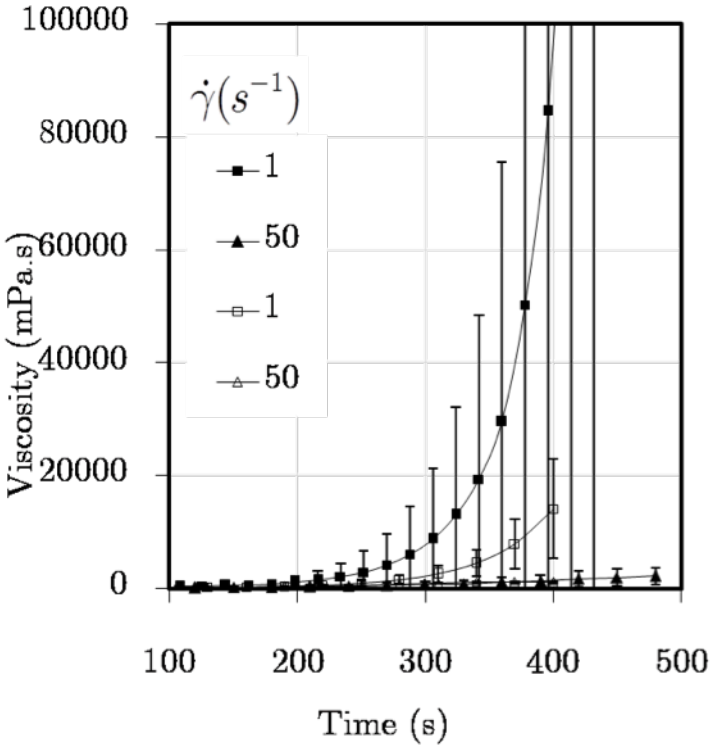

Figure 4.14. Viscosity vs. time at later reaction times at 40 °C : full symbols - mixed outside rheometer, open symbols - mixed at rheometer.

Viscosity value at the last registered point at a reaction time of 500 s, for OTO method without the premixing interval is approx. 600 mPa.s for all shear rates studied. While for the samples mixed with the magnetic stirrer, viscosity decreases as shear rate increases, resulting in the deviation between the value for $1\,s^{-1}$ and $50\,s^{-1}$ of 38%. Viscosity value at 500 s for $1\,s^{-1}$ is double the value than the average of all shear rates for OTO. Based on these results and in order to control more efficiently the mixing of the reactants it was decided to conduct all future experiments by mixing the reactants directly on the plate and not in the magnetic stirrer.

4.4.3 Reaction shear rate effect

Previously observed viscosity rise dependence on shear rate and on the premixing procedure showed the need of further researching this subject. In the following experiments the reactants are added directly over the rheometer plate, and

measurements were carried out using two distinct methods for premixing in the rheometer: OTO and the HC. All the experiments were carried out by defining two intervals with different features at the rheometer:

- Premixing interval,
- Reaction interval.

The purpose of the premixing interval is to efficiently mix the reactants using the shearing caused by the rotation of the cone. In the RenCast datasheet pot life at $25\,^{\circ}\mathrm{C}$ is 6 – 8 minutes but mixing method was not specified. Based on the previous results of the viscosity rise after mixing in the magnetic stirrer for $30\,\mathrm{s}$, it was decided that duration of the premixing rheometer interval be $100\,\mathrm{s}$. The premixing time effect on the gel point is presented later in this document. Constant shear rate in premixing was set to $500\,\mathrm{s}^{-1}$, because this value corresponds to the conditions at the industrially used Reynolds number in RIM machines of 500 (see Appendix A). Premixing interval parameters were kept the same throughout the following experiments, in order to be able to compare the obtained data.

Depending on the objective of the experiments, measurements in the reaction interval were from:

- Rotational test, for viscosity rise and rheological behaviour measurements,
- Oscillatory tests, for gel point estimation.

Shear rate in rotational reaction interval was kept constant, with the following values being tested: $1\,\mathrm{s}^{-1}$,$50\,\mathrm{s}^{-1}$,$100\,\mathrm{s}^{-1}$,$500\,\mathrm{s}^{-1}$,$1000\,\mathrm{s}^{-1}$ and $3000\,\mathrm{s}^{-1}$. The shear values for the oscillatory reaction interval were lower in order to keep the sample in the linear viscoelastic region, strain constant in all tests and set to 1% and angular frequency values were $1\,\mathrm{s}^{-1}$,$2\,\mathrm{s}^{-1}$, $5\,\mathrm{s}^{-1}$ and $20\,\mathrm{s}^{-1}$.

Viscosity rise, rheological behaviour and gel time estimation were measured by both methods OTO and the HC and obtained results compared at temperature of 25 °C and 40 °C.

4.4.4 Edge fracture

Viscosity rise graphs at 25 °C at shear rates $1\,s^{-1}$, $50\,s^{-1}$, $100\,s^{-1}$, $500\,s^{-1}$, $1000\,s^{-1}$ and $3000\,s^{-1}$ for both premixing methods are represented in Figure 4.15 to Figure 4.20. Throughout all the experiments and all the shear rates employed torque did not exceed the limit value of 150 mNm. Plot at $1\,s^{-1}$ (see Figure 4.15) is the only case where the viscosity did not drop during the experiment time duration, representing no edge fracture. Maximum registered value of the viscosity at $1s^{-1}$ was at the last point for 1210 s and it was: for OTO, approx. 4 kPa.s while for the HC the viscosity value was ten times less, 0.4 kPa.s.

At shear rate of $50\,s^{-1}$ (see Figure 4.16) viscosity rise has a slight drop at approx. 500 s for both methods after what it continues to increase up to 850 s for the HC and 940 s for OTO and then it drops again. Torque did not exceed its maximum for both methods.

At $100\,s^{-1}$ slight drop in viscosity at 500 s followed with the viscosity increase for the HC method was also observed and is presented in Figure 4.17. The same slight drop in viscosity was not observed for OTO method. The edge fracture shown as a rapid drop in viscosity at $100\,s^{-1}$ for OTO was registered at 640 s and for the HC at 850 s. Maximum value of torque was not exceeded for neither of the methods. Maximum viscosity obtained for OTO was approx. 3000 mPa.s at 650 s and for the HC 500 mPa.s at 500 s.

At higher shear rates such as $500\,s^{-1}$ (see Figure 4.18) and $1000\,s^{-1}$ (see Figure 4.19) maximum viscosity before the sudden drop indicating fractured sample edge was achieved at the same time for both methods which occurred approximately at 700 s.

Up to this time torque remained lower than the maximum limit. Maximum viscosity value at $500\,s^{-1}$ for OTO was 3 times higher than for the HC. At $1000\,s^{-1}$ maximum viscosity value measured for the OTO was approx. 2.5 times higher than for the HC method.

From all the above observations it can be concluded that the edge fracture was detected for every shear rate excepting for $1s^{-1}$ and therefore viscosity at $1s^{-1}$ achieved values of a few kPa.s. For the shear rates of $50\,s^{-1}$ and $100\,s^{-1}$ a specific pattern is shown representing a very slight viscosity drop at approx. 500 s that may indicate the gel point occurrence, after which viscosity continued to rise up before the sudden drop typical for the edge fracture.

At $3000\,s^{-1}$ which is represented in Figure 4.20 the maximum viscosity value is the same for both methods, approximately 1300 mPa.s at 600 s. After a sudden decrease in viscosity it is observed for the HC without exceeding the maximum torque value. For OTO after 600 s the torque exceeded its maximum value of 150 mPa.s and those points are not taken into account. That pattern was not shown for shear rates higher than $100\,s^{-1}$. For shear rate of $500\,s^{-1}$ and $1000\,s^{-1}$ a typical edge fracture occurred at 700 s. For shear rates lower than $3000\,s^{-1}$ the viscosity rise of the HC method was slower than of the OTO, which is the consequence of the delayed contacting between the two reactants, due to the separator of the holding cell equipment. The time of the sudden drop in viscosity decreases to 600 s for the shear rate of $3000\,s^{-1}$, and the difference in the viscosity rise between the two methods is not significant. By increasing the shear rate in early reaction times, viscosity is expected to rise faster because the mixing is favoured by the higher shear rate. Later in the reaction times when polymeric chains start to entangle and form network the shear rate may have two opposite influences on the polymer formation: it may still promote the transport of monomers and smaller oligomeric chains into growing macromolecular chains and increase the molecular weight and viscosity or it may break down the existing network and decrease the viscosity.

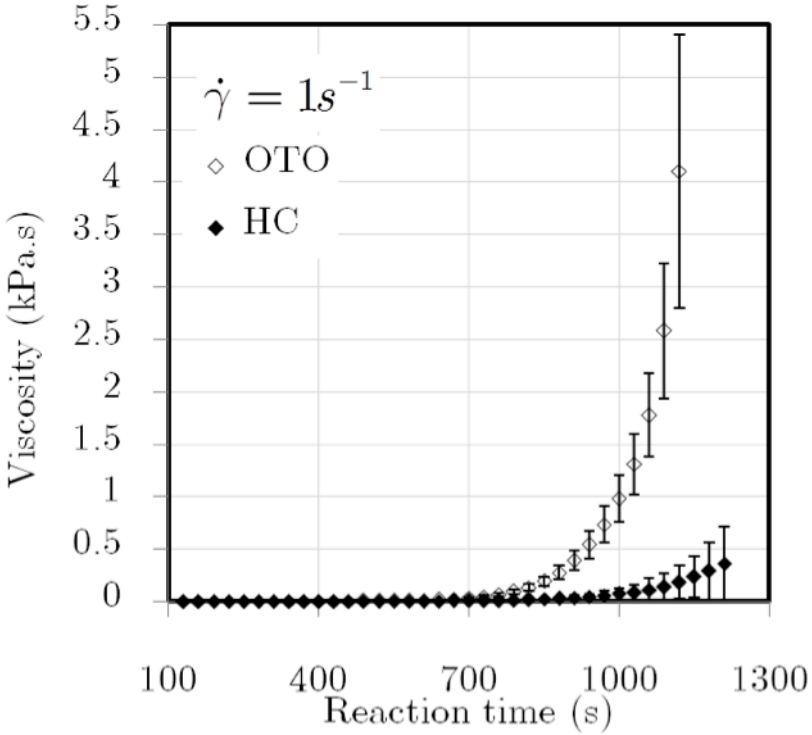

Figure 4.15. OTO vs. the HC: viscosity rise with standard deviation at $1\,s^{-1}$ and $25\,^{\circ}C$.

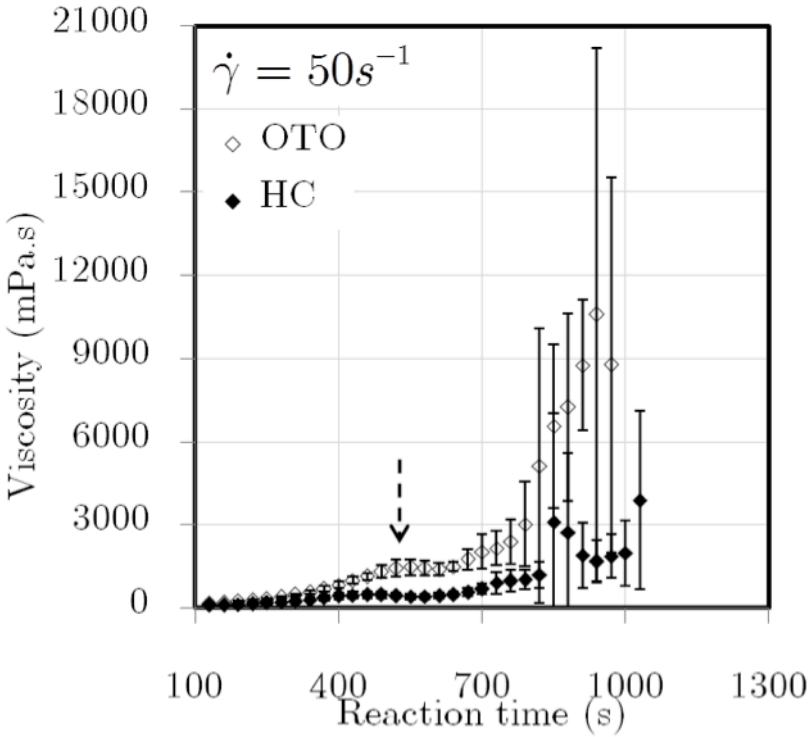

Figure 4.16. OTO vs. the HC: viscosity rise with standard deviation at $50\,s^{-1}$ and $25\,^{\circ}C$.

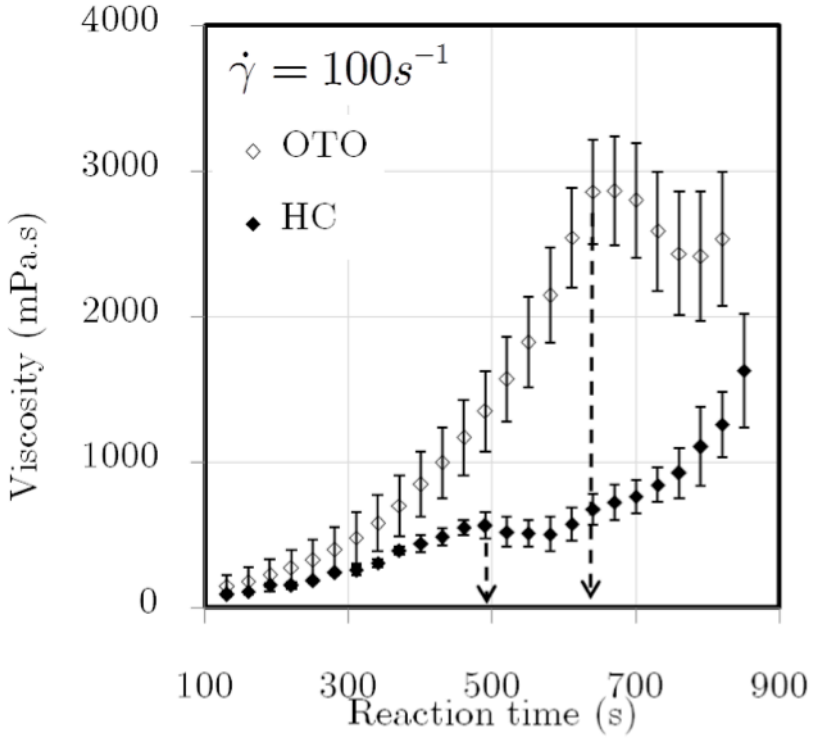

Figure 4.17. OTO vs. the HC: viscosity rise with standard deviation at $100\,s^{-1}$ and $25\,°C$.

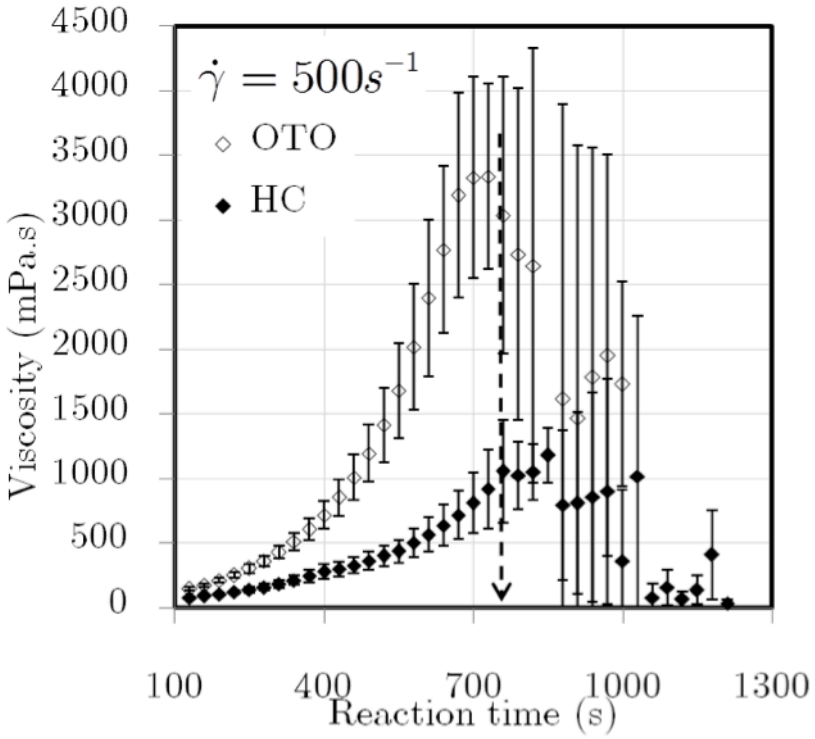

Figure 4.18. OTO vs. the HC: viscosity rise with standard deviation at $500\,s^{-1}$ and $25\,°C$.

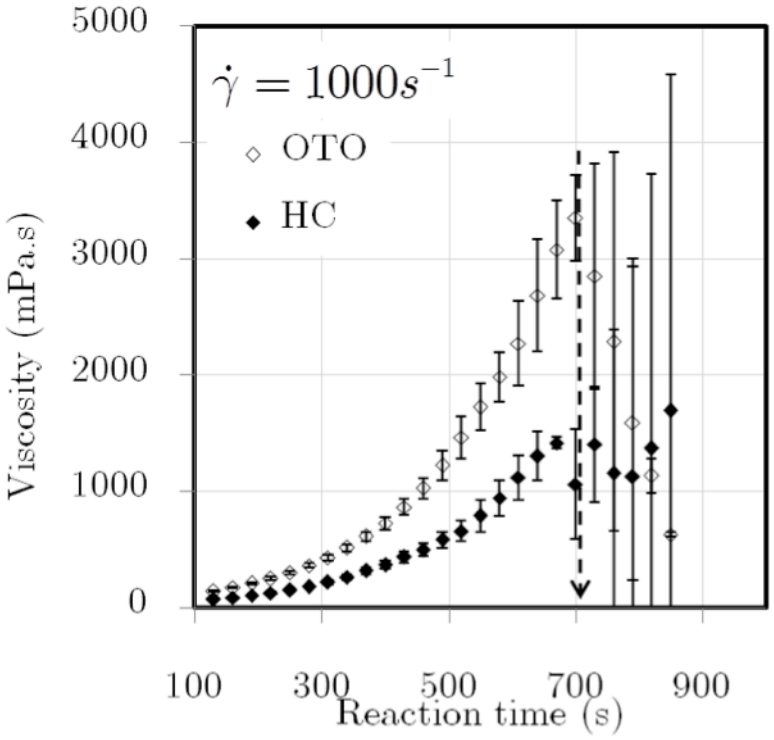

Figure 4.19. OTO vs. the HC: viscosity rise with standard deviation at $1000\,s^{-1}$ and $25\,^{\circ}C$.

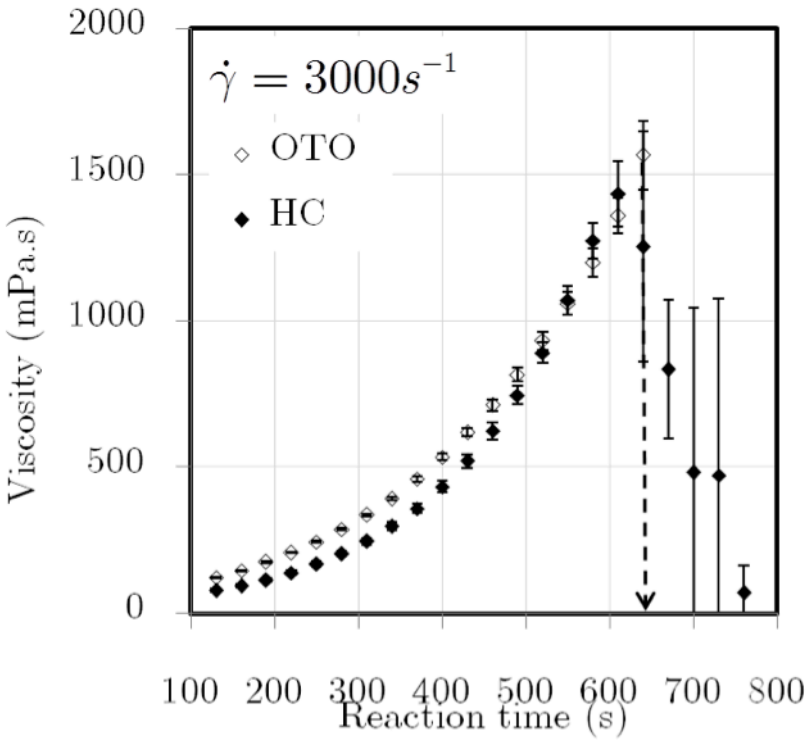

Figure 4.20. OTO vs. the HC: viscosity rise with standard deviation at $3000\,s^{-1}$ and $25\,^{\circ}C$.

Viscosity rise data at $40\,^{\circ}\mathrm{C}$ for both mixing methods is presented from Figure 4.21 to Figure 4.26.

For shear rates $1\,\mathrm{s}^{-1}$ (see Figure 4.21), $50\,\mathrm{s}^{-1}$ (see Figure 4.22) and $100\,\mathrm{s}^{-1}$ (see Figure 4.23) no drop in viscosity is detected for up to at least $700\,\mathrm{s}$ indicating that in this time range no edge fractures of the samples occurred. Maximum viscosity at $600\,\mathrm{s}$ for $1\,\mathrm{s}^{-1}$ and $50\,\mathrm{s}^{-1}$ was in the range $50-2000\,\mathrm{Pa.s}$. At shear rate of $100\,\mathrm{s}^{-1}$ maximum viscosity achieved at $500\,\mathrm{s}$ was less than $2\,\mathrm{Pa.s}$, which is significantly lower value than for $1\,\mathrm{s}^{-1}$ and $50\,\mathrm{s}^{-1}$ at the same time. No maximum torque was exceeded.

Typical drop in viscosity at higher shear rates for $500\,\mathrm{s}^{-1}$ (see Figure 4.24), $1000\,\mathrm{s}^{-1}$ (see Figure 4.25) and $3000\,\mathrm{s}^{-1}$ (see Figure 4.26) indicate the fractured sample edge occurred later in time as the shear rate increased. For OTO method drop in viscosity was registered at $350\,\mathrm{s}$, $400\,\mathrm{s}$ and $450\,\mathrm{s}$ for shear rates $500\,\mathrm{s}^{-1}$, $1000\,\mathrm{s}^{-1}$, and $3000\,\mathrm{s}^{-1}$ respectively; for the HC method at $680\,\mathrm{s}$, $890\,\mathrm{s}$ at $500\,\mathrm{s}^{-1}$ and $1000\,\mathrm{s}^{-1}$, respectively. For this method at $3000\,\mathrm{s}^{-1}$ torque reached it maximum value at $580\,\mathrm{s}$, and the points after this time were not taken into account as significant. No maximum torque was exceeded.

It is concluded that at $40\,^{\circ}\mathrm{C}$ samples did not suffer from edge fracture at relatively low shear rates of $1\,\mathrm{s}^{-1}$, $50\,\mathrm{s}^{-1}$ and $100\,\mathrm{s}^{-1}$. At higher shear rates, edge fracture appeared later in time as the shear rate increased for both methods. Furthermore, it seems that there is no difference in comparison of the shape of the viscosity rise curves at $1\,\mathrm{s}^{-1}$ between OTO and the HC. For all the other shear rates employed, viscosity increased faster for OTO than for the HC method.

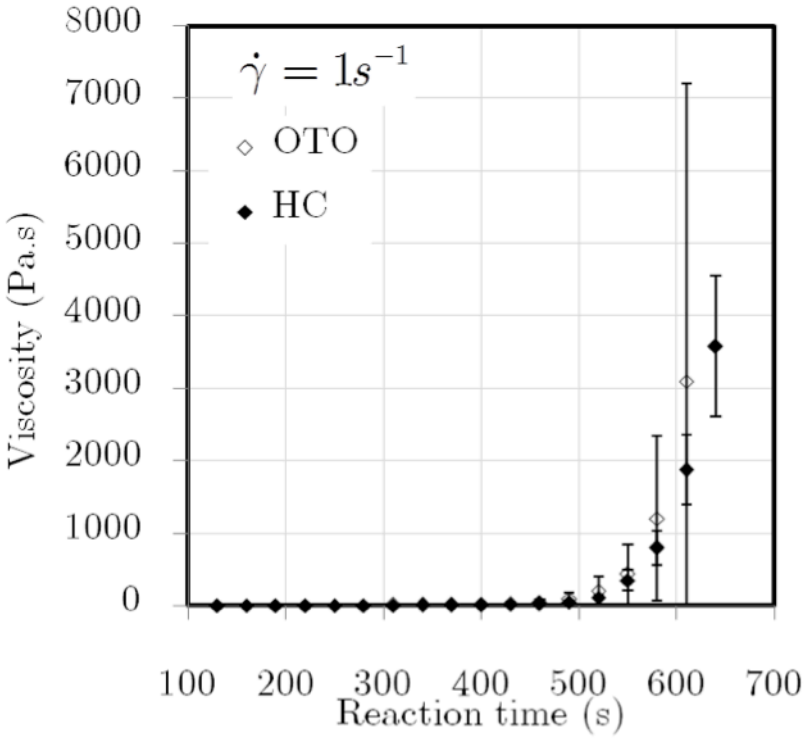

Figure 4.21. OTO vs. the HC: viscosity rise with standard deviation at $1\,s^{-1}$ and 40 °C.

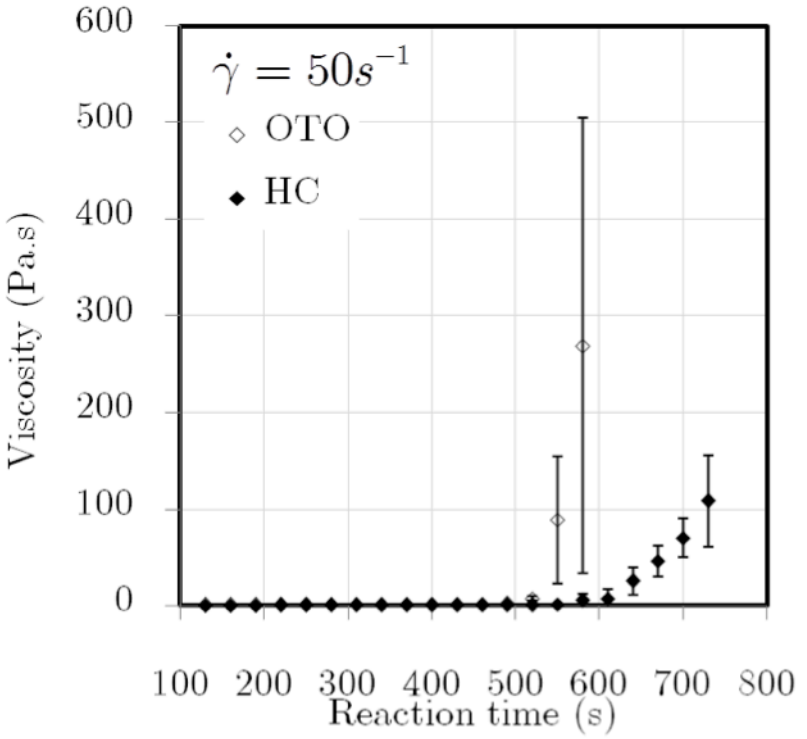

Figure 4.22. OTO vs. the HC: viscosity rise with standard deviation at $50\,s^{-1}$ and 40 °C.

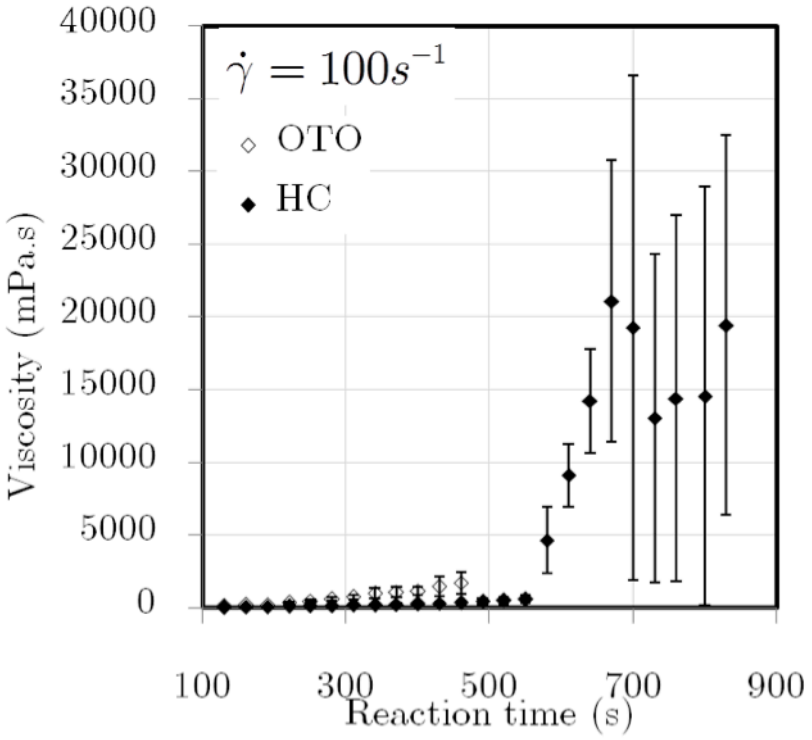

Figure 4.23. OTO vs. the HC: viscosity rise with standard deviation at $100\,s^{-1}$ and $40\,^{\circ}C$.

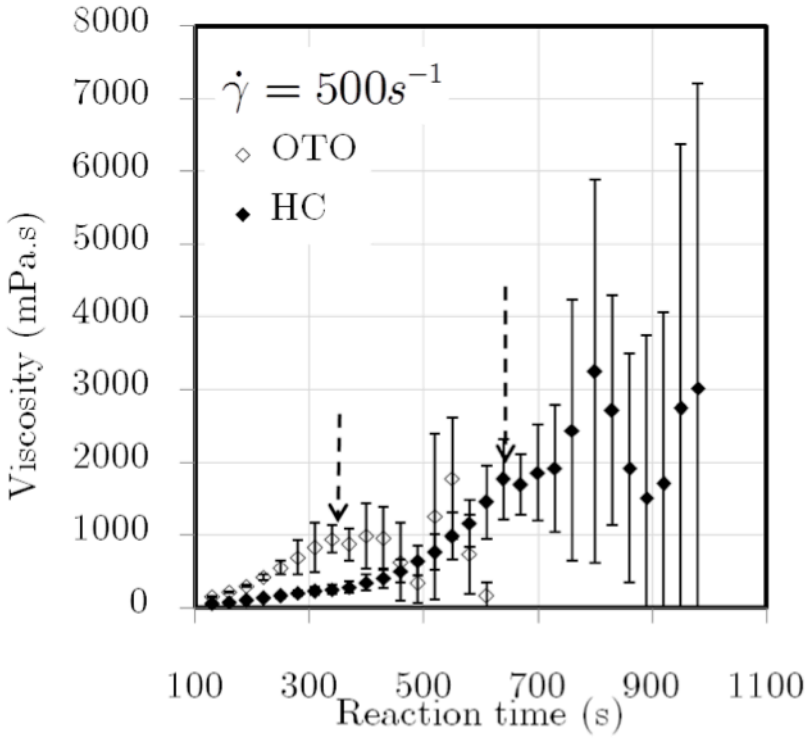

Figure 4.24. OTO vs. the HC: viscosity rise with standard deviation at $500\,s^{-1}$ and $40\,^{\circ}C$.

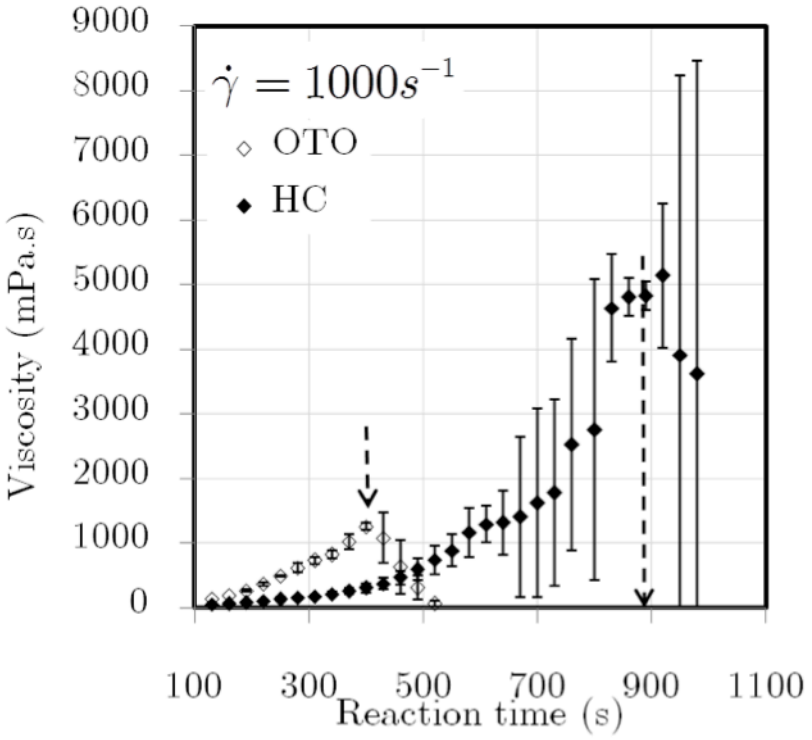

Figure 4.25. OTO vs. the HC: viscosity rise with standard deviation at $1000\,s^{-1}$ and $40\,^{\circ}C$.

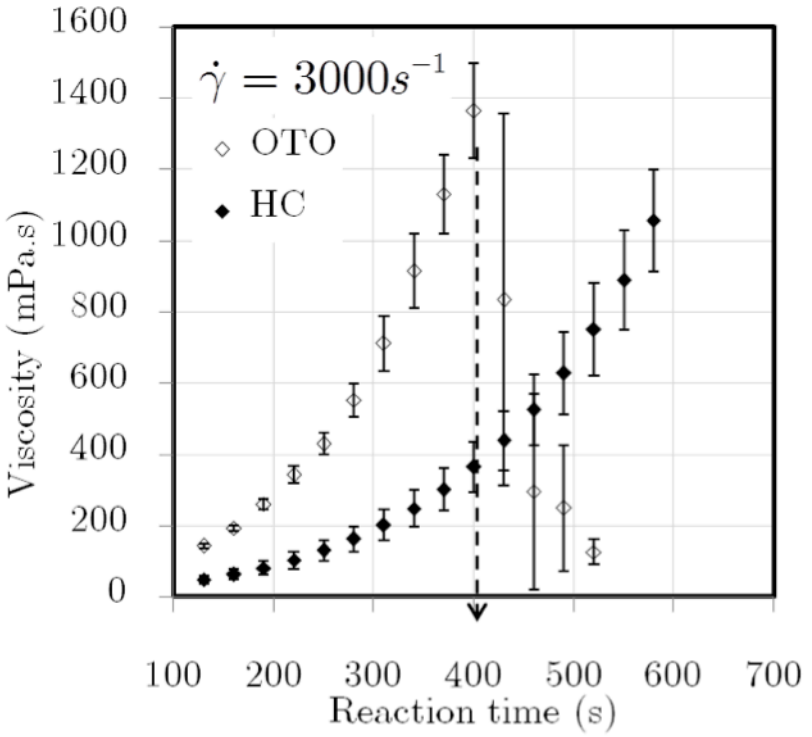

Figure 4.26. OTO vs. the HC: viscosity rise with standard deviation at $3000\,s^{-1}$ and $40\,^{\circ}C$.

In the previous sections it was observed that shear rate has influence on the viscosity rise, therefore viscosity versus reaction time is represented from Figure 4.27 to Figure 4.30 for different shear rates. All the graphics have the same scale; at $25\,^{\circ}\mathrm{C}$ maximum time was $600\,\mathrm{s}$ and viscosity $3000\,\mathrm{mPa.s}$; at $40\,^{\circ}\mathrm{C}$ maximum time plotted is $500\,\mathrm{s}$ and viscosity $2000\,\mathrm{mPa.s}$. In all of them, except the HC at $25\,^{\circ}\mathrm{C}$ viscosity at $1\,\mathrm{s}^{-1}$ rose much faster than at the other shear rates. Rise in viscosity is a consequence of the increase in molecular weight of the polymer. Factors that affect rise in molecular weight are: mixing efficiency - as mixing is more efficient, more interfacial area is generated between the reacting monomers, which results in higher number of macromolecular chains generated (the case of the HC method); branching – this is the most probable cause of the exceptionally fast viscosity rise at $1\,\mathrm{s}^{-1}$, since shearing is very slow the conditions of the formation of the branched chains are favourable, resulting in the rise in molecular weight and therefore in viscosity.

Besides the exception at $1\,\mathrm{s}^{-1}$, for the other shear rates used at all mixing methods and all temperatures tests, no specific pattern was observed. Other conditions that could cause the viscosity deviation and poor reproducibility are the deviations in stoichiometry and in temperature. Therefore, the most probable cause of the viscosity deviation at different shear rates is the very small deviation in stoichiometry due to the lack of the more accurate sampling method. It is observed that the difference in viscosity rise for shear rates $50\,\mathrm{s}^{-1}$,$100\,\mathrm{s}^{-1}$,$500\,\mathrm{s}^{-1}$,$1000\,\mathrm{s}^{-1}$ and $3000\,\mathrm{s}^{-1}$ and is the smallest for the HC method at $40\,^{\circ}\mathrm{C}$.

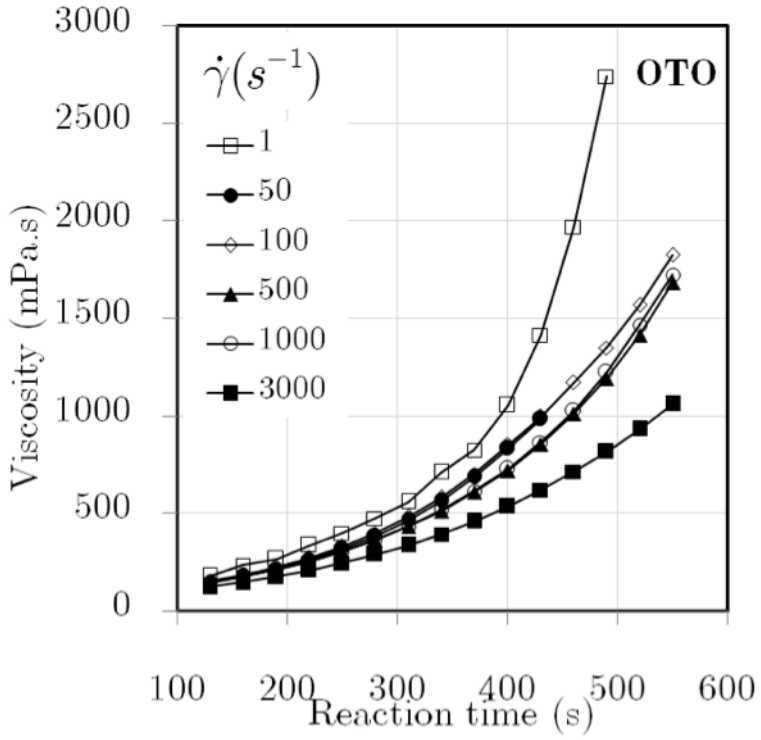

Figure 4.27. Viscosity vs. reaction time with shear rate as changing parameter at 25°C for OTO method.

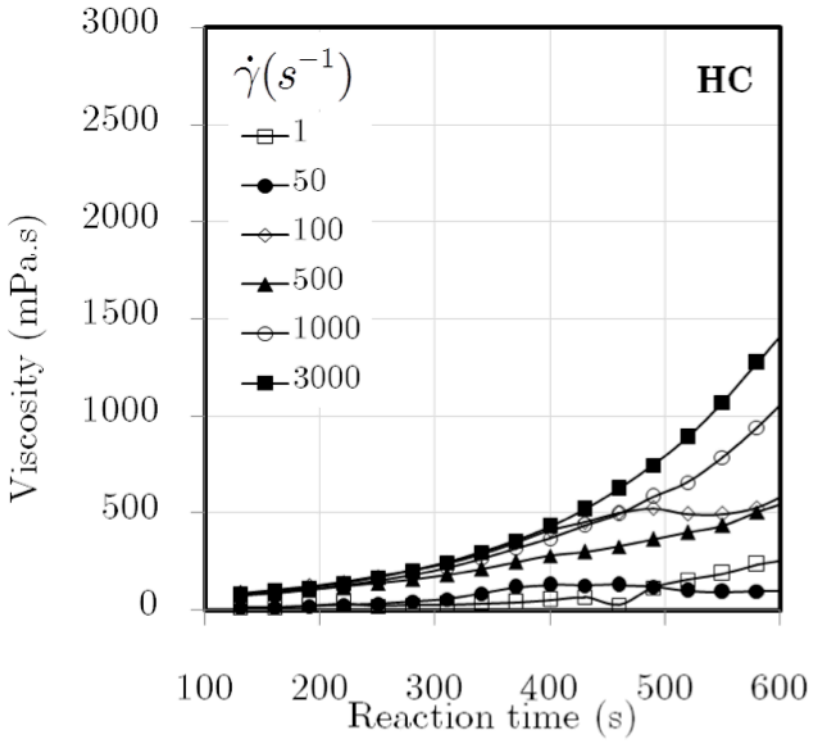

Figure 4.28. Viscosity vs. reaction time with shear rate as changing parameter at 25°C for the HC method.

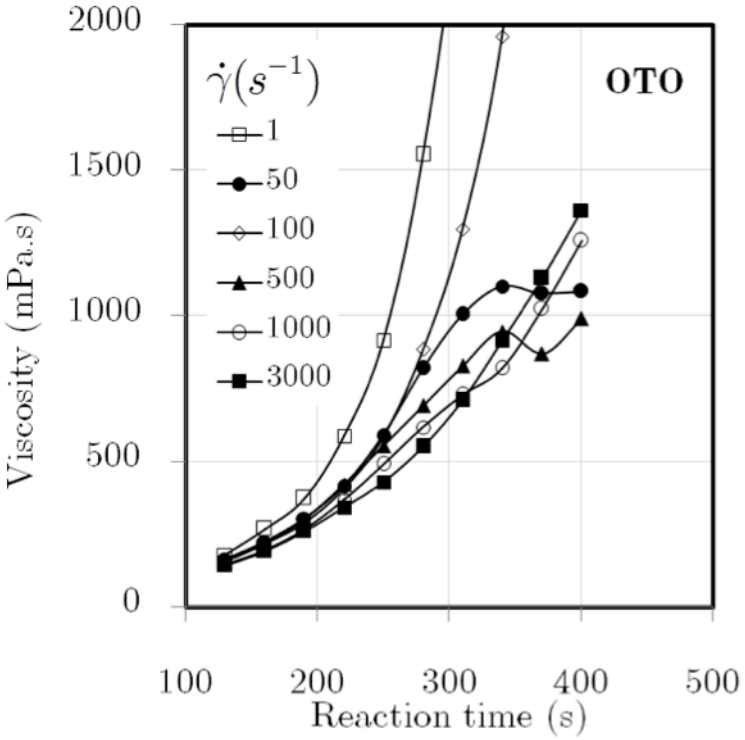

Figure 4.29. Viscosity vs. reaction time with shear rate as changing parameter at 40°C for OTO method.

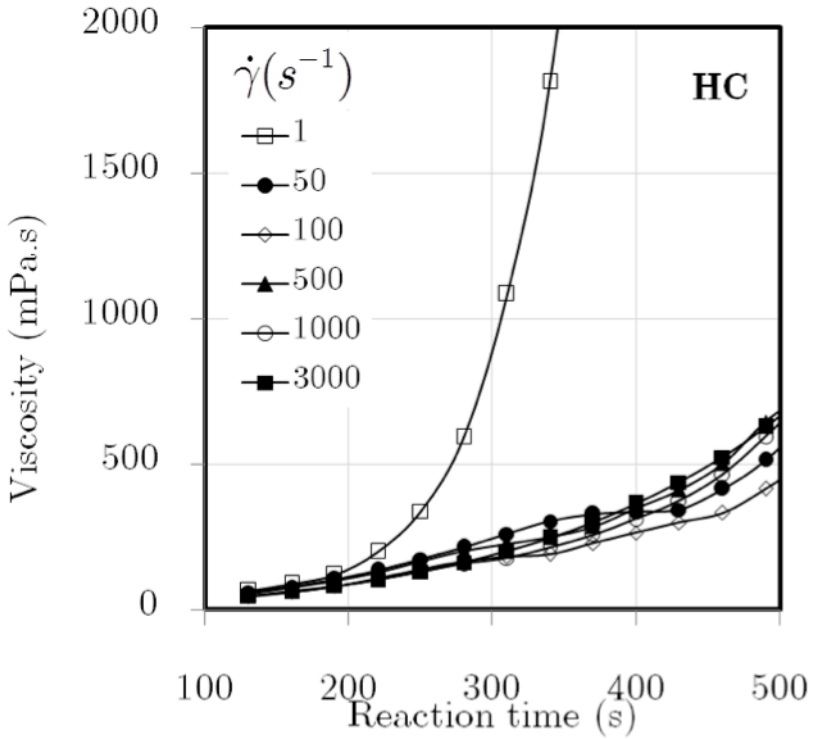

Figure 4.30. Viscosity vs. reaction time with shear rate as changing parameter at 40°C for the HC method.

4.4.5 Viscosity power-law model

Viscosity rise might be modelled by power-law model and it is useful to predict viscosity of the reactive formulations over time (Malkin and Kulichikhin 1991). The model used in this study is:

$$\eta = \alpha t^{n} \tag{4.4}$$

where model parameters are α which represents zero time viscosity and n is a constant. Model parameters were obtained by using Solver from Excel application, using linear regression method and experimental viscosity rise at $25\,^{\circ}C$ and $40\,^{\circ}C$ obtained with OTO method.

The viscosity rise at $25^{\circ}C$ was modelled in different time ranges $100-600\,s$, $100-500\,s$ and $100-400\,s$ for all the shear rates and only the best fit results are presented here. The best parameters fit of this model at $25\,^{\circ}C$ was found for the time range $100-400\,s$ including the shear rates lower than $100\,s^{-1}$ and model parameters and coefficient of determination R^2 are represented in Table 4.3.

Table 4.3. Power-law parameters for OTO at $25\,^{\circ}C$.

Shear rate $[s^{-1}]$	$\alpha(\times 10^2)$	n	R^2
1	1.44	1.86	0.98
50	1.20	1.85	0.98
100	1.46	1.82	0.99
500	3.61	1.64	0.99
1000	3.03	1.68	0.99
3000	6.89	1.49	0.99

Values of α and n which are valid for the whole range of shear rates are calculated as an arithmetic mean value of the set of the values for each shear rate from the Table 4.3. The model is represented with

$$h = 0.03t^{1.72} \tag{4.5}$$

At $40\,^{\circ}\mathrm{C}$ the viscosity rise was modelled in different ranges of time $100-400\,\mathrm{s}$ and $100-300\,\mathrm{s}$ and the best parameters fit were found for the time range $100-300\,\mathrm{s}$. Model parameters and coefficient of determination for all the shear rates are shown in Table 4.4.

Table 4.4. Power-law parameters for OTO at $40\,^{\circ}\mathrm{C}$.

Shear rate [s^{-1}]	$\alpha(\times 10^3)$	n	R^2
1	0.000124	4.14	0.99
50	1.25	2.38	0.99
100	2.42	2.20	1.00
500	8.79	2.00	1.00
1000	8.81	1.98	1.00
3000	7.06	2.00	0.99

Model parameters that are valid for any shear rate in the range from $1-3000\,\mathrm{s}^{-1}$ are calculated as arithmetic mean values from the Table 4.4 and the viscosity rise model for the polyurethane reactive mixtures at $40\,^{\circ}\mathrm{C}$ for polymerisation duration up to $300\,\mathrm{s}$ is represented with

$$h = 0.05t^{2.45} \tag{4.6}$$

Viscosity rise obtained experimentally (points) and power-law model curve (line) are represented at $25\,^{\circ}\mathrm{C}$ in Figure 4.31 and at $40\,^{\circ}\mathrm{C}$ in Figure 4.32. A reasonably good fit between the experimental results and the model curve is observed for all the shear rates studied at both temperatures.

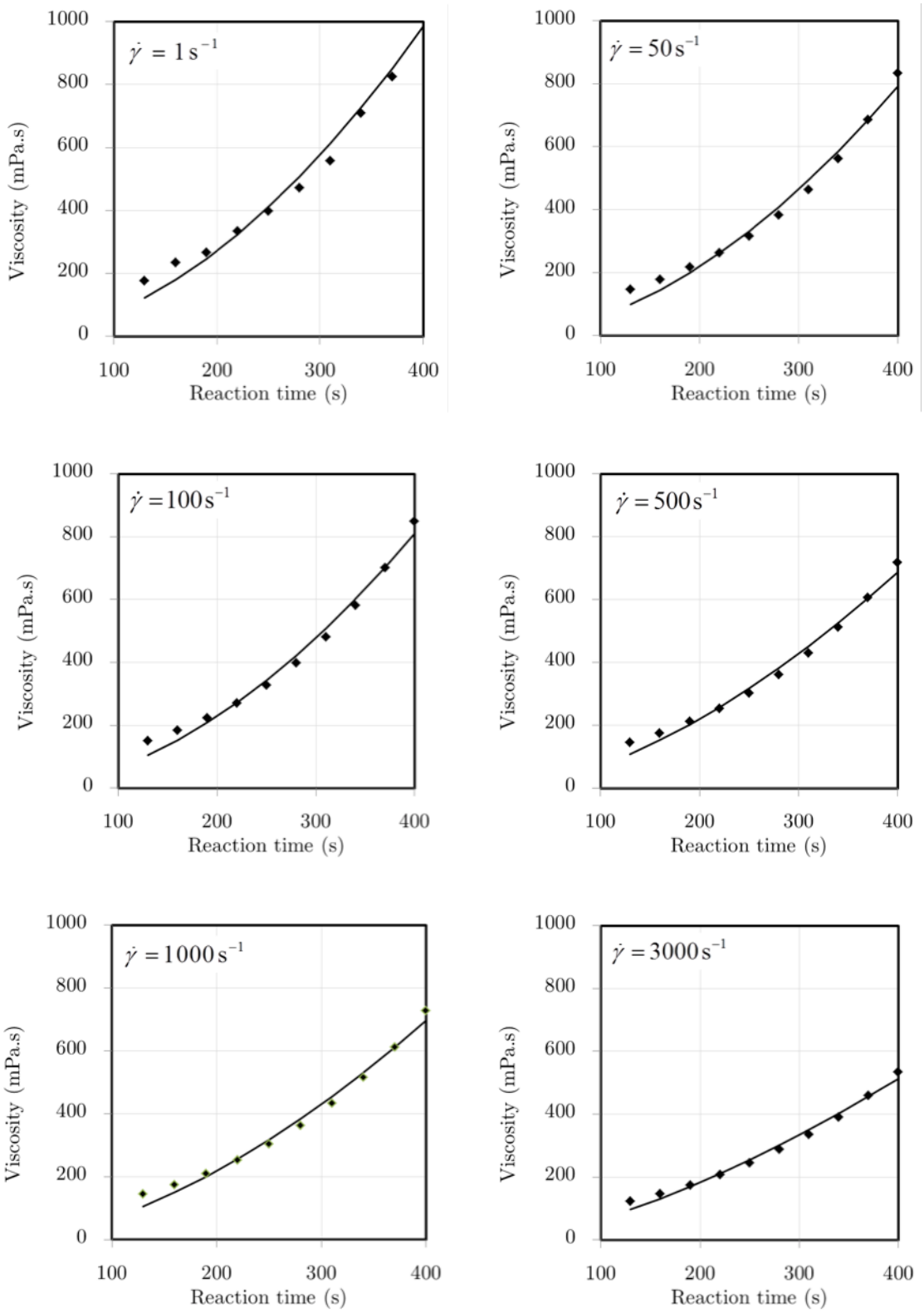

Figure 4.31. Rheometry and power-law viscosity rise for OTO at 25°C.

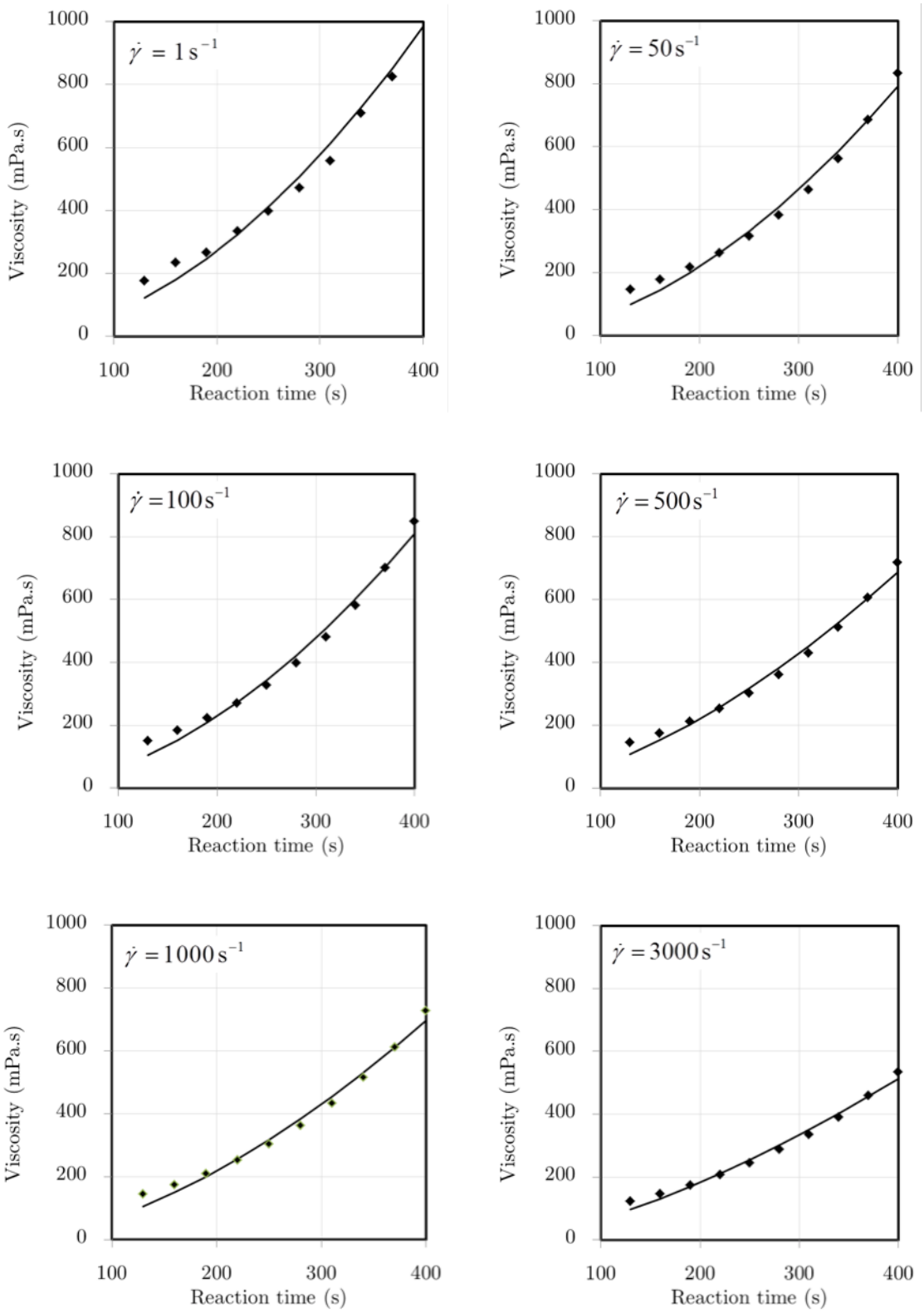

Figure 4.32. Rheometry and power-law viscosity rise for OTO at 40°C.

4.5 Newtonian behaviour

Different values of the viscosity at different shear rates as was seen in the previous chapter lead to the doubt that the reactive mixture might exhibit non-Newtonian behaviour although many authors already reported that viscosity of the reactive mixture does not depend on shear rate (Castro and Macosko 1980, Chen and Macosko 1996, Kim and Macosko 1996, Sun, Toth et al. 1997, Ivankovic, Incarnato et al. 2003, Dimier, Sbirrazzuoli et al. 2004, Haddadi, Nazockdast et al. 2008). Therefore it was decided to design an experiment in order to determine whether the viscosity of the RenCast reactive formulation is dependent on the shear rate. Most appropriate test mode found for this purpose was one test with many consecutive intervals each with identical shear rate sweep. Measuring gap was set to $50\,\mu m$ and geometry used was cone and plate, cone diameter $50\,mm$ and 1^{o} angle. Since the reactants start to react and viscosity to rise (as shown above) from the moment they enter into contact, there was no need to carry out the premixing interval. Reactants were therefore placed onto the plate by the aid of the holding cell and separator, afterwards the experiment was started. Two tests were designed with the difference in the shear rate range. Both of the tests consisted of 20 identical and consecutive rotation intervals at $25\,^{o}C$, each containing 10 points, with $3\,s$ of measuring point duration and total time of experiment was $600\,s$. Shear rate range of the first test was in logarithmic ramp from $5\,s^{-1}$ to $500\,s^{-1}$ and of the second experiment was in logarithmic ramp from $100\,s^{-1}$ to $3000\,s^{-1}$.

Furthermore, RenCast results were compared with glycerol, which is known to have a shear rate not dependent on viscosity. Viscosity of glycerol was measured using the same parameters except the temperature which was lowered to $10\,^{o}C$ in order to decrease the viscosity of the glycerol.

Results of glycerol are shown in the Figure 4.33 where viscosity and torque are plotted versus the total time of experiment. In this figure is seen that torque increases exponentially in each interval, which is followed with the sudden decrease

through the beginning of the next interval. Viscosity remains constant at approx. 2.8 Pa.s until 300 s. After this viscosity starts slowly to drop, which corresponds to a small decrease in the torque at high shear rates (up to 500 s^{-1}) in each interval.

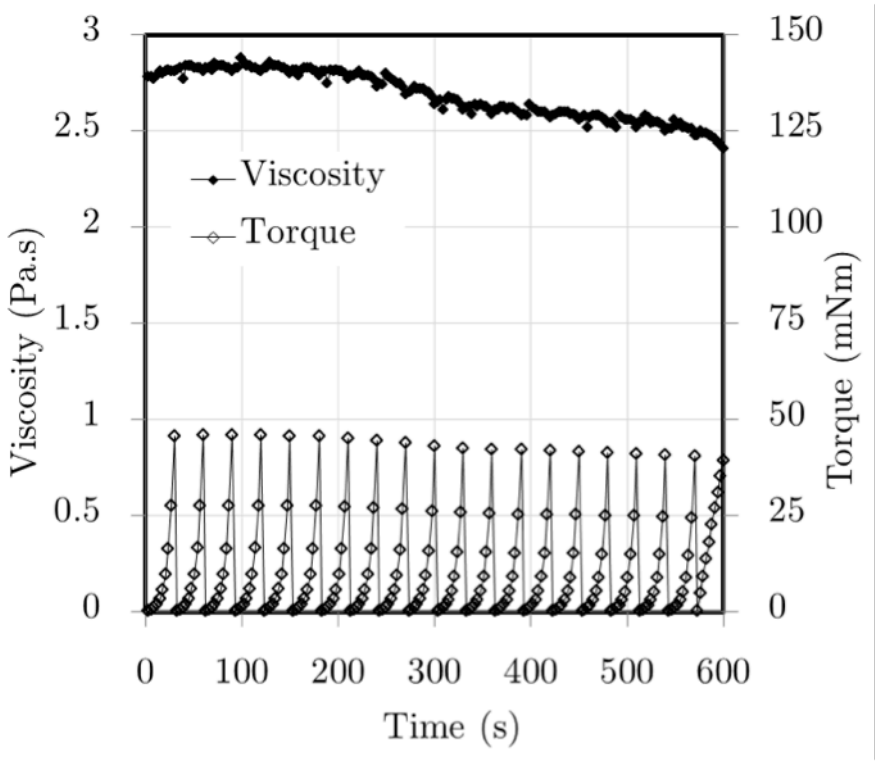

Figure 4.33. Viscosity vs. shear rate for glycerol at 10 °C.

Results for the reactive mixture at 25°C for the shear rate range 5 s^{-1} to 500 s^{-1} are shown in Figure 4.34. Towards the end of the experiment torque increases in each interval, which is the consequence of the molecular weight increase due to the polymerisation. It is observed that torque remains lower than the upper limit of 150 mNm. General trend throughout all the experiment time is the increase in viscosity up to approx. 2.5 Pa.s at 600 s. Looking at each interval, it is observed a sudden jump in viscosity at the first point of each interval, the point that corresponds to the sudden decrease in shear rate from 5 s^{-1} to 500 s^{-1}. This result is in the accordance with the results of the viscosity rise for the constant and low shear rate (1 s^{-1}), implicating faster viscosity rise and higher viscosity values at low shear.

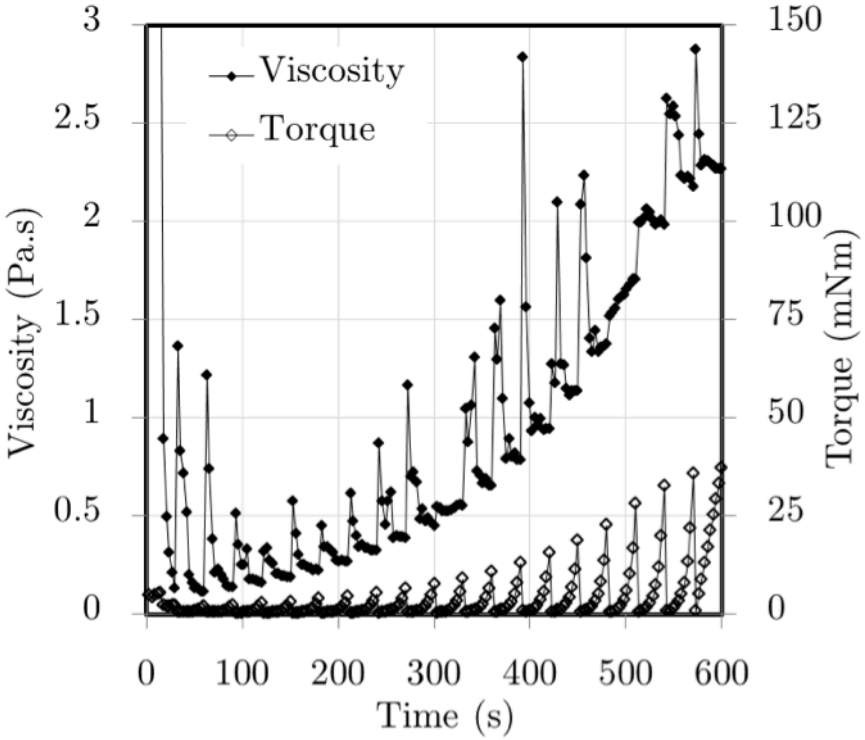

Figure 4.34. Viscosity and torque vs. time in shear rate sweep ranging $5-500\,s^{-1}$ for RenCast at $25\,^{\circ}C$.

Results for shear rate range $100\,s^{-1}$ to $3000\,s^{-1}$ are represented in Figure 4.35. General trend throughout all the experiment is the rise of the viscosity, reaching approx. $1.5\,Pa.s$ at $600\,s$, which is followed to the maximum equipment torque value of $150\,mNm$ at the same time. Sudden decrease in shear rate from $100\,s^{-1}$ to $3000\,s^{-1}$ at the end of one interval and beginning of the next interval was not followed with such a sudden increase in viscosity as was observed for the previous experiment, where shear rate decreased from $5\,s^{-1}$ to $500\,s^{-1}$. This is the result of the growth in molecular weight at low shear rates, lower than $500\,s^{-1}$.

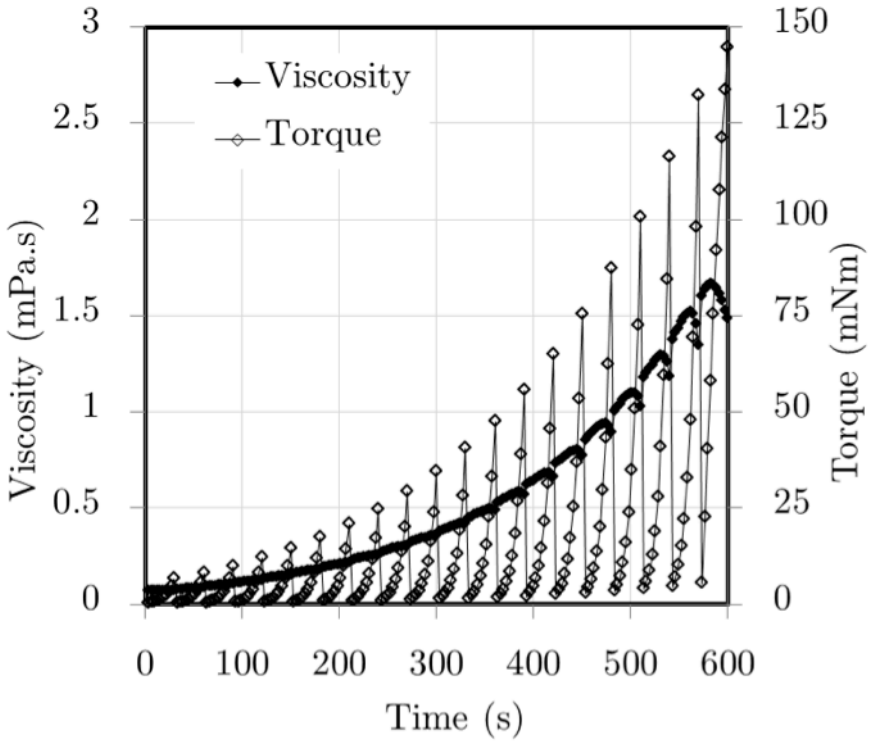

Figure 4.35. Viscosity and torque vs. time in shear rate sweep ranging $100-3000\,s^{-1}$ for RenCast at $25\,^{\circ}C$.

From Figure 4.27, Figure 4.28, Figure 4.29 and Figure 4.30 it was not clear whether the RenCast reactive mixture exhibits Newtonian behaviour or not. Viscosity rise curves for low shear rates (lower than $100\,s^{-1}$) diverge from the other curves for higher shear rates. Therefore experiments with shear rate ramp were necessary to confirm the rheological behaviour of the mixture. Viscosity rise at lower shear rate ramp presented in Figure 4.34 still does not show certain proof whether the mixture is dependent or not on the shear rate because of the appearances of the sudden increases in the viscosity at the beginning of each interval. Viscosity rise at higher shear rate ramp results presented in Figure 4.35 did not show those dramatic sudden increases of the viscosity at the beginning of each interval, and exponential rise of the viscosity observed here is the confirmation that the RenCast reactive mixture has Newtonian behaviour.

4.6 Gel point estimation

4.6.1 Angular frequency effect

For the gel point determination, experimental conditions of the premixing rotation interval were kept identical as for the viscosity rise determination (constant shear rate $500\,s^{-1}$ for $100\,s$) and in the reaction oscillation interval angular frequencies used were $1\,s^{-1}, 2\,s^{-1}$, $5\,s^{-1}$ and $10\,s^{-1}$, while strain was kept constant at 1% for both studied temperatures $25\,^{\circ}C$ and $40\,^{\circ}C$. These parameters ensured that the experimental conditions are in the region of the linear viscoelasticity.

In oscillatory rheometry test the gel point is usually assessed as a point where elastic and loss modulus curves intersect in a graph of viscoelastic moduli versus time. In early reaction times the reactive mixture is liquid, so the loss modulus is much higher than the elastic modulus. With the progress of the polymerisation reaction, both moduli grow with loss modulus keeping larger values than the elastic modulus up to the gel point where they match up, afterwards the elastic modulus grows faster than the loss because the mixture is now closer to the behaviour of a solid material than a liquid. The relation of the two moduli can be also represented by the loss factor, which is the ratio of the loss to storage modulus.

Oscillatory tests results for OTO method are shown as viscoelastic moduli versus reaction time with the angular frequency as a changing parameter at $25\,^{\circ}C$ and $40\,^{\circ}C$ in Figure 4.36 and Figure 4.37, respectively. Specific pattern is observed at both temperatures: with an increase in the angular frequency the viscoelastic moduli grows faster. Points where the viscoelastic moduli crossover, called gel points, versus angular frequency are represented at $25\,^{\circ}C$ in Figure 4.38 and at $40\,^{\circ}C$ in Figure 4.39 together with storage modulus at the gel point versus the angular frequency. At both temperatures it is observed that gel point decreases and elastic moduli increase with an increase in angular frequency. With an increase in temperature the difference between the gel points at different angular frequencies decreases. Gel point is the

point where the reactive mixture could be identified as one hypothetically large macromolecule that spreads throughout the whole sample (Djonlagic and Jovanovic 2004). With an increase in temperature gel point is achieved faster due to the faster rate of the reaction. At $40\,^{\circ}\mathrm{C}$ the angular frequency effect on the gel point is not as much as significant as at $25\,^{\circ}\mathrm{C}$, because the temperature effect on the polymerisation rate is the dominant effect. At $25\,^{\circ}\mathrm{C}$ the difference between the gel time, t(gel) , at $1\,\mathrm{s}^{-1}$ and $10\,\mathrm{s}^{-1}$ is 1.23 times, and at $40\,^{\circ}\mathrm{C}$ the same difference is 1.08 times.

When the rheometer is used for a production of the samples for mechanical tests, two parameters are used to assess the optimal demoulding time: gel point and elastic modulus. It is observed in Figure 4.38 and Figure 4.39 that the value of elastic modulus at gel point for the same frequency is higher at $25\,^{\circ}\mathrm{C}$ than at $40\,^{\circ}\mathrm{C}$. At higher temperature even though the gel points are achieved faster, the sample did not have enough time to gain as high elastic modulus as at $25\,^{\circ}\mathrm{C}$. As the temperature is higher the elastic modulus is lower, because at higher temperature the movements of the macromolecular chains are enabled (Fukuhara and Sampei 1996, Nakamae, Nishino et al. 1999).

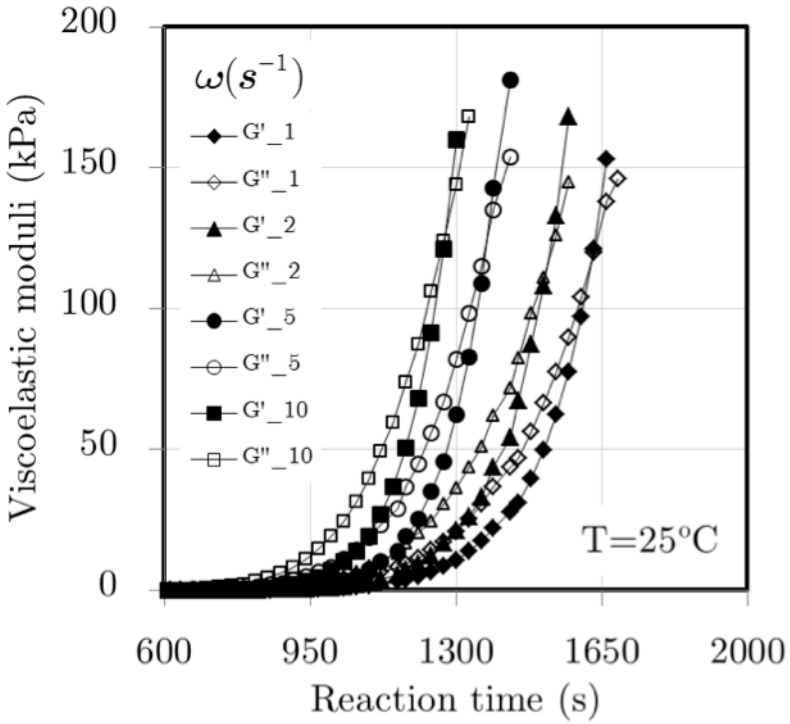

Figure 4.36. Viscoelastic moduli vs. reaction time at 25 °C.

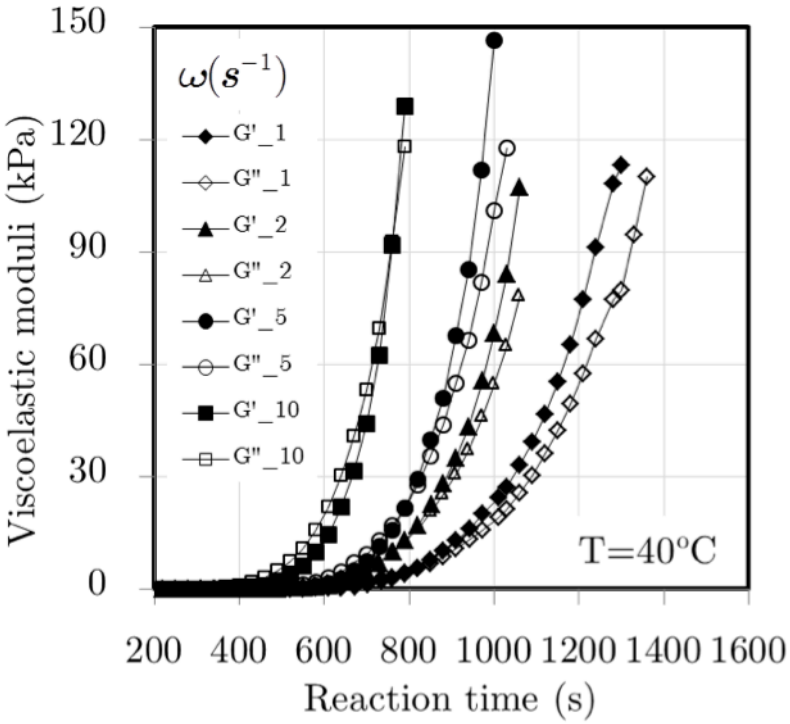

Figure 4.37. Viscoelastic moduli vs. reaction time at 40 °C.

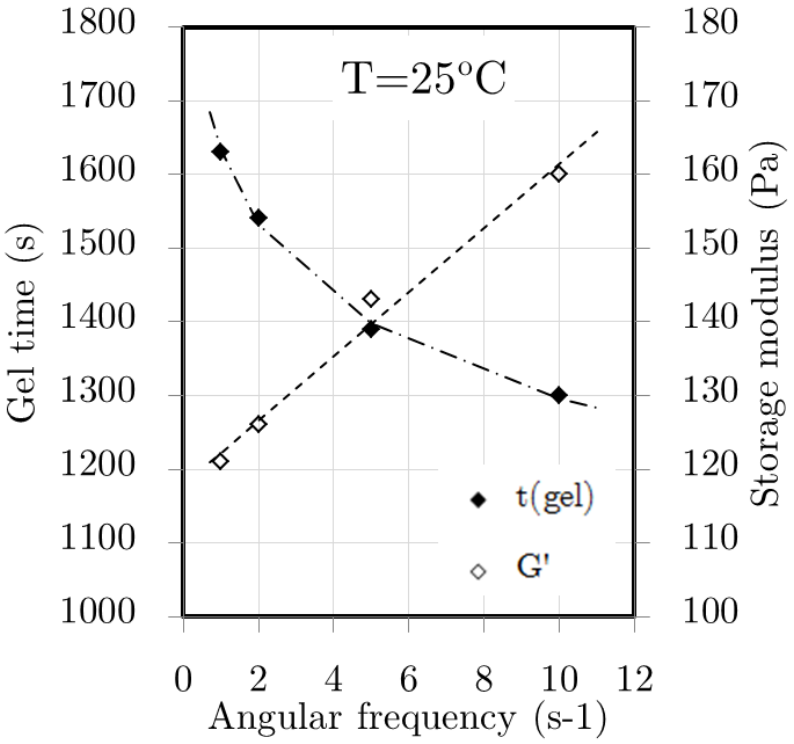

Figure 4.38. Gel time and storage modulus vs. angular frequency for OTO at 25°C.

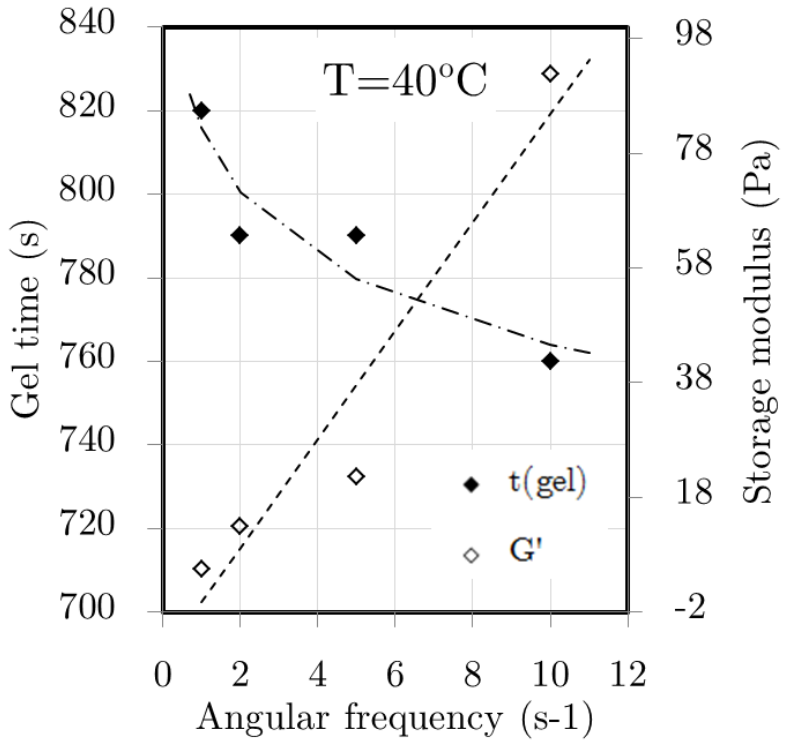

Figure 4.39. Gel time and storage modulus vs. angular frequency for OTO at 40°C.

Although the most precise way of gel point estimation is the elastic moduli crossover point, some authors reported that the gel point may be estimated as the point in

time when the loss factor becomes independent of the angular frequency (Chambon, Petrovic et al. 1986, Winter and Chambon 1986). For RenCast formulation it was already stated above that viscoelastic moduli and gel point depend on the angular frequency, but when the loss factor versus reaction time was plotted in Figure 4.40 and Figure 4.41 at $25\,^{\circ}\mathrm{C}$ and $40\,^{\circ}\mathrm{C}$ respectively, an important observation was made as follows. After the initial decrease in the loss factor, on the plot appears an inflexion in the loss factor curve in the time range $600-1000\,\mathrm{s}$ at $25\,^{\circ}\mathrm{C}$ and $200-6500\,\mathrm{s}$ at $40\,^{\circ}\mathrm{C}$. The time of the inflexion depends on the angular frequency, and it decreases as the angular frequency increase at both temperatures. When the loss factor decreases, the loss modulus grows faster than the elastic one. Situation where inflexion in loss factor appears is when the storage modulus grows faster than the loss modulus, but loss factor is higher than unity. This is most probably an indication of some rearrangement in the molecular level of the polymer at the point of the loss factor inflexion. The loss factor inflexion and value, as well as the ratio of the viscoelastic moduli are summarized in Table 4.5.

It appears to exist two points of intersection of the loss factor curves at each temperature: at $25\,^{\circ}\mathrm{C}$ the first point of the intersection is at $550\,\mathrm{s}$ and the second at $850\,\mathrm{s}$, and at $40\,^{\circ}\mathrm{C}$ at $475\,\mathrm{s}$ and $800\,\mathrm{s}$. Due to the fact that the formulated polyol is $5-15\%$ of propoxylated ethylene diamine, and that the rate of reaction of an aliphatic amine and aromatic isocyanate is higher than the rate of any other compound containing active hydrogen (Macosko 1989), this means that in early reaction times amine groups react with isocyanate groups and form urea hard segments. These segments get connected by the hydrogen bonds, forming an interconnecting physical network which is manifested by the *physical gel point* at the first intersection. At higher reaction times, hydrogen bonds of the physical network are being broken by the movement of the cone of the rheometer, which is manifested as a slight increase of the loss factor curves in Figure 4.40 and Figure 4.41. Further in the reaction, loss factor decreases for all used angular frequencies, until all curves crossover at the second intersection point, indicating the *chemical gel point*. At this

point crosslinked polyol -urethane network is being formed. In the end of the polymerisation, urea hard segments are dispersed in the crosslinked polyester-urethane network. Two identified gel times are: at 25°C 550s - the formation of the hydrogen bonded urea segments network, and at 850s - the formation of polyester-urethane crosslinked network, and at 40°C at 475s and 800s respectively.

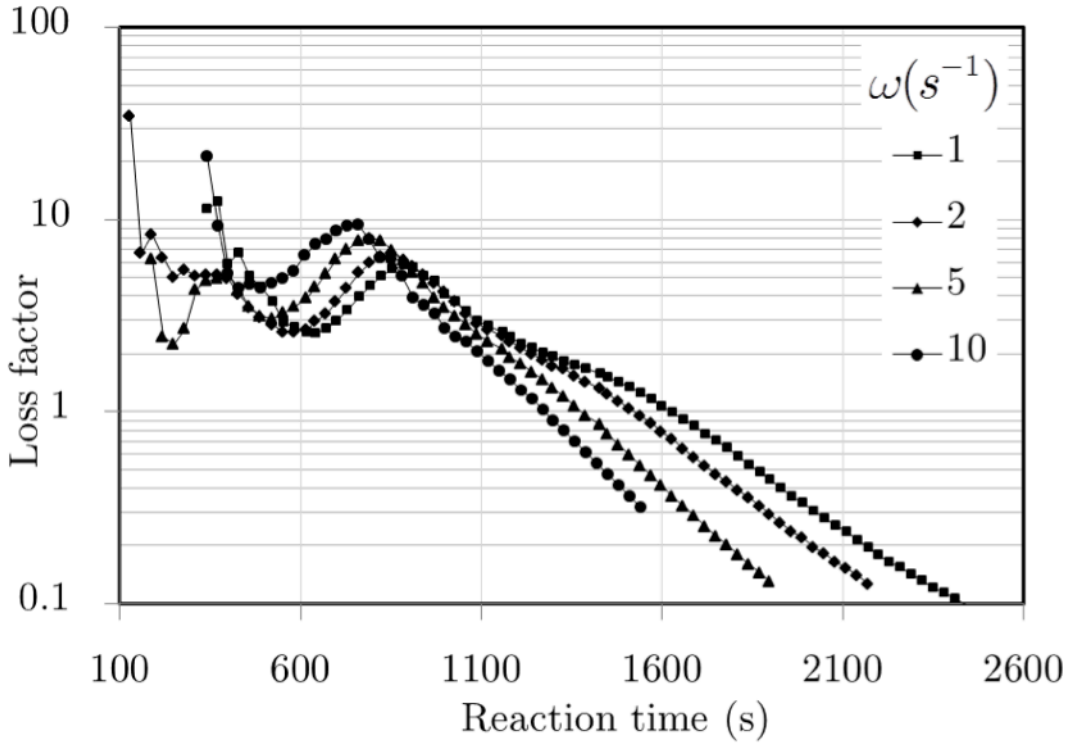

Figure 4.40. Loss factor vs. reaction time with angular frequency as a parameter at 25°C.

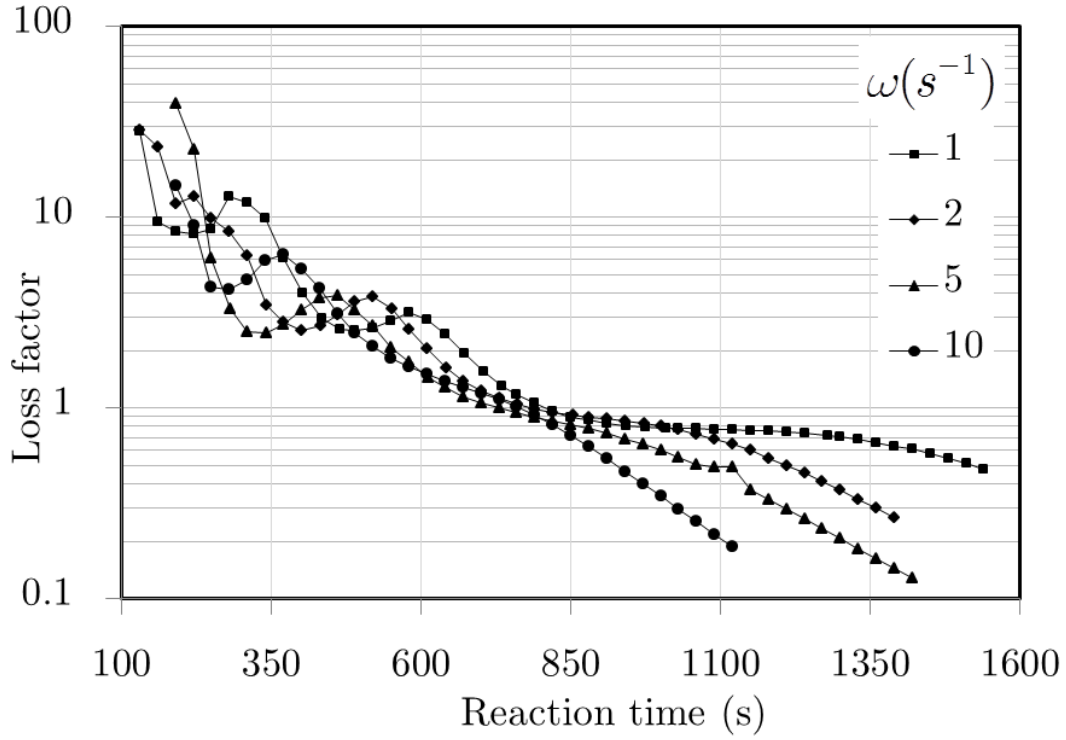

Figure 4.41. Loss factor vs. reaction time with angular frequency as a parameter at 40 °C.

Table 4.5. Loss factor and viscoelastic moduli evolution.

Loss factor inflection	Viscoelastic moduli relation	Loss factor value
$\tan\delta \searrow$		
$\tan\delta \nearrow$	$G" > G'$	$\tan\delta > 1$
$\tan\delta \searrow$		
$\tan\delta \searrow$	$G" < G'$	$\tan\delta < 1$

4.6.2 Premixing shear rate effect

In order to estimate the effect of premixing shear rate on viscosity rise as already mentioned before, premix shear rates of $100\,s^{-1}$, $500\,s^{-1}$, $800\,s^{-1}$ and $1000\,s^{-1}$ were studied at constant premixing time duration of $100\,s$. Oscillation parameters were kept constant in all experiments, using strain of 1% and angular frequency of $50\,s^{-1}$. The effect of the premix shear rate is assessed by comparing gel time points and storage modulus obtained in oscillation reaction interval at $40\,°C$ that is shown in Figure 4.42. It is observed that with an increase in premixing shear rate gel time decreases and storage modulus increases. Optimal premixing shear rate is assessed to

be in range $500-1000\,s^{-1}$, because for this range of shear rates, elastic modulus values are significantly higher (in the range of 90 kPa to 150 kPa) than for the shear rate of $100\,s^{-1}$ (elastic modulus approx. 30 kPa). Higher value of the elastic modulus is important for the successful demould of the product and it also affects the gel time, which should be as lower as possible in order to maintain the industrial production requirements. However, in order to measure rheological properties of the RenCast formulation for both mixing methods (OTO and the HC) it is chosen the unique premixing shear rate of $500\,s^{-1}$, because this rate of premixing enables slower polymerisation reaction, which is desirable for the accurate detection of the viscosity rise and gel point.

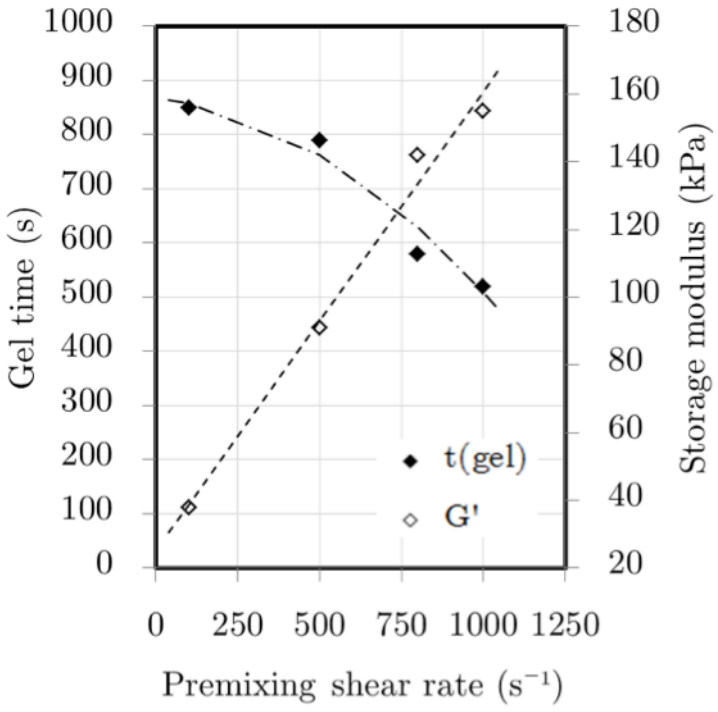

Figure 4.42. Gel point and storage modulus vs. premixing shear rate at 40 °C.

4.6.3 Premixing time effect

Premixing time effect with constant shear rate in rotation on the gel point and storage modulus was investigated at 40 °C. Premixing shear rate was set to $500\,s^{-1}$, and interval duration was different, 10 s, 50 s and 100 s. Oscillation reaction interval

had the same parameters for all the tests, using strain of 1% and angular frequency of $10\,s^{-1}$. Represented results are the average values of three measurements and they are shown in Figure 4.43 where gel time and storage modulus versus the premixing time are plotted at $40\,°C$. With an increase in premixing time the duration of the gel point decreases, and storage modulus increases. It is concluded that optimal premixing time should be $100\,s$ for efficient mixing.

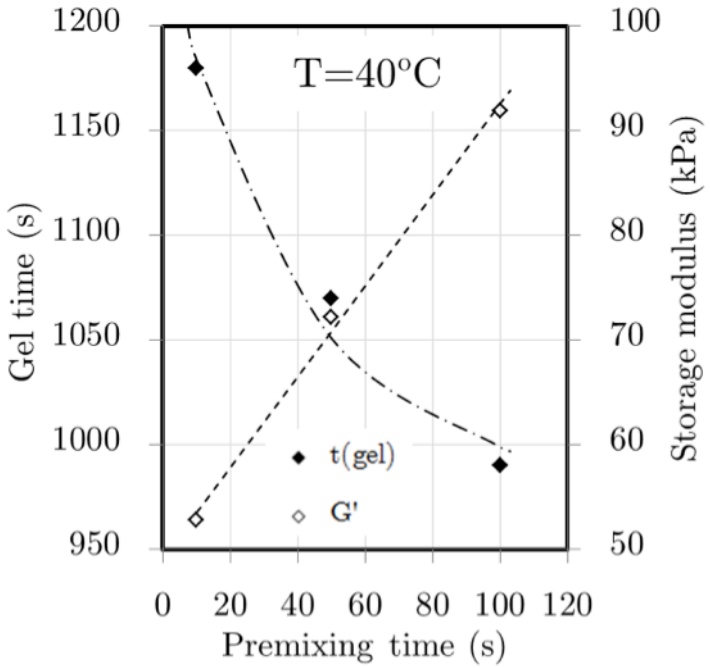

Figure 4.43. Gel point and storage modulus vs. premixing time at $40\,°C$.

4.7 Mechanical characterisation

Samples for the compression and deflection temperature measurements were produced at $40\,°C$ at the rheometer using the HC method. Premixing interval parameters were: $500\,s^{-1}$ shear rate and time duration of $100\,s$; reaction parameters 1% strain and $10\,s^{-1}$ angular frequency. The gap between the cone and the plate of the rheometer was set to 8 mm in order to obtain samples with the required thickness for the mechanical analysis. Different premixing shear rates were used $500\,s^{-1}$, $750\,s^{-1}$ $1000\,s^{-1}$ and $1500\,s^{-1}$ and the mechanical properties at each shear rate are compared. In order to guarantee reproducibility of the results, for both compression and

deflection temperature measurements, three samples for each premixing shear rate were produced and tested mechanically. A total of 12 samples for compression tests and 12 samples for deflection temperature determination were used. Prior to the measurements, samples produced at the rheometer were machined into the test specimens with the required size. From each sample, one test specimen was obtained. Only the average values of three identical measurements are presented in the following sections.

In compression tests, three material properties were measured (taken from the stress-strain curve under an axial force):

- Compressive stress at yield, σ_y, which is the limit of elastic region;
- Maximum compressive strength, σ_M, the maximum strength;
- Compressive strength at break, σ_B, which is achieved when the specimen breaks and it is the limit of the plastic region.

For the deflection temperature determination, samples were cut by machining into the specimens with the dimensions as represented in Figure 4.44, where L is the specimen length, w is the specimen width and t_s is the specimen thickness,

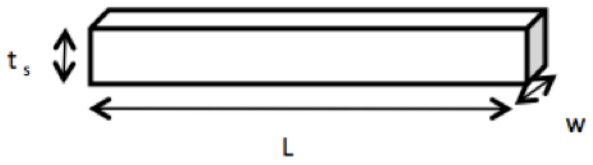

Figure 4.44. DMA specimens dimensions.

Loss factor $\tan(\delta)$ is defined as a ratio of the loss and the storage modulus in DMA tests. According to some authors (Menard 2008), loss factor is also called the *damping*, because it is a measure of material's lost of energy to the rearrangements in the molecular level and the internal friction.

One of material properties that is typically measured in DMA tests is the complex modulus, E^*, which is often called simply modulus. Since the force acting on the

sample is changing (dynamical), response of the viscoelastic sample consists of two parts: the elastic one and the viscous one. The elastic property of the sample is measured by the elastic modulus, E' and the viscous by the loss modulus E". The complex modulus is calculated from

$$E^* = E' + iE'' = \sqrt{\left(E'\right)^2 + \left(E'\right)^2} \tag{4.7}$$

4.7.1 Compression strength

In order to assess the effect of the premixing shear rate on the compressive properties of RenCast solid samples, compressive stress at yield, compressive strength and compressive strength at break from the stress-strain curves were made on the sample and are compared in Table 4.6. Samples name legend: C stands for samples for compression, $500 / 750 / 1000 / 1500\ s^{-1}$ are premixing shear rates. From data in Table 4.6 is observed that all measured compressive properties of the samples are significantly lower at $500\ s^{-1}$ than for other premixing shear rates, with differences of 5% from the average values of the other samples for the compressive stress and of 20% for compressive strength and compressive strength at break. No significant difference in the compressive properties at higher premixing shear rates was observed.

Table 4.6. Average values for some mechanical properties for each premixing shear rate.

Mechanical property	C500	C750	C1000	C1500
Compressive stress at yield [MPa]	32.9	34.0	35.1	34.7
Compressive strength [MPa]	35.1	44.4	46.3	41.1
Compressive strength at break [MPa]	32.1	42.0	40.6	40.8

It is concluded that the premixing shear rate for the production of samples for compression tests can be $750\ s^{-1}$.

4.7.2 Deflection temperature

In Table 4.7 are represented the sizes of all samples. For example in the sample labelled D500_1, D stands for deflection temperature test, 500 for premixing shear

rate, and _1 for the first run of the total number of runs, which was 3 for every premixing shear rate.

Table 4.7. Samples sizes for deflection temperature determination.

Sample name	Length [mm]	Width [mm]	Thickness [mm]
D500_1	10.00	5.00	5.00
D500_2	10.00	4.90	4.60
D500_3	10.00	4.80	4.90
D750_1	10.00	4.50	4.70
D750_2	10.00	5.10	4.90
D750_3	10.00	5.00	5.00
D1000_1	10.00	5.00	4.60
D1000_2	10.00	4.90	5.10
D1000_3	10.00	4.90	5.00
D1500_1	10.00	5.10	4.60
D1500_2	10.00	4.90	4.50
D1500_3	10.00	5.00	4.90

Maximum values of the loss factor and correspondent temperature are presented in Table 4.8. It was expected that as the premixing shear rate increases, deflection temperature would also increase. The lack of this pattern may be due to the problems with reproducibility of the results.

Table 4.8. Maximum value of loss factor and respective deflection temperature.

Sample	Max loss factor	Temperature [°C]
D500	0.714	103.8
D750	0.705	97.7
D1000	0.722	106.2
D1500	0.871	101.8

In Table 4.9 are represented values of the complex modulus for each premixing shear rate at different temperatures.

Table 4.9. Modulus at different temperatures for all samples.

	Modulus [MPa]				
Sample	25°C	80°C	100°C	120°C	140°C
D500	367	47.4	16.9	5.15	3.71
D750	275	24.5	7.83	3.21	2.97
D1000	309	36.1	16.8	4.33	3.52
D1500	415	58.5	20.3	5.1	4.38

It is concluded that the samples produced using the premixing shear rate $1500\ s^{-1}$ would have significantly higher modulus than the other samples. This result illustrates the critical role of mixing in RIM mixing chamber on the mechanical properties of produced parts (Kolodziej, Macosko et al. 1982, Kolodziej, Yang et al. 1986). Nevertheless, these results should be regarded with some care, because there is not a clear trend of the modulus with the premixing shear rate, and for example at 120°C approximately the same moduli values are obtained for D500 and D1500.

4.8 Mixing time versus shear rate

The mixing time is set by the premixing shear rate. Figure 4.45 shows the Computational Fluid Dynamics simulation of mixing of a white and black fluid in a cone and plate geometry, the first image is after a quarter of a cone turn and the second image is taken after one and a half turn. Considering that in each turn of the cone over the sample two layers of liquids form, the mixing scale is then decreased to half according to:

$$s = \frac{y}{2^N} \tag{4.8}$$

Where s is the scale of the lamina, y is the initial thickness of the lamina and N is the number of the cone turns. The number of cone turns is given by $N = t\omega$ where

ω is the rotational speed of the cone and t is the time. The rotational speed is related the de shear rate, $\dot{\gamma}$ according to:

$$\omega = \dot{\gamma} \tan \alpha \tag{4.9}$$

Where α is the angle of the cone. The scale of the monomer layers in the rheometer is then given by:

$$s\left(t\right) = \frac{y}{2^{t\dot{\gamma} \tan \alpha}} \tag{4.10}$$

For a cone with 50 mm the thickness of the fluid layer is around $400\,\mu\text{m}$, so this can be consider as the initial scale of mixing. After 1s this scale is kept almost the same for a shear rate of $\dot{\gamma} = 1\,\text{s}^{-1}$, while if $\dot{\gamma} = 1000\,\text{s}^{-1}$ the scale decreases to $2\,\text{nm}$.

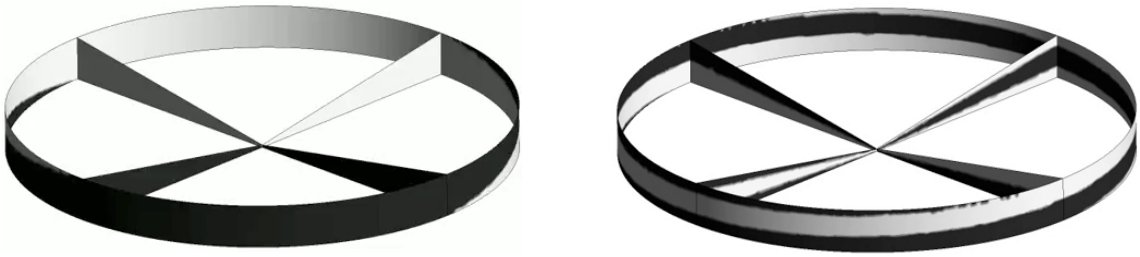

Figure 4.45. Concentration Maps from the Computational Fluid Dynamics simulation of the mixing of two fluids (black and white fluid) in cone and plate geometry. Maps a surface around the geometry and two radial cuts.

4.9 Conclusions

Rheological characterisation of the reactants was carried out. A method for the efficient premixing of the two reactants for a low temperature polyurethane formulation was developed, using two distinct periods: premixing period that enables efficient mixing; and reaction period that enables detection of material properties evolution, such as gel point and viscosity rise due to the polymerisation reaction. These values are useful for the mould design in RIM machines, to predict the

demoulding time and the viscosity rise inside the mixing chamber and during mould filling. This method can be used for other polymerisation reactions.

Main results of this study are:

- Reactive mixture shows Newtonian behaviour;
- Viscosity rise at both temperatures is affected by the shear as follows: for shear rates lower than $100\,s^{-1}$ no edge fracture occurs, for shear rates higher than $100\,s^{-1}$ edge fracture may occur;
- Mixing efficiency may be assessed with gel time and storage modulus. Lower gel point and higher storage modulus are consequences of more efficient mixing; more efficient mixing is favoured with higher premixing shear rates and longer premixing duration times;
- Two premixing methods were tested and compared OTO and the HC. Better control of the reaction is obtained with the HC;
- From the oscillatory experiments, for RenCast reactive formulation due to the reactants formulations, two gel points were observed physical and chemical gel points indicating existence of the initial phase-separated polymeric structure which later in the reaction becomes dominated by the chemically connected polymer network;
- The optimal premixing shear rate for the production of samples with thickness of 8 mm for compression tests is $750\,s^{-1}$;
- Deflection temperature measurements shown significantly higher modulus when using larger premixing shear rate, $1500\,s^{-1}$.

4.10 References

Castro, J. M. and C. W. Macosko (1980). "Kinetics and rheology of typical polyurethane reaction injection molding systems." Society of Plastics Engineers (Technical Papers): 434-438.

Chambon, F., Z. S. Petrovic, et al. (1986). "Rheology of model polyurethanes at the gel point." Macromolecules**19**(8): 2146-2149.

Chen, Y.-T. and C. W. Macosko (1996). "Kinetics and rheology characterisation during curing of dicyanates." Journal of Applied Polymer Science**62**(3): 567-576.

Dimier, F., N. Sbirrazzuoli, et al. (2004). "Curing kinetics and chemorheological analysis of polyurethane formation." Polymer Engineering & Science**44**(3): 518-527.

Djonlagic, J. and S. M. Jovanovic (2004). Hemija makromolekula. Beograd, Tehnolosko-metalurski fakultet.

Fonte, C. P., R. J. Santos, et al. (2011). "Quantification of Mixing in RIM Using a Non-Diffusive Two-Phase Flow Numerical Model." International Journal of Chemical Reactor Engineering**9**(A114).

Fukuhara, M. and A. Sampei (1996). "Temperature dependence of elastic moduli and internal dilational and shear frictions of polyimide." Journal of Polymer Science, Part B: Polymer Physics**34**(9): 1579-1582.

Haddadi, H., E. Nazockdast, et al. (2008). "Chemorheological characterisation of thermosetting polyurethane formulations containing different chain extender contents." Polymer Engineering and Science**48**(12): 2446-2453.

Huntsman (2007). Advanced Materials. Rencast FC 52 Isocyanate / Rencast FC 52 Polyol.

Huntsman (2007). Safety data sheet: Rencast FC 52 Polyol

Huntsman (2011). "Safety Data Sheet: Rencast FC 52/53 Isocyanate."

Ivankovic, M., L. Incarnato, et al. (2003). "Curing kinetics and chemorheology of epoxy/anhydride system." Journal of Applied Polymer Science**90**(11): 3012-3019.

Kim, D. S. and C. W. Macosko (1996). "Reaction kinetics and chemorheology of a highly reactive PU system." Korea Polymer Journal**4**(1): 54-60.

Kolodziej, P., C. W. Macosko, et al. (1982). "The influence of impingement mixing on striation thickness distribution and properties in fast polyurethane polymerisation." Polymer Engineering & Science**22**(6): 388-392.

Kolodziej, P., W. P. Yang, et al. (1986). "Impingement Mixing And its Effect on the Microstructure of RIM Polyurethanes." Journal of Polymer Science, Part B: Polymer Physics**24**(10): 2359-2377.

Macosko, C. W. (1989). RIM, Fundamentals of Reaction Injection Molding, Hanser

Macosko, C. W. (1994). Rheology: Principles, Measurements, and Applications, Wiley-VCH.

Malkin, A. Y. and S. G. Kulichikhin (1991). "Rheokinetics of curing." Advances in Polymer Science**101**: 216-257.

Menard, K. P. (2008). Dynamic Mechanical Analysis: A Practical Introduction, CRC Press.

Nakamae, K., T. Nishino, et al. (1999). "Temperature dependence of the elastic modulus of the crystalline regions of poly(p-phenylene benzobisthiazole)." Polymer**40**(16): 4629-4634.

Sun, X., J. Toth, et al. (1997). "Chemorheology of poly(urethane/isocyanurate) formation." Polymer Engineering & Science**37**(1): 143-152.

Tucker, C. L. and N. P. Suh (1980). "Mixing for reaction injection molding. I. Impingement mixing of liquids." Polymer Engineering & Science**20**(13): 875-886.

Winter, H. H. and F. Chambon (1986). "ANALYSIS OF LINEAR VISCOELASTICITY OF A CROSSLINKING POLYMER AT THE GEL POINT." Journal of Rheology**30**(2): 367-382.

5 Polyamides by Ring-opening Polymerisation

5.1 Introduction

The developed rheological methodology for the mixing and curing of reactive polymerisations was previously described for the polyurethane casting resin. This chapter uses the same methodology with a different measuring system in the rheometer, which is required due to the high processing temperature of polaymide-6 formulation for RIM. The differences between the polyurethane system used in Chapter 4 and polyamide-6 formulation studied in this thesis are:

- Polyurethane is a low temperature formulation reacting in the temperature window 20 °C to 40 °C to yield a solid product having gel times in the order of 15 to 20 minutes, and therefore it is well suited for the accurate measurement of its rheological characteristics during the polymerisation; Polyamide-6 formulation is a higher temperature formulation requiring at least 100 °C to 120 °C to form the solid product in less than a minute.
- Polyurethane reactants, especially handling of isocyanates is delicate, since it reacts with a large number of compounds including itself and air. In the reactions between isocyanate and other compounds in most cases are formed

polyurethanes or polyureas and they get glued to any surface they get into contact. Removal of these undesired by-products is found to be extremely difficult, requiring significant amounts of dichloromethane (DCM) solvent and mechanical action. Toxicity of isocyanate and DCM are very high. Polyamide-6 reactants do not show many difficulties in handling, and their reactivity and toxicity at room temperature is low;

- Polyurethane formulation is a thermoset while the polyamide-6 is a thermoplastic. Chemical structure of thermosets can be characterised by swelling and by partial chemical degradation. Molecular weight and size measurement make sense for the small amount of soluble fraction which can be present. Determination of the gel and melting temperature for the thermosetting polyurethane sample is not possible, because its very dense network structure is stable on high temperatures. At temperatures as high as the degradation temperature, the structure begins to collapse and the polymer starts to carbonize and desegregate. Strong covalent bonds of the polyurethane network prevent the sample to dissolve in the common solvents such as tetrahydrofuran. Practice showed that only dichloromethane can start breaking the sample out in a small amount, which is not sufficient for the molecular weight techniques.
- While for polyurethane formulation only mechanical tests were applicable, for nylon-6 formulation besides the mechanical tests, the determination of the molecular weight, gel point and melting point was also possible to carry out.

The melting temperature of polyamide-6 is $200\,^{\circ}\mathrm{C}$ and the glass transition temperature $75\,^{\circ}\mathrm{C}$.

5.2 Method and experiment

5.2.1 Experimental set up

In Figure 5.1 are shown the rheometer with electrically heated hood EH-TEK350 and temperature controller TC-20 which is connected to both the lower fixed plate of the

rheometer, and also to the hood TEK350. Since the temperature controller is based on an electrical resistance placed directly in the plate and hood, the set temperature both at plate and at hood is achieved very quickly. TEK350 hood is also connected to the compressed air for cooling and can be seen from the black tubes in the photo in Figure 5.2. Due to the fact that the exothermic chemical reaction for the formation of nylon-6 occurs inside the hood, overheating may occur and the generated heat be transferred through the cone axis to the rheometer motor. In order to avoid any heat caused damages, cooling of the hood is necessary, which it made by circulating compressed air through the hood whenever the temperature raises above the set point.

Figure 5.1. Rheometer equipped with thermostat units TEK350 and TC20.

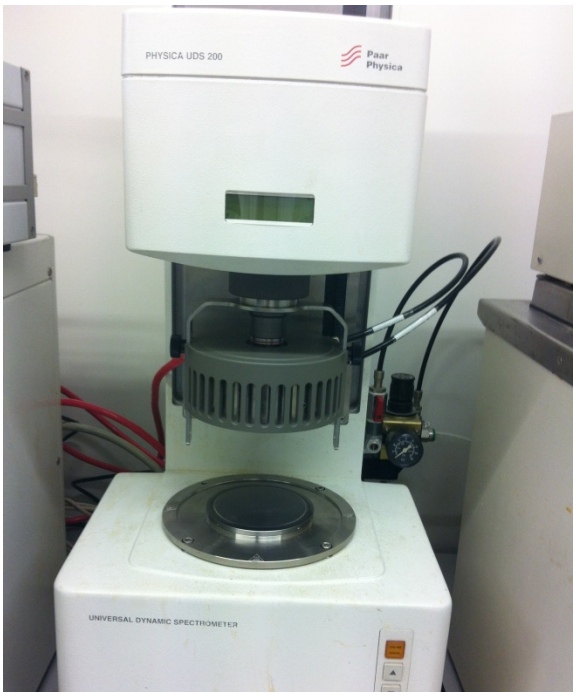

Figure 5.2. TEK350 hood with compressed air inlet and outlet.

5.2.2 Reactants and their preparation

The polyamide-6 formulation was supplied by the Bruggemann Chemicals and it consisted of the three reactants: caprolactam monomer, and a mixture of the initiator in the monomer, and a mixture of the catalyst in the monomer as shown in the Table 5.1.

Table 5.1. Reactant names.

Reactant	Name	Short name
Monomer	Caprolactam, anionic grade	CL
Initiator	Sodium caprolactamate in caprolactam	BruggolenC10
Catalyst	Hexamethylene-1,6-dicarbamoyl-caprolactam in caprolactam	BruggolenC20P

Sodium-caprolactamate(Na-CL) is an organometallic compound also called Grignard reagent able to create carbon-carbon bonds. In the synthesis of polyamide-6 the sodium caprolactamate in caprolactam (trade name C10) is used as a catalyst. The melting point of C10 is $62\,^{\circ}\mathrm{C}$. Hexamethylene-1,6-dicarbamoyl-caprolactam (B-iso) is used as an initiator. This compound is a difunctional blocked isocyanate which at temperature higher than $160\,^{\circ}\mathrm{C}$ de-blocks itself into de-blocking reaction and as a

result generates a product with free isocyanate group. Concentration of sodium-caprolactamate (Na-CL) in C10 and of hexamethylene-1,6-dicarbamoyl-caprolactam (B-iso) in C20 is 17wt.%.

Reactant properties such as molecular weight M_W, and melting temperature T_m are shown in Table 5.2.

Table 5.2. Reactant properties.

Physical property	CL	C10	C20
$M_w\left[g/mole\right]$	113.16	135	392
$\rho\left[g/cm^3\right]$	1.01	1.12	1.20
$T_m\left[^oC\right]$	69.2	62.2	60
$T_b\left[^oC\right]$	270.8	270	85

All the reactants were kept separately in well-closed glass bottles and were kept in the oven at $50\,^oC$ for at least 6 hours before experiments.

5.2.3 Reactants preparation

Necessary quantities of all reactants (see Appendix B) were measured and two tanks were prepared, monomer and initiator and monomer and catalyst. Each tank was heated to $80\,^oC$ on a hot plate and mixed while melted for 30 minutes with magnetic stirring bars.

5.3 Reactants viscosity

Monomer viscosity was measured using TEK350 at constant temperature, for the following temperatures: $75, 80, 85, 90, 95, 100$ and $105\,^oC$. Before the rheological test, the solid monomer was weighted and put on the hot rheometer plate. After few seconds on the hot plate the monomer melts. The cone is then lowered to the measuring position and the rheological test is started. Experimental parameters used were: 20 points, total duration time 200 seconds, shear rate within linear ramp $10-500\,s^{-1}$. Figure 5.3 represents the viscosity versus temperature for caprolactam

monomer. Since the caprolactam melting temperature is 69.2 °C (see Table 5.2) first point of viscosity is measured at 75 °C and it was 9.4 mPa.s, and the last point measured at 100 °C was 3.3 mPa.s. Viscosity value at 100 °C is in the order of magnitude of water at room temperature which is 1mPa.s (Barnes, Hutton et al. 1989). Since the mixtures (A/B) of the caprolactam and C10/C20 have predominantly caprolactam (between 96wt.% and 98wt.%) it is assumed that the viscosity of the mixtures is equal to the viscosity of the pure caprolactam.

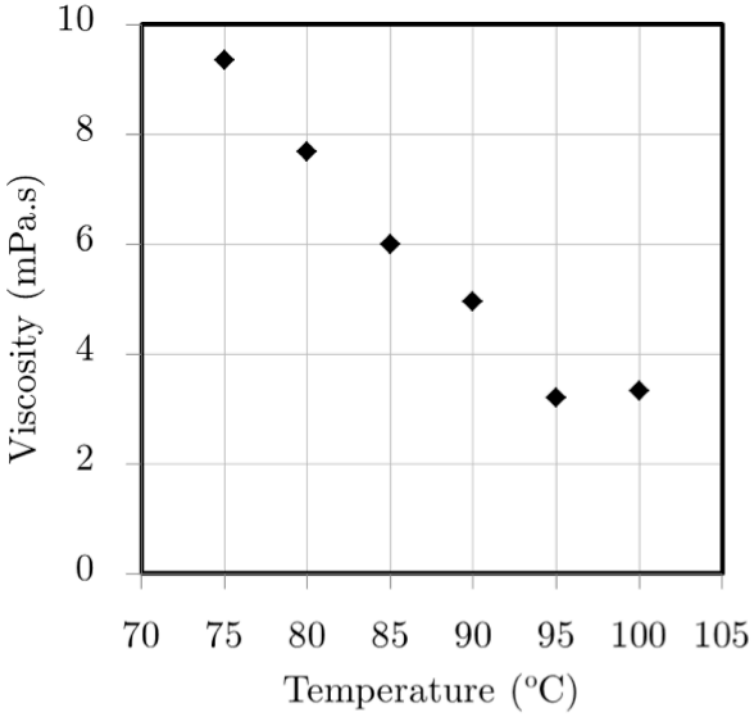

Figure 5.3. Viscosity vs. temperature for AP-caprolactam.

5.4 Experiments

Different formulations and different experimental conditions, such as premixing time and temperature, are measured and assessed for each formulation in order to determine optimal processing conditions for the production of the polyamide-6. Melting temperature of the monomer and initiator/catalyst are approx. 80 °C and the polymerisation temperature window to obtain the crystalline polyamide-6 is in the range 140 − 150 °C (van Rijswijk, Bersee et al. 2006).

Two experimental methods were tested and assessed by the measurement of the time when abrupt increase in complex viscosity is observed:

- Monomer and initiator/catalyst melting in around-bottom flask at $80\,^{o}\mathrm{C}$ and their transfer to the rheometer plate;
- Monomer and initiator/catalyst melting directly at the rheometer plate before the measurement.

5.5 Formulation 1

The lowest initiator/catalyst formulation was tested first by rheometry using the HC method. In the final solid sample, concentration of the Na-CL initiator (from C10) was 0.97 wt.% and blocked isocyanate (from C20) was 0.52 wt.%. Reactants were melted in round-bottom flask closed with a glass adapter at temperature of $80\,^{o}\mathrm{C}$. In order to melt the monomer in the round-bottom flasks, higher amount of reactants is required, and it is calculated on the 5 ml of mixture in each flask. In further text round-bottom flask is equal to tank A or tank B. The calculated masses and mass fractions are shown in Table 5..

Table 5.3. Reactants masses for Formulation 1.

Tank A		Tank B	
$\omega^{A}_{Na-Cl}\left[\%\right]$	2	$\omega^{B}_{B-iso}\left[\%\right]$	1
$V^{A}\left[ml\right]$	5	$V^{B}\left[ml\right]$	5
$m^{A}_{tot}\left[g\right]$	5.6	$m^{B}_{tot}\left[g\right]$	6
$m^{A}_{Na-Cl}\left[g\right]$	0.112	$m^{B}_{B-iso}\left[g\right]$	0.06
$m^{A}_{CL,tot}\left[g\right]$	5.49	$m^{B}_{CL,tot}\left[g\right]$	5.94
$\omega^{C10}_{Na-CL}\left[\%\right]$	17	$\omega^{C20}_{B-iso}\left[\%\right]$	17
$m^{C10}_{Na-Cl}\left[g\right]$	0.55	$m^{C20}_{B-iso}\left[g\right]$	0.29
$m^{A}_{CL,add}\left[g\right]$	4.9	$m^{B}_{CL,add}\left[g\right]$	5.6
$m^{A}_{C10}\left[g\right]$	0.66	$m^{B}_{C10}\left[g\right]$	0.35
$m^{samp}\left[g\right]$	11.6	$m^{samp}\left[g\right]$	$m^{samp}\left[g\right]$
$\omega^{samp}_{Na-CL}\left[\%\right]$	0.97	$\omega^{samp}_{B-iso}\left[\%\right]$	0.52

In the tank A $4.90\,g$of CL monomer was added together with $0.66\,g$ of C10. In the tank B $5.60\,g$ of CL monomer and $0.35\,g$ of C20 were blended. Both tank A and tank B made of glass were closed by the glass adapter and placed on a hot plate and left for 15 minutes at $80\,^{o}C$ until their contents melted. After, $0.35\,ml$ of each mixture was placed at the rheometer plate on each side ofthe holding cell. The rheometer cone was descended over the rheometer plate, the separator on the holding cell was removed, and the experiment started.

This experiment consisted of three consecutive intervals:

- Mixing rotational interval at $500\,s^{-1}$ at $100\,^{o}C$ for $60\,s$;
- Temperature ramp interval from $100\,^{o}C$ to $140\,^{o}C$ for $90\,s$;
- Reaction oscillation interval at strain of 5% and angular frequency of $10\,s^{-1}$ at temperature from $145\,^{o}C$ for $440\,s$.

Viscosity rise during premixing and complex viscosity rise in reaction interval are represented in Figure 5.4. Figure 5.4 represents slow and unsteady increase in the

complex viscosity in the oscillation interval. After 600 s from the beginning of the reaction, the complex viscosity values were still very low, approx. 60 - 70 mPa.s. This experiment was stopped at 600 s because the solid sample should be obtained in the time range 2-3 minutes when the concentrations of initiator/catalyst are correct (Davé, Kruse et al. 1997). In this formulation even at 600 s the complex viscosity rise was not fast enough (300 mPa.s) in order to obtain solidified sample at typical times for anionic polymerisations of nylon-6. So, it was considered that this formulation does not contain an adequate concentration of initiator/catalyst for the production in RIM process.

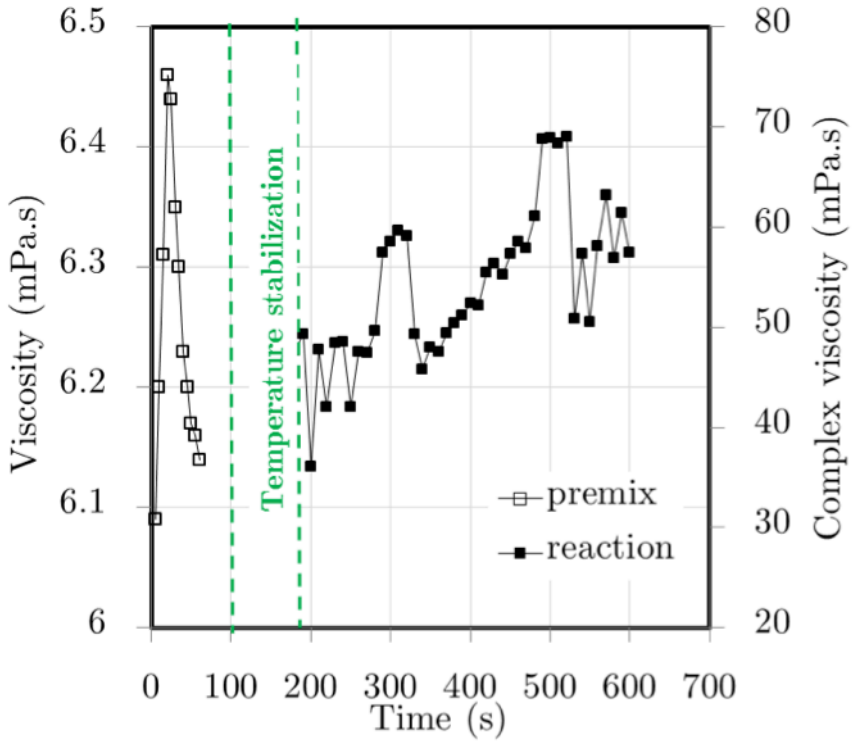

Figure 5.4. Viscosity rise at premixing interval (0 s - 80 s) and complex viscosity rise at reaction interval (200 s - 600 s) for Formulation 1.

5.6 Formulation 2

Medium concentration initiator/catalyst formulation was tested by rheometry using the HC method. In the final solid sample, concentration of the Na-CL catalyst (from C10) was 1.93 wt.% and blocked isocyanate (from C20) was 1.03 wt.%. Reactants

were melted in round-bottom flask closed with a glass adapter at hot plate at temperature of $80\,^{\circ}\mathrm{C}$. In order to melt in round-bottom flask higher amount of reactants is required, $5\,\mathrm{ml}$ of mixture in each flask. The round-bottom flasks are referred to as tank A or tank B. The calculated masses and mass fractions are represented in Table 5.4.

Table 5.4. Reactants masses for Formulation 2.

Tank A		Tank B	
$\omega^{\mathrm{A}}_{\mathrm{Na-Cl}}\left[\%\right]$	4	$\omega^{\mathrm{B}}_{\mathrm{B-iso}}\left[\%\right]$	2
$\mathrm{V}^{\mathrm{A}}\left[\mathrm{ml}\right]$	5	$\mathrm{V}^{\mathrm{B}}\left[\mathrm{ml}\right]$	5
$\mathrm{m}^{\mathrm{A}}_{\mathrm{tot}}\left[\mathrm{g}\right]$	5.6	$\mathrm{m}^{\mathrm{B}}_{\mathrm{tot}}\left[\mathrm{g}\right]$	6
$\mathrm{m}^{\mathrm{A}}_{\mathrm{Na-Cl}}\left[\mathrm{g}\right]$	0.22	$\mathrm{m}^{\mathrm{B}}_{\mathrm{B-iso}}\left[\mathrm{g}\right]$	0.12
$\mathrm{m}^{\mathrm{A}}_{\mathrm{CL,tot}}\left[\mathrm{g}\right]$	5.38	$\mathrm{m}^{\mathrm{B}}_{\mathrm{CL,tot}}\left[\mathrm{g}\right]$	5.88
$\omega^{\mathrm{C10}}_{\mathrm{Na-CL}}\left[\%\right]$	17	$\omega^{\mathrm{C20}}_{\mathrm{B-iso}}\left[\%\right]$	17
$\mathrm{m}^{\mathrm{C10}}_{\mathrm{Na-Cl}}\left[\mathrm{g}\right]$	1.09	$\mathrm{m}^{\mathrm{C20}}_{\mathrm{B-iso}}\left[\mathrm{g}\right]$	0.59
$\mathrm{m}^{\mathrm{A}}_{\mathrm{CL,add}}\left[\mathrm{g}\right]$	4.3	$\mathrm{m}^{\mathrm{B}}_{\mathrm{CL,add}}\left[\mathrm{g}\right]$	5.3
$\mathrm{m}^{\mathrm{A}}_{\mathrm{C10}}\left[\mathrm{g}\right]$	1.32	$\mathrm{m}^{\mathrm{B}}_{\mathrm{C10}}\left[\mathrm{g}\right]$	0.71
$\mathrm{m}^{\mathrm{samp}}\left[\mathrm{g}\right]$	11.6	$\mathrm{m}^{\mathrm{samp}}\left[\mathrm{g}\right]$	11.6
$\omega^{\mathrm{samp}}_{\mathrm{Na-CL}}\left[\%\right]$	1.90	$\omega^{\mathrm{samp}}_{\mathrm{B-iso}}\left[\%\right]$	1.03

5.6.1 Experimental conditions I

This experiment consisted of three consecutive intervals:

- Mixing rotational interval at $500\,\mathrm{s}^{-1}$ at $110\,^{\circ}\mathrm{C}$ for $60\,\mathrm{s}$;
- Temperature ramp interval from $110\,^{\circ}\mathrm{C}$ to $145\,^{\circ}\mathrm{C}$ for $90\,\mathrm{s}$;
- Reaction oscillation interval at strain 5% and angular frequency $10\,\mathrm{s}^{-1}$ at temperature $145\,^{\circ}\mathrm{C}$ for $20\,\mathrm{s}$.

Experimental data is represented in Figure 5.5 where is seen that the viscosity of the mixture in the premixing interval rises from $6.6\,\mathrm{mPa.s}$ to $11.7\,\mathrm{mPa.s}$ at temperature

110 °C. Second interval of 90 s was necessary to increase the temperature from 110 °C to 145 °C. In the third interval, complex viscosity rise was measured and it was observed that it rises abruptly in 10 s from 1 Pa.s to 217 kPa.s. In the end of experiment at 170 s solid polymer is obtained.

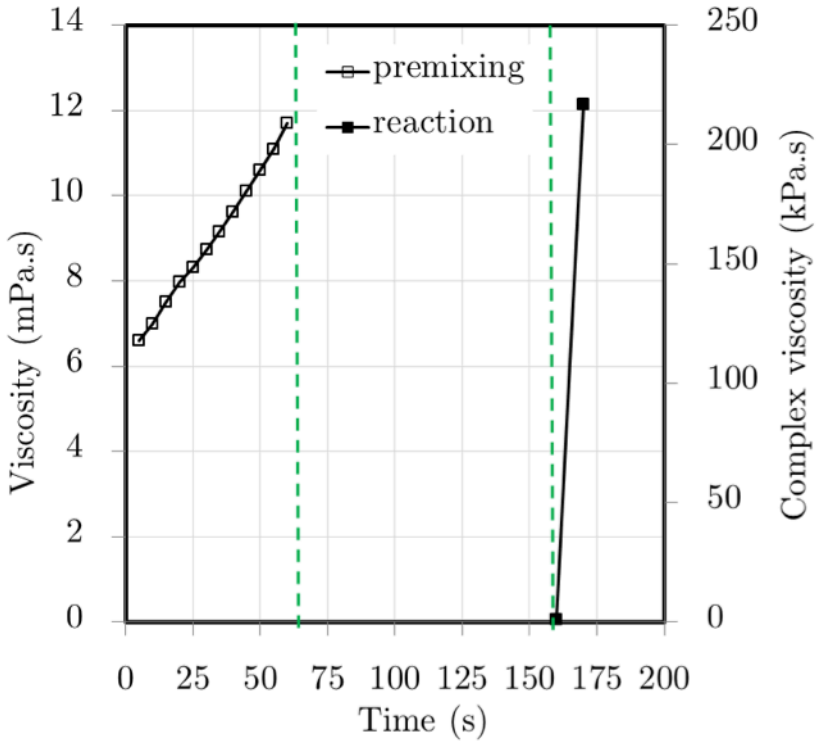

Figure 5.5. Viscosity rise at premixing interval (0 s - 75 s) and complex viscosity rise at reaction interval (160 s - 200 s) for Formulation 2.

5.6.2 Experimental conditions II

Effect of the premixing temperature on the complex viscosity rise is studied using the following experimental conditions:

- Mixing rotational interval at 500 s^{-1} at 140 °C for 30 s;
- Temperature stabilisation interval at 140 °C for 40 s;
- Reaction oscillation interval at 5% and 100 s^{-1} at temperature 140 °C for 5 s

.

Results are shown in Figure 5.6 where viscosity in the premixing interval and complex viscosity in the reaction interval are represented as a function of time. Since the premixing interval was carried out at $140\,^{\circ}\mathrm{C}$ viscosity rises from approx. $700\,\mathrm{mPa.s}$ to $5000\,\mathrm{mPa.s}$. Higher value of the premixing viscosity at $140\,^{\circ}\mathrm{C}$ compared to the premixing viscosity at $110\,^{\circ}\mathrm{C}$ is the direct consequence of the temperature: higher temperature makes the reaction faster, resulting in larger molecular weight of the reacting polymer and thus larger viscosity values. At $73\,\mathrm{s}$ a solid polymer is obtained having complex viscosity of $90\,\mathrm{kPa.s}$.

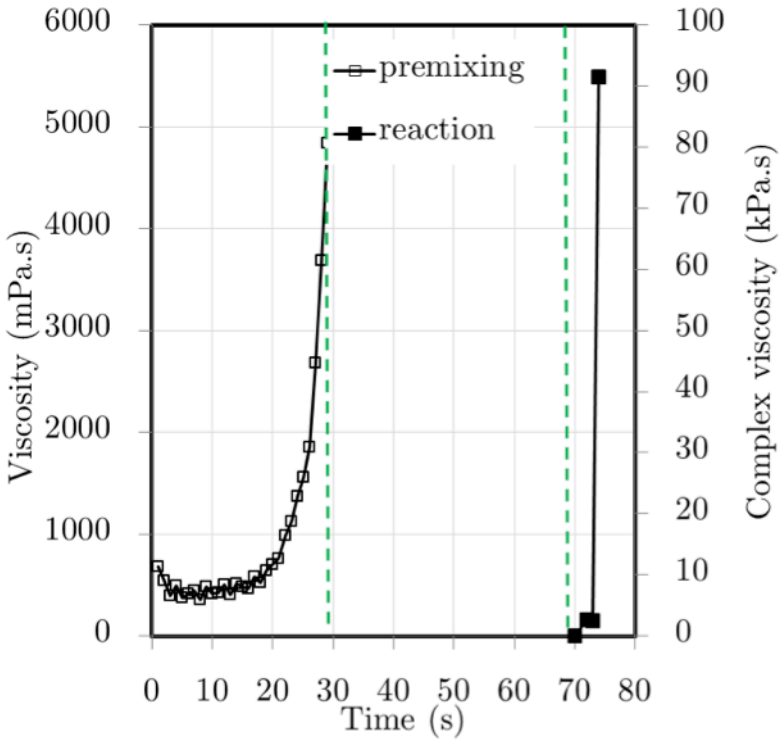

Figure 5.6. Viscosity rise at premixing interval ($0\,\mathrm{s}$ - $30\,\mathrm{s}$) and complex viscosity rise at reaction interval ($70\,\mathrm{s}$ - $80\,\mathrm{s}$) for Formulation 2.

5.7 Formulation 3

The highest concentration initiator/catalyst formulation was tested by rheometry using the HC method. In the final solid sample, concentration of the Na-CL catalyst (from C10) was $2.9\,\mathrm{wt.\%}$ and blocked isocyanate (from C20) was $1.55\,\mathrm{wt.\%}$. The calculated masses and mass fractions are represented in Table 5.5. Reactants were

placed directly on the rheometer plate, in order to have in total 0.7 ml of sample, 0.30 g of caprolactam and 0.14 g of C10 were place in one compartment of the holding cell and in another one 0.30 g of caprolactam and 0.07 g of C20.

Table 5.5. Reactants masses for Formulation 3.

Tank A		Tank B	
$\omega^{A}_{Na-Cl}\left[\%\right]$	6	$\omega^{B}_{B-iso}\left[\%\right]$	3
$V^{A}\left[ml\right]$	0.35	$V^{B}\left[ml\right]$	0.35
$m^{A}_{tot}\left[g\right]$	0.39	$m^{B}_{tot}\left[g\right]$	0.42
$m^{A}_{Na-Cl}\left[g\right]$	0.02	$m^{B}_{B-iso}\left[g\right]$	0.01
$m^{A}_{CL,tot}\left[g\right]$	0.37	$m^{B}_{CL,tot}\left[g\right]$	0.41
$\omega^{C10}_{Na-CL}\left[\%\right]$	17	$\omega^{C20}_{B-iso}\left[\%\right]$	17
$m^{C10}_{Na-Cl}\left[g\right]$	0.11	$m^{C20}_{B-iso}\left[g\right]$	0.06
$m^{A}_{CL,add}\left[g\right]$	0.30	$m^{B}_{CL,add}\left[g\right]$	0.30
$m^{A}_{C10}\left[g\right]$	0.14	$m^{B}_{C10}\left[g\right]$	0.07
$m^{samp}\left[g\right]$	0.80	$m^{samp}\left[g\right]$	0.80
$\omega^{samp}_{Na-CL}\left[\%\right]$	2.90	$\omega^{samp}_{B-iso}\left[\%\right]$	1.55

Effect of the premixing temperature on the complex viscosity rise is studied using the following experimental conditions:

- Mixing rotational interval at $500\,s^{-1}$ at $140\,^{o}C$ for $30\,s$;
- Temperature stabilization interval at $140\,^{o}C$ for $40\,s$;
- Reaction oscillation interval at $5\,\%$ and $100\,s^{-1}$ at $140\,^{o}C$ for $5\,s$.

The measured data is represented in Figure 5.7 and steady increase in the premixing viscosity is observed up to 900 mPa.s. In the oscillation interval abrupt increase in viscosity is observed in 4 s from 0.5 kPa.s to 23 kPa.s.

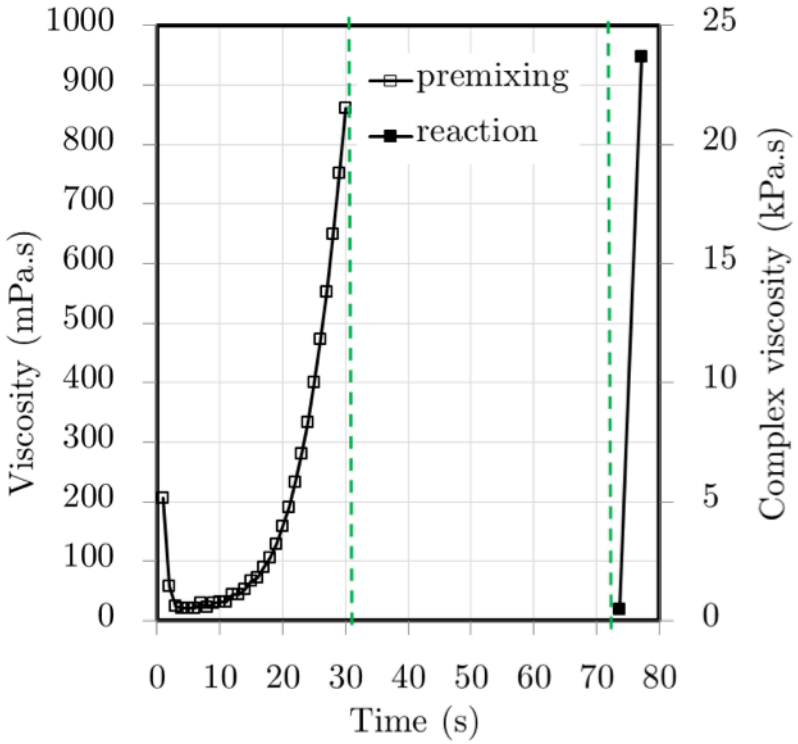

Figure 5.7. Viscosity rise at premixing (0 s - 30 s) and complex viscosity rise at reaction interval (70 s - 80 s) for Formulation 3.

5.8 Conclusions

The optimal conditions for production of the polyamide-6 from AP-caprolactam, Bruggolen C10P and Bruggolen C20P in RIM process were studied by rheometry and it was concluded:

- Formulation 1 containing 0.97 wt.% Na-CL and 0.52 wt.% B-iso is not suitable for the production in RIM process because it is characterised with too slow complex viscosity increase in order to obtain solid product for the optimal time in less than 3 minutes.
- Formulation 2 containing 1.93 wt.% and 0.93 wt.% B-iso depending on the experimental conditions is possible to cure into a solid product in shorter period than 3 minutes, which makes it suitable for the production in RIM process. The effect of the premixing temperature on the complex viscosity rise of this formulation was studied and higher premixing temperature such as

140 °C after 30 s of the premixing interval would yield a viscosity rise of the reacting polymer up to 5000 mPa.s and complex viscosity of 90 kPa.s in 75 s from the beginning of the experiment.

- Formulation 3 containing 2.90 wt.% Na-CL and 1.55 wt.% B-iso is also suitable for RIM yielding in a solid product of complex viscosity of 23 kPa.s after 75 s.

- When comparing Formulation 2 to Formulation 3 at the same experimental conditions of premixing, Formulation 2 yields higher complex viscosity for the same demoulding time than the Formulation 3. This is the consequence of the method of melting and mixing of the reactants between the two formulations. In Formulation 2 reactants were melted separately in the glass beakers on the hot plate for 15 minutes, which assured homogenous mixture of caprolactam and Na-CL/B-iso. In the Formulation 3 melting was carried out on the rheometer plate for a shorter period (approx. 10 s), which was not enough to melt the solid monomers into a homogenous mixture and thus the final value of the complex viscosity was lower.

5.9 References

Barnes, H. A., J. F. Hutton, et al. (1989). An Introduction to Rheology Elsevier.

Davé, R. S., R. L. Kruse, et al. (1997). "Polyamides from lactams via anionic ring-opening polymerisation: 3. Rheology." Polymer **38**(4): 949-954.

van Rijswijk, K., H. E. N. Bersee, et al. (2006). "Optimisation of anionic polyamide-6 for vacuum infusion of thermoplastic composites: Influence of polymerisation temperature on matrix properties." Polymer Testing **25**(3): 392-404.

6 Functionalisation of nanoparticles for production of polyurethane nanocomposites

6.1 Nanocomposites with HAp

Polymeric nanocomposites with inorganic particles pose several process challenges that mainly stem from the fact that inorganic nanoparticles tend to agglomerate into microsized structures when dispersed into polymeric matrices. Once inorganic nanoparticles are surrounded by organic molecules, polar groups from nanoparticles tend to repel nonpolar groups of organic molecules, and due to van der Walls forces nanoparticles agglomerates into stable and larger structures (Rozenberg and Tenne 2008). In order to prevent the agglomeration it is necessary to functionalize nanoparticles. These microstructures that are nanostructured microparticles can introduce spots of higher tension due to lack of affinity to the polymeric matrix and cause mechanical vulnerabilities, such as cracks.

A new nanocomposite product based on RenCast formulation and HAp was developed in this work. HAp was chosen because it is not toxic and it is biocompatible. In order to obtain a polyurethane matrix reinforced with HAp

nanoparticles, a functionalisation method of HAp is developed and it is described in this chapter. The functionalisation increases the affinity of the nanoparticles to the polymer. Once functionalized nanoparticles were obtained, they were mixed with polyol and/or isocyanate to form stable dispersion and this dispersion is mixed with the other RenCast component using the methods represented in Chapter 4.

6.1.1 Experimental method

In this study RenCast polyurethane formulation and hydroxyapatite (HAp) 15 wt.% water paste (commercial name nanoXIM) and hydroxyapatite dried powder were used. RenCast formulation consists of two reactants, formulated polyester based polyol (viscosity 80 mPa.s at $25^{\circ}C$) and formulated MDI based isocyanate (viscosity 20 mPa.s at $25^{\circ}C$). HAp is a calcium-phosphate with hydroxyl functional groups. From now on, HAp water paste is designated as HAp-past and powder as HAp-pow. The formula of hydroxyapatite is $Ca_{10}(PO_4)_6(OH)_2$. The ethylene glycol molecule is represented in Figure 6.1 and it is used to functionalise the polyol from RenCast formulation.

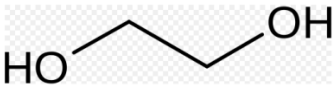

Figure 6.1. Ethylene glycol molecule.

The dispersion of HAp was mixed in one of the RenCast components, the polyol component was chosen because it does not show reactivity with the HAp (both have hydroxyl functional groups) and it is not as toxic as the isocyanate component, which poses some handling issues. The developed functionalisation method assumes that in order to mix HAp nanoparticles with formulated high molecular weight polyol, HAp should be first mixed with another alcohol of lower molecular weight to increase the HAp affinity to the polymer matrix. For this purpose, ethylene glycol supplied by Sigma Aldrich was chosen (from now on it is designated as EG). Both HAp paste and powder were produced by NetMix technology and supplied by Fluidinova, Engenharia dos Fluidos S.A. Distillation to extract water was performed at $110^{\circ}C$.

Molecular weight M and density ρ, which are used for the calculation of necessary quantities for the functionalisation of HAp with ethylene glycol (EG), are given in Table 6.1.

Table 6.1. Molecular weight and density of materials.

Material	$M\left[g/mole\right]$	$\rho\left[g/cm^3\right]$
Crystalline hydroxyapatite	1004.6	3.16
Ethylene glycol molecule	62.07	1.1132

Table 6.2 shows the boiling points of water and EG.

Table 6.2 Boiling points of water and ethylene glycol.

Substance	$T_b\left[^oC\right]$
Water	100
Ethylene glycol	196

Sample names and their description are shown in Table 6.3 and these are going to be used from now.

Table 6.3 Sample names and description.

Sample name	Sample description
f-HAp	HAp functionalised with EG
Ren	RenCast
Ethylene glycol	RenCast reacted with EG
f-HAp-Ren	RenCast reacted with f-Hap
A2	RenCast reacted with f-HAp-past
A3	RenCast reacted with HAp-pow

6.1.2 Calculation of the reactant quantities

The minimum volume ratio of HAp nanoparticles (HAp-past) and EG is computed in order that total area of HAp nanoparticles that is contained in reference mass of $1\ g$ of pure HAp nanoparticles is covered with the molecules of EG. For the calculation of the total volume of HAp nanoparticles it is considered that both HAp nanoparticles and EG molecules are cylindrical, characterised with diameter D and length L.

- Area A of a single HAp nanoparticle and a single EG molecule are calculated from:

$$A = \pi D(L + \frac{D}{4}) \tag{6.1}$$

- The values of diameters, lengths and the calculated areas are shown in Table 6.4. Diameter and length of EG molecule are approximately calculated based on the covalent bonds length and angles between atoms.

Table 6.4. Geometrical properties of reactants molecules.

Material	$D\left[nm\right]$	$L\left[nm\right]$	$A\left[nm^2\right]$
Single HAp nanoparticle	10	50	1727
Single EG molecule	0.109	0.63	0.234

- For the calculation of the volume V' of a single HAp nanoparticle is used,

$$V' = \pi \frac{D^2}{4} L \times 10^{-21} \tag{6.2}$$

- For further calculation, a reference mass m_{HAp} of HAp is set, $1\,g$, and total volume V_{HAp}^{tot} of $1\,g$ of HAp nanoparticles is calculated from:

$$V_{HAp}^{tot} = \frac{m_{HAp}}{\rho_{HAp}} \tag{6.3}$$

- To calculate total number N^{tot} of HAp nanoparticles in $1\,g$ of it, it is used:

$$N^{tot} = \frac{V^{tot}}{V'} \tag{6.4}$$

- Calculated values of a single nanoparticle volume and number of nanoparticles in $1\,g$ of mass of HAp are shown in Table 6.5.

Table 6.5. Calculated volumes and total number of nanoparticles of HAp.

Material	$V_{HAp}^{'}\left[ml\right]$	$V_{HAp}^{tot}\left[ml\right]$	N_{HAp}^{tot}
HAp	3.9E-18	0.32	8.1E+16

- For the calculation of the total volume of EG molecules it is first calculated mass m'_{EG} of EG molecules to cover one HAp nanoparticle:

$$m'_{EG} = 2 \times \frac{M_{EG}}{N_A} \left(\frac{A_{HAp}}{A_{EG}} \right) \quad \textbf{(6.5)}$$

- Where M_{EG} is the molecular weight of EG, N_A is Avogadro's number, $\left(\frac{A_{HAp}}{A_{EG}} \right)$ is the ratio of areas of a single HAp nanoparticle to a single EG molecule. Total mass m_{EG}^{tot} of EG molecules to cover 8.1E+16 nanoparticles of HAp is then calculated from:

$$m_{EG}^{tot} = N_{HAp}^{tot} m'_{EG} \quad \textbf{(6.6)}$$

- The total volume of EG molecules, V_{EG}^{tot}, that corresponds to m_{EG}^{tot} is given by:

$$V_{EG}^{tot} = \frac{m_{EG}^{tot}}{\rho_{EG}} \quad \textbf{(6.7)}$$

- Calculated values of mass of a single molecule m'_{EG}, and mass and volume of EG molecules to cover the area of $1\,g$ of mass of HAp, m_{EG}^{tot} and V_{EG}^{tot}, respectively, are shown in Table 6.6.:

Table 6.6. Calculated masses and volume of EG.

Material	$m'_{EG}\,[g]$	$m_{EG}^{tot}\,[g]$	$V_{EG}^{tot}\,[ml]$
EG	1.52E-18	0.122	0.110

- From Table 6.5 and Table 6.6 it is obtained the minimum volume ratio of solid HAp nanoparticles (and therefore HAp paste) and EG and it is:

$$\frac{V_{HAp}^{tot}}{V_{EG}^{tot}} = 2.89 \quad \textbf{(6.8)}$$

- Total volume of 15 wt.% HAp water paste $V_{HAp,p}^{tot}$ is calculated from:

$$V_{HAp,p}^{tot} = V_{HAp}^{tot} + \frac{m_{HAp}}{0.15 \cdot \rho_{H_2O}} \quad \textbf{(6.9)}$$

- And therefore it is obtained the minimum volume ratio of EG and HAp 15 wt.% water paste:

$$\frac{V_{EG}^{tot}}{V_{HAp,p}^{tot}} = \frac{1}{138.7} = 1.45 \times 10^{-2} \quad \textbf{(6.10)}$$

In order to obtain stable dispersion of hydroxyapatite in ethylene ethylene glycol, volume ratio of EG and HAp 15 wt.% water paste must be higher than 1.45×10^{-2}.

6.1.3 Functionalisation of HAp with EG

A method for functionalisation of hydroxyapatite from HAp 15 wt.% water paste is developed and described as follows. The method is based on mixing the HAp water paste with EG which is followed by the operations of distillation and/or spray drying in order to eliminate water and EG until the amount of EG reaches minimum content to coat hydroxyapatite particles, which was determined by DSC-TG mass loss measurements as a function of temperature. In order to produce HAp particles from hydroxyapatite 15 wt.% water paste functionalized with EG molecules, next procedure was adopted:

- Measure the calculated volume of HAp paste, $V_{HAp,p}^{tot}$, in a glass recipient;
- Add the calculated volume of EG, V_{EG}^{tot}, into the 15 wt.% HAp paste and stir with the aid of magnetic stirrer for 15 minutes;
- Distil the mixture of HAp-paste and EG at $110\,^{o}C$ or $190\,^{o}C$ to extract water;
- Resultant dispersion of HAp particles in ethylene glycol containing functionalised HAp nanoparticles, f-HAp, after the distillation was left to cool down to the room temperature;

- Mix f-HAp with the chosen volume of RenCast polyol and stirred for 15 minutes at magnetic stirrer before further use. This dispersion was called from now on dispersion of f-HAp in polyol.

6.1.4 Rheometry

Samples produced and tested by SEM are synthesised by different routes and have different weight fractions of hydroxyapatite. The list of all routes and obtained sample is shown here:

- Formulation 1 is characterised with the ratio $\frac{V_{EG}^{tot}}{V_{HAp,p}^{tot}} = \frac{5ml}{1ml} = 5$. This sample (sample A2) was synthesised from $1\,ml$ of Hap 15 wt.% paste and $5\,ml$of EG were distilled at $110^{o}C$; $2\,ml$ of the resultant HAp dispersion in EG was mixed with $20\,ml$ of RenCast polyol and it was stirred. In the final step $0.35\,ml$ of HAp/EG/polyol dispersion was pipetted onto the rheometer plate together with $0.35\,ml$ of RenCast isocyanate by the HC method. Rotational and oscillatory tests were conducted. A2 sample was seen by SEM-EDS and no HAp was observed.
- Sample A3 also consisted of RenCast formulation mixed with HAp-pow. $0.15\,g$ of HAp powder was stirred with $20\,ml$ of polyol, and afterwards $0.35\,ml$ of that dispersion was placed on the rheometer plate together with $0.35\,ml$ of isocyanate using the HC method. Cured sample was tested by SEM-EDS and microsized agglomerates of HAp were seen, confirming that without functionalisation of the HAp powder it is not possible to obtain nanocomposite.
- Formulation 2 is characterised with this ratio $\frac{V_{EG}^{tot}}{V_{HAp,p}^{tot}} = \frac{95ml}{102.6ml} = 0.93$. In order to make a dispersion of HAp in EG $102.6\,ml$ of HAp 15 wt.% water

paste and 95 ml of EG are added in the distillation flask and distilled at 110°C to extract water. The resulting suspension was spray-dried and the obtained powder was tested by DSC-TG and DRIFTs in order to check the amount of the water inside the powder sample. A reference HAp powder sample was obtained by spray-drying 102.6 ml of HAp 15 wt.% water paste at 110°C and it was compared with the f-HAp-past dried sample.

Hydroxyapatite weight fraction in the PU samples is summarized in Table 6.7.

Table 6.7. HAp weight fraction in the final sample.

Sample	ω(final) [%]
A2	0.34
A3	0.38

6.1.5 Formulation 1 (Sample A2)

1 ml of HAp paste and 5 ml of EG were mixed into the distillation flask, and the distillation at 110°C was performed until approximately 1 ml of water and ethylene glycol solution was distilled during 20 minutes. In this formulation with ethylene glycol excess, the distillate residue which is the suspension of HAp in EG left after the distillation is directly used for the rheological characterisation. The distilled water (the distillate) was disposed of.

In the next step, 2 ml of HAp suspension in EG was mixed with 20 ml of RenCast polyol in a magnetic stirrer during 1 hour. This dispersion was prepared to be mixed with RenCast isocyanate in the rheometer.

6.1.6 Formulation 2

For the functionalisation of HAp nanoparticles from Hap 15 wt.% water paste, 102.6 ml of HAp 15 wt.% water paste and 95 ml of EG are added in the distillation flask and distilled at 110°C to extract water. The amount of distilled water collected

was 80 ml. The distillate residue, which is as calculated to be 13 wt.% suspension of the HAp in EG, also called feed suspension (for spray-dryer), was then dried in spray-dryer at 200 °C which is the boiling point of EG. From visual inspection it is observed that a *dry* powder was obtained. In Table 6.8 are summarized the parameters of the spray-dryer used for this operation.

Table 6.8 Feeding parameters of the spray-dryer.

Parameter	Value
T(inlet)	200°C
Feed suspension flow rate	30%
Nitrogen feed pressure	5 bar
T(EG condensation)	25°C

In order to assess the amount of the functionalisation with EG of HAp, another sample was prepared. 103 ml of pure HAp paste was dried in spray-dryer at 110 °C in order to eliminate water. From visual inspection it is observed that a *dry* powder was obtained.

In Table 6.9 are summarised parameters of the spray-dryer used for this operation.

Table 6.9 Feeding parameters of the spray-dryer.

Parameter	Value
T(inlet)	100 °C
Feed suspension flow rate	30%
Nitrogen feed pressure	5 bar

Two powder samples hydroxyapatite and functionalised-hydroxyapatite, which are designated as HAp and f-HAp, respectively, that were prepared by the previously described method are analysed by DSC-TG and DRIFTs in order to determine the quantity of hydroxyl compounds, water and EG entrapped within HAp nanoparticles.

6.1.7 Formulation 1: Results

6.1.7.1 Shear rate effect

In order to assess the shear rate effect on viscosity rise of RenCast reinforced with f-HAp, rotation experiments were performed using the HC method as follows:

- Premixing rotation test at $500\,s^{-1}$ during $100\,s$;
- Reaction rotation test at $100\,s^{-1}$, $500\,s^{-1}$ and $1000\,s^{-1}$ during $600\,s$.

In the initial phase of experiments, measurements were performed at $25\,^{\circ}C$ in order to compare with results of pure RenCast polyurethane. After performing the test at $25\,^{\circ}C$ it was observed that the viscosity rise is faster when f-HAp is part of the formulation, therefore it was decided to perform the same experiments at lower temperature such as $10\,^{\circ}C$. Results of viscosity rise at $10\,^{\circ}C$ and $25\,^{\circ}C$ with different reaction shear rate are represented in Figure 6.2 and Figure 6.3, respectively. At both temperatures it was observed that viscosity rise is faster when the shear rate is larger. After the premixing interval which purpose was to premix the reactants, the shear rate value affects the viscosity rise in different ways: higher shear rate causes faster viscosity rise, due to the fact that it promotes faster and more effective mixing of the reactants (isocyanate, polyol, ethylene glycol and HAp).

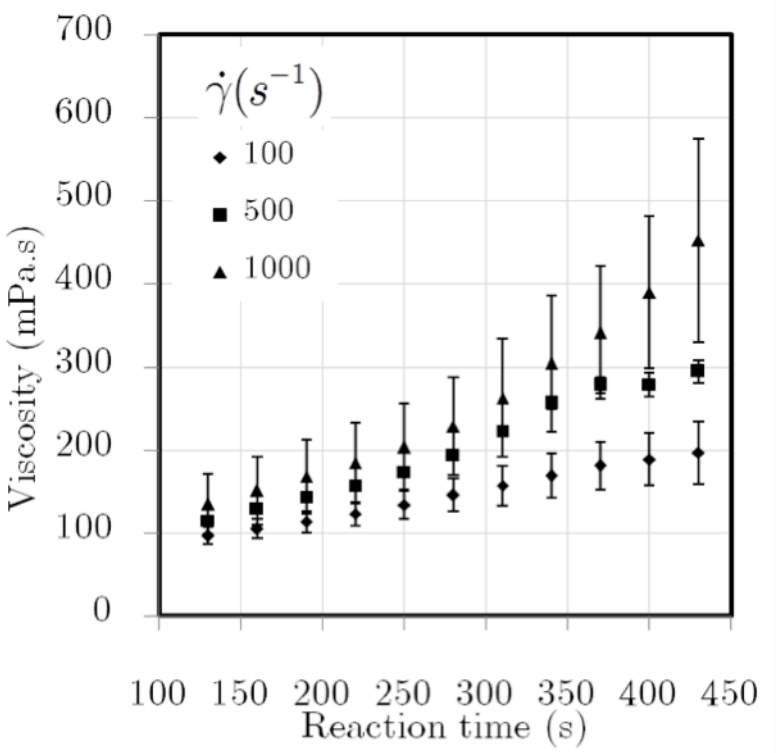

Figure 6.2. Plot of the average viscosity and standard deviation of Formulation 1 reaction for shear rates $100\,s^{-1}$, $500\,s^{-1}$ and $1000\,s^{-1}$ at $10\,^{\circ}C$.

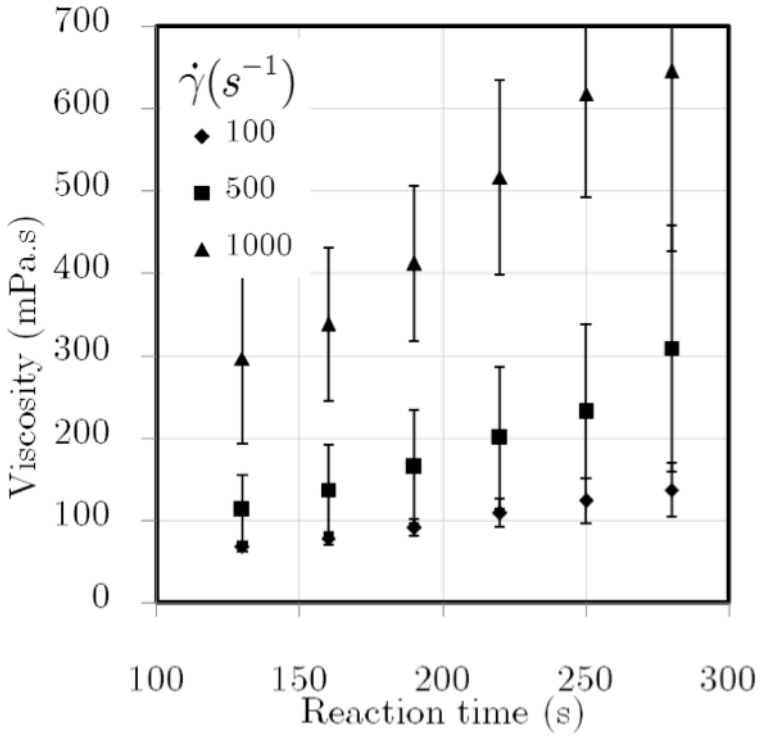

Figure 6.3. Plot of the average viscosity and standard deviation of Formulation 1 reaction for shear rates 100 s^{-1}, 500 s^{-1} and 1000 s^{-1} at 25°C.

6.1.7.2 Temperature effect

Temperature effect on viscosity rise at constant reaction shear rate can be seen from Figure 6.4 to Figure 6.6. For all shear rates, viscosity rise is faster at higher temperature, because increase in temperature increases reaction rate which influences and increases molecular weight and therefore viscosity. The divergence of the viscosity rise at two studied temperatures 10°C and 25°C is higher as the shear rate is higher. This suggests that for the lower shear rates the polymerisation reaction rate is limited by mass transfer, and thus changing the temperature only causes a slight change of reaction rate. For larger shear rate values the mixing is faster and the rate of reaction becomes clearly a function of the temperature which influences the rate of chemical reaction. Thus, for larger shear rates the reaction is in chemical regime, i.e. the limiting step for reaction is not diffusion but the reaction rate.

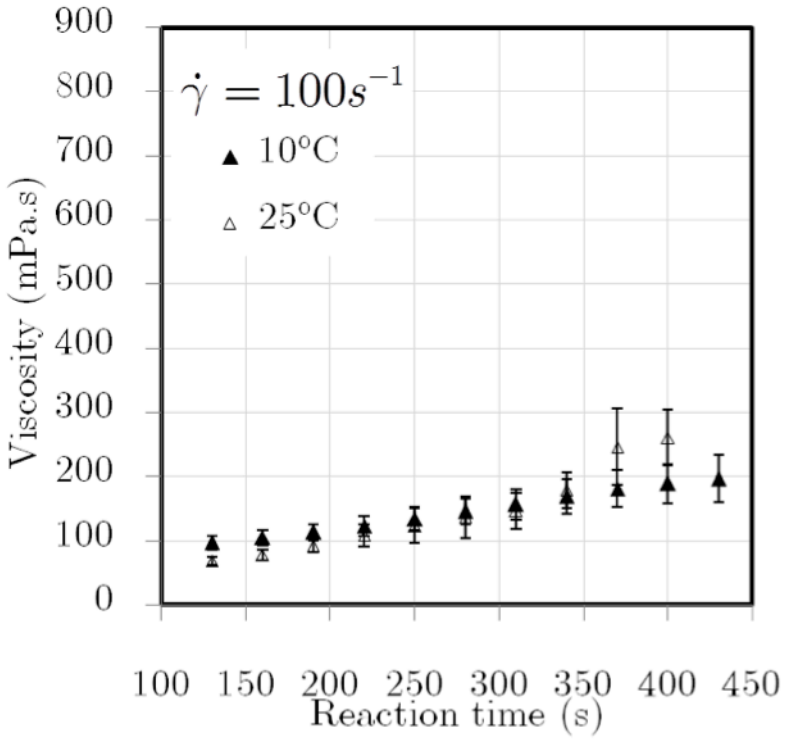

Figure 6.4. Plot of viscosity and standard deviation of Formulation 1 reaction at 100 s^{-1} at 10°C and 25°C.

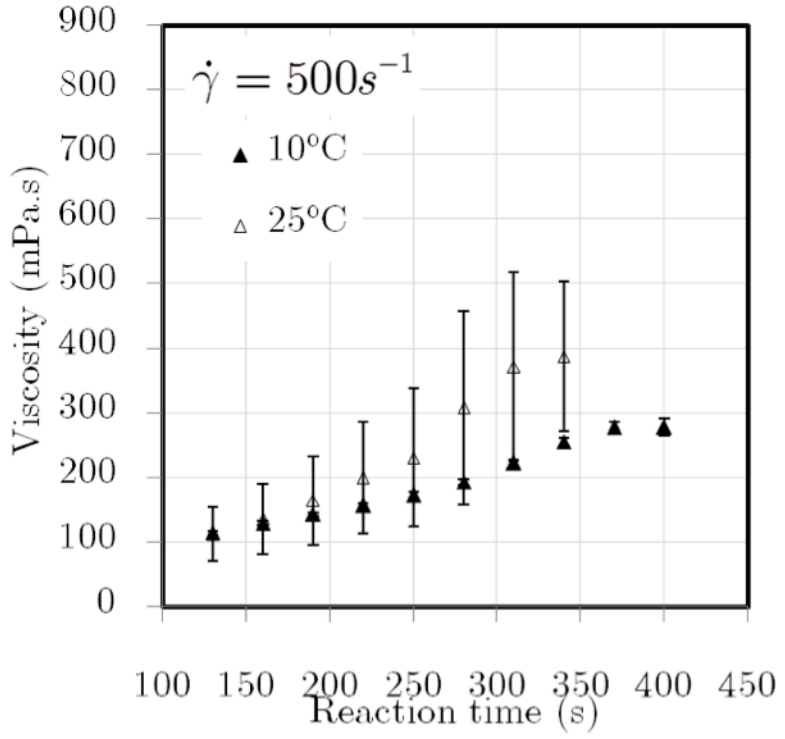

Figure 6.5. Plot of viscosity and standard deviation of Formulation 1 reaction at 500 s^{-1} at 10°C and 25°C.

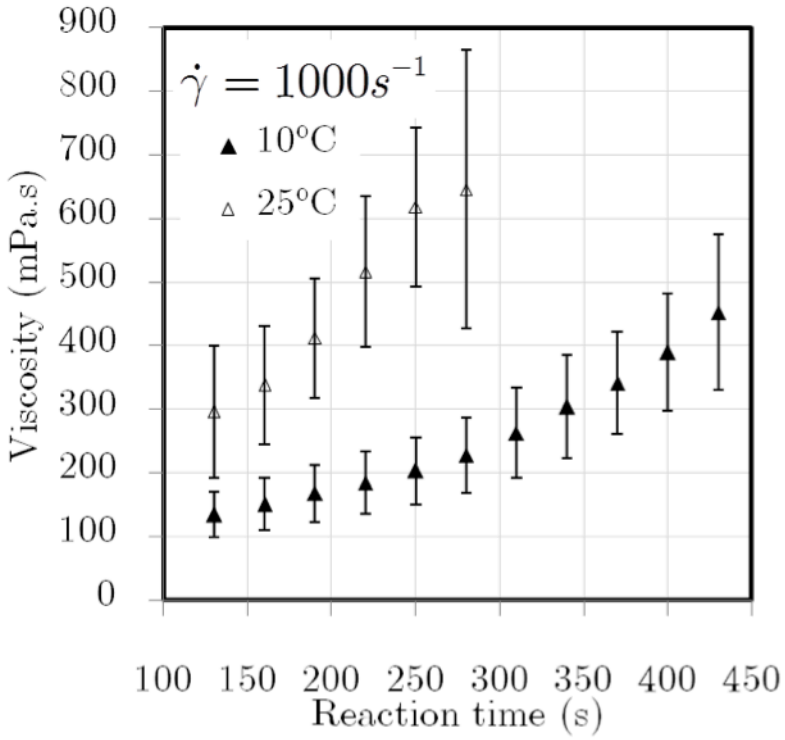

Figure 6.6. Plot of viscosity and standard deviation of Formulation 1 reaction at 1000 s^{-1} at 10°C and 25°C.

6.1.7.3 Ethylene glycol and f-HAp-paste effect

In order to get a grasp on the individual effect of ethylene glycol and f-HAp on viscosity rise of reactive formulation, viscosity as a function of reaction time for Ethylene glycol and f-HAp-paste at 100 s^{-1}, 500 s^{-1} and 1000 s^{-1} is shown from Figure 6.7 to Figure 6.9, respectively. The viscosity rise pattern at 100 s^{-1} is different than for 500 s^{-1} and 1000 s^{-1}. At 100 s^{-1} viscosity rise of sample Ethylene glycol is faster than of sample f-HAp-paste. At 500 s^{-1} and 1000 s^{-1} sample f-HAp-paste is characterised with faster viscosity rise than sample Ethylene glycol.

EG sample consists of RenCast isocyanate, RenCast polyol and EG. F-HAp-paste sample consists of RenCast isocyanate, RenCast polyol, ethylene glycol and HAp. Introducing EG into the RenCast formulation changes rheological behaviour as follows: the EG molecules are short and will compete with longer molecules of polyol to react with isocyanate, since the EG is a smaller molecule its diffusion into the ends of forming polymeric chains is faster than the diffusion of polyol, which increases the

overall polymerisation rate resulting in faster viscosity rise. Introducing the HAp nanoparticles in the formulation act as a "nuclei" of the polymerisation, i.e. HAp particles will be the initial points of the formation of the macromolecular chain between isocyanate and EG/polyol. When the shear rate is lower, the reaction rate is mainly controlled by mass transfer limitations, and under such conditions the addition of HAp slows down the polymerisation rate, as can be seen from Figure 6.7. Under the presence of HAp more time is necessary for the EG and polyol molecules to reach HAp particles and meet the isocyanate functional groups and orientate around them in order to start the polymerisation.

For larger shear rate values, the reaction occurs under regimes that are mainly limited by the reaction rate, and under such conditions the presence of HAp is associated to an increase on the reaction rate. So the HAp enhances the chemical reaction rate but slows down the mass transfer during the polymerisation, which explains the different effect of HAp presence observed for different shear rates.

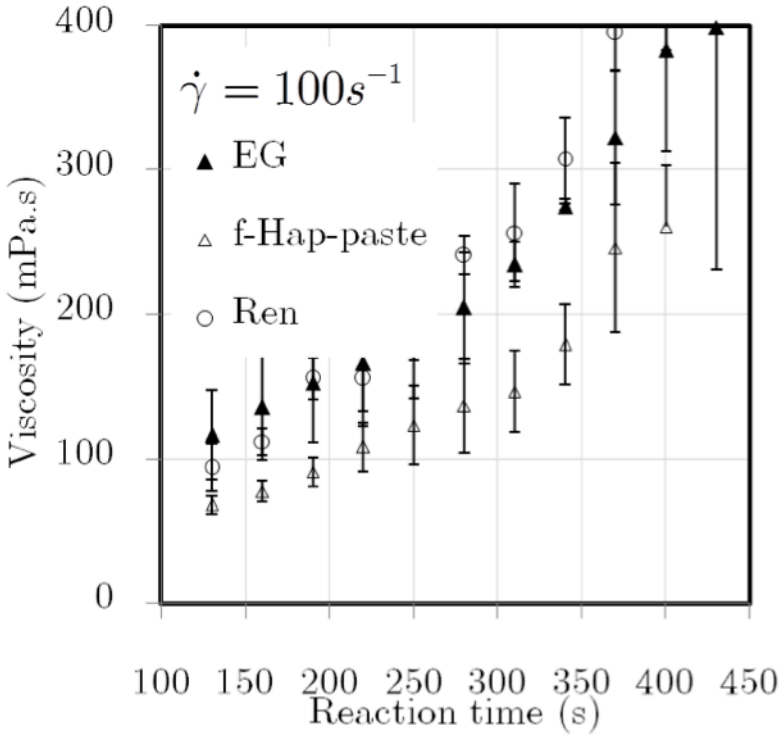

Figure 6.7. Plot of viscosity vs. reaction time: ethylene glycol and HAp-paste effect at 100 s^{-1} at 25 °C.

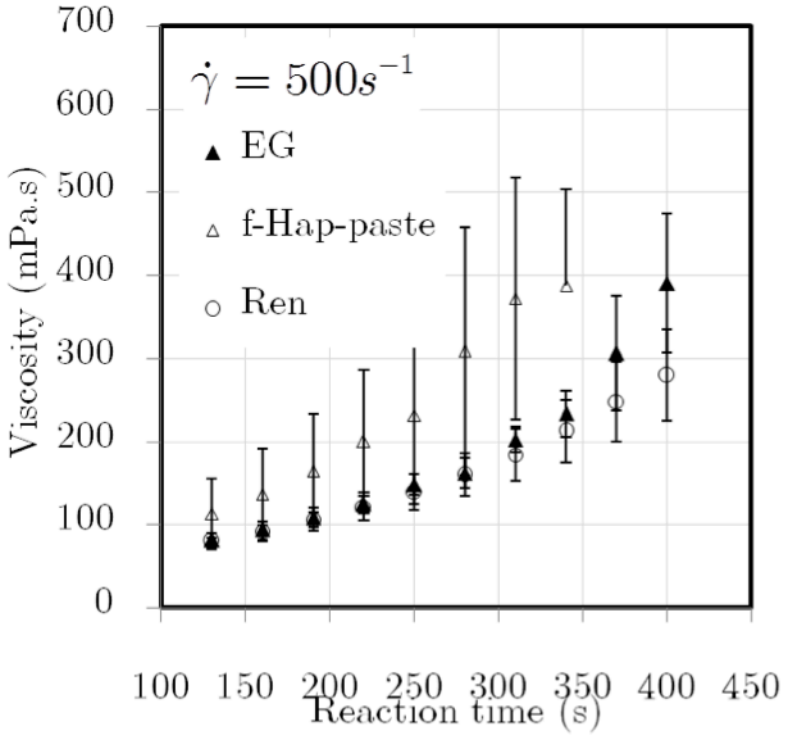

Figure 6.8. Plot of viscosity vs. reaction time: ethylene glycol and HAp-paste effect at 500 s^{-1} at 25 °C.

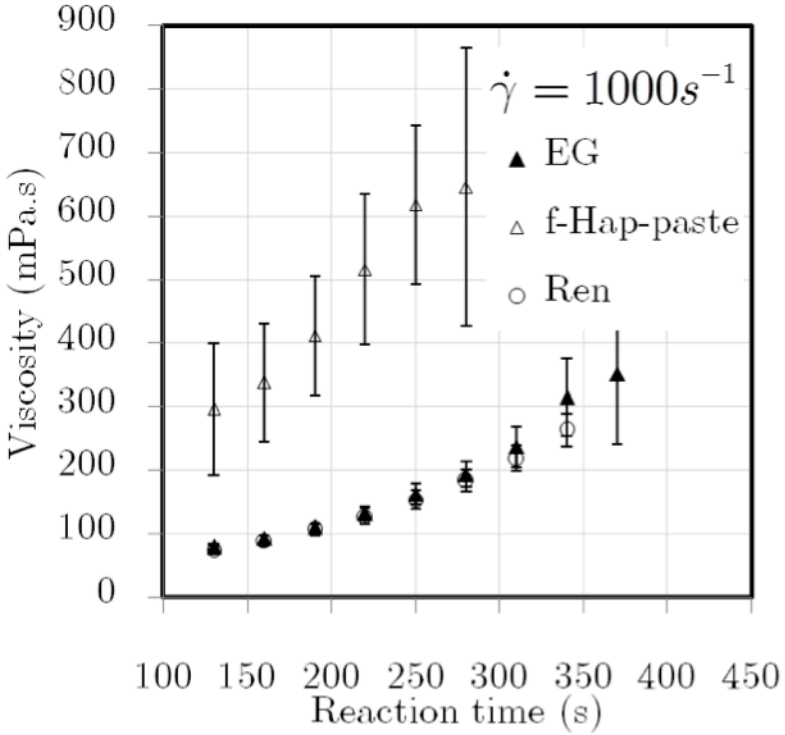

Figure 6.9. Plot of viscosity vs. reaction time: ethylene glycol and HAp-paste effect at 1000 s^{-1} at 25 °C.

6.1.7.4 F-HAp-pow effect (sample A1=mix3)

Functionalised hydroxyapatite powder f-HAp, was mixed in RenCast polyol and stirred during 15 minutes before the rheological test. The resulting rheogram of viscosity rise at different reaction shear rates of reactive formulation of RenCast mixed with f-HAp powder at $25^{\circ}\mathrm{C}$ is represented in Figure 6.10. It is observed that viscosity rises faster with the shear rate. In this plot full symbols represent points where viscosity increases, and open symbols points where viscosity decreases due to the edge fracture. The time taken for edge fracture to occur at $25^{\circ}\mathrm{C}$ for all shear rates was assumed to be $340\ \mathrm{s}$.

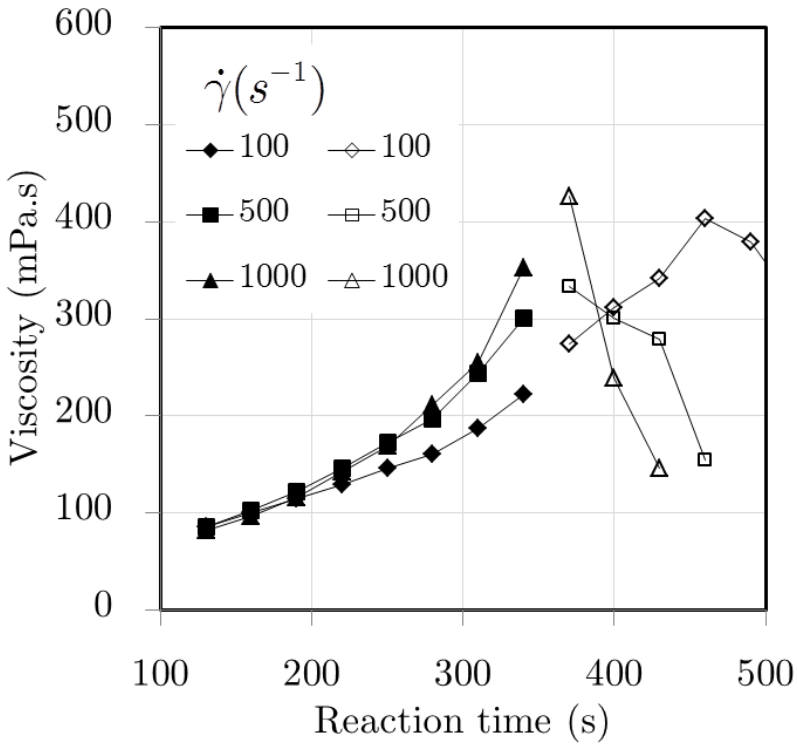

Figure 6.10. Plot of viscosity versus reaction time for HAp-pow for shear rates $100\ \mathrm{s}^{-1}$, $500\ \mathrm{s}^{-1}$ and $1000\ \mathrm{s}^{-1}$ at $25^{\circ}\mathrm{C}$.

6.1.8 Gel point of modified PU

6.1.8.1 Ethylene glycol effect

Figure 6.11 represents viscoelastic moduli (storage and loss modulus) versus reaction time. The addition of ethylene glycol into the RenCast PU decreases the gel time for

this formulation. Gel time for Ren is 1630 s, and for EG is 1380 s. In RenCast formulation, where only formulated RenCast polyol can react with isocyanate, only soft segments may be formed. By adding ethylene glycol, isocyanate reacts with hydroxyl groups both from ethylene glycol and from polyol, which may introduce phase separation. As a consequence, gel time is achieved faster when ethylene glycol is introduced.

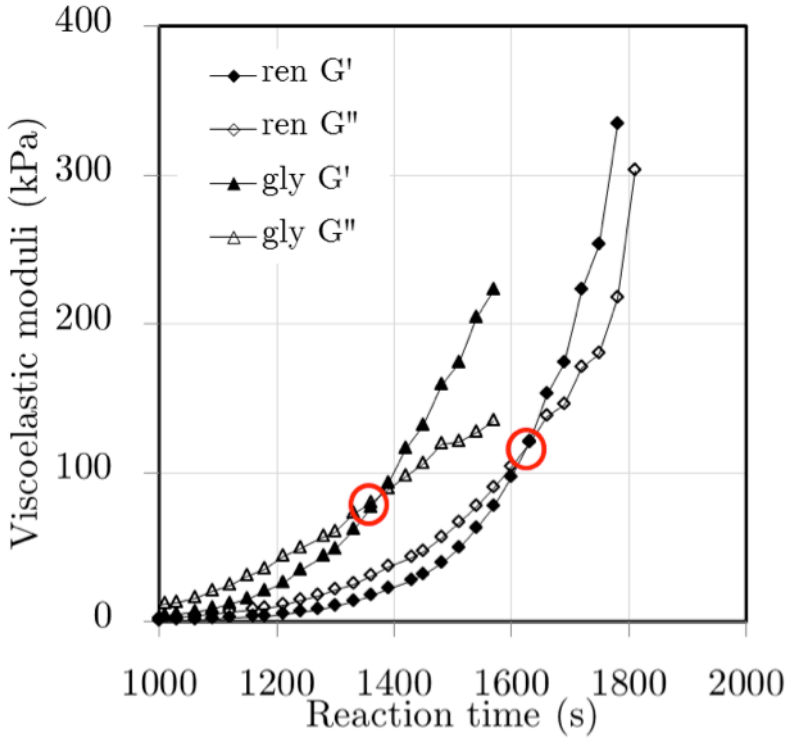

Figure 6.11. Viscoelastic moduli versus reaction time for determination of gel time, for Ren and Ethylene glycol.

In Figure 6.12 is represented gel time and storage modulus as a function of angular frequency for sample EG at 25°C. It is observed that with an increase in angular frequency the gel time decreases although the value for storage modulus can not be related with angular frequency in the same way.

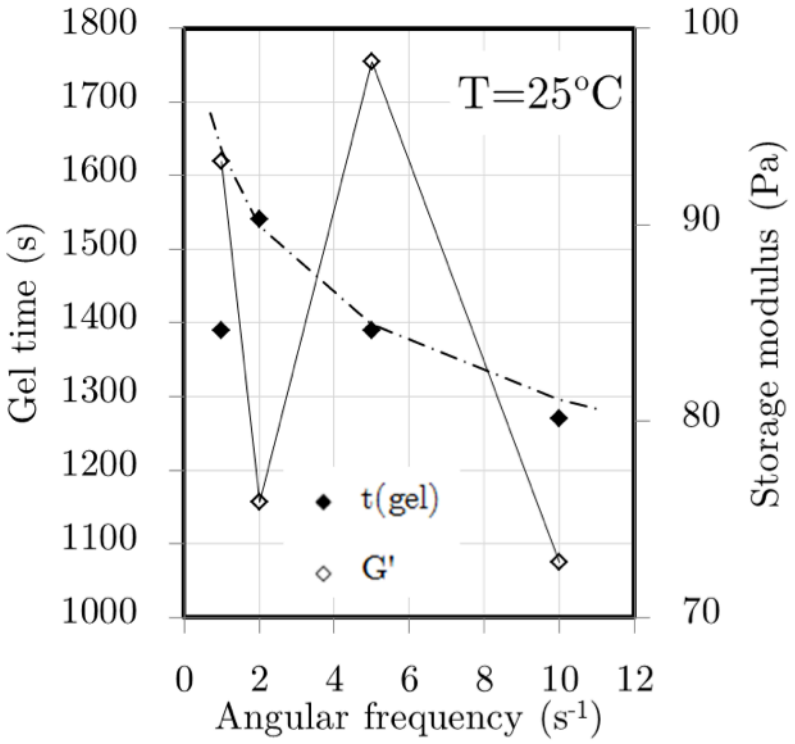

Figure 6.12. Gel time and storage modulus vs. angular frequency for Ethylene glycol at 25°C.

6.1.8.2 HAp effect in different samples

All studied samples Ren, EG, HAp, and f-HAp were compared by plotting the gel time measured with oscillatory test against the reaction time at $25\,^{\circ}\mathrm{C}$ in Figure 6.13. Oscillation parameters were: strain 1% and angular frequency $1\,\mathrm{s}^{-1}$. Oscillation interval was preceded by the premixing rotation interval with parameters: shear rate $500\,\mathrm{s}^{-1}$ and interval duration $100\,\mathrm{s}$. Gel time was measured and it was in the following order from the shortest to the largest: f-HAp-pow>Ethylene glycol>Ren>HAp.

Short gel time is the consequence of the high molecular weight of the product that is being formed, which is the consequence of the high polymerisation rate. Due to the fact that the gel time of f-HAp-pow sample is shorter than pure polyurethane Ren sample, and the gel time of HAp-pow is longer of Ren sample it is believed that it is the ethylene glycol and not the hydroxyapatite that increases the polymerisation

rate. This result is also in the concordance with the rotation results (see Figure 6.7 and Figure 6.8).

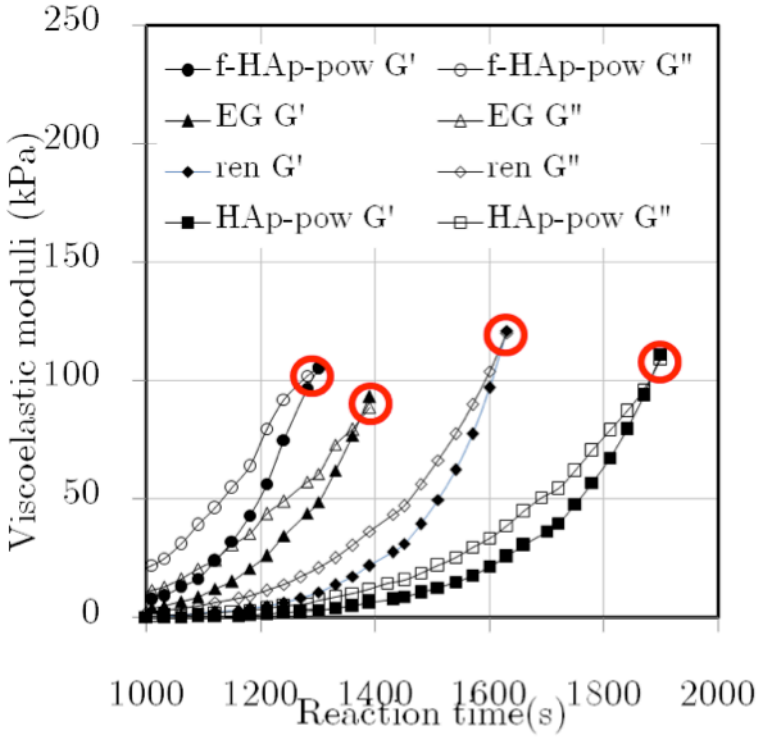

Figure 6.13. Viscoelastic moduli versus reaction time, for samples Ren, Ethylene glycol, HAp-pow G' and HAp-pow G".

Gel time and storage modulus versus the angular frequency for samples Ren, HAp and f-HAp are represented in Figure 6.14, Figure 6.15 and Figure 6.16, respectively. All the samples show similar pattern with an increase in the angular frequency, gel time decreases and the storage modulus increases.

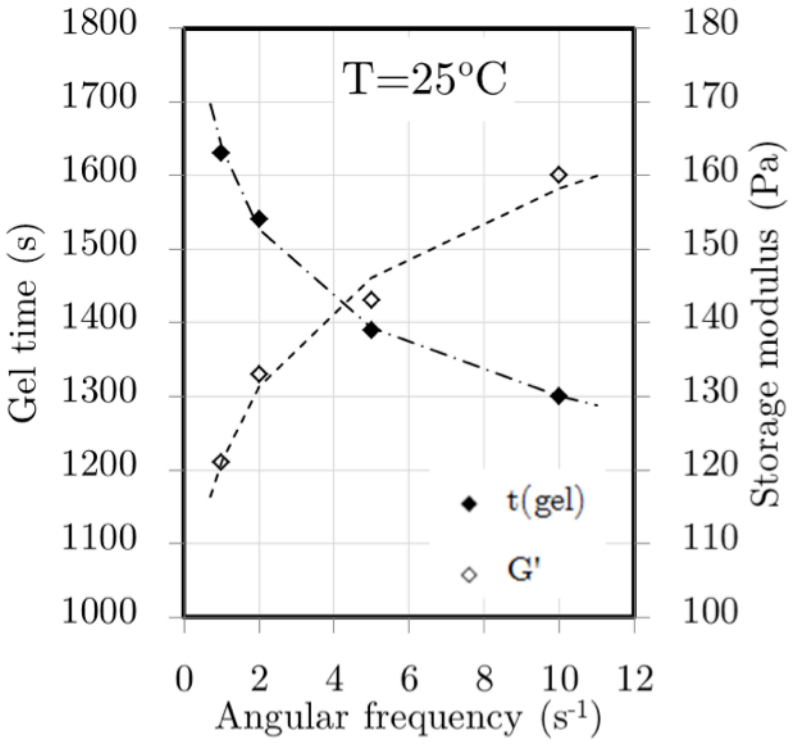

Figure 6.14. Gel time and storage modulus vs. angular frequency for Ren at 25°C.

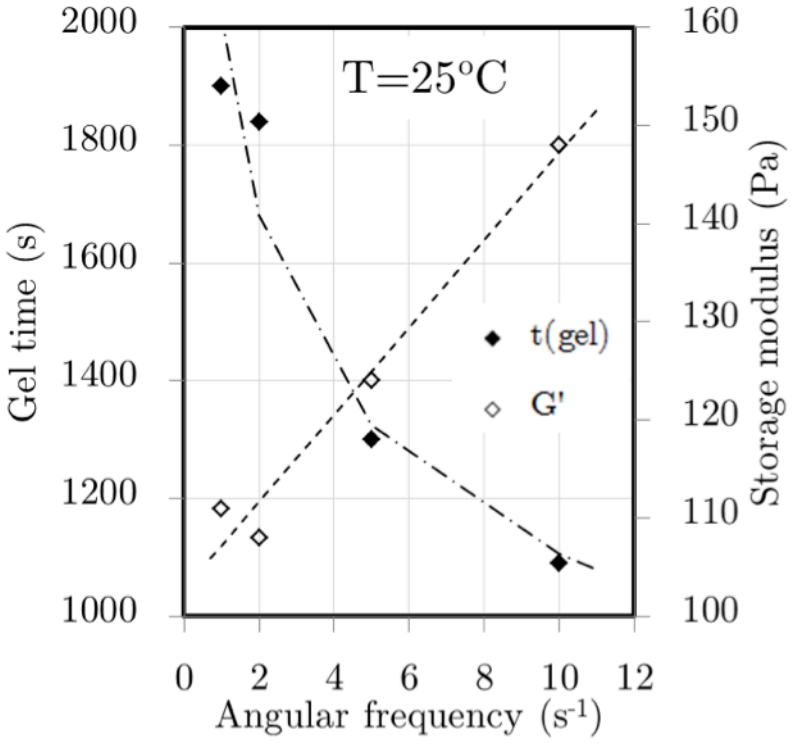

Figure 6.15. Gel time and storage modulus vs. angular frequency for HAp at 25°C.

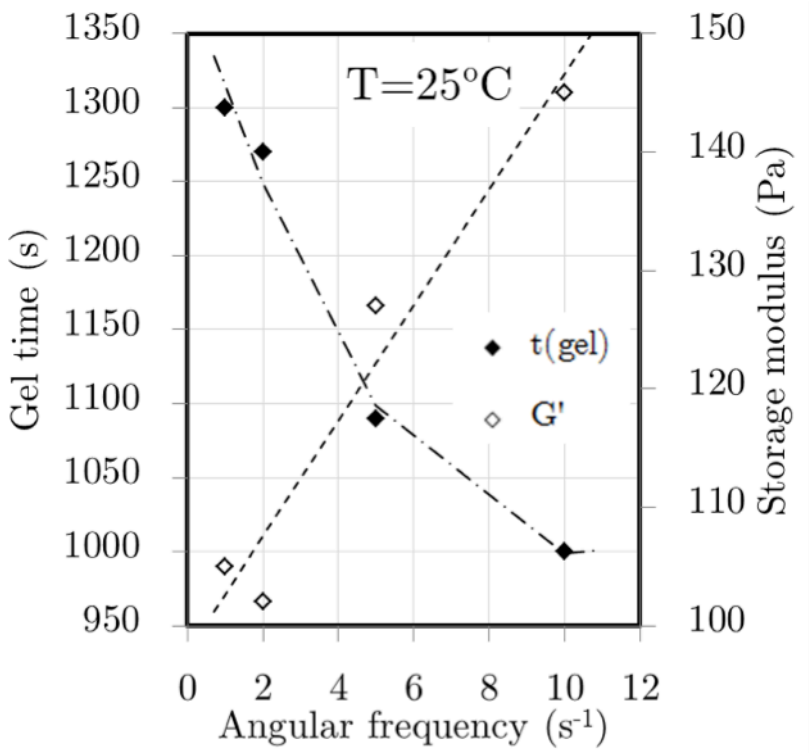

Figure 6.16. Gel time and storage modulus vs. angular frequency for f-HAp at 25°C.

All the samples HAp, Ren, EG and f-HAp were compared at one plot in Figure 6.17 where gel times are represented at each studied angular frequency. For samples HAp, Ren, and f-HAp with an increase in angular frequency gel time decreases. This is an indication that in the oscillatory tests the reaction is limited by mass transfer, and increase of the oscillation frequency enhances the mass transfer.

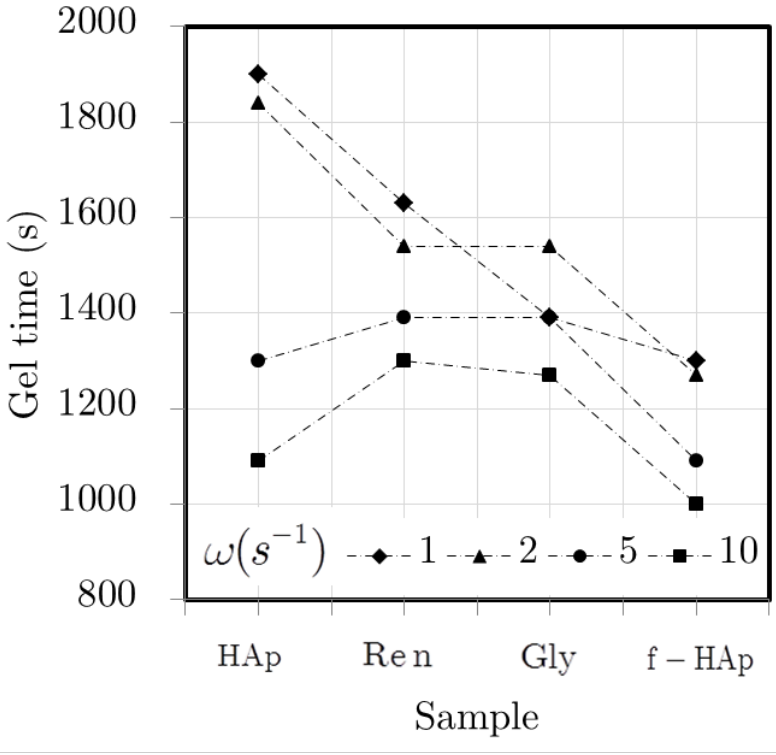

Figure 6.17. Gel time for different sample with angular frequency as a parameter at 25°C.

6.1.9 Formulation 2: Results

6.1.9.1 Determination of hydroxyl compounds by DSC-TG and DRIFTs

DSC-TG is used in order to measure the mass loss of samples, and in this particular case is used to calculate the quantity of evaporated water and ethylene glycol. Samples were heated under nitrogen flow from $50^{\circ}C$ to $400^{\circ}C$ at the heating rate of $5^{\circ}C/\min$.

Figure 6.18 represents data obtained by DSC, the heat flow versus temperature for both samples HAp and f-HAp. Positive values of the heat flow, indicating exothermic transitions are in the temperature range from $50^{\circ}C$ to $185^{\circ}C$ for HAp, and from $50^{\circ}C$ to $165^{\circ}C$ for f-HAp. Since the evaporation is an endothermic transition, transitions that may occur in these temperature ranges can not be assigned to the water evaporation. Negative values of the heat flow for HAp are in the temperature range from $185^{\circ}C$ to $400^{\circ}C$, and for f-HAp ranging $165^{\circ}C$ to $400^{\circ}C$, which are an

indication of possible endothermic transitions such as evaporation of water or ethylene glycol.

Mass derivative and respective temperature difference for HAp and f-HAp samples are represented in Figure 6.19. Mass loss of HAp sample in the temperature range from $185\,^{\circ}\mathrm{C}$ to $400\,^{\circ}\mathrm{C}$ is of 2.25%. Since, it is known that hydroxyapatite has ability of physically adsorbing water (to its surface), as well as to chemically react forming hydrogen bonding(Gomes, Silva et al. 2009), the transition at this temperature range can be assigned to the evaporation of the water that is entrapped in hydroxyapatite crystal structure of the HAp sample. For the sample f-HAp and for temperatures higher than $165\,^{\circ}\mathrm{C}$ the mass loss is of 2.60%, and the transition in this temperature range is possibly evaporation of ethylene glycol and water.

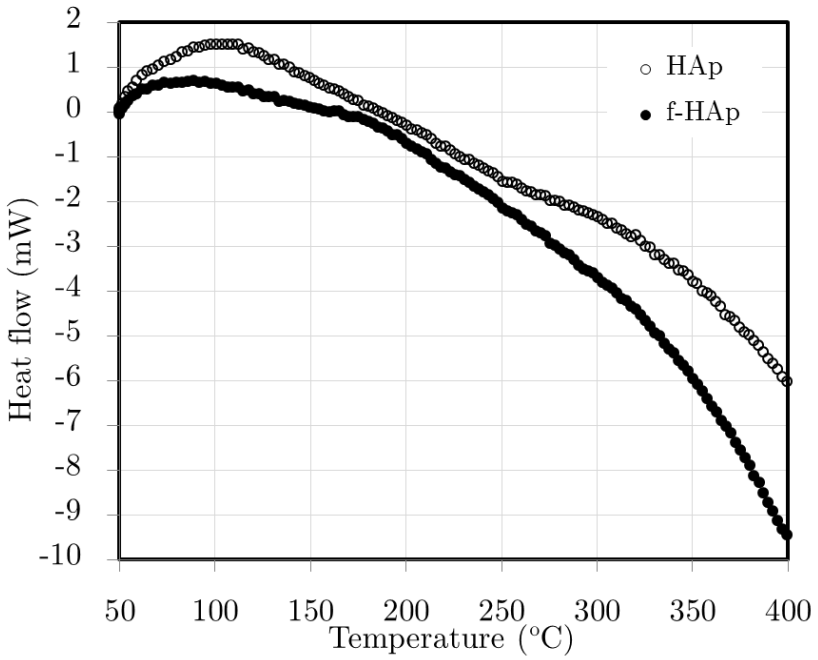

Figure 6.18. Heat flow vs. temperature for HAp and f-HAp.

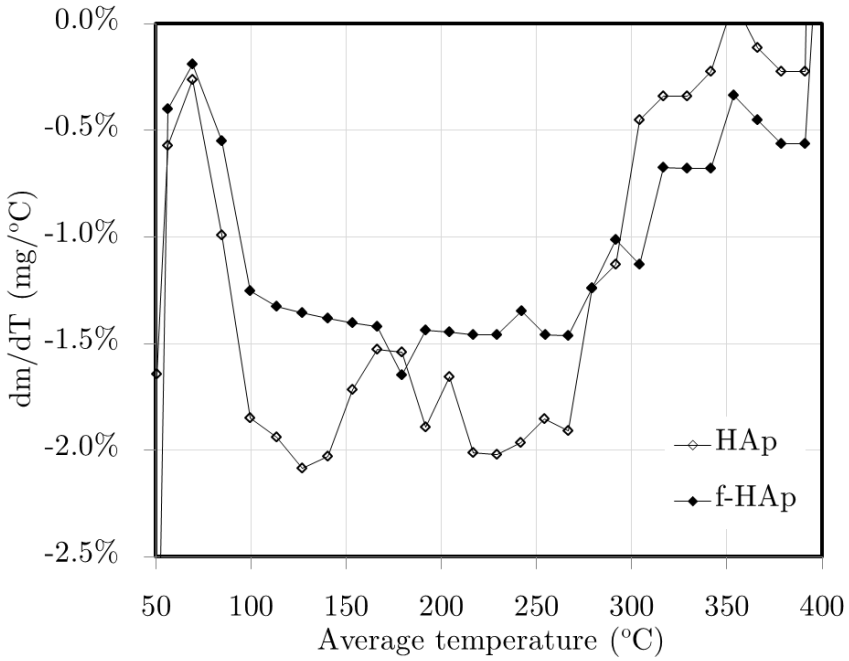

Figure 6.19. Mass derivative vs. average temperature for HAp and f-HAp.

In order to get better insight into quantities of hydroxyl groups of water and EG, DRIFTs was carried out. The objective of this analysis was to determine the difference of intensity in hydroxyl group peak of HAp (assigned to water) and f-HAp (assigned to ethylene glycol/water). DRIFTs data of samples HAp and f-HAp is plotted in Figure 6.20 as Kubelka-Munk versus wavelength.

All dilutions were made with KBr that was previously dried in the oven at $100\,^{o}\mathrm{C}$ for 4 hours. Appropriate quantities of sample and KBr were weighted and mixed manually in an eppendorf, and then further mixed with a mortar and pestle. The background was made using the same KBr, treated by the same process. Experimental parameters used for both background and samples were: 128 scans, $4\ \mathrm{cm}^{-1}$ resolution, Gain: 64, Vel. 1.5825 and Aperture: 100.

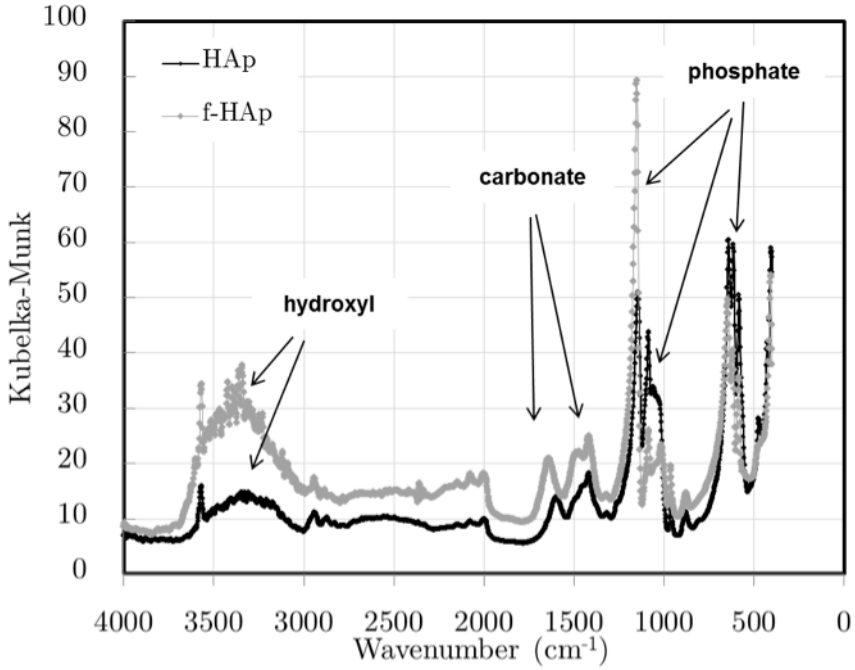

Figure 6.20.DRIFTs analysis: Kubelka-Munk (absorbance function) versus wavenumber for HAp and f-HAp.

In Figure 6.20 broad peak at $3000\,\mathrm{cm^{-1}}$ to $3500\,\mathrm{cm^{-1}}$ is assigned to hydroxyl groups that can be either parts of water or ethylene glycol molecules entrapped within hydroxyapatite crystal structure. Looking at this figure, higher intensity of hydroxyl group peak from f-HAp sample indicates higher concentration of hydroxyl groups in this sample than in HAp.

The peak at approximately $1200\,\mathrm{cm^{-1}}$ is caused by the reflectance of the f-HAp sample.

6.1.9.2 Formulation 1: Structure visualisation by SEM

In Figure 6.21 is shown the structure of sample A3, of RenCast reinforced with the HAp powder. In Figure 6.21 (a) the magnification of 1000x shows some wide plane areas, which are surrounded by valleys filled with spheres. Although there are some groups of spheres all over the plane areas, higher concentrations of spheres are seen inside the valleys. In Figure 6.21 (b) zone ZO from (a) is magnified 2500 times, and the diameter of the spheres is observed to be in the range from $3\,\mu\mathrm{m}$ to $5\,\mu\mathrm{m}$. Diameter of HAp nanoparticles is generally $50\,\mathrm{nm}$, and the size of agglomerates of

nanoparticles is up to $5\,\mu m$, therefore these spheres are agglomerates of HAp. Magnification of 10^4 times is shown in Figure 6.21 (c) where it is seen an agglomerate of smaller bubble-like structures. This agglomerate is magnified 4×10^4 times at Figure 6.21 (d) where it is clearly seen the bubble-like structures.

Zones Z1 and Z2 from Figure 6.21 are analysed by Energy Dispersive X-Ray spectroscopy (EDS) and the spectra obtained are shown in Figure 6.22 (a) for Z1 and (b) for Z2. Aluminium, gold, and palladium peaks are generated from the sample coating for SEM. Carbon and oxygen peaks belong to the atomic structure of polyurethane, and silica peak is probably some impurities. Calcium and phosphor peaks in (a), and lack of those peaks in (b) prove that bubble-like structures in zone Z1 are hydroxyapatite and there is no HAp in Z2.

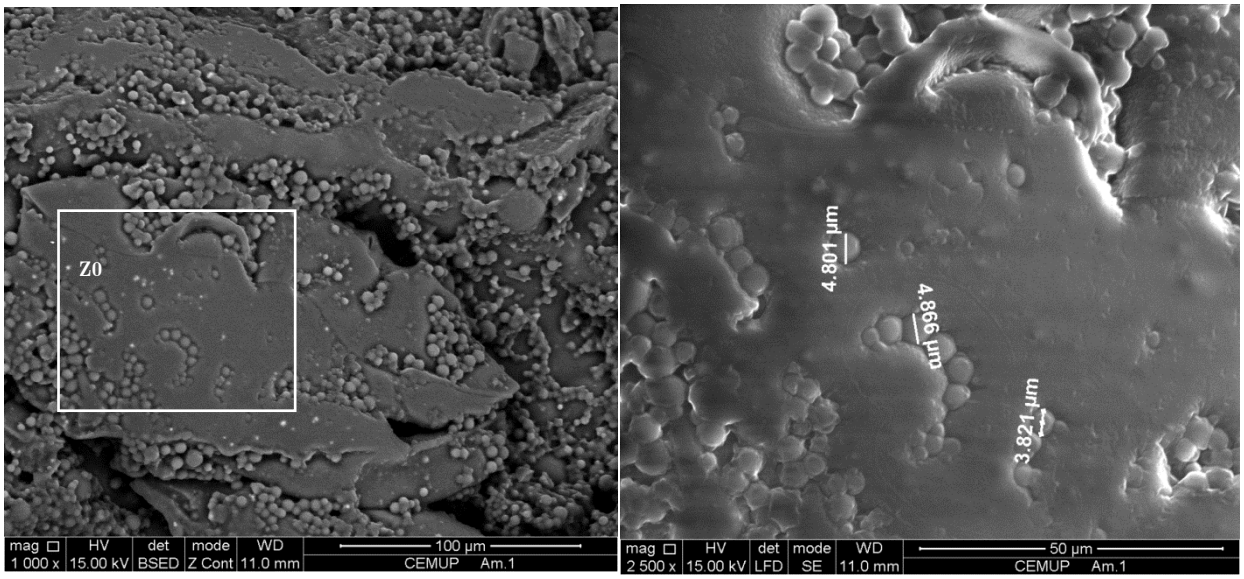

(a) (b)

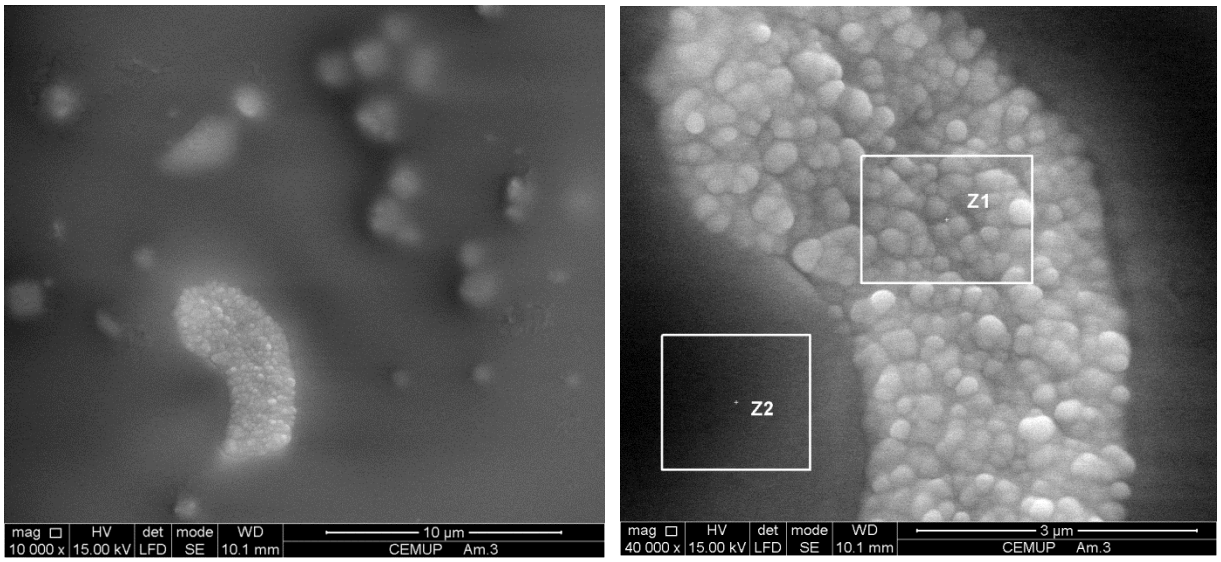

(c) (d)

Figure 6.21. SEM photos of RenCast reinforced with f-HAp with magnification of: (a) 10^3 times, (b) 2.5×10^3 times, (c) 10×10^3 times and (d) 40×10^3 times.

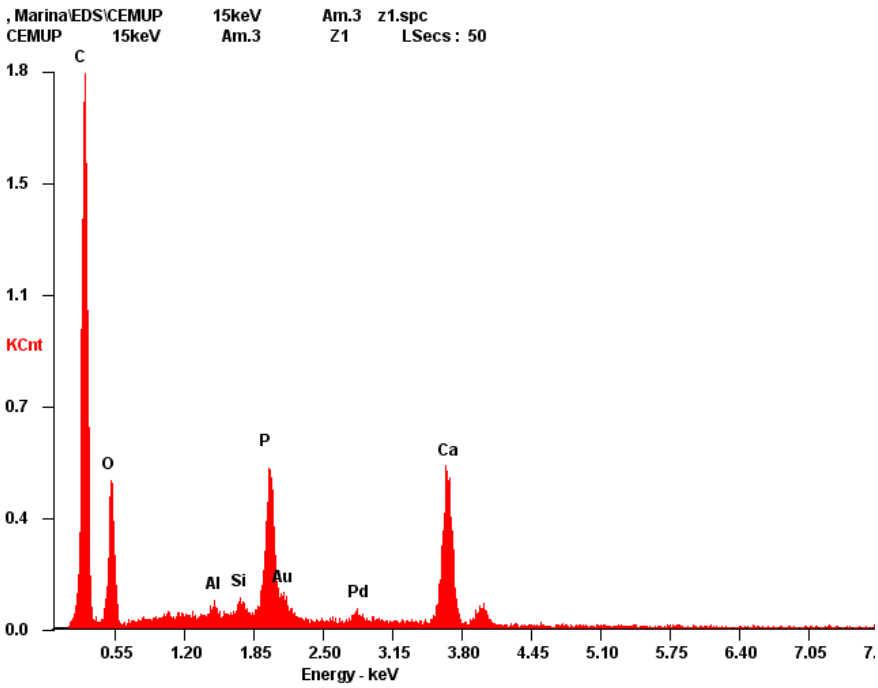

(a)

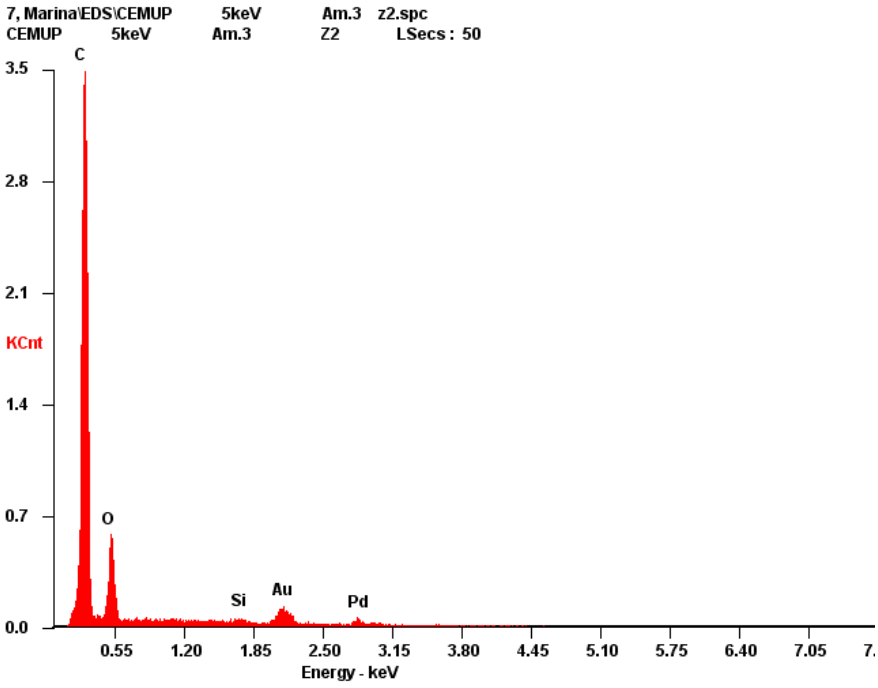

(b)

Figure 6.22. EDS spectra of RenCast reinforced with f-HAp, sample A3. (a) zone Z1, (b) zone Z2.

6.2 Nanocomposite with ZnO nano particles

6.2.1 Production of ZnO

Zinc oxide was produced from the reaction between zinc acetate and sodium hydroxide that yields in solid particles of zinc oxide, sodium acetate and water molecule as follows (Viswanatha, Amenitsch et al. 2007),

$$Zn(CH_3CO_2)_2 + 2NaOH \rightarrow ZnO(s) + 2Na(CH_3CO_2)_2 + H_20 \quad \textbf{(6.11)}$$

Reaction is carried out in isopropanol solvent. Synthesis method isas it follows:

- 0.44 g of zinc acetate is dissolved in 500 ml of isopropanol at $50^{o}C$;
- 0.13 g of sodium hydroxide is dissolved in 500 ml of isopropanol at $65^{o}C$;
- Solutions of zinc acetate and sodium hydroxide in propanol were mixed in a T-jets reactor;
- The ZnO suspension was mixed in the Rencast polyol and after distilled (evaporated) at $83^{o}C$ to extract the isopropanol.

In Table 6.10 are shown the physical properties of reactants and products of the reaction.

Table 6.10. Physical properties of reactants. (Legend: *n.k.*= not known)

Physical property	ρ' $\left[g/cm^3\right]$	M' $\left[g/mole\right]$	c' $\left[M\right]$	V' $\left[ml\right]$	n' $\left[mole\right]$	m' $\left[g\right]$	V' $\left[ml\right]$
ZnAc	1.735	219.5	0.0040	50	0.0002	0.0439	2.53E-05
NaOH	2.13	40.0	0.0064	50	0.00032	0.0128	0.0060
Isopropanol	0.786	60.1					
ZnO	5.606	81.41	0.0016	100	0.00016	0.0130	0.0023
Polyol	0.98	n.k.					
Isocyanate	1.12	n.k.					

Three concentrations of zinc oxide solutions were made based on the following calculation. Number of moles of ZnO, n', is calculated from

$$n' = c' \frac{V'}{1000} \tag{6.12}$$

The weight m' of reactants and products is calculated from

$$m' = n' M' \tag{6.13}$$

where M' is the molecular weight.

Volume of each reactant and product V' is calculated from

$$V' = \frac{m'}{\rho'} \tag{6.14}$$

Three concentrations of zinc oxide solutions were made based on the three different volumes of isopropanol V_{prop} and zinc oxide (see Table 6.11). Total volume (V_{tot}) is a sum of the volume of isopropanol (V_{prop}) and a volume of zinc oxide (V_{ZnO}). Since $V_{ZnO} = V_{prop}$, it is assumed that the total volume is equal to the volume of isopropanol $V_{tot} = V_{prop}$.

Zinc oxide mass m_{ZnO} is calculated from

$$m_{ZnO} = \frac{m'_{ZnO}}{a} \tag{6.15}$$

Where m'_{ZnO} is elementary mass of zinc oxide (mass calculated for $100\ ml$ of generated zinc oxide volume) and a is the dividing factor. The dividing factor is calculated from

$$a = \frac{V_{tot}^{ini}}{V_{tot}} \tag{6.16}$$

Where V_{tot}^{ini} is set to $1000\ ml$ of solvent.

Weight fraction of zinc oxide expressed in ppm is calculated from

$$\text{ppm} = \frac{m_{ZnO}}{m_{pol} + m_{iso}} 10^6 \tag{6.17}$$

Where polyol and isocyanate mass m' are calculated from

$$m' = V_{pol}\rho' \tag{6.18}$$

Where $V_{pol} = V_{iso}$ because the reaction is carried out in equal volumetric ratio.

Table 6.11. Total sample volumes and polyol volumes.

Sample name	$V_{tot}\,[\text{ml}]$	$V_{pol}\,[\text{ml}]$	$c\,[\text{ppm}]$
sample 1	1000	10	620
sample 2	100	10	62
sample 3	50	100	3

6.2.2 Rheometer characterisation

6.2.2.1 Premixing study

RenCast isocyanate was mixed with a mixing ratio of 1:1 with the RenCast polyol having ZnO nanoparticles with 3 concentrations of ZnO: $3\,\text{ppm}$, $66\,\text{ppm}$ and $665\,\text{ppm}$.

All the experiments were carried out at $25\,^{\circ}\text{C}$, and the sample prepared in the rhemoeter has a thickness $2\,\text{mm}$ for all runs. Premix interval was followed by the reaction interval, using rotational and oscillatory mode, respectively. In Table 6.12 are represented sample names, premix duration and gel times. Other parameters were kept constant in all runs, as follows: premixing shear rate $500\,\text{s}^{-1}$, strain 1% and angular frequency $1\,\text{s}^{-1}$ for the oscillatory tests.

Table 6.12 Experimental conditions.

Run	Sample name	Concentration [ppm]	Premix duration [s]	Gel time [s]
1	3 ppm _1	3	100	1300
2	3 ppm _2	3	50	2460
3	66 ppm _1	66	50	no evidence
4	66 ppm _2	66	50	560
5	66 ppm _3	66	50	650
6	665 ppm _1	665	50	290
7	665 ppm _2	665	50	410
8	665 ppm _3	665	50	314
9	665 ppm _4	665	50	390

Sample names consisted of two numbers, the first one corresponding to concentration of the ZnO in polyol, and the second one corresponding to the number of the run.

6.2.2.2 End of experiment

In rheological measurements of the reactive mixtures, sample is being modified from liquid, through gel, to a solid state material. These changes are monitored by the rheometer and are associated to an increase in rheological characteristics of the sample such as storage modulus, loss modulus and complex viscosity.

In the onset of the reaction when the mixture is liquid, loss modulus is higher than the storage modulus. With the development of the polymerisation, both of the moduli increase until they reach the point of the intersection, which is in literature defined as the gel point of the polymer (Haddadi, Nazockdast et al. 2008). After this point, elastic modulus increases faster than the loss modulus. Polymerisation is also manifested by an exponential increase in the complex viscosity, where the gel point is defined as the time when viscosity approaches to the infinity. The rate of an increase in the viscoelastic moduli and the complex viscosity is specific for each reactive mixture and it differs with the change in the experimental conditions as was determined experimentally.

It has been checked experimentally that if the maximum torque has not been achieved, the optimal parameter for the demoulding is the complex viscosity ranging from $50\,\mathrm{kPa.s}$ to $100\,\mathrm{kPa.s}$. In this range of complex viscosity, independently of the reactive system and experimental conditions, it is checked that the sample is completely solid and still has some flexibility.

All the experimental runs using reactive mixture with ZnO were stopped before achieving maximum torque of the rheometer, when the complex viscosity was in the range of $50\,\mathrm{kPa.s}$ to $100\,\mathrm{kPa.s}$. Experimental run "PU" reactive mixture without ZnO was stopped after the maximum torque was reached.

6.2.2.3 Effect of the concentration of the ZnO on gel point

The effect of ZnO on the polymerisation is assessed from the gel time of the samples. Figure 6.23 shows viscoelastic moduli versus reaction time for PU reinforced with ZnO in three concentrations and compared with the pure PU. The rate of viscosity increases, when the concentration of ZnO increases. So, the ZnO have a catalytic effect on the polymerisation reaction.

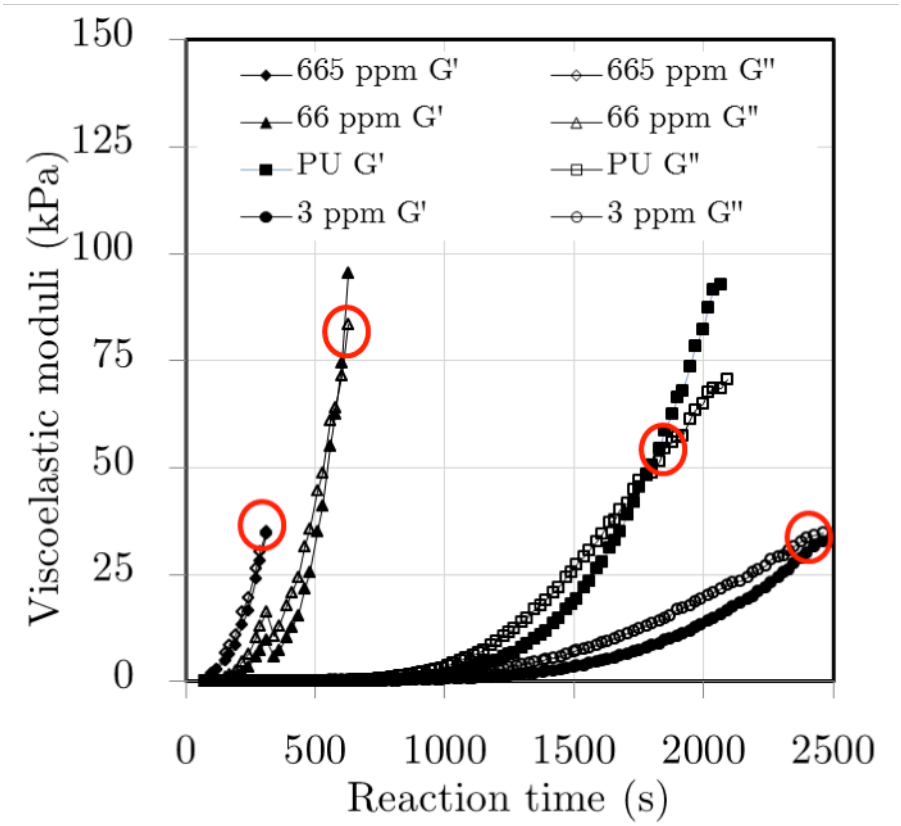

Figure 6.23 Viscoelastic moduli versus reaction time at 25°C for pure PU and PU reinforced with three concentrations of ZnO.

In Table 6.13 is summarized the gel times for the RenCast PU and the RenCast PU reinforced with ZnO.

Table 6.13 Influence of the concentration of ZnO on the gel time of PU reinforced with ZnO.

Sample	Gel time (s)
Average 665 ppm	340
Average 66 ppm	602
PU	1630
3 ppm _2	2460

6.2.2.4 Effect of the each reactant on the gel point composite

To study the effect of the reactants used to synthesize the ZnO on the kinetics of polymerisation of the RenCast PU, three reactants were added to the polyol: ZnAc – solid zinc acetate dissolved in isopropanol, NaOH – solid sodium hydroxide dissolved in isopropanol and pure isopropanol. Each one of the new reactants was premixed with RenCast polyol, and then the polymerisation of the RenCast PU was carried out standard in the rheometer.

Figure 6.24 represents viscoelastic moduli versus reaction time for pure RenCast polyurethane sample (PU) and for RenCast reinforced with zinc acetate (ZnAc).

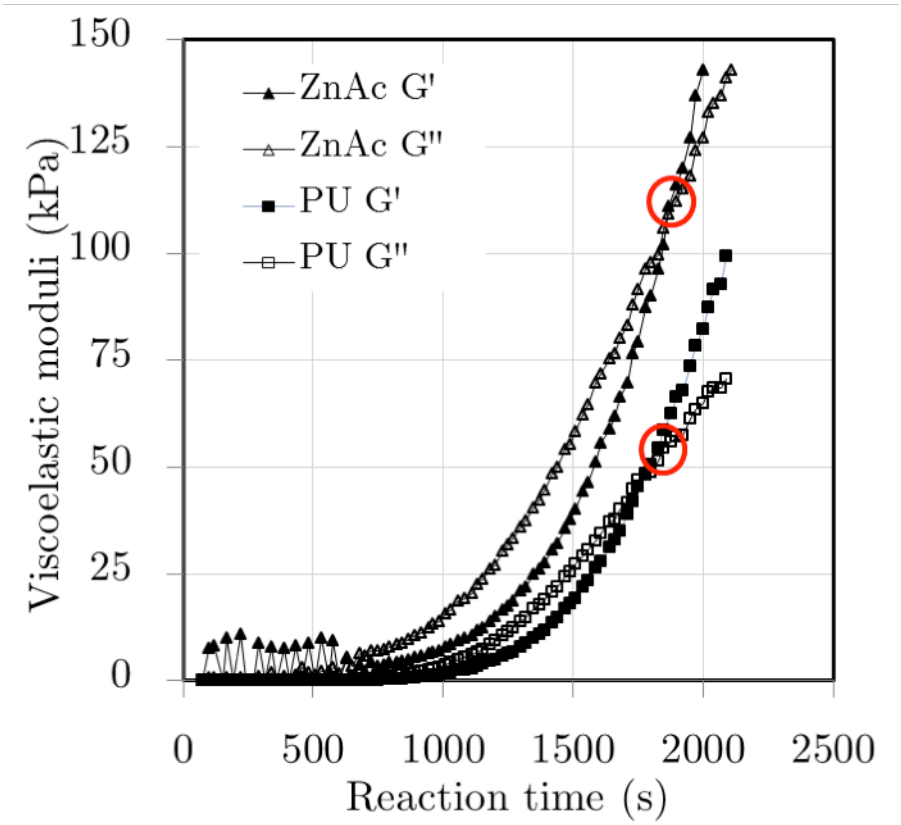

Figure 6.24 Viscoelastic moduli versus reaction time at 25°C for pure PU and PU with 10 vol.% of zinc acetate solution in isopropanol

Viscoelastic moduli versus reaction time for RenCast sample with sodium hydroxide (NaOH) is represented in Figure 6.25. Gel time at 25∫C is measured to be 1880 s. Although the dump and storage modulus change with the addition of the different reactants, the gel time remains approximately de same, and so it is the ZnO that is catalysing the polymerisation of RenCast PU.

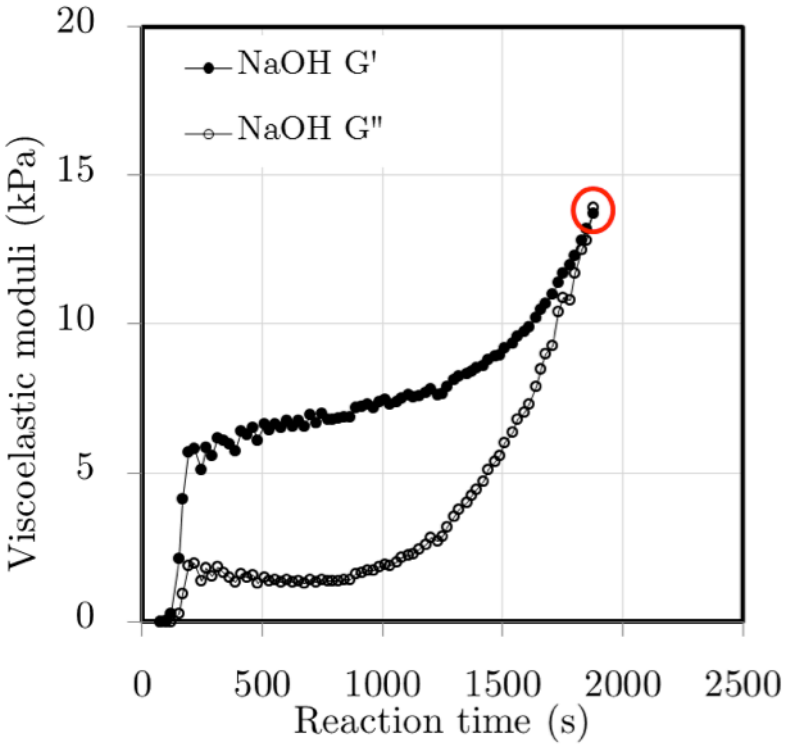

Figure 6.25 Viscoelastic moduli versus reaction time at 25°C for PU with 10 vol.% of isopropanol.

6.3 Conclusions

The effect of adding functionalised hydroxyapatite on the rheological characteristics and kinetics of the RenCast PU polymerisation was assessed, and it was observed that:

- The shear rate has huge effect on the process kinetics, if the shear rate is not high enough the reaction becomes diffusion limited a phenomenon that is more relevant under the presence of HAp nanoparticles.
- If the reaction is not limited by diffusion the temperature increases the reaction rate, which is clear indication that the reaction is in chemical regime, i.e. limited by the polymerisation kinetic constants.
- It was observed that ethylene glycol and f-HAp-paste have different effects on viscosity rise for different reaction shear rates: at $100\,s^{-1}$ viscosity rise of sample EG is faster than of sample f-HAp-paste. At $500\,s^{-1}$ and $1000\,s^{-1}$ sample f-HAp-paste is characterised with faster viscosity rise than sample EG.

The HAp dual effect is due to the fact that HAp probably hinders mass transfer while on the other hand catalyses the polymerisation reaction.

- Gel time for Ren sample is $1630\,\mathrm{s}$, and for EG is $1380\,\mathrm{s}$, so the ethylene glycol increases the reaction rate due to the fact that it has more mobility than polyol molecules.
- When functionalised f-HAp is incorporated into the solid RenCast sample by rheometry using the HC method it acts as a centre of the formation of macromolecular chains.
- When non functionalised HAp powder incorporated into the solid RenCast, it remains agglomerated in a few micrometers structure.

RenCast formulation was reinforced with ZnO nanoparticles of three concentrations: $3\,\mathrm{ppm}$, $66\,\mathrm{ppm}$ and $665\,\mathrm{ppm}$. Solid samples were synthesised by the HC method by rheometry and it was found that the the ZnO catalyses the polymerisation of RenCast PU.

6.4 References

Gomes, P. J., V. M. Silva, et al. (2009). "A Highly Reproducible Continuous Process for Hydroxyapatite Nanoparticles Synthesis." Journal of Nanoscience and Nanotechnology **9**(6): 3387-3395.

Haddadi, H., E. Nazockdast, et al. (2008). "Chemorheological characterisation of thermosetting polyurethane formulations containing different chain extender contents." Polymer Engineering and Science **48**(12): 2446-2453.

Rozenberg, B. A. and R. Tenne (2008). "Polymer-assisted fabrication of nanoparticles and nanocomposites." Progress in Polymer Science (Oxford) **33**(1): 40-112.

Viswanatha, R., H. Amenitsch, et al. (2007). "Growth kinetics of ZnO nanocrystals: A few surprises." Journal of the American Chemical Society **129**(14): 4470-4475.

7 Final Remarks

7.1 Conclusions

The principal conclusions of the thesis are presented in the following subchapters in the following order: polyurethanes, polyamide-6 for RIM and nanocomposites. The particular conclusions in each of these materials, are part of a bigger picture where the main result is the characterisation of a methodology to study the chemorheology of polymer formulations that are suited for RIM.

7.1.1 Polyurethanes

The main objectives of this work were to determine the best conditions for the rheological characterisation of polymerisation reactions aiming to get data that enables the optimization of RIM process parameters for each specific formulation. A new mixing method for rheometry called the HC was developed and showed more controlled contacting of the monomers and so more repeatable results.

The effect of shear rate and angular frequency on viscosity evolution and on the gel point were researched and it was found that by increasing the shear rate/angular frequency the viscosity rise and gel point are achieved faster. This was correlated

with the enhancement of diffusion of the monomer molecules inside the sample and faster onset of the polymerisation, which promotes a faster rate of polymerisation and therefore faster viscosity rise.

Mechanical properties, namely compressive strength and deflection temperature were measured on RenCast samples of 8 mm thickness produced by the HC method and correlated with the premixing shear rate. Optimal premixing shear rate for the production of samples for compression tests is found to be $750\,s^{-1}$. Deflection temperature measurements showed that significantly higher modulus compared to other premixing shear rates employed was obtained using premixing shear rate of $1500\,s^{-1}$.

Main results from the rheological characterisation of RenCast PU can be summarized as:

- The RenCast reactive mixture has a Newtonian behaviour in a time window large enough to comprise the time for mould filling;
- Shear rate has a strong effect on the viscosity rise at $25\,^{o}C$ and $40\,^{o}C$, setting the polymerisation regime from diffusion limit to chemical limited;
- For shear rate $\dot{\gamma} < 100\,s^{-1}$ no edge fracture occurs, for $\dot{\gamma} \geq 100\,s^{-1}$ edge fracture may occur;
- Larger premixing shear rates and longer premixing time that stand for a higher degree of mixing, yield lower gel times and higher storage modulus at the gel point which indicates larger growth rates of the macromolecules;
- Physical and chemical gel points were determined by the oscillatory experiments, which indicates the existence of the initial phase-separated polymeric structure which later in the reaction becomes dominated by the chemically connected polymer network.

7.1.2 Polyamide-6 for RIM

Three formulations containing different ratio of initiator/catalyst of polyamide-6 reactive formulation for RIM were tested. The summary of the formulations is shown in Table 7.1.

Table 7.1. Active compounds concentration in each formulation.

ω_{AC}^{samp}, %	Na-CL	B-iso
Formulation 1	0.97	0.520
Formulation 2	1.93	0.930
Formulation 3	2.90	1.55

The optimal concentration of initiator/catalyst and optimal rheometry procedure for The Holding Cell method were found and are as it follows:

- The complex viscosity rise of the formulation 1 is higher than 5 minutes which is not suitable for most RIM industrial applications (Van Rijswijk, Bersee et al. 2006).
- Formulations 2 and 3 are both suitable for RIM yielding in a solid product with complex viscosity at 75 s of 90 kPa.s and of 23 kPa.s, respectively.
- Two methods to melt the reactants were compared: melting in the closed glass beakers for 15 minutes at the hot plate (formulation 2) and directly on the rheometer plate during 10 s with exposition to atmospheric air (formulation 3) and other experimental conditions were kept identical. Formulation 2 yielded higher complex viscosity for the same time window.

7.1.3 Nanocomposites

A method for the functionalisation of hydroxyapatite from hydroxyapatite nanometric water paste 15 wt.% and from hydroxyapatite micrometric powder was developed. The method consists of mixing hydroxyapatite paste with ethylene glycol followed by the distillation at 110 °C to extract water. The obtained dispersion of hydroxyapatite in ethylene glycol is ultrasonicated for dispersion of the HAp. The

dispersion was blended in polyol and the polymerisation reaction was characterized using the HC rheological method and depending on the experiment the viscosity rise and gel point are measured. Solid sample was also possible to obtain and its morphology was studied by SEM. The main conclusions that were withdrawn from this study are as follows:

- Viscosity rise of the reactive mixture at both studied temperatures ($10\,^{\circ}\mathrm{C}$ and $25\,^{\circ}\mathrm{C}$) was faster as the shear rate was higher;
- At $\dot{\gamma} = 100\ \mathrm{s}^{-1}$ viscosity rise of sample EG is faster than of sample f-HAp-paste, which is clear indication that in this case the polymerisation rate is diffusion limited and the addition of nanoparticles poses an additional barrier to the molecules reorganizations;
- At $\dot{\gamma} = 500\ \mathrm{s}^{-1}$ and $\dot{\gamma} = 1000\ \mathrm{s}^{-1}$ f-HAp-paste sample is characterised with faster viscosity rise than sample EG, which shows that when the polymerisation rate is only chemically controlled the HAp acts as a catalyst;
- Gel time for Ren sample is $1630\ \mathrm{s}$, and for EG is $1380\ \mathrm{s}$, due to the fact that ethylene glycol molecules have more mobility that the polyol they will increase the polymerisation rate;
- Functionalised HAp with ethylene glycol are incorporated into the solid PU and it acts as a centre of the formation of macromolecular chains;
- Not functionalised HAp powder remains agglomerated in a few micrometer structures in RenCast polyurethane;

The effect of the nanometric zinc oxide on the gel time of the reactive formulations of RenCast and zinc oxide is assessed by the oscillatory tests in rheometry using the HC method. Zinc oxide nanoparticles were previously synthesised by wet precipitation method from zinc acetate and sodium hydroxide. Zinc oxide in the concentrations as high as $66\ \mathrm{ppm}$ and $666\ \mathrm{ppm}$ acts as a catalyst for the nanocomposite yielding lower gel time at room temperature than the gel time of the RenCast polyurethane.

7.2 Future work

The presented work shows the insight of the effects of the mixing methods on the viscosity rise and gel point of the reactive formulations which can be used to assess the optimal processing parameters for RIM machines. Additional work can be suggested here in order to complete this study, such as:

- Assessment of the effect of the mixing by the laboratory scale impingement mixer on the viscosity rise and the gel point of the reactive formulations used in this thesis (RenCast polyurethane and polyamide-6 for RIM). This objective would require construction of the mentioned lab scale mixer.
- Determination of the kinetics of the formulations by FTIR to be used in chemorheology study.
- Construction of a higher diameter holding cell (for example $75\ \mathrm{mm}$) which can be used with cone of the same diameter in order to produce larger samples that can be afterwards tested by other mechanical analysis method (compressive modulus, the required sample length is $50\ \mathrm{mm}$).

7.3 References

Van Rijswijk, K., Bersee, H.E.N., Jager, W.F., Picken, S.J., 2006. Optimisation of anionic polyamide-6 for vacuum infusion of thermoplastic composites: Choice of activator and initiator. Composites Part A: Applied Science and Manufacturing 37, 949-956.

A. Chamber shear rate of industrial RIM machines

A.1 Shear rate correlation with the Reynolds number for Newtonian fluid

The Reynolds number of injectors Re_{inj} in RIM machines is defined as a ratio of inertial to viscous forces in the material,

$$\mathrm{Re}_{inj} = \frac{\rho v_{inj} d_{inj}}{\mu} \tag{A.1}$$

where ρ and μ are density and viscosity of the polyol or isocyanate, and v_{inj} velocity of the fluid at the injectors and d_{inj} diameter of the injector. Flow inside the injector can be represented as a flow inside a circular duct. Axial velocity in the circular duct is obtained from

$$v_{ax} = 2\overline{v}\,\frac{R^2 - r^2}{R^2} \tag{A.2}$$

where v_{ax} is the axial velocity of the fluid jet, $\overline{v}$ is the average velocity, and r is the radial coordinate and R is the radius of the duct (injector) and it is also $R = \frac{d}{2}$.

Shear rate in a circular duct (injector) for Newtonian fluid is calculated from

$$\dot{\gamma} = \frac{\partial v_{ax}}{\partial r} = -\frac{4\overline{v}}{R^2} r \qquad \textbf{(A.3)}$$

At the centre of the injector where $r = R$, v_{ax} becomes equal to the maximum velocity v_{max}.

$$\dot{\gamma}_{\max} = -\frac{8 v_{\max}}{d} \qquad \textbf{(A.4)}$$

Combining Eq. (A.1) and Eq. (A.4) and substituting $v_{\max} = v_{inj}$, $d = d_{inj}$ and $\mathrm{Re} = \mathrm{Re}_{inj}$ maximum shear rate is obtained

$$\dot{\gamma}_{\max} = \frac{8\,\mathrm{Re}\,\mu}{\rho d^2} \qquad \textbf{(A.5)}$$

In order to make rheometer shear rate comparable to the shear rate in RIM machine, calculation was based on the shear rate inside the mixing chamber. The reason for this is that at rheometer shearing is applied on the reactive mixture and not separate reactants. In RIM machine reactive mixture flow inside the circular duct is obtained inside the mixing chamber.

Reynolds number in the mixing chamber Re_{ch} was calculated from

$$\mathrm{Re}_{ch} = \mathrm{Re}_{iso} \frac{d_{iso}\mu_{iso}\rho_{mix}}{D\mu_{mix}\rho_{iso}} + \mathrm{Re}_{pol} \frac{d_{pol}\mu_{pol}\rho_{mix}}{D\mu_{mix}\rho_{pol}} \qquad \textbf{(A.6)}$$

where μ_{pol} and μ_{iso} are viscosities of the polyol and isocyanate and ρ_{pol} and ρ_{iso} are densities of the polyol and isocyanate at $25\,^{\circ}\mathrm{C}$ and their values are represented in

Table A.1. Viscosity of the mixture μ_{mix}, was measured by rheometer at $25^{\circ}\mathrm{C}$ and taken as the first registered point of value $60\ \mathrm{mPa.s}$. Density of the mixture at $25^{\circ}\mathrm{C}$ ρ_{mix} was calculated from

$$\rho_{mix} = \frac{\rho_{pol} + \rho_{iso}}{2} \tag{A.7}$$

And it is $1\ \mathrm{g/cm^3}$. Polyol injector diameter d_{pol} was chosen to be $1.5\ \mathrm{mm}$, isocyanate d_{iso} $1\ \mathrm{mm}$ and chamber diameter D $10\ \mathrm{cm}$ which are the values of typical industrial RIM machines.

$$\dot{\gamma}_{ch} = \frac{8\,\mathrm{Re}_{ch}\,\mu_{mix}}{\rho_{mix} D^2} \tag{A.8}$$

Calculated shear rates from the injectors Reynolds numbers and chamber Reynolds number at $25^{\circ}\mathrm{C}$ are represented in Table A.1 and at $40^{\circ}\mathrm{C}$ at Table A.2.

Table A.1. Industrial Reynolds numbers and corresponding shear rates at $25^{\circ}\mathrm{C}$.

Re_{iso}	Re_{pol}	Re_{ch}	$\dot{\gamma}_{\mathrm{ch}}\left[\mathrm{s}^{-1}\right]$
1	1	0	1
50	50	14	56
100	100	28	112
500	500	140	560
1000	1000	280	1120
1500	1500	420	1680
2000	2000	560	2240
3000	3000	840	3360

Table A.2. Industrial Reynolds numbers and corresponding shear rates at $40^{\circ}\mathrm{C}$.

Re_{iso}	Re_{pol}	Re_{ch}	$\dot{\gamma}_{\mathrm{ch}}\left[\mathrm{s}^{-1}\right]$
1	1	0	1
50	50	14	40
100	100	29	80
500	500	143	400
1000	1000	286	800
1500	1500	429	1200

2000	2000	571	1600
3000	3000	857	2400

B. Preparation method for nylon-6

B1. Calculation of the reactants quantities

Three reactants were used in this synthesis:

- C10 (mixture of Na-CL and CL);
- C20 (mixture of B-iso and CL);
- Pure CL monomer (anionic grade).

C10 and C20 were supplied in packages with equal weights of $m_{pack}^{C10} = m_{pack}^{C20} = 1\,kg$.

The weight fraction of Na-CL in package C10, ω_{Na-CL}^{C10} and the weight fraction of B-iso in package C20, ω_{B-iso}^{C20} were equal and $\omega_{Na-CL}^{C10} = \omega_{B-iso}^{C20} = 17$ wt.% .

Recommended values by Bruggemann Chemicals of the weight fraction of Na-CL in tank A is to be $\omega_{Na-CL}^{A} = 4$ wt.% and the weight fraction of B-iso in tank B is to be $\omega_{Na-CL}^{B} = 2$ wt.%.

The objective of this calculation is to determine masses to be weighed by the next order:

- Tank A contains mixture of pure CL and C10;
- Tank B contains mixture of pure CL and C20.

In the following text, necessary weights of pure monomer caprolactam (CL) to be added into tanks A and B, $m^{A}_{CL,add}$ and $m^{B}_{CL,add}$, respectively; and of C10 and C20, m^{A}_{C10} and m^{B}_{C20} to be added into tanks A and B, respectively are calculated from the following:

- Necessary sample volume for MK22 cone is $0.7\ \text{ml}$, which is divided into two equal parts: $0.35\ \text{ml}$ from tank A and $0.35\ \text{ml}$ from tank B. Therefore the volume of the mixture in each tank is $V = V^{A} = V^{B} = 0.35\ \text{ml}$. From these volumes and densities of the mixture A and B which are assumed to be equal and also equal to the caprolactam monomer, $\rho^{A} = \rho^{B} = \rho_{CL} = 1.01\ \text{g}/\text{cm}^3$ (see Table 5.2) mixture mass in tanks A and B is calculated:

$$m^{A}_{tot} = m^{B}_{tot} = V\rho_{CL} \qquad \textbf{(B.1)}$$

From this value and m^{A}_{tot} and m^{B}_{tot} the weight fraction of Na-CL in tank A is to be $\omega^{A}_{Na-CL} = 4\ \text{wt.}\%$ and the weight fraction of B-iso in tank B is to be $\omega^{B}_{B-iso} = 2\ \text{wt.}\%$, masses of Na-CL in tank A, $m^{A}_{Na-\ CL}$ and of B-iso in tank B, $m^{B}_{B-\ iso}$ are calculated

$$m^{A}_{Na-CL} = \omega^{A}_{Na-CL} m^{A}_{tot} \qquad \textbf{(B.2)}$$

$$m^{B}_{B-iso} = \omega^{B}_{B-iso} m^{B}_{tot} \qquad \textbf{(B.3)}$$

- In the next step total mass of the caprolactam in tank A, $m^{A}_{CL,tot}$ and B, $m^{B}_{CL,tot}$ is calculated from

$$m^{A}_{CL,tot} = m^{A}_{tot} - m^{A}_{Na-\ CL} \qquad \textbf{(B.4)}$$

$$m^{B}_{CL,tot} = m^{B}_{tot} - m^{B}_{B\text{- iso}} \quad \textbf{(B.5)}$$

- From the datasheet of C10 and C20 it is known that the weight fraction of the active compounds, Na-CL in C10 and B-iso inC20, is equal and, $\omega^{C10}_{Na-CL} = \omega^{C20}_{B-iso} = 17$ wt.%. It is assumed that the mass of the Na-CL in tank A equals to the mass of Na-CL from C10 ($m^{C10}_{Na\text{- CL}} = m^{A}_{Na\text{- CL}}$) and that the mass of the B-iso in tank B equals to the mass of B-iso from C20 ($m^{C20}_{B\text{- iso}} = m^{B}_{B\text{- iso}}$). From these values, mass of caprolactam monomer from C10, m^{C10}_{CL} and caprolactam monomer from C20, m^{C20}_{CL} is calculated from

$$m^{C10}_{CL} = m^{C10}_{Na-CL} \frac{1-\omega^{C10}_{Na-CL}}{\omega^{C10}_{Na-CL}} \quad \textbf{(B.6)}$$

$$m^{C20}_{CL} = m^{C20}_{B-iso} \frac{1-\omega^{C20}_{B-iso}}{\omega^{C20}_{B-iso}} \quad \textbf{(B.7)}$$

- Now it is possible to calculate necessary weights of C10, m^{A}_{C10} and C20, m^{B}_{C20} to be added into tanks A andB, respectively from

$$m^{A}_{C10} = m^{C10}_{CL} + m^{C10}_{Na\text{- CL}} \quad \textbf{(B.8)}$$

$$m^{B}_{C20} = m^{C20}_{CL} + m^{C20}_{B\text{- iso}} \quad \textbf{(B.9)}$$

- Finally, it is possible to calculate the necessary weight of pure caprolactam monomer CL to be added into tank A, $m^{A}_{CL,add}$ and into tank B, $m^{B}_{CL,add}$.

$$m^{A}_{CL,add} = m^{A}_{CL,tot} - m^{C10}_{CL} \quad \textbf{(B.10)}$$

$$m^{B}_{CL,add} = m^{B}_{CL,tot} - m^{C20}_{CL} \quad \textbf{(B.11)}$$

- The quantity of caprolactam in tank A, $m^{A}_{CL,add}$, and in tank B, $m^{B}_{CL,add}$, and necessary weights of C10 in tank A, m^{A}_{C10}, and of C20 in tank B, m^{A}_{C20}, are weighted, melted and put on the rheometer plate where the experiment is started. In the end a solid sample is obtained.
- In order to calculate the weight fraction of active compound (Na-CL and B-iso) in the solid sample, the next procedure was adopted: total solid sample weight is obtained from

$$m^{samp} = m^{A}_{CL} + m^{B}_{CL} + m^{A}_{C10} + m^{B}_{C20} \tag{B.12}$$

- Weight fraction of Na-CL in the final polymerised sample is calculated from

$$\omega^{samp}_{Na-CL} = \frac{m^{A}_{Na-CL}}{m^{samp}} \tag{B.13}$$

- Weight fraction of B-iso in the final polymerised sample is calculated from

$$\omega^{samp}_{B-iso} = \frac{m^{B}_{B-iso}}{m^{samp}} \tag{B.14}$$

In this thesis three formulations are tested, by changing the mass fraction of the active compounds and they are listed in Table B.1.

Table B.1. Formulations with different mass fraction of active compounds.

Formulation n°	$\omega^{samp}_{Na-CL}\left[\%\right]$	$\omega^{samp}_{B-iso}\left[\%\right]$
1	0.97	0.52
2	1.93	1.03
3	2.90	1.55